UNIVERSITY OF SOUTHAMPTON

School of Civil Engineering and the Environment

Internal Fluidisation of Granular Material

By

Majed Omar Ahmad Alsaydalani

A Thesis Submitted in Fulfilment of the Degree of Doctor of Philosophy in the School of Civil Engineering and the Environment of the University of Southampton

August, 2010

This work is dedicated to my parents,

my wife and my son Omar.

UNIVERSITY OF SOUTHAMPTON

ABSTRACT

SCHOOL OF CIVIL ENGINEERING AND THE ENVIRONMENT

Doctor of Philosophy

INTERNAL FLUIDISATION OF GRANULAR MATERIAL

By Majed Omar Alsaydalani

Uncontrolled seepage flow due to defects or imperfect joints in civil engineering structures (such as dams, levees, dry-dock, seepage barriers, and sheet piles interlocking) or from fractured underground pipes is a major concern. The result of such leakage is increased water pressure and hydraulic gradients at the source of leakage making the behaviour of the surrounding material complex. This is because of the interaction of particles with the source of flow, turbulent flow in the surrounding bedding and the potential of developing additional mechanisms at the source of flow. Evidence of the occurrence of internal fluidisation has been reported in a number of fields, and yet not much is known about it.

In this fundamental study experimental apparatus and techniques have been developed to investigate the mechanism of internal fluidisation of granular material due to localised flow. A two-dimensional experimental model was created for the study, in which a machined box with variable orifice openings was designed and built to simulate an idealised crack for a localised leak. The box was fitted inside a modified seepage tank to fluidise a bed of granular material. Various parameters were investigated: flow rate, excess pore water pressure in the bed, pressure upstream of the orifice, particle size, particle shape, height of the bed, and orifice size on the observed mechanism. Image analysis techniques based on the Particle Image Velocimetry (PIV) have been developed in this study to monitor the behaviour of the fluidised zone.

Results and observations of this study suggest that the mechanism of internal fluidisation in a bed of granular materials is associated with an uplift mechanism of the grains in the active region of the bed. This is attributed to the drag force exerted by seepage flow overcoming the downward bulk weight of the bed. From the results

and observations of this study a mathematical model based on the concept of force equilibrium has been proposed to predict the pore pressure at the onset of internal fluidisation. The results show that high pressure heads can be sustained upstream of the orifice without the internally fluidised zone breaking through to the bed surface. They also show that the onset of this mechanism in a bed of granular material is highly dependent on packing properties (grain size, grain shape, height of the bed), seepage velocity and orifice size.

Keywords: *internal fluidisation, hydraulics gradient, excess pore water pressure, granular, localised flow, turbulent flow, Particle Image Velocimetry (PIV).*

"Water is essential for life on our planet; however, too much in the wrong places under the wrong conditions can have detrimental effects. Throughout recorded history there is evidence that mankind has feared and respected the destructive power of water. Out in the open, in the form of tides and floods, it is one of the most powerful forces of nature. Hidden in rock crevices and in soil pores, under the downward pull of the force of gravity it exerts unbelievable forces that tear down mountainsides and destroy engineering works. Railroad engineers, highway people, dam designers and builders, and many others have long known of the great importance of controlling water in pores and cracks in earth and rock formations. When ground water and seepage are uncontrolled, they can cause serous economic losses and take many human lives"

Harry R. Cedergren

CONTENTS

LIST OF TABLES

LIST OF FIGURES

LIST OF SYMBOLS

A	Area of flow in the soil
A_o	Area of the orifice
b	Breadth of the gap
CSF	Corey's shape factor
C_d	Discharge coefficient
dh	Differential bed height
d_j	Jet diameter
d_p	Particle diameter
F	Shape factor of the soil
g	Acceleration due to gravity
H	Height of the bed
i_c	Critical hydraulic gradient
I	Hydraulic gradient
k	Coefficient of permeability of the soil
k_c	Cavitation number
L	Length of the flow path in the soil
L_0	Width of the orifice opening
n	Porosity of the material
OS	Orifice / soil number
h	Pressure head
h_c	Orifice head loss
h_s	Soil head loss
p_d	Pressure downstream of the orifice
p_v	Vapour pressure of water

PIV	Particle Image Velocimetery
Q	Flow rate
Re	Reynolds number
S	Smallest dimensions of a particle
SEES	Scalene equivalent ellipsoid sphericity
U	Superficial fluid velocity
U_o	Initial velocity at the orifice
U_m	Decreasing axial velocity
w	Width of the orifice
Δh	Head losses within the soil
Δl	Length of flow path
ΔP	Differential pressure
ρ_f	Fluid density
ρ_s	Solids density
μ	Dynamic viscosity of fluid
ϕ_s	Particle shape factor
ψ_o	Krumbein's operational sphericity
ψ_p	Projection sphericity
ε	Porosity
$\bar{\gamma}$	Submerged unit weight
γ_w	Unit weight of water

ACKNOWLEDGEMENTS

The author sincerely thanks the expertise, the useful advice, discussion, and the constant support and guidance of his supervisor, Prof C.R.I. Clayton. During the research period, Professor Clayton guided the author in the right direction to achieve the research goals. I also express my gratitude and appreciation to Dr. Arif Anwar for his valuable comments and discussion.

Part of this acknowledgment goes to the lab-supervisor Mr. Harvey Skinner, for all his help in the lab with electrical and electronic components and in troubleshooting various technical problems in the lab. I also would like to thank the member of technical workshop: Mr. Earl Peters for his help with the mechanical components, and Mrs. Jacqui A. Holmes, the research secretary/postgraduate program coordinator, for her kindly supports during the research.

Above all, the Author would like to express his deep gratitude to his parents, who brought him up in love, who constantly encourage his study, who always wish all the best to the Author.

I offer my profound thanks to the Saudi Arabian Cultural bureau specifically, and the Saudi Arabian government generally, for their spiritual and financial support.

CHAPTER 1 INTRODUCTION

1.1 Background

Fluidisation of granular material refers to the state when solid particles are caused to behave like a viscous fluid i.e. when they are transformed from a solid like state to a dynamic fluid like state. This phenomenon occurs when a fluid (liquid or gas) flows through a bed of granular material and creates a drag force sufficient to support the weight of the grains (Leave, 1959). It can occur in an open bed, but also can occur under confined conditions.

The phenomenon of fluidisation is a multidisciplinary issue governed by the principles of various disciplines including hydraulics, granular media mechanics and fluid dynamics. It is relevant to various industrial, coastal, geological, and geotechnical applications, and can be either useful or detrimental depending on the occurrence in engineering applications. For example, in the field of chemical engineering, fluidisation has been used for many years to improve chemical reactions, and for drying and mixing particles (e.g. Wen and Yu, 1966; Hartman and Coughlin, 1993). Similarly in the field of coastal engineering it has been applied as a useful tool for sand management as it has been used for maintenance of navigable waterways and in sand bypassing at tidal inlet and harbour mouths (e.g. Weisman et al., 1988; Ledwith and Weisman, 1990). It is also seen to be an important phenomenon in the field of geology. In this field fluidisation has been invoked to explain the structure and geometry of volcaniclastic materials within kimberlite[1] pipes which are known to be sources of diamonds (Walters et al. 2006; and Gernon et al., 2009). The reported studies on fluidisation in the above flelds often make reference to "local", "partial" or "internal" fluidisation within which the particles circulate (move) in a localised confined zone. However, very little is known about this phenomenon which appears, surprisingly, to have attracted little attention.

[1] Kimberlites are ultramafic, volatile-rich volcanic rocks occurring in continental settings (e.g., South Africa), (Walter et al., 2006).

Nevertheless, internal fluidisation of granular material may have important civil engineering and fundamental interests. For example, uncontrolled seepage flow due to defects or imperfect joints in engineering structures (such as dams, levees, dry-docks, seepage barriers, and sheet plies interlocking) or from fractured buried pipes is a major concern. Excessive leakage has been reported through many of these structures and has been identified to be the cause of many failure incidents of these structures resulting in different failure mechanisms. An example of this is the catastrophic failure of Teton Dam, in the United Sates, in 1976, which resulted in the deaths of 11 people and caused over $1 billion in property damages (see Figure 1.1). Different failure mechanics have been suggested to be responsible for the failure of the dam, one of which is the formation of a hydraulic fracture in the core of the dam (Pillai et al., 2004). This may involve the mechanism of internal fluidisation, and yet not much is known about it in the hydraulic and geotechnical literature. Unfortunately, when a structure fails due to localised flow the evidence is often washed away with the structure.

It is postulated that the build up of pore water pressure and increase in hydraulic gradients at the point source of leakage may lead to the occurrence of an internally fluidised zone. This phenomenon is complex in nature and may not be detected until it has progressed enough to be visible or detected by measurements. This thesis considers this problem and makes a contribution to this field by improving the understanding of the internal fluidisation of granular material.

1.2 Objectives of this research

The main aim of the study is to develop an understanding of the mechanism of internal fluidisation of granular media. The secondary aims are to:

- Development of an experimental apparatus and techniques for monitoring fluidisation.

- Assessment of the effect of grains characteristics (in term of size and form of the grain) on internal fluidisation.

- Assessment of the effect of orifice (i.e. crack) size on the onset of internal fluidisation.

- Development of a mathematical model for predicting the pore water pressure at the onset of internal fluidisation.

1.3 Organisation of this thesis

This thesis is divided into five chapters; the content of each of these chapters is briefly described below.

- This chapter has provided a brief background on this subject and states the scope and the objectives of the work.

- **Chapter 2** presents a detailed literature review on various topics that are necessary to accomplish the objective of this research.

- **Chapter 3** presents the experimental development and techniques used to accomplish this study. It also presents typical results obtained from the study.

- **Chapter 4** brings together the information presented in previous chapters, compares it with the literature wherever appropriate and draws further conclusions.

- **Chapter 5** presents the conclusions derived from this research, practical implications of this research, and recommendations for future research.

Figure 1.1a: Failure of Teton dam. Photo by Mrs. Eunice Olson, 5 June 1976. Arthur Gibbs Sylvester, University of California[2]

Figure 1.1b: Failure of Teton dam. Photo by Mrs. Eunice Olson, 5 June 1976. Arthur Gibbs Sylvester, University of California[2]

[2] http://www.geol.ucsb.edu/faculty/sylvester/Teton_Dam/welcome_dam.html

CHAPTER 2 LITERATURE REVIEW

This chapter provides a detailed literature review of the background topics such as (i) definitions of internal fluidisation, (ii) its occurrence in civil engineering and other fields, (iii) flow through granular materials and orifices, (iv) combined flow (seepage/ orifice flow interaction), (v) onset of fluidisation, and (vi) previous studies on internal fluidisation. It then summarises the main points (that are relevant to this research) from the literature.

2.1 Definition of internal fluidisation

Due to the large body of literature that has been found related to fluidisation, and the fact that this phenomenon is a multidisciplinary issue related to the fundamentals of different subjects including hydraulics, soil mechanics, and chemical processing it was essential to define this term before proceeding with this review.

The term fluidisation has been widely used in the field of chemical engineering, and is defined as the operation by which solid particles are transformed into a fluid like state through contact with gas or liquid (Kunii and Levenspiel, 1991). The particles become separated and in motion with the pore fluid. This can be achieved by pumping a fluid upwards through a bed of granular materials. When the upward fluid flow creates a drag force sufficient to support the weight of the bed then fluidisation occurs (Leva, 1959).

In the literature of soil mechanics there is a phenomenon termed piping. This phenomenon is also sometimes known as fluidisation. However, the definitions found in the literature describing the piping phenomenon encompass internal erosion processes. For example Terzaghi (1939) defined piping as the progressive backward erosion of particles from an exit point of concentrated leakage. This mode of piping is the classic backward erosion which results in the formation of a continuous passage or pipe along the base of the structure. Piping of this type is initiated by Darcy flow at the exit point, where the flow is laminar. Other definitions of piping which involve internal erosion include: concentrated leak piping; suffusion, and

heave (Foster and Fell, 1999). Heave is usually followed by backward erosion if piping is to occur (Foster and Fell, 1999).

Interestingly, the term fluidisation is found in Wikipedia[1], where it is defined as "a process similar to liquefaction whereby a granular material is converted from a static solid-like state to a dynamic fluid-like state". However, the term liquefaction is normally used for the loss of stability of a saturated granular media subjected to loads of very short duration such as occur during earthquakes (Holtz and Kovacs, 1981). Additionally, liquefaction occurs over a large area.

In summary, the terms "fluidisation", "piping" in all its forms, and "liquefaction" have all been used to describe the conditions where granular materials are transformed to behave like a viscous fluid. However, the term piping is used to describe the condition resulting from seepage flow which involves the **removal** of soil particles and occurs in localised channels. The term liquefaction is used if the condition occurs as a result of shock loads (e.g. earthquake) and occurs over a large area.

In this thesis the term 'internal fluidisation' is defined as the phenomenon in which granular media are forced by seepage flow, due to the build of water pressure and increased in hydraulic gradients, to behave like a heavy fluid circulate with a jet of fluid in a localised zone. If internal fluidisation occurs in the middle of soil or in the bedding material around fractured buried pipelines, it may not be observed at the surface. Such a phenomenon may be transparency-limited until it has progressed enough to be visible or detected by measurements.

[1] http://en.wikipedia.org/wiki/Fluidization

2.2 Occurrence in Civil Engineering and other fields

Internal fluidisation of granular materials can occur in a number of situations when there is a source of localised fluid flow into a body of granular materials. It can occur in the field of civil engineering as a result of uncontrolled seepage flow due to defects or imperfect joints in engineering structures built to contain or transport water. However, it can also occur in other fields such as chemical engineering, costal engineering and geology. Many of the processes and applications in chemical engineering and coastal engineering fields require contact between granular materials and a fluid. In such processes and applications the fluid is normally fed into the bed of materials through a distributor or pipe for fluidisation. In the field of geology, fluidisation is also seen to be an important process where it is invoked to explain the structure and geometry of materials within kimberlite pipes. Analogue laboratory studies of these systems have been reported within which internal fluidisation has been observed. More about these is presented in the following subsections.

2.2.1 Civil Engineering

Uncontrolled seepage flow due to defects or imperfect joints in engineering structures such as dams, levees, seepage barriers, sheet piles interlocking and from fractured buried pipes is a major concern. The build up of pore water pressure and increase in hydraulic gradients around the source flow may lead to the occurrence of internal fluidisation, and eventually lead to failure of the structure.

Internal fluidisation in the field of civil engineering may take place inside the bedding materials around fractured pipes, in the vicinity of defects in the seepage barrier, around sheet piles wall interlocks, and in the middle body of dams (e.g. dam cores). In all these situations there is high potential for uncontrolled leakage flow to develop due to defects or imperfect joint connections leading to the occurrence of this phenomenon.

Fractured pipes

Fractured underground water pipes are one major source of seepage flow into the surrounding bedding. On average, leakage rate from these systems around the world is thought to be about 35% of the total supplied (Global Leakage Summit, 2008).

Leakage from water pipes can be attributed to several causes, including: high internal pressure, materials defects, as a result of corrosion, and due to differential settlements arising from poor backfilling beneath the pipe. Depending on the type of cause, leakage can occur in different components of the distribution systems; through joints, ferrule connections, holes and fractures. The last of these is thought to be the most significant contributor to the overall leakage rate.

A significant body of literature on the failure mechanisms of water pipes has shown that the majority of failures in these pipes occur in cast iron pipes, particularly in small (e.g. 100 mm) diameter pipes (O'Day, 1982; Ciottoni, 1983; Habibian, 1994; Rajani et al, 1996; O'Shea, 2000; Makar et al., 2001; Silinis and Franks, 2007; Kunkel et al., 2008). These small diameter pipes mainly fail by circumferential cracks, indicating that bending forces were applied to the pipe resulting in beam failure (O'Day, 1982; Rajani et al., 1996; Makar et al., 2001). Circumferential cracks could also result from tensile forces applied on the pipe as a result of the seasonal swelling and shrinkage of clay soils (Clayton et al., 2010).

Leakage flow from fractured underground pipes into the surrounding bedding can lead to the build up of pore water pressure and increases in hydraulic gradients resulting in unstable bedding (Al-Karni, 2000; Noack and Ulanicki, 2006). This may be a potential place for internal fluidisation to occur.

Seepage barriers

Another situation for internal fluidisation to take place in the field of civil engineering is around the boundaries of seepage barriers. Seepage barriers (e.g. slurry walls, concrete walls, jet grouted walls or sheet piles walls) are used to control underseepage of water through pervious parts of embankments dams, foundations, or abutments. However, in practice the cut-off efficiency of these structures is imperfect i.e. does not achieve complete water-tightness (e.g. Telling et al., 1978, Casagrande, 1961). Water tightness is quantified in term of the degree of imperfection which is defined by Ambraseys (1963) as the ratio of cut-off wall area that has not been sealed. For instance, in the case of steel sheet piling the degree of imperfection is represented by the proportion of the joint gap (i.e. clutch gap) to the cut-off wall

area. Details of clutch interlocking are presented in Figure 2.1. The width of clutch gaps may vary but an average value of 2 mm may be representative of a loosely driven piling (Telling, 1978), and this corresponds to a degree of imperfection of about 0.5%. Based on theoretical studies Ambraseys (1963) showed that very small openings in the sheeting ($\leq 1\%$ of the total area) will lead to a significant reduction in the cut-off efficiency from (100% to 10% efficiency) Figure 2.2.

Even though nowadays in practice sheet wall piles with expanding materials located in the interlocking sealing joint are being used to reduce leakage, the sheet piles may be damaged during installation. Driving piles into dense materials or materials containing boulders may create cracks in the sheet piling materials or separation of interlock joint and this reduces the efficiency (Guertin and McTigue, 1982).

Rice and Duncan (2010) have recently published the result of a study of 30 case histories of dams in the United States with seepage barriers in place for over 10 years. The results of this study showed that several of the case histories showed direct evidence of the development of cracks or leaks in seepage barriers after construction. As reported by Rice and Duncan (2010) evidence of leaks in the barriers was detected in a number of dams: Wolf Creek (Zoccola et al. 2006), Navajo (Davidson 1990), and Crane Valley (Perkins 1932; Garber 1972). They also believe that post-construction cracking may have occurred in many other barriers; however, most of these cracks remained undetected because of the locations of instrumentation. When leakage through these cracks intensifies it can potentially lead to build up of hydraulic pressure and gradients which eventually may end up with the formation of internal fluidisation in the body of the dams or its foundations.

Dam cores

A dam core is another place where internal fluidisation of the materials can arise. Normally embankment dams are constructed of different zones of different materials in order to control seepage through the dam body. An embankment dam usually has an impervious core acting as a hydraulic barrier, which is adjusted to zones of coarser materials (acts as filter) to provide seepage control, in addition to rock-fill and gravel in order to provide stability for the construction (Figure 2.3).

However, dams are subjected to different forms of loads which may result in a variety of deformation and settlement. Different compressibility of the various zones might lead to redistribution of internal stress and uneven settlement, and this may cause cracks or soft zones in the body of a dam increasing the potential of initiation of internal fluidisation. Figure 2.4 presents locations of internal differential settlement cracks in embankment dams suggested by Sherard et al. (1963). The locations of these cracks are potential places for internal fluidisation to occur.

Load transfer may occur in dams as a result of the arching effect or "load shed" caused by dam's differential settlement. When the core is less stiff than the fill on each side, the settlement in the core becomes larger than that in the fill; and as a result of this the core material is left "hanging" on the shoulder of the coarser fills materials. As a consequence of this, the total stress in the middle of the core at some points drops below the weight of the overburden and thereby the water pressure exceeds it, leading to hydraulic fracture, and this causes effective stress to drop to zero (Squier, 1970; Bjerrum et al., 1972; Kulhawy and Gurtowski 1976; Sherard, 1986). The tendency for hydraulic fracturing ought to be more pronounced in central core type dams, particularly with a relatively thin core, as they favour load transfer from the core to the shells (Lofquist 1986; Sherard 1986; Foster 2002).

Excessive leakage attributable to hydraulic fracturing in the core of dams has been reported in a number of cases. Examples of these are the Hyttejuvet Dam in Norway (Kjaernsli and Torblaa, 1968), and Teton Dam in the USA (Independent Panel to Review Cause of Teton Dam Failure, 1976) both of which suffered from failure during the filling of the reservoirs. In both cases, high leakage rate has been reported which is believed to occur due to hydraulic fracture in the core of the dams. This may involve at some stage the occurrence of an internally fluidised zone in the dams cores.

2.2.2 Chemical Engineering

Fluidisation of granular materials has been widely used in the field of chemical engineering processing for wide applications. For example it has been used for gas adsorption, solid drying, filtering, petroleum refining and for ore reduction (MacDonald and Bridgwater, 1997). Such processes need a contact between a bed of granular materials and a fluid. Generally in such applications, a fluid injected through a distributor or a feed pipe is required for fluidisation (MacDonald and Bridgwater, 1997). When the fluid is injected at high velocity into the bed of materials it may lead to the occurrence of internal fluidisation. Such a phenomenon has been reported in various studies in the field of chemical engineering (e.g. Apte et al., 1990, MacDonald and Bridgwater, 1997, and Sastry et al., 2003, Zhang 2003, Chen et al., 2007), and is know as a cavity formation, and sometimes is termed a "raceway cavity". In all the reported studies a jet of air has been introduced into a bed of granular materials.

Fluidisation of packed beds of changing cross sectional area has also been used in many industrial processing applications. For instance, in the case of tapered fluidised beds extensive mixing can be achieved because of changing flow geometry, leading to various applications (Peng and Fan, 1997). Such systems are designed with cross sectional area that changes with height. The area of the flow increases along the height of the bed from the bottom to the top. Under such conditions the fluid velocity is relatively high at the bottom of the bed and decreases in the vertical direction, where it becomes relatively low at the top of the bed. This higher velocity at the bottom of the bed can be expected to lead to formation of internal fluidisation in this region. "Local" or "partial" fluidisation in beds of changing cross sectional area (flow geometry) have been reported in a number of studies (e.g. Peng and Fan, 1997; Zhang et al., 2003).

2.2.3 Coastal Engineering

Fluidisation has also been seen to be a useful tool in the field of coastal engineering. Laboratory and analytical research has been undertaken to design fluidiser systems for maintaining of navigable water ways and in sand bypassing at tidal inlets and harbour mouths (e.g. Weisman et al., 1988; Lennon et al., 1990; Ledwith et al., 1990;

Weisman and Lennon, 1994). In such applications, water jets have been produced from small horizontally-aligned holes in the walls of buried pipes at high pressures and flow rate to fluidise the region above the pipes.

Flow emerging from these holes, in the source pipes, has largest gradient near the holes and this can be expected to create internal fluidisation. Such a phenomenon has been reported by Weisman and Lennon, (1994) who indicated that initiation of fluidisation occurs when a local boil of sand occurs along the weakened path from the source pipe to the bed surface. Eventually when flow becomes sufficiently high the localised boil of sand enlarges and combines until the bed above the source pipes is fluidised completely (Weisman and Lennon, 1994).

2.2.4 Geology

Fluidisation has been seen to be an important process in volcanic systems. It has been invoked as a major process in pyroclastic flows (Sparks, 1976; Wilson, 1980, 1984). It is also seen to explain the structure and geometry of volcaniclastic materials within kimberlite pipes (Woolsey et al., 1975; Walters et al., 2006; Sparks et al., 2006, Gernon et al., 2009). Figure 2.5 presents a model of a kimberlite body that has been recognised (Field and Soctt Smith, 1999), which is typical of many kimberlites in Southern Africa (Walters et al., 2006). It consists of a steep sided shaped pipe (Figure 2.5) and is thought to consist of three different zones (i) the root zone, (ii) the pipe zone and (iii) the crater zone (Hawthorne, 1975).

Recent laboratory studies on fluidisation, as analogue to volcanic systems, have been reported in the literature of geology (e.g. Walters et al., 2006; and Gernon et al., 2008). Walter et al. (2006) studied the role of fluidisation in the formation of volcaniclastic materials within kimberlite pipes. In this study they introduced high pressure gas, fed into a bed of sand from a 5 mm diameter point source. This resulted in the formation of an upward diverging pipe structure of thoroughly mixed fluidised materials bounded by non-fluidised zone. Walter et al. (2006) also observed in this study that when a strong upward gas flowed along the centre of the pipe led to internal circulation of sand at the bottom of the bed. Based on the results of this study

Walter et al. (2006) concluded that fluidisation could be a major control on the structured and sorting of deposits in kimberlite pipes.

In another analogue study Gernon et al. (2008) performed experiments to investigate gas fluidisation behaviour on particles in straight sided and tapered beds. They observed in the case of tapered bed fluidised particles are limited to a central region and marginal non-fluidised.

2.3 Flows through granular materials and orifices

When considering internal fluidisation of granular materials it is essential to look at the theory of fluid flow; flow through granular media and flow through orifices. An orifice may be considered as representative of an idealised defect (i.e. crack or hole) in engineering structures where it could be a source for a localised flow. The following sub-headings will look at flow through granular materials followed by flow through orifices.

2.3.1 Flow through granular material

Fluid flow through granular media can be classified to be either laminar or turbulent depending on flow velocity, which can be characterised by Reynolds's number (Re). High flow velocity may lead to piping in coarse materials or hydraulic fracturing in fine (low permeable) materials.

Laminar flow

Darcy, in 1856, established the first law of flow through a saturated porous medium, which is known as Darcy's law. He carried out a series of experiments using a vertical column filled with sand particles and allowed water to flow through the sand column Figure 2.6. Based on these experiments, Darcy concluded that the rate of flow through the porous media is linearly proportional to the total head loss across the sand column (ΔH) and the cross sectional area (A) of the flow and inversely proportional to the packed bed height of the column (L).

$$Q = K\ A\ (\frac{\Delta H}{L}) \tag{2.1}$$

another form of this equation is:

$$v = k \cdot i \tag{2.2}$$

Where *(v)* is flow velocity, *(i)* is the hydraulic gradient and *(k)* is the hydraulic conductivity (which is a function of both porous medium and the fluid properties).

It was recognised later by Reynolds, in 1883, that the linear proportional relationship between flow rate and head only holds true for laminar flow. Laminar flow through granular materials may be described as smooth flow in which flow lines, not necessarily parallel, remain distinct and follow the general vector direction of overall flow (Watson, 1993). This type of flow occurs at low velocity for which viscous forces predominate over inertial forces. The flow regime is characterised by Reynolds number ($\mathrm{Re} = \rho VD / \mu$, where V is the discharge velocity, D is the average diameter of the particle). The critical Reynolds number value at which the flow through porous media changes from laminar to turbulent flow has been found to range between 1 and 12 (Harr, 1962).

In the field of soil mechanics it is generally believed that flow through soil is laminar, in which case the rate of flow is linearly proportional to the applied head, following Darcy's law. Terzaghi (1943) examined the range of the validity of Darcy Law and found that the law is valid for a wide range of soils and hydraulic gradients. Similarly, Muskat (1937) conclude that " in the great majority of flow systems of physical interest the flow will be strictly governed by Darcy's law." Taylor (1948) has also indicated that flow through most soil is generally laminar. He found that under a hydraulic gradient of unity, typical for most flow situations, soil with a grain size of 0.5 mm or smaller will always have laminar flow.

However, there are a number of situations where the flow is expected to be non-laminar. For example in the case of flow through coarse sand and gravels Darcy's law is not strictly applicable (Cedergren 1989), in which case non-laminar flow may occur.

Turbulent flow

Darcy's law, which suggests a linear relationship between flow rate and head, is only valid for low flow velocity where the flow is laminar. At higher flow velocity turbulent flow may occur in porous media for which a nonlinear relationship between flow and head is expected to occur. Turbulent flow occurs at the high Reynolds numbers for which inertial forces predominates over viscous forces. According to Bear (1972) turbulent flow is not observed in a porous medium until the pore Reynolds number is 60 to 150.

Forchheimer (1901), the first to suggest a non linear relationship between flow and head, suggested that Darcy's law be modified for high flow velocities (where a nonlinear relationship between the flow and hydraulic gradient occurs). He suggested including a second order term in the velocity:

$$I = aV + bV^2 \tag{2.3}$$

where a and b are constants to be determined. The values of the constant parameters a and b could be obtained for a given physical system by solutions of the Navier-Stokes equations and relating pressure and velocity fields, for the corresponding boundary conditions (Hlushkou and Tallarek, 2006). However, due to the complexity of the geometry of porous media and nonlinearity of the Navier-Stokes equations the numerical solution of the problem is very complex (Hlushkou and Tallarek, 2006). This has led many investigators to focus on obtaining an empirical relationship between head loss and velocity in porous media. Forchheimer (1901) found that for flow through pervious gravels the above equation takes the form of:

$$I = \frac{1.77}{10^3}V + \frac{3.18}{10^4}V^2 \tag{2.4}$$

In equation 2.4, the velocity is in m/day.

Later Ergun (1952), in the field of chemical engineering, studied the nonlinear relationship between pressure drop and fluid velocity. He examined this phenomenon using a column, similar to that of Darcy, filled with granular materials, and allowed gas to flow through the bed. Ergun (1952) examined its dependence on flow rate,

size and shape of the particle, porosity of the bed, and fluid properties. Based on this study, Ergun developed an equation by equating the fluid energy loss to the sum of viscous energy and kinetic energy losses, giving the pressure loss per length of a packed bed:

$$\frac{\Delta P}{L} = A\frac{\mu}{\phi_s^2 d_p^2}\cdot\frac{(1-\varepsilon)^2}{\varepsilon^3}U + B\frac{\rho_f}{\phi_s d_p}\cdot\frac{(1-\varepsilon)}{\varepsilon^3}U^2 \qquad (2.5)$$

Where

μ is the dynamic viscosity of fluid;

d_p is the particle diameter;

ρ_f is the fluid density;

ϕ_s is the particle shape factor (sphericity);

ε is the porosity;

U is the superficial fluid velocity (defined by $U = Q/A_c$)

Q is the total flow rate through a cross section of area, A_c

Ergun (1952) analysed a large quantity of experimental data, and concluded that the best fit could be obtained by values for A = 150 and B=1.75. This equation (equ. 2.5) is similar to Forchheimer's (1901) empirical form (2.3).

The Ergun model, equation (2.5), has been the most widely accepted relationship describing the dependence of pressure loss on fluid velocity and packing properties (Hlushkou, 2006). This is due to the fact that it takes into account the effect of pressure losses due to viscous energy loss resulting from laminar flow at low velocity; and losses due to kinetic energy or inertial losses from the onset of flow separation effects and other "shock losses" within the porous media (Niven, 2003), at higher flow velocity. Figure 2.7, demonstrates the capability of the Ergun model to cover, in good agreement with the experimental data, a wide range of velocities in a packed granular beds from laminar to turbulent flow (Bird et al., 2002; Hlushkou and

Tallarek, 2006). The transition from laminar to turbulent flow has been described by Ergun to be gradual and smooth (See Figure 2.7).

The cause of the non-linearity (i.e. the second power) of the second term in equation (2.5) has been discussed by many researchers (e.g. Bear, 1972; Niven, 2002; 2003; Hlushkou and Tallarek, 2006). As reported by Bear (1972), Forchheimer (1901) attributed the non-linearity to the appearance of turbulent flow, as the head gradient through a pipe in turbulent flow is proportional to the square of the velocity. However, Bear (1972) suggested that this explanation is rather questionable, as there seem to be basic differences between the two cases (i.e. flow through porous media and through pipes). These are:

(i) In turbulent flow through pipes the linear form does not appear;

(ii) In flow through pipes the transition from laminar to turbulent is rather sharp and not gradual as described by Ergun, (1952); and

(iii) The critical Reynolds number at which the transition takes place in pipes is several orders of magnitude higher than in flow through porous media.

For fluid flow in pipes, laminar flow behaviour is normally observed up to Reynolds numbers of about 2000, whilst fully turbulent flow occurs above Re of about 4000. In a packed bed, however, the flow is laminar at Re up to about 10, and the onset of turbulent flow is not observed in a porous medium until the pore Reynolds number is in the range of 60 to 150 (Bear, 1972). Based on these results the deviation from Darcy's law (which may occur at Re = 1 to 10) cannot be attributed to turbulent flow (Bear, 1972; Niven, 2002; and Niven, 2003). Instead the deviation from Darcy's law (at low Re, less than 10) is attributed to inertial forces (Scheidegger, 1960; Bear, 1972; Niven, 2002; and Niven, 2003). This arises from the onset of "local" losses - sometimes termed "shock," "minor" or "fitting" losses - as a result of laminar flow through the expansions, contractions, and changes in flow direction within the porous medium (Scheidegger, 1960; Bear, 1972; Niven, 2002; 2003). Niven (2003) has indicated that just as expansions, contractions and bends in a pipe produce local energy losses, due to flow separation effects within the fittings, the constantly expanding and contracting flow between the narrow pore necks and wider pore

pockets in a granular material - as well as the curved flow paths around soil particles - also generates local losses. This result is an additional velocity squared term in the head loss equation, which may not be the result of turbulence (Niven, 2003).

On this basis, Hlushkou and Tallarek (2006) indicated that three regimes of liquid flow through porous media can be identified (Figure 2.8); Darcian flow (where viscous forces dominates and pressure loss is linearly proportional to the fluid velocity), (ii) turbulent flow (inertial forces dominates; pressure loss is proportional to square of the velocity) and (iii) transient or nonlinear laminar flow (in which viscous and inertial forces effects exist, and pressure loss varies nonlinearly with fluid velocity, but flow remains laminar). Pressure loss due to kinetic energy loss dominates at high Re. According to Bear (1972) turbulent flow is not observed in a porous medium until the pore Reynolds number is 60 to 150.

Piping

When fluid flow through granular media becomes sufficiently high then piping may occur. A substantial amount of research has been found related to piping and internal erosion in the literature of geotechnical engineering (e.g. Terzaghi, 1922; Skempton and Brogan, 1994; Foster, 1999; Foster et al., 2000; Fell et al., 2005; and Richards and Reddy, 2007). They are considered to be the main causes of failures and incidents in embankment dams (Sherard et al., 1963, Foster et al. 2000, 2002; and Fell et al., 2005).

The term piping found in the literature encompasses the range of internal erosion processes as follows (Foster and Fell, 1999):

(i) *Backward erosion piping*: defined by Terzaghi, (1922) as the progressive backward erosion of particles from an exit point of seepage resulting in the formation of a continuous passage or pipe. This form of piping is the classic backward erosion piping and is initiated by Darcy's flow.

(ii) *Concentrated leak piping*: involves the development of a crack or concentrated leak from the source of leakage to an exit point, and erosion starts along the walls of concentrated leak.

(iii) *Suffusion*: involves the removal of internal fine particles by seepage flow through internally unstable materials.

(iv) *Piping due to heave*: occurs as a result of high pore water pressure at the down stream toe of the structure and causing a zero effective stress condition (Terzaghi, 1922). This is normally followed by backward erosion if piping is to occur (Foster and Fell, 1999).

Conceptual models for development of failure by piping and internal erosion for the first two processes have been described by Foster and Fell (1999) as a four phase process consisting of (i) initiation, (ii) continuation, (iii) progression, and (iv) breach Figure 2.9. The sequence of the events causing failure by the two models is basically similar, but the mechanisms associated with initiation and propagation phases are different. For example, in the backward erosion piping process the initiation stage occurs at the exit point of seepage and progresses backwards, whereas in the case of concentrated leak piping process it occurs due to flow through crack and progresses by enlargement of concentrated leak.

Terzaghi (1922) first developed a theory for piping potential in a uniform sand column. The developed theory was specifically for upwards vertical flow, and is based on the summation of the vertical upward forces due to seepage flow and the downwards weight of the submerged sand particles. According to this theory, when the hydraulic head reached a critical value i.e. causing a zero effective stress the point at which the upwards seepage force by water pressure at a certain level is in balance with the bulk weight of the sand column at that level, then piping will occur Figure 2.10. Terzaghi (1922) termed this as piping failure due to heave and the critical hydraulic gradient for this to occur is given by:

$$i_c = (1-n)(1-\rho) = \bar{\gamma} / \gamma_w \qquad 2.6$$

Where

i_c is the critical hydraulic gradient;

n is the overall porosity of the material;

ρ is the specific gravity of the grains;

$\bar{\gamma}$ is the submerged unit weight; and

γ_w is the unit weight of water.

According to the above Terzaghi's theory, piping will occur at a critical upward hydraulic gradient i_c typically about 1.0.

However, Skempton and Brogan (1994) have shown experimentally that piping may occur at hydraulic gradients different from that suggested by Terzaghi's theory. They carried out piping experiments in sandy gravel using a cylindrical apparatus measured 139 mm in diameter and 155 mm in length (Figure 2.11). In their tests the samples were subjected to upward flow increased in small steps until piping occurred. Skempton and Brogan (1994) observed initially in all their tests a linear increase in flow velocity with increasing hydraulic gradient, following Darcy's law for laminar flow. But when the gradient increased further, a disproportionate increase in flow occurred, resulting in failure by piping (Figure 2.12). As reported by the authors, this occurs initially with movement of the finer particles followed by general movement, or by creating a crack (below or around the mid-depth of the sample) and then creates its way upwards until piping occurs throughout the whole sample. In these tests Skempton and Brogan (1994) found that for stable materials, having a coefficient of uniformity less than 10, the critical hydraulic gradients at which piping occurred was approximately at the full theoretical gradient (i_c=1). However, for the unstable materials, with a coefficient of uniformity of greater than 20, the critical hydraulic gradients at which piping occurs was far lower, i.e. one third to one fifth, than that given by Terzaghi's theory. One important conclusion from Skempton and Brogan's (1994) work is that the distribution of internal stress may influence piping potential (Richards and Reddy, 2007).

Based on the above discussion it can be concluded that the mechanical role of the hydraulic gradient on failure by piping is not well known. The available theory of failure by piping suggests that the critical hydraulic gradient at which piping would occur is about one (based on Terzaghi's failure theory). However, recent literature has indicated that the actual critical hydraulic gradient can be different from that

proposed in the theory. There are some instances of failure by seepage flow where it has occurred at a hydraulic gradient below unity. It has been suggested by some researchers that distribution of internal stress may influence failure potential.

Hydraulic fracture

Fluid flow through porous media, particularly media with low permeability such as clay, can generate sufficiently high pore water pressure that may lead to failure by hydraulic fracture (Bjerrum et al., 1972). Hydraulic fracture is defined as "the condition leading to the creation and propagation of a thin physical separation in a soil or rock mass due to the high fluid pressure" (Independent Panel to Review Cause of Teton Dam Failure, 1976). According to Bjerrum et al. (1972) hydraulic fracture takes place once the water pressure at any point in the ground exceeds the minor total principal stress.

Hydraulic fracture has been recognised in dam engineering and identified to be the cause of excessive leakage in many dams around the world (e.g. Hyttejuvet Dam in Norway, low level flood control dams in Oklahoma and Mississippi, Stockton Creek Dam, Wister Dam, Yard's Creek Upper Reservoir Dam, Balderhead Dam, and Teton Dam (reported in Jaworski et al. (1981)). Even though it has not been possible to prove by direct observation that hydraulic fracture occurred in all these cases, a significant amount of evidence has been gathered to indicate that hydraulic fracture could in fact take place. In the paper by Sherard (1986) evidence is accumulated to supporting the conclusion that concentrated leaks due to hydraulic fractures occur commonly in well-designed and constructed dams without being noticed. The evidence is presented in the following categories (Sherard, 1986):

(i) *"Concentrated leaks which appear soon after the first reservoir filling through well-constructed homogeneous dams with no internal filter or drain, sometimes leading to breaching failure;*

(ii) *Erosive leaks through central core dams with inadequate filters ,usually occurring soon after the first relatively rapid reservoir filling;*

(iii) Records of well constructed and designed central core dams in which nearly full reservoir pressure was measured in piezometers at the downstream face of the core, and in which exploratory borings in the dam made to study this condition showed conclusively that near horizontal, water-filled cracks existed in the core;

(iv) FEM calculations showing that only relatively small differential settlements will easily create stress conditions in most dams under ordinary conditions which will allow hydraulic fracturing to occur; and

(v) The discovery of 'wet seams' inside impervious dam sections, with water content higher than can be accounted for reasonably by any other mechanism than the entry of water into an open crack."

Sherard (1986) also indicated that the width of the hydraulic fracturing cracks depends mainly on the water pressure entering the crack (and height of the reservoir above the crack). For low dams the cracks are probably generally very narrow for example as small as a fraction of a millimetre, whereas for high dams the crack can be opened up for several centimetres (Sherard, 1986).

Hydraulic fracture was confirmed for the first time, in geotechnical engineering, by a series of laboratory tests using a small scale piezometer in a tank filled with soft clay (Bjerrum et al., 1972). The tests were performed as constant head permeability tests (i.e. applying constant head with increased increments while observing the rate of flow). After the application of the excess head a fundamental change in the rate of flow was observed. This was indicated by a sudden rapid rise in the rate of flow of water into the soil resulting of the hydraulic fracture. Figure 2.13, shows a photograph of the developed crack.

Since Bjerrum et al. (1972), hydraulic fractures have been reported in a number of experimental studies (e.g., Jaworski et al., 1981, Murdoch, 1993). In all of these studies the tests were performed on low permeable materials. For example, Jaworski

et al. (1981) carried out laboratory tests on soil samples taken from the core of the remainder of Teton Dam after its failure. They performed their tests, in a similar way to Bjerrum et al. (1972), by increasing the water pressure in a model borehole until a fracture was developed in the sample. Based on the results of their study, they hypothesised that (i) hydraulic fracturing is a "weak link" phenomenon, in which crack will occur in the soil with least resistant subjected to the build-up of water pressure; and (ii) for hydraulic fracturing to occur it may require a discontinuity, for which water pressure can wedge its way in the soil. In this study Jaworski et al. (1981) also reviewed previous field and laboratory tests on hydraulic fracture and indicated that the mechanism of hydraulic fracturing around model boreholes in the laboratory is similar to that in the field.

Other experimental studies on hydraulic fractures have also been reported in other fields (e.g. Nichols et al., 1994, Valverde et al., 1998; Watson et al., 2001). In experiments on a fluid escape structure Nichols et al. (1994) reported horizontally water-filled cracks when over-pressurised water flowed upward through horizontal layers of fine-grained glass ballotini (74-149 micrometer) and silicon carbide (180-250 micrometer). Valverde et al. (1998) and Watson et al. (2001) have also observed hydraulic fractures when they studied experimentally the tensile strength of homogenous cohesive powders (organic polymers) by forcing gas upward through columns of particles. They reported that cracks were formed when the fluid overpressure rose above the weight of the overburden. But hydraulic fracture could occur at excess water pressure lower than the effective overburden pressure at the point of measurement as presented earlier by Bjerrum et al. (1972).

The above discussion indicates that there is a high potential for hydraulic fracture to take place in embankment dams, without even been observed. When hydraulic facture takes place then water starts to flow rapidly. Flow along these cracks is expected to be non-laminar, as pressure increases, the move from Darcy flow to hydraulic fracturing can be expected to produce higher flow leading to internal fluidisation of the surrounding materials.

2.3.2 Flow through orifices

An orifice is a small opening (i.e. small compared to the head producing flow), usually circular but can any shape, through which fluid is discharged in the form of a jet, normally into the atmosphere (Douglas et al., 1979). The hydraulic behaviour of the orifice can be affected by various factors including its geometry (size, shape, and roughness), and type of the flow (which can be laminar, turbulent, and cavitation flow). Blockage of an orifice with objects such as grains may also affect its hydraulic behaviour.

Laminar flow through an orifice occurs at low flow velocity for which viscous forces predominate over inertial forces. According to Idelchik, (1994) flow through an orifice is defined to be laminar at Reynolds numbers (Re) below about 10. The Reynolds number for an orifice opening can be written as:

$$\mathrm{Re} = \frac{\rho V D_h}{\mu} \tag{2.7}$$

Where

ρ is the density of the fluid;

V is the velocity;

D_h is the hydraulic diameter $(= 4R_h)$

R_h is the hydraulic radius of the orifice (defined as flow area A divided by the wetted perimeter P); and

μ is the viscosity of the fluid.

A laminar flow regime is characterised by individual fluid "particles" following paths that do not cross those of neighbouring "particles" (Massey and Ward-Smith, 1998). The development of laminar flow through thick orifice plates (e.g. long tube length) is shown in Figure 2.14. When a fluid enters the orifice, at first the velocity profile across the orifice is uniform (position A), then retarding effects of the boundaries takes place (position B), and eventually the profile becomes a parabolic distribution (position C), which is referred to as fully developed laminar flow. According to Massey and Ward-Smith (1998) laminar flow is independent of the surface

roughness of the walls, as long as the roughness is not so great that it constitutes an appreciable change on the cross sectional area.

Fully developed laminar flow through a thick orifice plate (i.e. constant gap with smooth parallel sides) may be described by Poiseuille's equation as follows:

$$Q = \frac{b\ w^3}{12\ \mu}\frac{\Delta P}{L} \tag{2.8}$$

Where

Q is the rate of flow through the gap;

w is width of the orifice;

L is the length of the orifice;

ΔP is the differential pressure;

b is the breadth of the gap; and

μ is the viscosity of the fluid.

However, most orifice flow under free discharge condition occurs at high velocity (i.e. high Reynolds numbers) for which inertial forces dominate over viscous forces. Under such conditions turbulent flow through the orifice is expected to occur.

A ***turbulent*** flow regime is characterised by irregular movement of fluid flow "particles" which mix strongly with each other (Idelchik, 1994). Idelchik (1994) indicated that flow through an orifice transforms from laminar to turbulent flow at Reynolds numbers of about 4000-5000.

The hydraulic behaviour of orifice flow under turbulent conditions has been studied extensively in the fluid mechanics literature, and can be predicted with some degree of certainty. It is typically described by the orifice flow theory which suggests that the rate of flow is proportional to the square root of the pressure drop across the orifice, according to the following equation:

$$q = C_d A_o \sqrt{2gh} \tag{2.9}$$

Where

q is the flow rate;

C_d is the discharge coefficient;

A_o is the orifice area;

g is the acceleration due to gravity; and

h is the pressure head.

The above equation (eq. 2.9) is derived based on Bernoulli's principle which describes the conversion of pressure head into kinetic energy, and is applicable for an incompressible steady-state flow. The discharge coefficient C_d in the equation is added to overcome the loss of energy and the reduction of jet diameter at the vena contracta, downstream of the orifice. Its value is dependent on various parameters: the ratio of the orifice diameter to the thickness of the tank wall, the sharpness of the edge of the orifice, the roughness of the inner surface, and the temperature of the water (Brater and King, 1976). Normally a constant value of the coefficient of discharge for turbulent conditions is assumed. For example for small sharp edged orifices a constant value for C_d between 0.6 and 0.62 is usually adopted (Brater et al., 1996).

The diffusion of a submerged turbulent jet issuing from an orifice into a body of the same fluid is shown in Figure 2.15 (Rajaratnam, 1976). As a result of the shear against the surrounding fluid, the jet spreads radially, forming three flow regions. These are: a potential core of the original velocity U_o; a transition region beyond the core with different flow profiles, and a zone of established flow, with a decreasing axial velocity U_m, with similar velocity profiles (Albertson et al., 1950, cited in Niven and Khalili, 1998). The central velocity U_m is decreases linearly in the x direction from the tip of the jet:

$$\frac{U_m}{U_o} = \beta \frac{d_j}{x} \tag{2.10}$$

Where

U_o is the initial velocity;

U_m is the decreasing axial velocity;

β is constant (6.3 for air and water (Albertson et al., 1950, cited in Niven and Khalili, 1998);

d_j is jet diameter; and

x is the distance from jet tip.

Cavitation (boundary layer separation)

One of the factors that influences the behaviour of fluid flow through orifices is the cavitation phenomenon. This phenomenon involves the formation of vapour bubbles in the region of high flow velocity and occurs when the pressure in this region is reduced below the vapour pressure of the fluid (Douglas et al., 1979, Koivula, 2002).

A substantial amount of research has been carried out on cavitation in the field of fluid mechanics (e.g. Wiklund and Svedberg, 1996; Myllykyla, 1999; Koivula, 2002); as this phenomenon can affect the performance of fluid power systems in different ways. Cavitation can reduce the efficiency of the systems while increasing vibration and noise level (Douglas et al., 1979; Koivula 2002). Another serious effect of cavitation on fluid power systems is local erosion of metals surfaces by a process called "cavitation erosion" (Douglas et al., 1979 and Koivula 2002). Erosion of metal surfaces by this phenomenon occurs when the bubbles formed during cavitation collapse suddenly when in contact with metal surfaces (Douglas et al., 1979). When the bubbles are transformed from a low pressure region into high pressure region they can generate very large forces with which the liquid hits the surface, resulting in local erosion (Douglas et al., 1979).

The effect of cavitation on the efficiency of fluid systems has been examined in many research studies (e.g. Wiklund, 1996; Myllykyla, 1999, Koivula, 2002). Wiklund (1996) and Myllykyla (1999) have examined pumping capability of different pumps, and found that a significant reduction in flow is associated with cavitation in the suction line of the pump.

In another study Koivula (2002) investigated the effect of cavitation on flow behaviour of a small hydraulic orifice (1 to 5 mm internal diameter). In this investigation Koivula measured the rate of flow as the pressure down stream was decreased. Koivula observed that the pressure-flow rate relationship followed the orifice flow theory until a particular point, after which it started to deviate. It is observed that at this point the rate of flow through the orifice does not increase as the downstream pressure is decreased, due to cavitation effects (Figure 2.16). The stage is referred to as "choked flow".

From the theory of fluid mechanics, the intensity of cavitation can be estimated by a non-dimensional number which relates the static pressure, which resists cavitation to dynamic pressure which promotes cavitation as follows (e.g. Douglas et al., 1979):

$$k_c = \frac{2(p_d - p_v)}{\rho v^2} \tag{2.11}$$

Where

k_c is the cavitation number;

p_d is the pressure downstream of the orifice;

p_v is the vapour pressure of the fluid;

ρ is the density of the fluid; and

v is the mean velocity through the orifice.

The higher the cavitation number the less likely is the cavitation to occur. According to Lamb (1987) a critical cavitation number of between 0.2 and 1.5 is reported below which the cavitation is likely to appear in orifices, depending on geometry.

The effect of orifice geometry on the occurrence of cavitation has been studied by many researchers (e.g. Nurick, 1976; Reitz and Bracco, 1982; Su et al., 1995; and Koivula, 1998 and 2002). Nurick (1976) indicated that cavitation occurring in a sharp edged orifice causing flow separation from the orifice wall depends on the orifice aspect ratio (L/D) and the flow conditions. Su et al. (1995) investigated sharp and round-edged orifices and found that sharp edged orifices have a lower coefficient

of discharge compared to round edged orifices, as a result of cavitation. Similarly, Koivula (2002) studied experimentally the influence of orifice geometry on cavitation. He examined sharp and chamfered-edged orifices and found that a chamfer edged orifice passes more flow than a sharp edged orifice. Koivula (2002) found that in sharp edged orifices the flow detaches easily from the orifice wall, and cavitation occurs more easily.

The above studies indicate that the degree of cavitation is strongly dependent on the orifice geometry at the inlet point and the injection velocity. The sharper the edges of the orifice at the entrance the more likely is cavitation to occur as a result of the fluid flow separation at the orifice flow entrance Figure 2.17.

Orifice blockage

Fluid flow through an orifice under the free discharged condition is assumed to be proportional to the square root of the pressure drop across the orifice; following the orifice flow theory (equation 2.9). A constant value of the coefficient of discharge C_d is normally assumed in the equation depending on the orifice geometry. For example, for sharp edged orifices a value for C_d between 0.6 and 0.62 is normally adopted (Brater et al., 1996).

However, when the orifice becomes blocked or obstructed with objects (e.g. soil particles) then the flow behaviour is expected to be disturbed. Studies on this type of flow have been rare. Massimilla et al. (1963) studied the rate of fluid-particle flow from fluidised beds through small orifices. They examined the effect of the ratio of orifice to particle diameter on the flow behaviour. The result of this study showed that for beds of greater than 70% liquid the rate of flow was analogous to that of homogenous liquid (i.e. liquid alone). Massimilla et al. (1963) indicated that under such conditions the orifice flow equation with a coefficient of discharge identical to that of the liquid alone can be used. However, at some critical bed solids concentration (35% - 50%) the particles started to interfere with the orifice and the coefficient of discharge for the flow decreased. They observed, under these conditions, a reduction in the value of the coefficient of discharge by about 22 % of that at high liquid rate.

The interaction of soil particles with the orifice expected to modify the downstream jet behaviour, while perhaps also block part of the orifice itself (Massimilla et al., 1963 and van Zyl and Clayton, 2007). Water seeping through these particles meets with more resistance than water flowing freely through the unblocked orifice. Under such situations it is expected that more energy is required to deliver more flow.

2.4 Combined flow (seepage / orifice interface)

Very few studies have been carried out on seepage through combined granular materials and orifices (e.g. Ledwith et al., 1990; Walski et al., 2006; Zoueshtiagh and Merlen, 2007). Walski et al. (2006) considered two elements of head loss; loss due to flow through an orifice (h_o), and loss due to flow through soil by Darcy's law (h_s), and derived a dimensionless "orifice/soil " (OS) number to characterise their importance.

$$OS = \frac{h_o}{h_s} = \frac{KAQ}{2gL}\left(\frac{1}{C_d A_o}\right)^2 \tag{2.12}$$

Where

K is the hydraulic conductivity of the soil,

A is the area of flow in the soil,

Q is the flow rate,

L is the length of the flow path in the soil,

C_d is the coefficient of discharge of the orifice, and

A_o is the area of the orifice.

When OS is less than unity, they claimed that soil head losses predominate. When OS is larger than unity orifice head losses were thought to predominate. As OS with a magnitude of 1 indicates that both the soil loss and orifice loss are important.

Walski et al. (2006) examined this theory by measuring head loss versus flow relationship for a range of OS numbers. Two test apparatuses were used: a "short"

apparatus and "tall" apparatus. The former was cylindrical, 48 cm in height with an inside diameter of 38 cm, and the latter was tall and narrow made from a PVC pipe with a height of 1.57 m and a diameter of 10.2 cm. They carried out various tests with different pressures, flows, orifice sizes and soils. Walski et al. (2006) observed in these tests that for head loss to be controlled by the soil (a low OS number), a relatively high flow rate is needed. Also, the soil matrix had to be secured to avoid fluidisation of the soil. They found that without a pressure plate (i.e. a screen that allows water to pass through but retains the soil) in the tall apparatus to prevent the soil from fluidising, conditions could not be created with a low OS number. Based on these observations, they concluded that "in most real-world cases, the OS number is large" so that the orifice head loss dominates.

However, other literature indicates that seepage head may dominate, and indeed that it is possible to maintain significant heads in a water pipe whilst fluidising a shallow bed of soil. Burnell and Race (2000) demonstrated that leakage from their supply pipes had a linear correlation with internal pressure, suggesting that leakage in that case had been controlled by soil head loss. Furthermore, using a two-dimensional fluidisation experimental apparatus, Ledwith et al. (1990) investigated fluidisation pipe pressures and the flow rate required to achieve initial and full fluidisation. These tests were performed on fine, medium and coarse sands at depths of 25.4 and 42 cm, using 12 orifices with different sizes with diameters ranging between 1.59 and 6.35 mm. The results of this study showed that the bed of soil, although only 42 cm deep, could sustain a pressure head in the pipe of up to 33 m of water before being fully fluidised.

Moreover, van Zyl and Clayton (2007) have expressed some doubt about the analysis that led to Walski et al.'s conclusion; i.e. that soil has no effect on leakage rate. They indicated that an equation for the combined systems cannot be properly defined by a direct coupling of the orifice equation with the soil seepage equation as has been proposed above. This is because of the incompatibility between the two analyses; soil seepage analysis and the orifice flow analysis. They also indicated that the Darcy

flow equation is depends on a number of assumptions that are not generally valid for seepage around a fractured pipe. These are:

- In soil seepage analysis it is safe to neglect the velocity component of the total head because it is very small. The velocity of flow through soil under a hydraulic gradient of unity ranges from value of 10^{-2} m/s for clean coarse sand to less than 10^{-8} m/s and smaller for clays (Harr, 1962). However in comparison, the orifice flow equation (equation ((2.9)) predicts very high velocities at the orifice- grain interface.

- In most geotechnical seepage conditions, upstream and downstream boundaries can be assumed to have fixed geometries and head conditions. However, the downstream boundary conditions in the ground surrounding a fractured pipe are not generally constant.

- Darcy's law, which suggests a linear relationship between head and flow rate, is only valid for laminar flow. Flow through soil is found to be laminar at Reynolds number less than 10 (Bear 1972). In many soil seepage situations, laminar flow can expected to occur in sands and finer materials at low hydraulic gradients ($\Delta h/\Delta l << 1$). Yet, around a fractured leaking pipe, hydraulic gradients are expected to be much larger. Normally water distribution pipes are buried at depth of about 1 m and have a pressure head of about 30 m. Thus, flow around a leaking fractured pipe is expected to be non-laminar.

- The way in which flow takes place within a bed of granular materials is affected by the stress conditions. For example, for materials such as soil, if the pore water pressure at any point in the ground exceeds the minor total stress, then hydraulic fracture takes place (Bjerrum et al., 1972). Soil cracks through which water preferentially flows, in order of magnitude. Under such a condition soil seepage analysis is no longer applicable, as flow along these cracks is expected to be non-laminar.

- The traditional soil seepage analysis also is not applicable if fluidisation takes place. In the literature of soil mechanics this phenomenon is known as "piping" and occurs in granular materials if the uplift force due to seepage exceeds the self weight of the grains. Based on the available theory, piping occurs at hydraulic gradient approximately equals to unity (Terzaghi, 1922).

The complexity of combined flow (flow through granular materials and orifice flow) has been shown in a number of studies (e.g. Niven and Khalili, 1998; Zoueshtiagh and Merlen, 2007). Zoueshtiagh and Merlen (2007) studied experimentally the effect of a vertically flowing water jet underneath a granular bed. They observed that three distinct regimes are associated with the flow rate that appeared to outline the bed's behaviour. Regime (i): at sufficiently low flow rate the bed remained motionless and acted as a porous medium. When the applied flow rate was large enough, regime (ii) occurred, in which local deformation was observed at the bed surface (See Figure 2.18). Zoueshtiagh and Merlen (2007) indicated that this bump shape deformation occurred at the centre of the tank just above the injection (Figure 2.18 b and c). They considered this regime as a transitional situation from a packed bed regime to fluidisation. The observation by Zoueshtiagh and Merlen (2007) of regime (ii) suggests that there is high potential for internal mechanisms that may occur at the orifice-particle interface. However, the limitations of their experimental design, which studied the problem in three dimensions, did not allow them to observe such mechanisms. When flow rate increased further, Zoueshtiagh and Merlen (2007) observed regime (iii), in which local fluidisation at the bed surface was observed, and this was limited to the area above the injection hole. They observed that the fluidised area was similar to a cylindrical and vertical chimney in which the grains are in motion.

Based on the above discussion it can be concluded that the interaction between seepage through granular materials and orifice flow is complex. In such a situation it is unlikely that the relationship between head and flow rate will be either a linear relationship, following Darcy's law, or follow the orifice flow theory. This can be attributed to the interaction of grains with the orifice, orifice blocking, turbulent flow

in the bed of materials, and initiations of additional mechanisms such as piping, hydraulic fracturing and internal fluidisation in the bedding material.

2.5 Onset of fluidisation

Almost all theoretical and experimental studies on fluidisation come from the literature of chemical engineering. Further, most emphasis has been on gas-fluidised systems, with few studies on liquid-fluidised systems (e.g. Shi et al, 1984; and Peng and Fan, 1997).

The onset of complete fluidisation in a bed of granular material occurs when the upward drag force exerted by the fluid becomes equal to weight of the bed. In other words it occurs when the upward pressure is in equilibrium with the buoyant weight of the materials (Hartman and Coughlin, 1993):

$$\frac{\Delta P}{L} = (1-\varepsilon)\ (\rho_s - \rho_f)\ g \tag{2.13}$$

The pressure drop in the bed at the onset of fluidisation can be predicted using the widely known Ergun's equation (Ergun, 1952):

$$\frac{\Delta P}{L} = A\frac{\mu}{\phi_s^2 d_p^2}\cdot\frac{(1-\varepsilon)^2}{\varepsilon^3}U + B\frac{\rho_f}{\phi_s d_p}\cdot\frac{(1-\varepsilon)}{\varepsilon^3}U^2 \tag{2.14}$$

The above equations are valid for uniformly distributed flow along a columnar fluidised bed. However, the start of fluidisation from a localised flow such as that resulting from underground leaking pipe may require an energy input greater than that required for fluidisation itself. If the bedding materials for example were composed of interlocked, very angular particles, then more energy is needed to overcome grain interlocking (Weisman et al., 1988; Hartman and Coughlin, 1993). This may be considered as fluidisation "activation energy" (Niven and Khalili, 1998). In addition to this is the amount of energy dissipated in the orifice.

2.6 Previous studies on internal fluidisation

Several studies have been carried out to investigate internal fluidisation in a bed of granular materials (e.g. Apte et al., 1990; MacDonald and Bridgwater, 1997; Niven and Khalili, 1998; and Sastry et al., 2003). Apart from the study by Niven and Khalili

(1998) from the literature of hydraulic engineering, where a jet of water was used in their study, all the others come from the literature of chemical engineering where a jet of gas was injected into the bed of material.

Niven and Khalili (1998) investigated the scour of granular material by an *internal* downwardly-directed vertical water jet. They conducted experiments on different granular materials and jet diameters; using tanks of different sizes made of plexiglass. In some of these experiments the jet was adjacent to the tank wall to visualise the scour zone. Niven and Khalili (1998) observed from these experiments the formation of an in-situ fluidised zone, (defined in their study as the fluidisation of granular materials by a jet), surrounded by a circular ridge of eroded, re-deposited materials. With increasing jet depth, the fluidised zones changed from an open, axisymmetric, approximately ellipsoidal form to an asymmetric, spouted profile, and thence to a submerged fluidised cavity as shown in Figure 2.19. Based on their study they observed that the fluidised zone profile was approximately constant in shape for any given material, jet diameter, and flow rate. They also observed that its geometry was controlled by two mechanisms:

(i) Scour below the jet tip, which follows the linear velocity decrease of a submerged jet; and
(ii) The ability of the flow to maintain fluidisation, which controls the zone diameter.

Others laboratory experiments where internal fluidisation has been observed were carried using two-dimensional models (e.g. Apte et al., 1990; and Sastry et al., 2003). Apte et al. (1990) used a two-dimensional experimental model to measure the static pressure profile in a packed bed above a cavity formed by air jet in upward direction. This was performed using a rectangular container (570 mm long × 920 mm high with inside widths of 14, 20, and 30mm). The container included a slot opening (about 1 mm) through its bottom, running across the bed width. Static pressure measurements through the bed were obtained by drilling 1.65 mm diameter holes in the face of the enclosure. Granular materials (i.e. glass and plastic) with a sphere diameter ranging from 3-3.4 mm were used for the tests. Apte et al. (1990) started

the tests by increasing blast flow rate; while observing the cavity size and the static pressure profile in the cavity and the bed. They observed abrupt changes in the pressure and gas velocity near the roof of the cavity. The pressure increased inside the cavity, reaching a maximum value at the inner boundary of the cavity zone.

In another study Sastry et al. (2003) used two-dimensional glass models to investigate void formation and breaking in a packed bed. They performed tests by injecting compressed air through a narrow rectangular slot (5 mm wide) flowing horizontally into the packed bed. Granular materials (quartz and polypropylene; with different diameters) were used as packing. Sastry et al. (2003) observed in these tests that as the air flow was gradually increased a small cavity formed in front of the slot Figure 2.20. By further increasing the air flow, the particles started moving inside the cavity forming a small raceway. As the air flow was gradually increased the raceway expanded in all direction, until eventually it broke through to the bed surface. Sastry et al. (2003) also observed in this study a variation in the pressure drop across the bed as flow rate increased initiating from cavity formation and up to braking of the cavity Figure 2.21. They observed that as the flow rate was increased the pressure drop across the outlet of the slot and pressure inside the cavity increased continuously; until a sudden drop in the pressure occurred due to collapse of the cavity (inset Figure 2.21).

2.7 Conclusions drawn from literature

- Uncontrolled seepage flow through defects or imperfect joints in engineering structures such as dams, levees, dry-docks, seepage barriers, sheet piles interlocking or from fractured underground pipes is of great concern. A large number of failures occur due to concentrated leakage from such structures. Failure by seepage flow is considered to cause among the most serious accidents in civil engineering.

- Traditionally, failure by seepage flow is perceived as resulting from a piping phenomenon, in which erosion of the soil initiates at the exit point of seepage,

and progressive backward erosion along its base results in the formation of a continuous passage or pipe. Piping is initiated by Darcy flow at the exit point where the flow is laminar. However, failures by seepage flow are very complex and may involve other different mechanisms. Unfortunately when a structure fails by seepage flow the evidence is often washed away with the structure.

- In soil seepage analysis, Darcy's law is generally applied, which suggests that the rate of flow, and hence seepage velocity, is linearly proportional to the hydraulic head and inversely proportional to the length of flow path. However, there are limits to the validity of Darcy's law in that it can only be applied to laminar flow. From a theoretical view, flow through defects in a structure does not adhere to Darcy's law. It has been suggested by some researchers that size of the opening may play a critical role.

- The literature review reveals that the mechanical role of the hydraulic gradient on failure is not well known. Seepage theory suggests that the critical hydraulic gradient at which fluidisation would occur is about one (based on Terzaghi's failure theory). However, recent literature has indicated that the actual critical hydraulic gradient can be different from that proposed in the theory. There are some instances of failure by seepage flow where it has occurred at hydraulic gradient below that of unity (about 1/3 to 1/5). It has been suggested by some researchers that distribution of internal stress may influence failure potential.

- A review of the literature on orifice flow indicates that the orifice flow equation is based on the Bernoulli principle, which is only applicable along streamlines of fluid flow. This however may not be relevant for the case of flow through defects in pipes or structures due to the interaction of particles with the orifice, and development of flow separation and cavitation at the orifice.

- Very limited research has been carried out on the interaction of soil particles with orifice flow, for example from a leaking pipe. What has been done suggests that soil has no effect on leakage rate because of fluidisation. It has been indicated that the possibility of soil fluidisation from a point source of leakage is very high. However, related literature (in other fields) suggests that the start of fluidisation from a fractured underground pipe requires an energy input greater than that necessary for the fluidisation itself. This has been referred to as the energy required to overcoming grain interlock and energy dissipation at the orifice.

- Theoretical models for estimating the hydraulic pressure in a packed bed of particulate material are already available in other scientific fields (e.g. the Ergun model), and which take into account the effect of vicious energy losses due to laminar flow and kinetic energy losses or inertial losses due to the onset of flow separation or turbulent flow in the bed. These, however, were developed on the hypothesis of uniform flow (i.e. parallel flow) in a columnar fluidised bed, and therefore may not be valid when the flow results from concentrated leakage where it is expected to be radial, as in the case of a leak through sheet wall pile interlocking, or from a buried pipe, as a result of hydraulic fracturing in an embankment dam, or through the seepage barrier of a dam.

- Experimental evidence available (in other scientific fields) indicates that an internal fluidised zone can form in a bed of granular material when fluid is injected into it. In most of these studies a jet of gas was used as the injection fluid.

- Surprisingly, very little is known about the phenomenon of internal fluidisation in the field of civil engineering, although it is seen be very important in designing, assessing, and monitoring of retaining structures where seepage flow is inevitable. Therefore research is required to develop

design methodologies based on a better understanding of the mechanisms involved with a localised flow.

- This study considers this problem and makes a contribution to this field by improving the understanding of internal fluidisation of granular materials. In order to achieve the purpose of this study it was required to design and develop experimental apparatus and techniques.

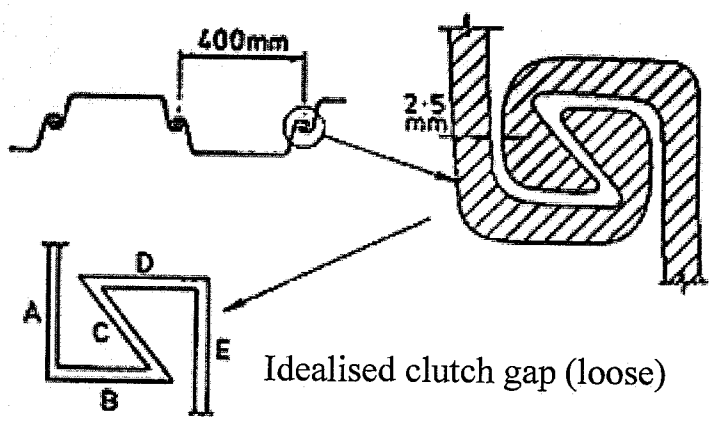

Figure 2.1: Type of sheet piling showing clutch details (Telling et al., 1978)

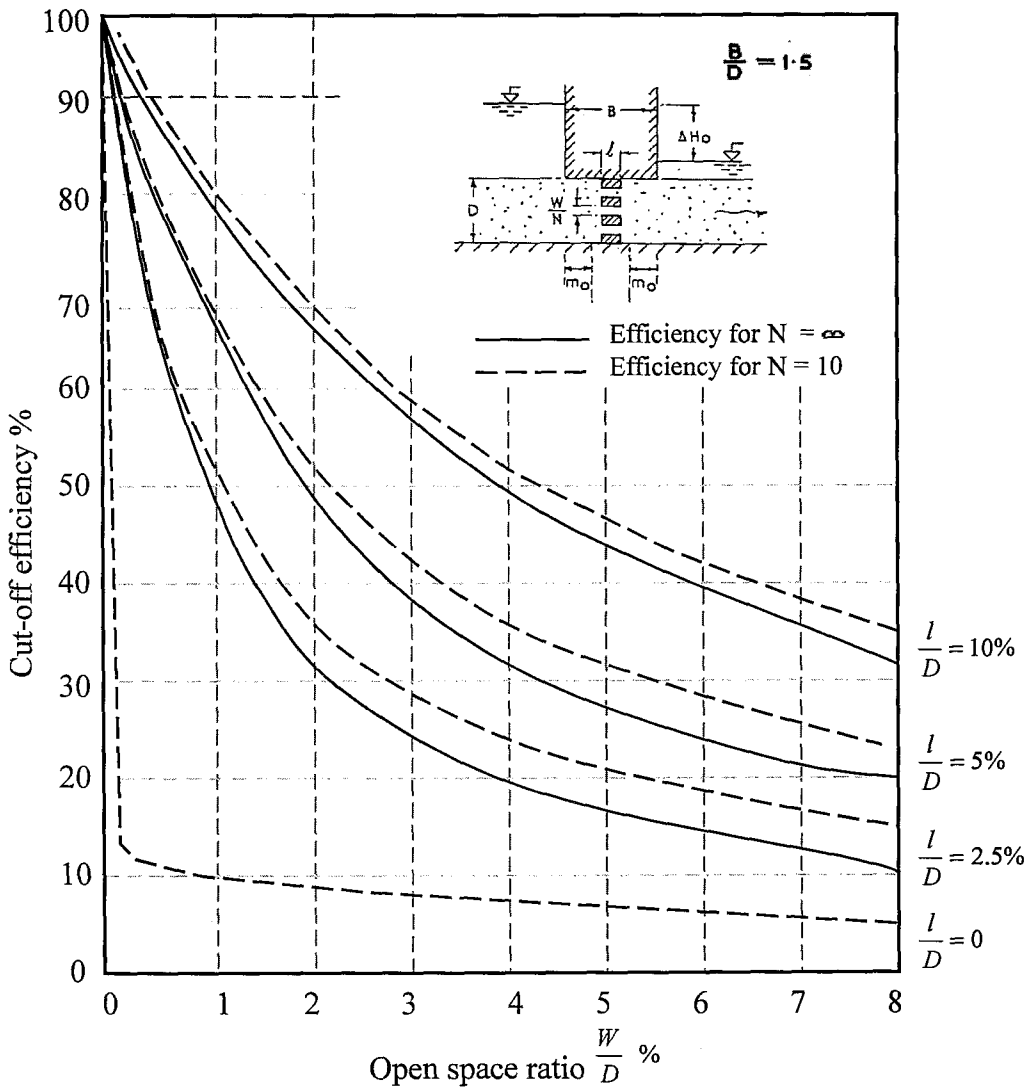

Figure 2.2: Cut-off efficiency versus open space ratio for imperfect cut-offs (Ambraseys, 1963).

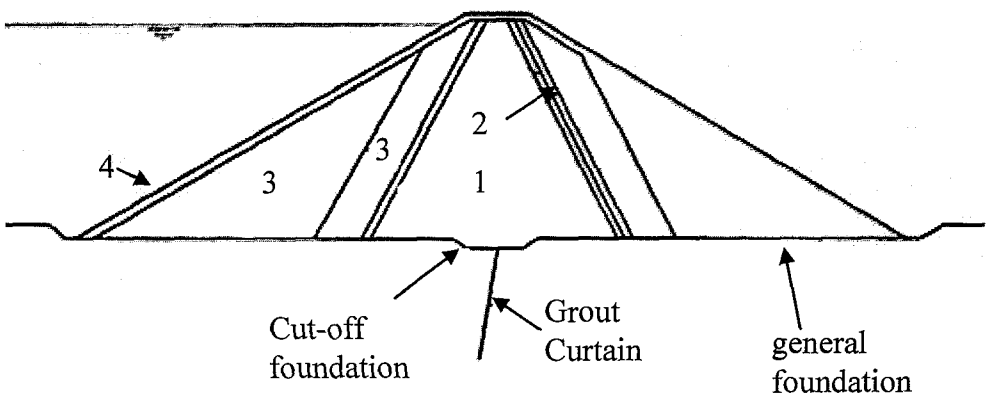

Figure 2.3: Example of a zoned embankment dam: (1) Core, (2) filter zones, (3) rockfill, (4) rip rap (Fell et al. 2005)

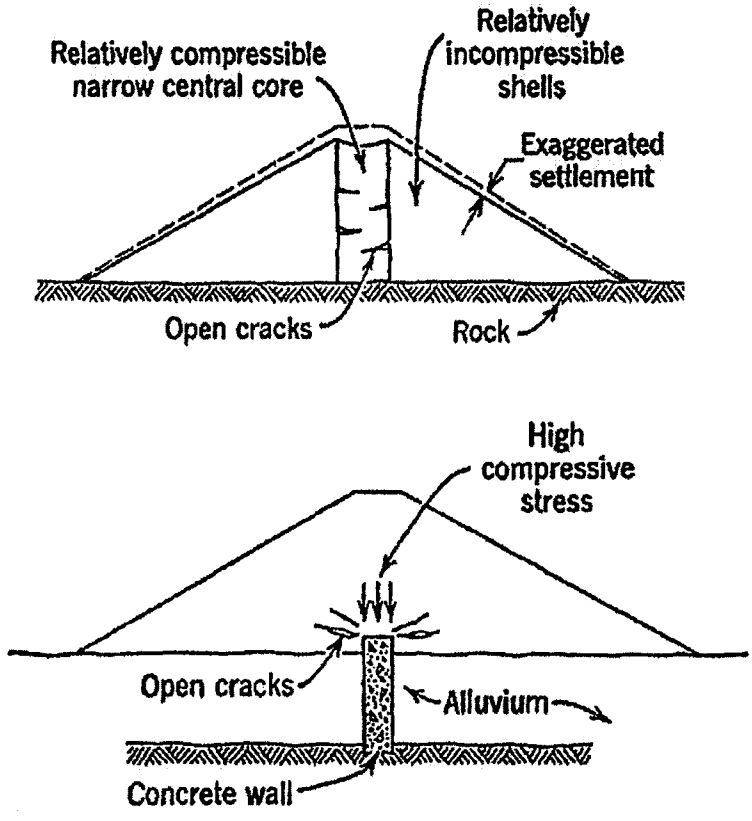

Figure 2.4: Typical internal differential settlement cracks in embankments (Sherard et al., 1963).

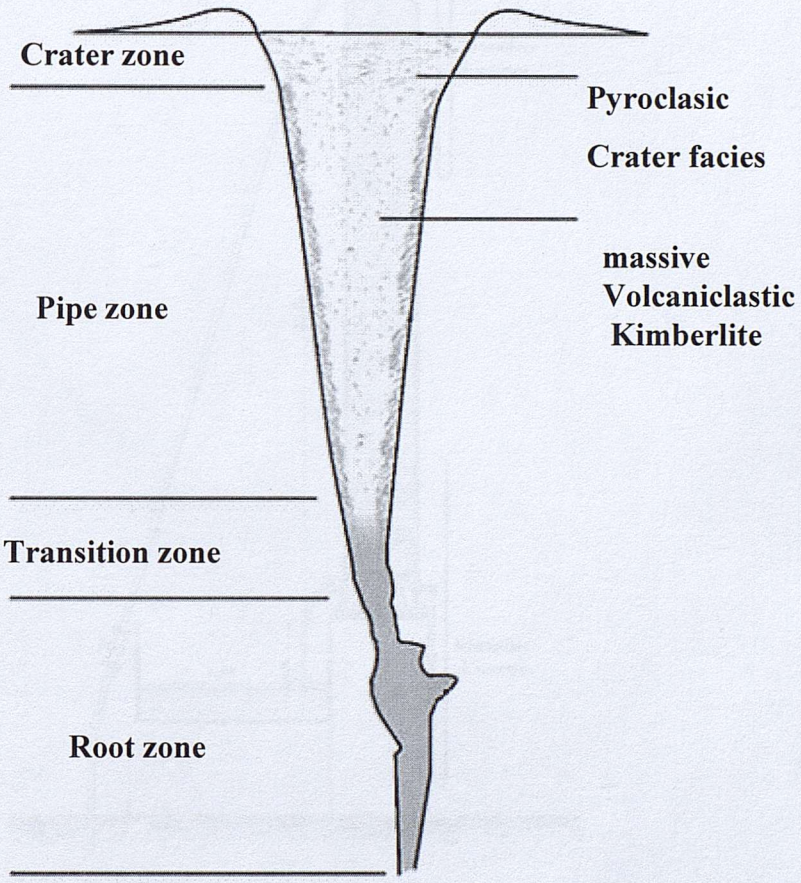

Figure 2.5: A model of Kimberlite pipe (taken from Walters et al., 2006, after Field and Scott Smith, 1999).

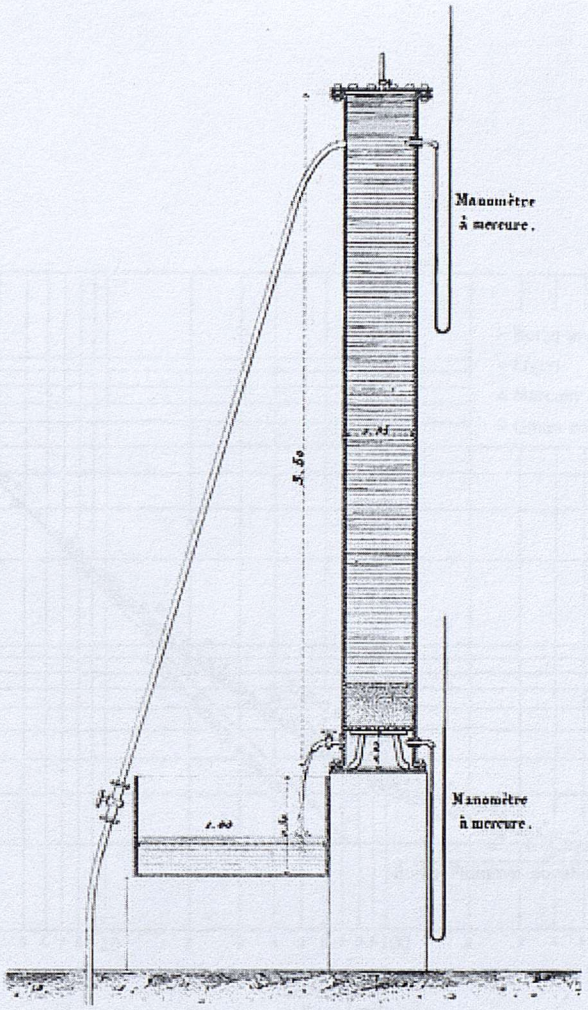

Figure 2.6: The original apparatus used by Darcy, 1856.

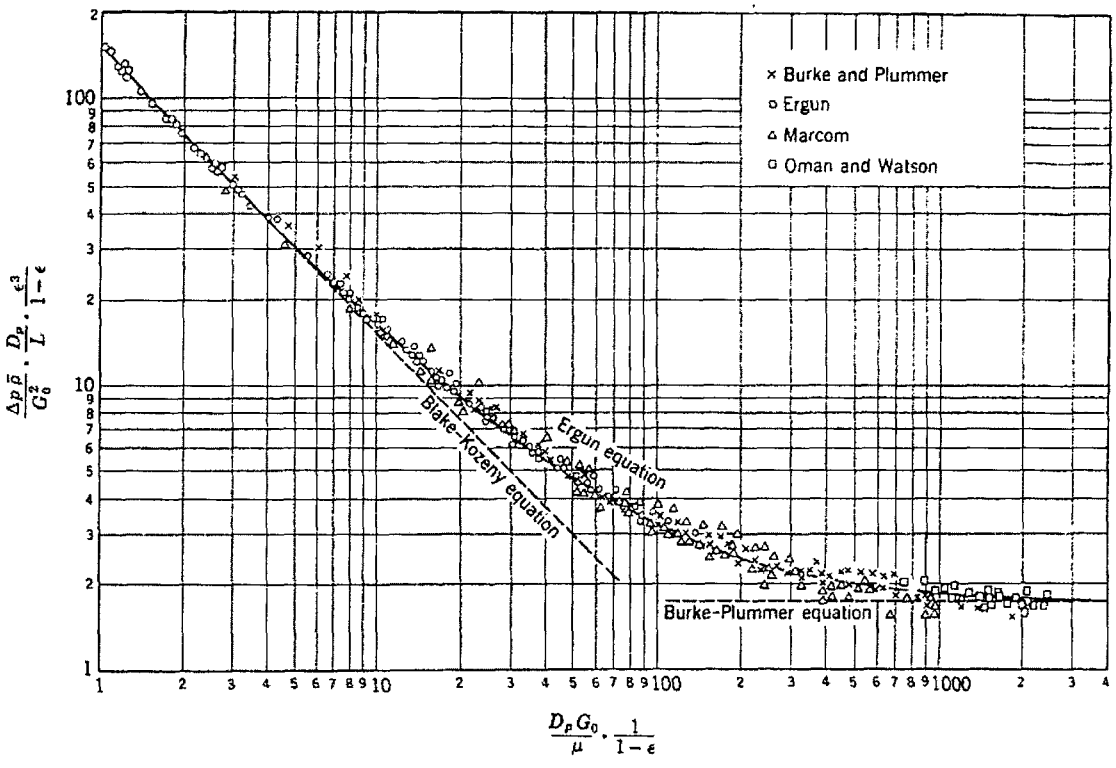

Figure 2.7: Normalised plot of the Ergun equation (after Ergun, 1952; Bird et al., 1960).

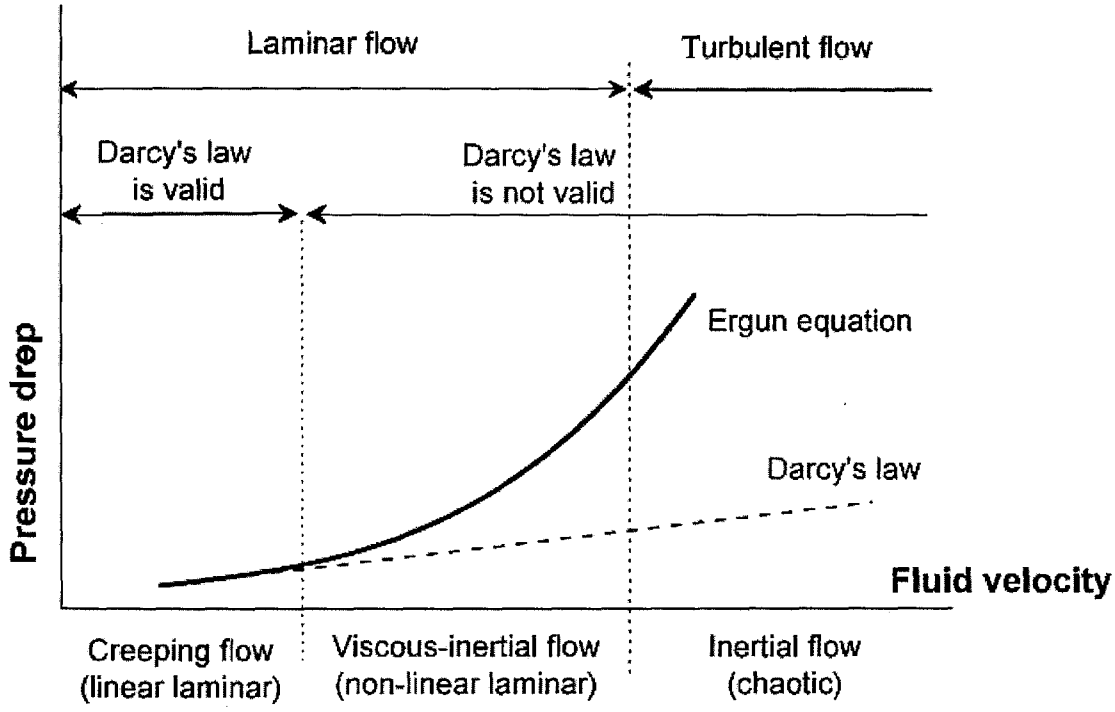

Figure 2.8: Characterization of different flow regimes in fixed beds by means of pressure drop-flow rate behaviour (After Hlushkou, Tallarek, 2006).

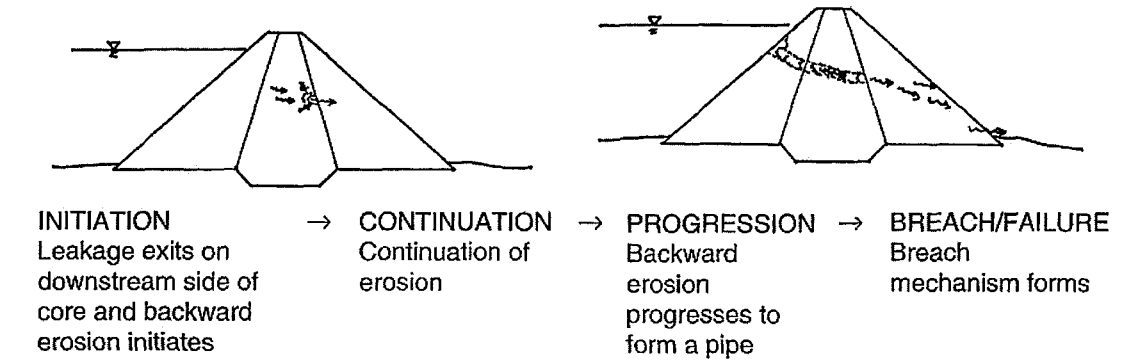

(a) Backward erosion piping

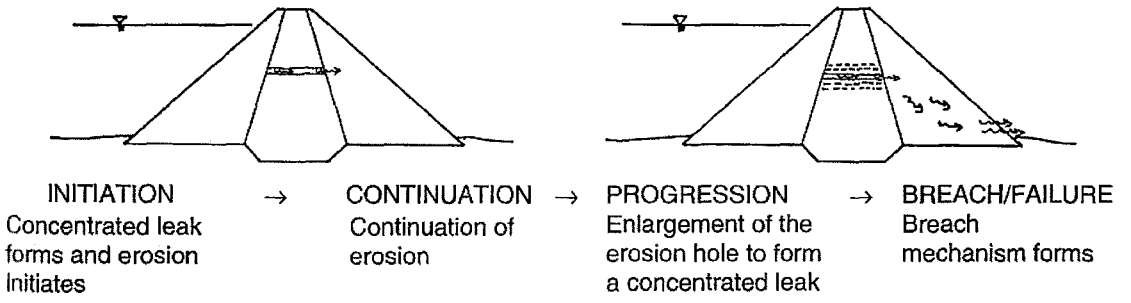

(b) Concentrated leak piping

Figure 2.9: Conceptual model for development of failure by piping in the embankment: (a) backwards erosion and (b) concentrated leak (Foster and Fell, 1999)

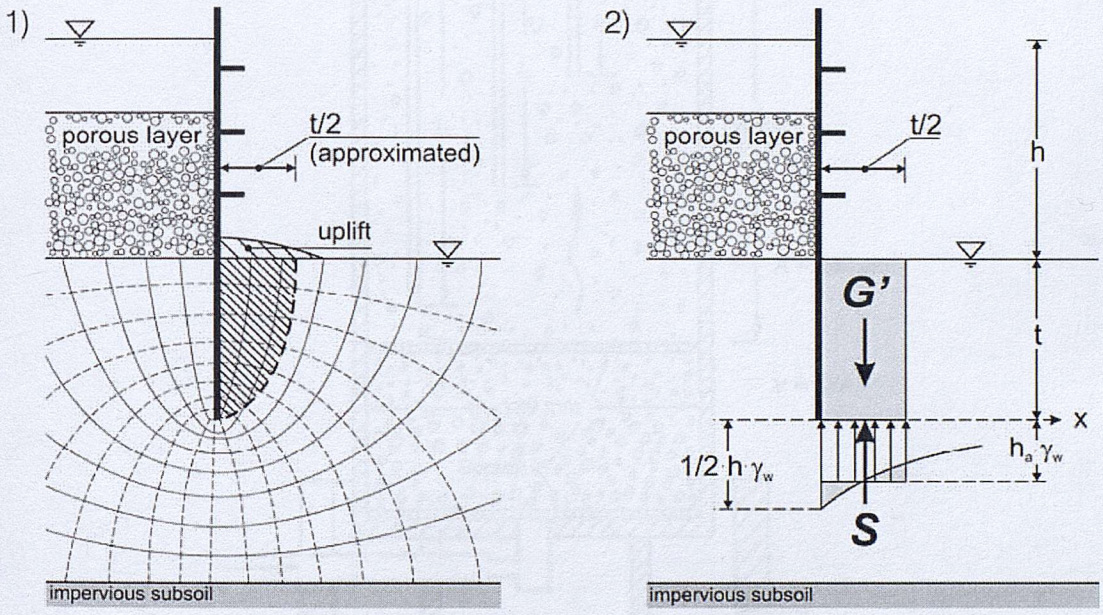

Figure 2.10: Failure by piping due to heave (Terzaghi and Peck, 1961)

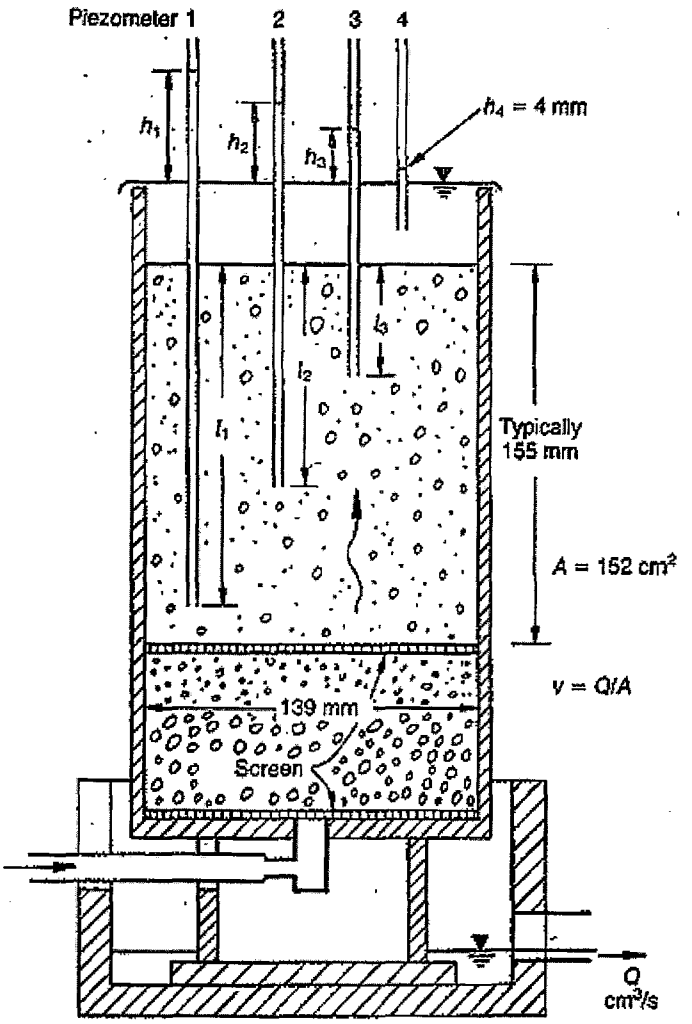

Figure 2.11 Experimental apparatus (Skempton and Brogan, 1994)

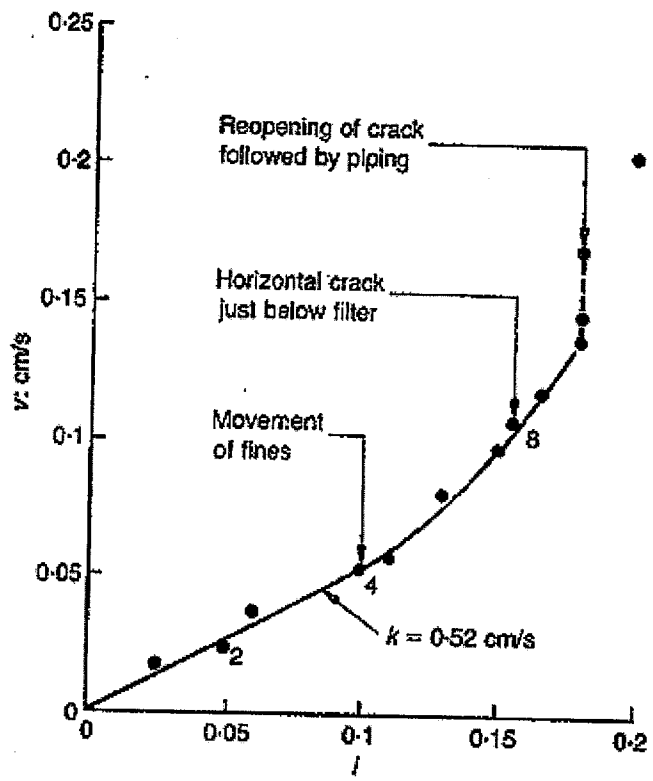

Figure 2.12: Failure by piping (Skempton and Brogan, 1994)

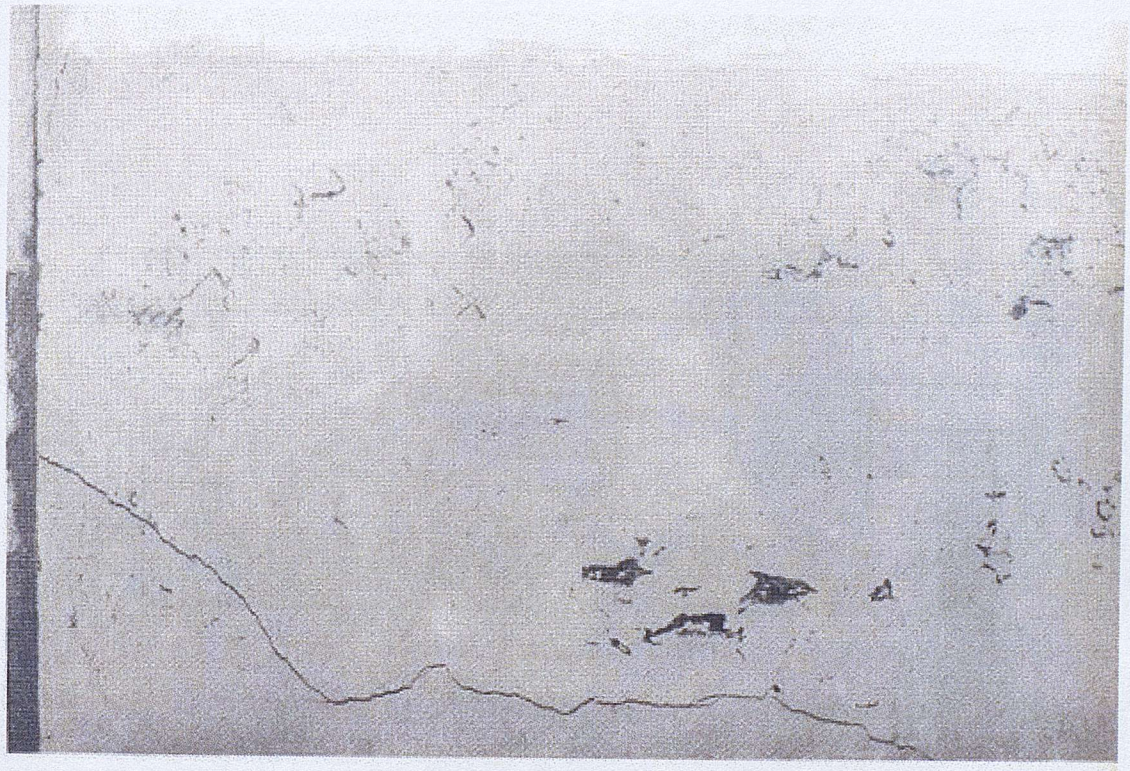

Figure 2.13: Crack development due to hydraulic fracture in clay (Bjerrum et al, 1972).

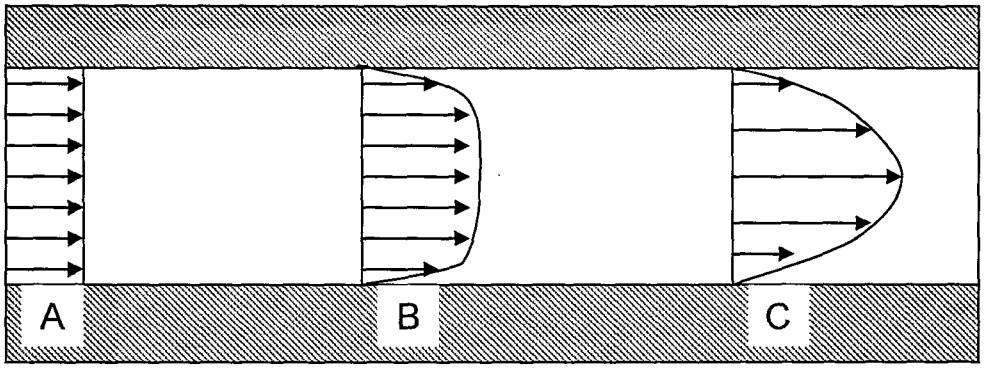

Figure 2.14: Development of laminar flow through a thick orifice plates.

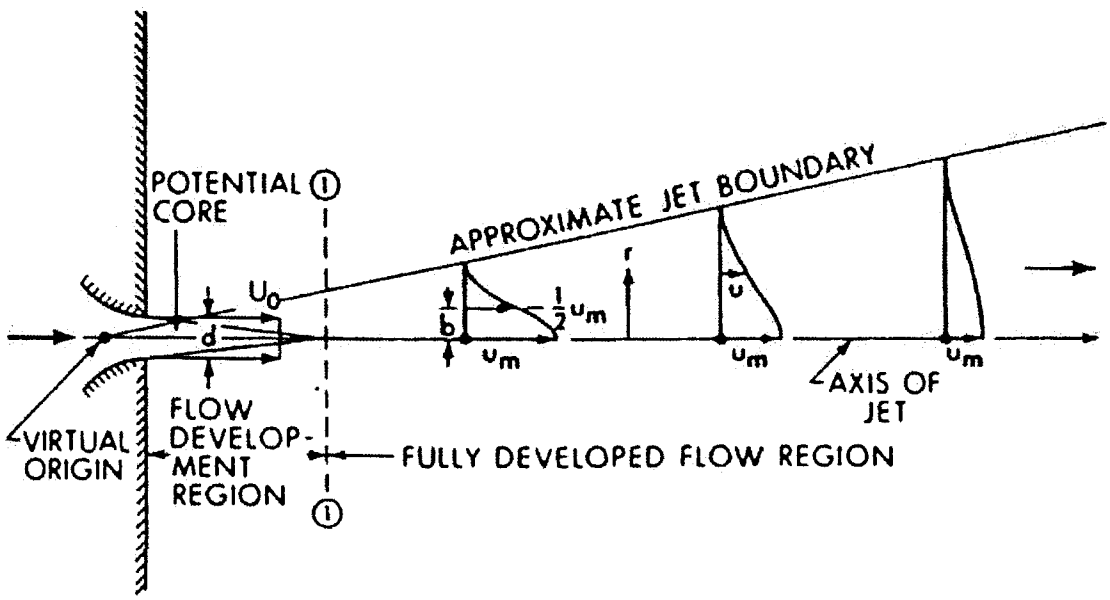

Figure 2.15: Schematic representation of jet diffusion (taken from Niven and Khalili after Rajaratnam, 1976).

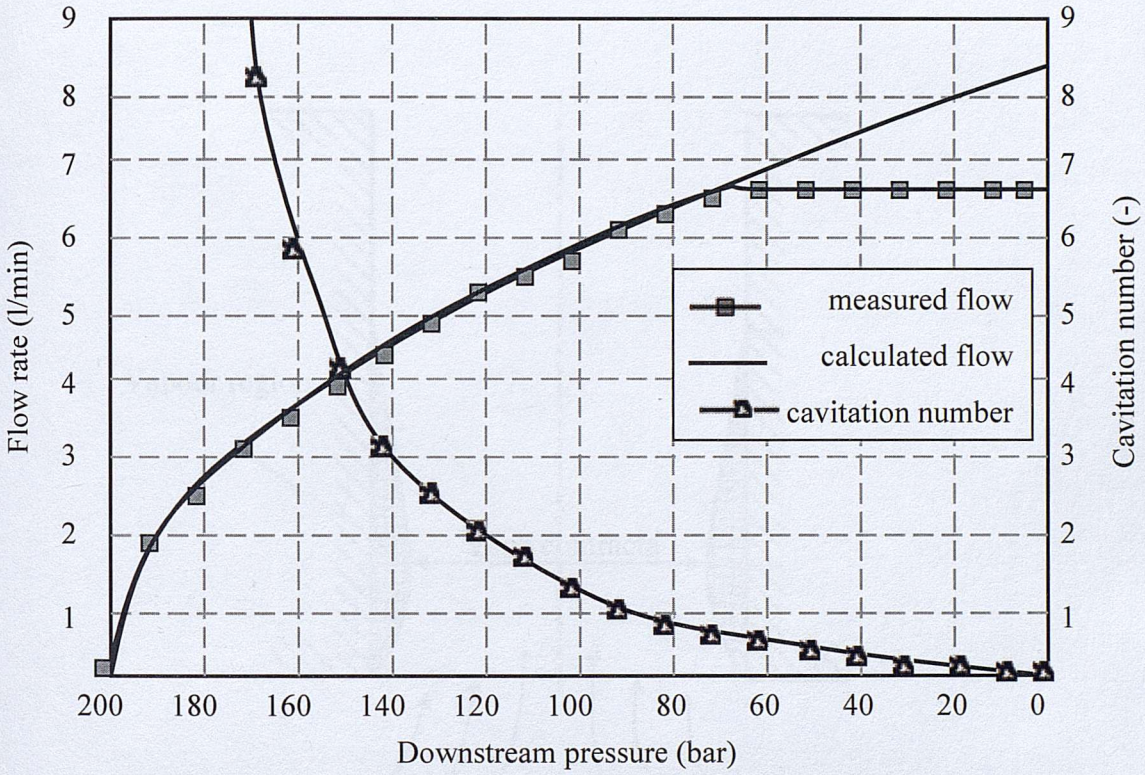

Figure 2.16: Flow rate and cavitation number against decreasing pressure down stream orifice (after Koivula, 2002).

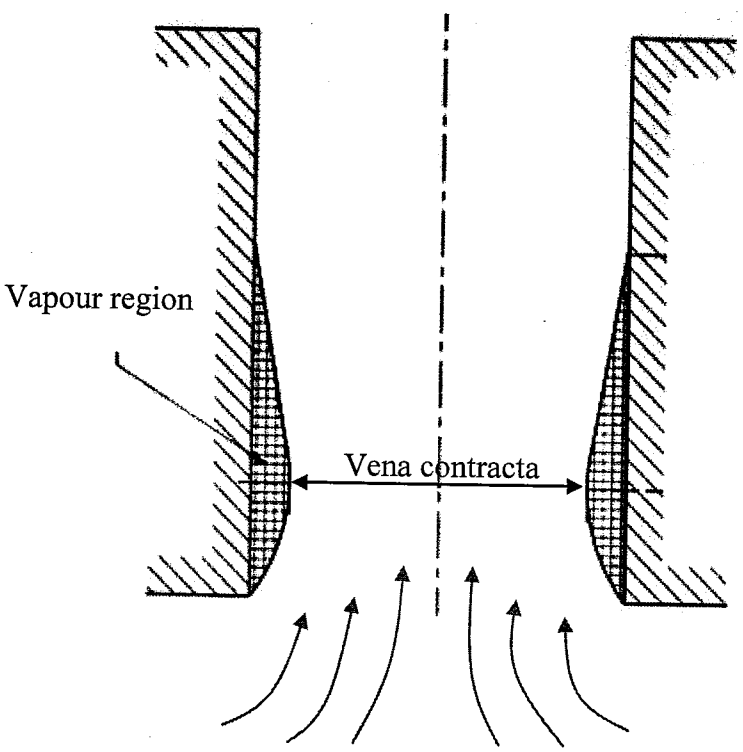

Figure 2.17: Flow separation in the orifice inlet corner and vena contracta formation (after Ramamurthi and Nandakumar, 1999).

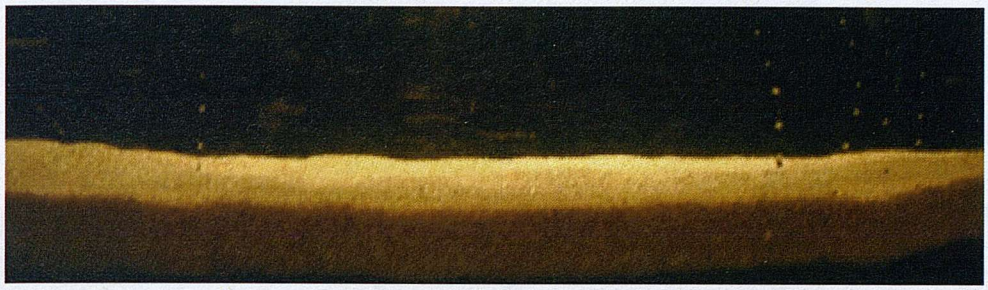

(a)

(b)

(c)

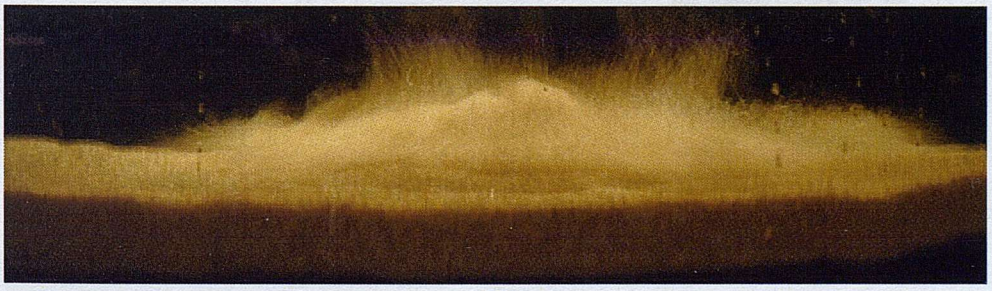

(d)

Figure 2.18: Elevation of the granular bed by water flow. The experimental parameters are water height=7 cm, sample height=10 cm, and flow rate (Q) = 80 l/h. the pictures are taken at (a) t=0 s, (b) t=1 s, (c) t=2 s, and (d) t= 3 s. the pictures show approximately 22 cm of cell's diameter (Zoueshtiagh and Merlen, (2007)).

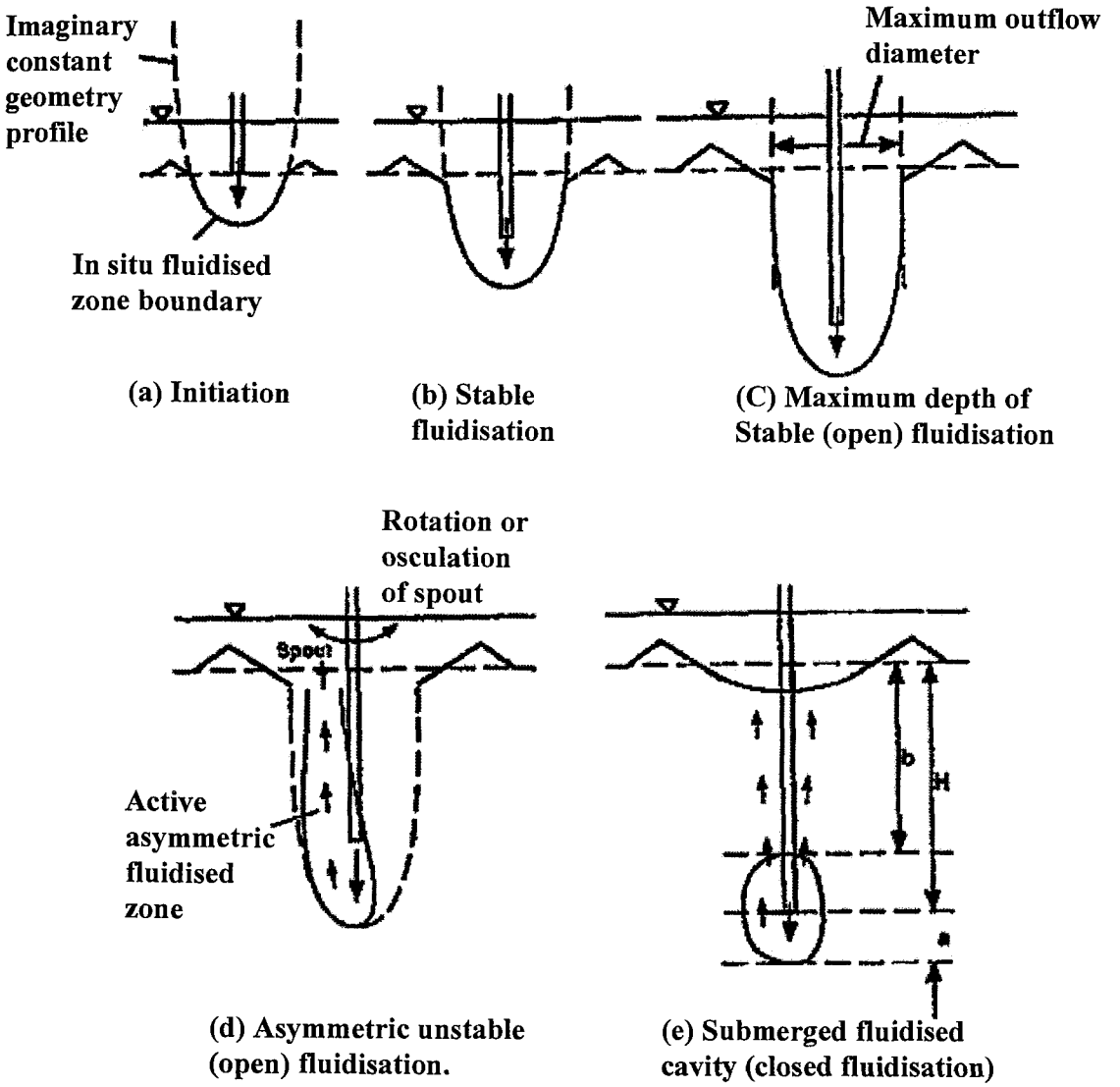

Figure 2.19: Schematic diagram of transition from stable in-situ fluidisation to cavity formation (Niven and Khalili, 1998).

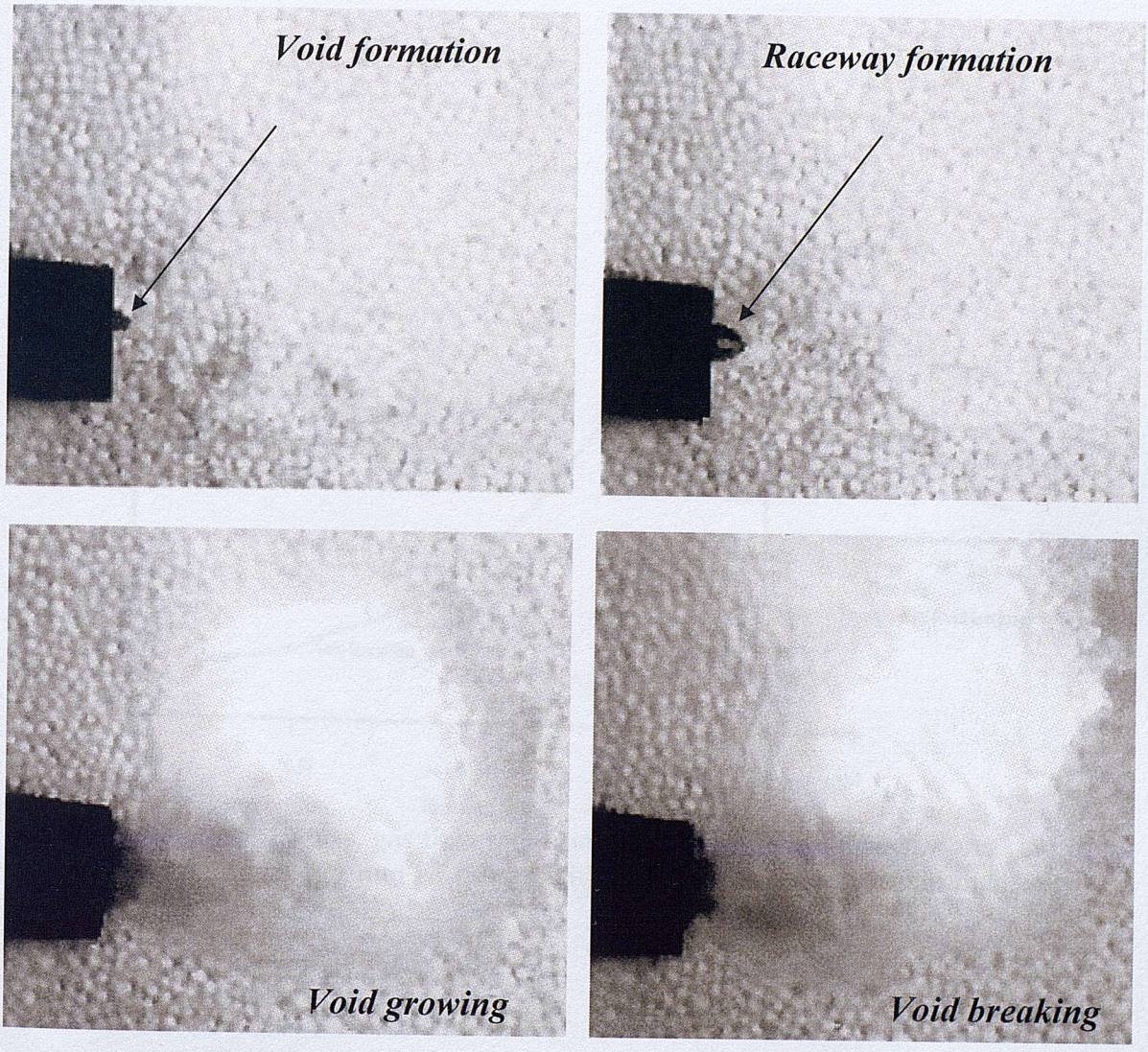

Figure 2.20: Photographs showing various stages of raceway development at different gas flow rates (Sastry et al., 2003).

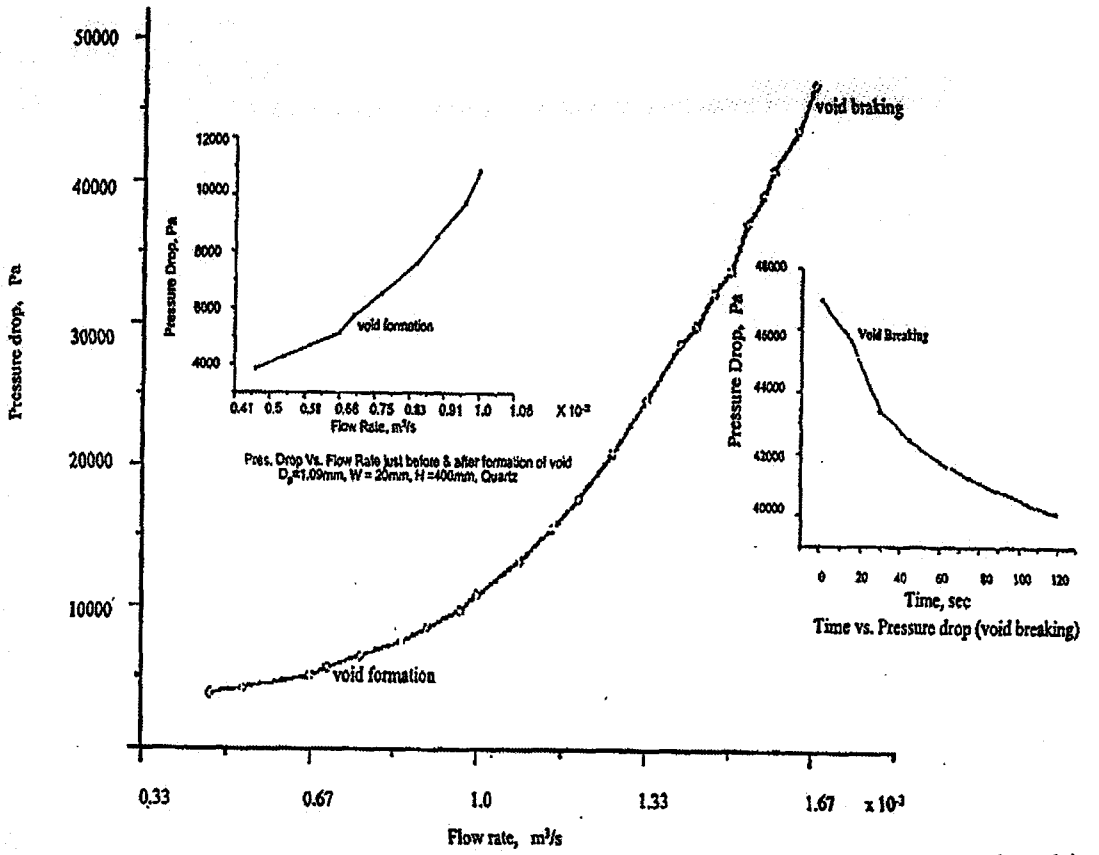

Figure 2.21: Pressure drop vs. gas flow rate from void formation to raceway breaking, bed height 400 mm of quartz with 1.09mm effective particle diameter (Sastry et al., 2003).

CHAPTER 3 EXPERIMENTAL DEVELOPMENT AND TECHNIQUES

3.0 Introduction

This chapter presents the methodology and experimental setup used in this research. It describes in detail the developed apparatus, and the techniques adopted to carry out the tests. It also provides descriptions of the materials used in the tests, and the sample preparation method. The test programmes and general procedures for the tests are also presented in this chapter, followed by the results of preliminary and final tests which are summarised at the end of the chapter.

3.1 Methodology

The literature review showed that there have been a significant number of failures by seepage flow resulting from localised leakage which would probably involve the mechanism of internal fluidisation of granular materials, and yet there is little known about it. Therefore the primary objective of this study was to improve the understanding of such mechanism. Further objectives were also to look at the effect of grains and orifice characteristics on the observed mechanisms. In order to accomplish the objectives of this study it was required to:

- Design and build an experimental apparatus to model a concentrated leakage.
- Develop techniques for monitoring the behaviour of a fluidised bed.
- Design a series of experiments to study the effect of grain characteristics on fluidisation.
- Design a series of experiments to study the effect of orifice characteristics on the observed mechanism.

The study was carried out by first setting up an experimental apparatus for preliminary tests, to ensure that procedures and equipment were optimised. Based on the outcomes of these results a final experimental setup was used for final tests.

3.2 Experimental Setup for preliminary tests

The experimental setup used for the preliminary tests in this research is shown schematically in Figure 3.1. It consisted of the following components:

- A machined aluminium box with an idealised opening crack,
- Seepage tank,
- Pump,
- Pressure gauge,
- Measuring cylinder,
- Tubes,
- A sight-tube panel assembly

3.2.1 The machined box

The machined aluminium box was designed with an idealised opening crack to model a localised (or concentrated) leakage such as might occur in the core of a dam, around a fractured buried pipe, due to cracks in sheet pile walls, and interlocking joints between sheet piles.

The box takes the dimensions: 330 mm length, 152 mm width, and 105 mm height. The crack was made of two aluminium plates put against each other on top of the machined box, as shown in Figure 3.2-3.3. One plate was held fixed by screws at one end and the other was connected to a nut, so that the crack opening could be controlled by the rotating of the nut using an Allen key. In this design, the maximum crack opening that could be produced was 3.6 mm. The assembly of the box was made watertight by means of an O-ring placed in a groove on the upper flange (Figure 3.4). Once the assembly of the box was completed it was then fitted inside a modified seepage tank, at its base, to fluidise the bed of grains (Figure 3.5). The box was fitted inside the tank using of silicon sealing compound.

3.2.2 The seepage tank

The tank used for conducting the experiments in this study was a seepage tank made of 20 mm thick Plexiglas. It measured 1060 mm x 550 mm x 153 mm, with steel

frames surrounding it. At one side of the tank two holes were drilled: with diameters of 32 mm and 10 mm. The former was for the inlet pipe that was used to supply the box with water; while the later was for the Allen key that was used to control the crack opening. These holes were made watertight by the use of an o-ring and silicon sealing compound.

3.2.3 Water supply and control system

A schematic diagram of the flow control system is shown in Figure 3.1. It consists of a plastic water tank, pump, control valves, inlet pipe, overflow tube, drainage chamber and outlet pipes.

The plastic water tank measured 600 mm length, 350 mm height, 380 mm width, and was filled with clean water, which was then pumped into the test tank through the inlet pipe.

The pump used in this study was manufactured by Karcher, model GP45. It was provided with a filter neck and window to allow water to be added, removing the air from the system (i.e. priming the pump). The maximum pressure head that could be supplied by the pump was 43 m of water and maximum flow rate was 3800 l/h. A 32 mm diameter inlet pipe connected into a flexible hose was used to connect between the machined box and the water tank.

Flow rate in the system was controlled using two valves (A and B, see Figure 3.1). One valve was used to divert the flow from the pump to the water tank when tests were conducted at low pressure (and low flow rate). The reason for this was to relieve the pump during this stage. The other valve was used to control the flow rate and/or pressure in the system through the crack. The water was then returned to the water tank from the overflow tube, flowing through the drainage chamber and then to the outlet pipe. Circulating the water into the storage tank avoided the problem of depressurising the system, which might otherwise cause air bubbles in the system, thus affecting the measured heads.

3.2.4 Instrumentation for preliminary tests

Pore water pressure measurement

Measurements of excess pore water pressure inside the fluidised bed were obtained using standpipes. Six holes, 3mm diameter each, were drilled through the back wall of the tank. These holes were constructed along the centreline of the orifice, at distances of 300, 220, 150, 102, 53, 10 mm above the orifice. A schematic layout of the hole locations is shown in Figure 3.6. Needles with 2 mm internal diameters were introduced through these holes. These were long enough (about 50mm each side) to provide a suitable point of attachment for the standpipes and reach to the centre line of the tank. In the current study, the dimensions of the tests sample prepared for the tests were 600 mm length, 300 mm height, and 146.6 mm width.

Before preparing the test sample in the tank, the needles inside it were covered with a screen (i.e. filter) in order to prevent grains from entering the pressure taps, thus avoiding blocking the taps which might otherwise affect the measured pressure in the bed.

Pore water pressure measurements were obtained by connecting each pressure tap with a vertically positioned water manometer, providing an accuracy of ±1 mm of water column.

Pressure measurement

Pressure upstream of the orifice was measured using a Bourdon pressure gauge, with a range of 4 bars and accuracy of 0.1bar. The typical calibration results for this gauge are presented in Appendix C, Figure C-1.

Flow rate measurement

Measurement of flow rate in the preliminary experimental setup was obtained by intercepting the out flow and collecting in a graduated cylinder for a specific time interval.

3.3 Monitoring behaviour of fluidised beds using Particle Image Velocimetry (PIV)

Various techniques have been employed to study the behaviour of fluidised beds, and most of these are published in the field of chemical engineering (e.g. Caicedo et al., 2003; Shen et al., 2004; and Halvorsen, 2005). The techniques may be classified into two categories depending on the nature of the sensors contacting the fluidised bed phase: 'intrusive' (e.g. optic fibre) or 'non-intrusive' (e.g. video, photographic). According to Caicedo et al. (2003) the use of intrusive techniques involves a greater source of error as a result of interference.

Nowadays, non-intrusive techniques offer good visual observation and supply a great quantity of information. As a result of the development in photographic technology, a recent technique: Particle Image Velocimetry (PIV) emerged, and is being widely used to study the behaviour of the fluidised beds and the movement of the particles in the beds.

Particle Image Velocimetry is a non-intrusive velocity measuring technique that was initially developed in the field of experimental fluid mechanics (Adrian, 1991). The principle behind PIV is the image pattern matching technique (i.e. cross correlation). The technique involves seeding the flow with tracer particles, illuminating the area of interest by a source of light (e.g. a laser sheet), and capturing a series of images of that area at known time intervals using a camera. The resulting images contain image pairs of each seed particle, which are then analysed using processing image software.

The technique has seen a steady increase and acceptance in a variety of disciplines. In the field of chemical engineering PIV has been widely applied to study the behaviour of fluidised beds (Santana et al., 2005; Busciglio et al., 2007; Laverman et al., 2007; Muller et al., 2007). In two dimensional gas fluidised beds studies, Santana et al. (2005) used PIV to study the initial particle movement of bubble eruption, while Muller et al. (2007) used PIV to study the motion of a single bubble as it approached and then broke through the top surface of the fluidised bed. It has also been applied in geotechnical engineering for measuring soil deformation (White, 2002; White et al., 2003). In granular flow it has been adapted to study particle movement. Lueptow, et al. (2000) used PIV for measuring particle displacement and

velocity field in granular flow. In their study, they used spherical solid glass beads with a nominal diameter of $200\,\mu m$. The images texture in their experiments was improved by using light and dark particles.

Several PIV codes are available in the literature, which use a cross-correlation function to compute the particle displacements. These include; MatPIV, UraPIV, VidPIV and Insight 6.0. The first two of these were developed using Matlab and are open sources for educational purposes. The second two codes are commercially distributed.

Shavit et al. (2006) used the above four PIV codes to evaluate the performance of the intensity capping (i.e. a method to improve cross-correlation PIV results which imposes a user-specified upper limit to the grayscale intensity of the images). In all the PIV analysis, interrogation windows 32x32 pixels with 50% overlap were used; producing velocity vectors every 16 pixels. He also noted that when using UraPIV, VidPIV, and Insight, only a single cross-correlation pass (iteration) was implemented; while a multiple-pass algorithm was performed when using MatPIV. In the first pass, an interrogation window of 64x64 pixels was used to calculate the particles displacement. Then the displacements results were used to find the centre of the interrogation window in the second pass. The other two passes were used to generate the final velocity using a 32×32 pixel window.

3.4 Particle Image Velocimetry (PIV) setup

The Particle Image Velocimetry (PIV) technique was adopted in this study to monitor the behaviour of grain fluidisation due to its advantages over others methods as discussed above. The setup for PIV is shown schematically in Figure 3.7. It consists of a light source, camera, a board with gridlines, and image processing software to track the movement of the particles.

Observations of the fluidisation were made on a 2D Fluidised bed with a field view of 600 mm length, 300 mm height, representing the actual size of the sample prepared for the tests. The front wall of the seepage tank was made of 20 mm thick clear Perspex, allowing observations of the fluidised zone. However, the results of the preliminary tests using the developed apparatus showed that when grains became

fluidised they moved in a downward direction, in a way that did not represent the expected motion of the particles. The reason for this was attributed to design limitation of the crack in the machined box. It is found that, when the machined box was fitted inside the seepage tank, the crack ends were about 8 mm away from the front and back walls of the tank (the thickness of the aluminium sheet that was used to make the box) see Figure 3.4. In order to overcome this problem, an 8 mm thick glass sheet (with 600 mm length and 300 mm height) was fitted inside and attached to the front wall of the tank. The movement of the particles in the fluidised bed near the wall then represented the actual motions of the particles.

In order to provide homogenous illumination of the fluidised bed; two 100 W lamps were installed, each placed at an angle of 45◦ as shown in Figure 3.5.

The behaviour of the fluidised bed was monitored using a Sony (HDR-SR11) digital video camera. The camera had a resolution of 1920× 1080 pixels and operated at 25 images per second. It was placed at a distance of 0.5 m from the front wall of the tank with the vision field of 600 mm × 300 mm.

During each experiment video recordings of the fluidisation process have been taken, and then analysed and converted to frames using PMB (Picture Motion Browser) software (supplied with the camera).

Once the images of the fluidised zone had been produced, they were analysed using the PIV technique. A computer code MatPIV was adopted in this study due to its advantages over the other available codes as discussed above. The code was written in MATLAB language by Sveen (2004). The principle behind PIV is the use of a cross correlation function to estimate particle movement, Figure 3.8.

For PIV analysis, after capturing two images of the area of interest at a known time interval, the area of the first image is divided into small regions (i.e. interrogation windows). The size of the interrogation window was iteratively reduced from 64 × 64 to 16 × 16 pixels, using four iterations. The displacement vector of each sub-window was then identified by extracting a search zone from the second image and cross correlating the two images. A peak in the correlation function indicated that the two images overlay each other (indicating the best area of match between the two

images). The correlation offset is equal to the displacement vector. In this manner, with a known time interval, and a local displacement, a velocity profile of the particle motion was obtained. In order to remove the outliers vectors of the velocity data, a Signal-To-Noise ratio (s/n) filter with a ratio of 1.3 (as suggested by Keane and Adrian, 1992), and global and local mean filters were applied.

3.5 Materials tested for preliminary tests

The tests were carried out on two different materials: Silica sand and Leighton Buzzard sand-fraction A (LBS-A). Electron micrographs of these materials are in Figure 3.9a and 3.9b shows that they are sub-rounded and slightly elongated and flattened. The particle size distributions of the tested materials are shown in Figure 3.10, showing that the silica sand has nominal particle diameters of 0.9 mm, while for the LBS-A this is 1.6 mm. Table 3.1 presents other properties of the materials (i.e. maximum and minimum dry density, Gs).

3.6 Characterisation of particle form

Particle form, sometimes termed 'sphericity', is a measure of the overall shape of the particle. It describes how closely a particle resembles a sphere. Wadell (1932), the first to suggest the term true sphericity, ψ , which was originally defined as the ratio of the surface area of a particle to that of a sphere of the same volume. As a result of the difficulty in measuring the surface area of a particle, Wadell (1933) suggested the use of an operational sphericity, ψ_o, which is the cubic root of the ratio of the volume of a particle to the volume of the circumscribing sphere.

Later Krumbein (1941) suggested a particle to be a triaxial ellipsoid having three diameters: namely, the largest, L, the intermediate, I, and the shortest, S, and proposed Krumbein's operational sphericity, ψ_o:

$$\psi_o = \sqrt[3]{\frac{(\pi/6)\ L \times I \times S}{(\pi/6)\ L^3}} = \sqrt[3]{\frac{I \times S}{L^2}} \qquad 3.1$$

Corey (1949) suggested that a particle generally falls with its largest projected area normal to the direction of flow, and proposed another particle form descriptor named

Corey's shape factor. Corey combined the two flatness ratios S/L and S/I to form the shape factor, which is the ratio of the cross section of the maximum inscribed sphere to the maximum projected area of the particles.

$$CSF = \sqrt{\frac{S}{L} \times \frac{S}{I}} = \frac{S}{\sqrt{L \times I}} \qquad 3.2$$

Corey's shape factor, CSF, is widely used in hydraulic engineering to express the effect of particle shape on the settling velocity (Blatt et al., 1980). CSF is a good measure of the flatness of the particle which has a significant effect on its falling velocity.

Sneed and Flok (1958) argued that Wadell's sphericity does not correctly express the dynamic behaviour of particles in fluid. They believed that the particle has a tendency to orient itself with the maximum projected area normal to the flow. Based on this they proposed another form descriptor i.e. maximum projection sphericity, ψ_p which is the cubic root of the ratio of the projected area of the inscribing sphere to the maximum projected area of the particle:

$$\Psi_p = \sqrt[3]{\frac{S^2}{L \times I}} \qquad 3.3$$

According to Sneed and Folk, (1958) and Krumbein and Sloss, (1963) the maximum projected sphericity shows a better linear correlation with the observed settling velocity than does Wadell's operational sphericity. This definition of sphericity looks similar to that of Corey's shape factor (equation 3.2).

More recently, Clayton et al. (2009) argued that the above methods cannot be easily applied to small particles or large numbers of variable particles, because it difficult and time consuming to obtain the three-orthogonal dimensions, especially the smallest dimension, S. In order to overcome this problem, they assumed the particles to be scalene ellipsoids with the equivalent volumes. The smallest dimension of the particles can then be estimated indirectly by determining the average volume of the particles. This new form descriptor is named "scalene equivalent ellipsoid sphericity" (SEES) and is defined as the ratio of the smallest to largest particle dimensions.

Particle form estimation

The method used to characterise the form of granular materials used in the tests was Corey's shape factor (CSF) due to its advantages over other methods. Corey's shape factor, defined as $S/\sqrt{L \times I}$, requires three dimensions; the largest, L, intermediate, I, and the smallest dimension, S,. These three dimensions were measured using an image analysis techniques combined with the volume method proposed by Clayton et al. (2009). The volume method is based on a volumetric equivalent scalene ellipsoid (i.e. assuming that the sand particles are scalene ellipsoids with the equivalent volumes). When non-spherical particles are dropped onto a microscopic slide, they normally reset on their largest surface with the short axis nearly vertical (Wadell, 1932). Clayton et al. (2009) assumed that the largest (L) and intermediate (I) dimension of sand particles are the circumscribed circle and the largest inscribed circle, respectively (Figure 3.11). From digital images of the granular materials the largest (L) and intermediate (I) dimensions were measured using Image-Pro plus software version 6.0, and were averaged. The smallest dimension, S, was then obtained indirectly using the following equation:

$$V = \frac{\pi}{6} L\ I\ S \qquad 3.4$$

Where V is the average volume of particles, which can be determined relatively easy. It can be obtained based on the weight of a specimen, the specific gravity, and the number of particles in the specimen. The number of particles in the specimen can be can be determined manually or automatically using image analysis software.

In this study, the largest (L), intermediate (I) and smallest (S) dimensions of a particle for the test materials were measured and presented in Table 3.2. From these data, Corey's shape factor (CSF) of the tested materials was calculated. Other sphericity descriptors of the materials include scalene equivalent ellipsoid sphericity, SEES, (Clayton et al., 2009) and operational sphericity, ψ_o, (Wadell, 1933) were also calculated and presented in Table 3.2.

3.7 Specimen reconstitution

The objective of the reconstitution technique was to produce uniform and saturated specimens. This was achieved by raining the soil through a funnel into the seepage tank half filled with water. The seepage tank was reduced in size to form a sample with dimensions of 600 mm length, 300 mm height and 146.6mm width, see Figure 3.1.

The soil specimen was prepared by pouring a known weight of dry sand from a funnel with a 16 mm diameter nozzle into the tank. The height of fall from the funnel was kept constant at 20 mm above the water level in the tank. Raining the soil particles into a depth of water minimised the amount of air between the particles, which might otherwise have occluded voids and reduced permeability in places, thus affecting measured heads.

Water pluviation tends to give a lower relative density than air pluviation because the soil particles have a slower falling velocity, and therefore lower impact energy. Thus, in order to achieve higher densities, compaction energy was applied into the specimen by gently tapping the base of the mould in a symmetrical pattern by means of rammer. Table 3.3 presents the initial conditions of the specimens in preliminary test series.

3.8 Test programme and procedures for preliminary tests

The purpose of carrying out preliminary tests using the developed apparatus was to:

- Ensure that the apparatus was working properly, and that there was no unwanted leakage.
- Develop a connection between the set up for the Particle Image Velocimetery (PIV) and the testing apparatus, and ensure that they were working properly.
- Establish a likely range of the controlled parameters to assist in selection of instrumentation for final tests.
- Establish initial understanding of the mechanism of internal fluidisation.

Therefore, three experiments were conducted during the preliminary tests. Table 3.4 shows the test programme of these tests. Two experiments were carried out on silica sand (d_{50}=0.9 mm) at two different orifice openings; namely 0.336 mm and 0.234mm, while the third one was conducted on LBS-A (d_{50}=1.6 mm) at an orifice opening of 0.234 mm. For all these experiment the bed height was constant at 300 mm.

Test procedure

Prior to commencing the test using the developed apparatus some arrangement need to be considered.

1- First, the crack opening in the machined box located at the bottom of the tank was adjusted to the required size opening using Allen key. It was then measured precisely using a set of flat feeler gauges. Due to design limitations of the machined box, the crack opening was not perfectly parallel. A number of measurements, therefore, were taken at different point along the crack and then an average value was calculated. Two orifice sizes were used in the preliminary experimental tests - 0.234 mm and 0.336 mm.

2- Once the size of the orifice was adjusted and measured, the system was primed. A water supply hose was used to fill the water tank with water. The pump was then primed by adding water through its supply window. After this, water was pumped from the water tank and was then allowed to flow through the orifice, by turning on valve A, into the test tank. Once the test tank was half filled with water (i.e. about 150 mm above the orifice), valve A was turned off, as was the pump.

3- The specimen was the then prepared in the test tank as described in (section 3.4), by pouring a known weight of dry sand through a funnel. Once the sample was prepared its density was then determined. The initial conditions of the specimens tested in this preliminary testing program are summarised in Table 3.3. At this point it worth noting that all the specimens were tested under fully saturated conditions and at quite high initial relative densities (>75%). After preparation, the specimen was allowed to stand for about 24 hour to ensure saturation.

4- Once the sample was prepared and was ready for the test, the sight-tubes were scanned for hydrostatic water level. Six tubes were scanned which were connected into the probes along the bed height.

5- Finally, the setup for the Particle Image Velocimetry technique was arranged as described in section 3.2.3.

By completing these arrangements the apparatus was ready for the test.

The preliminary tests were conducted at controlled pressure upstream of the injection point (which ranged between 10-250 kPa). During the test, water was pumped vertically through the orifice located at the bottom of the tank. Initially low pressures (i.e. 10 kPa) (and thus small flow rates) were applied, and these were then increased in increments until fluidisation was observed or the capacity of the apparatus was reached. At each increment in pressure, excess pore water pressures, and flow rates were recorded. They were allowed to stabilise for some time (five minutes was found to be sufficient length of time to reach this stage). Readings of excess pore water pressure in the bed of grain were measured from the sight tubes, while pressure in the pipe was recorded from the pressure gauge. The flow rate was obtained by intercepting the out flow and collecting water in a graduated cylinder for a specific time interval. At each increase in pressure the behaviour of the bed was monitored using a video camera, and the images produced were analysed using the Particle Image Velocimetry technique described in section 3.4. The same procedures were repeated at each increase in pressure.

3.9 Results of preliminary tests

Experiment A

Experiment A was conducted by injecting the flow into a 300 mm bed of silica sand (d_{50}=0.9 mm) through a crack opening of 0.336 mm. Figure 3.12 shows profile of excess pore water pressure (i.e. above hydrostatic for the upper water level) along the bed height as a function of pressure in the orifice. The line for a hydraulic gradient of unity is also plotted on the graph. It can be seen from the figure that increasing pressure behind the orifice, and thus the rate of flow through it, leads to progressive build up of the excess pore water pressure in the bed of grains, with a maximum value in the vicinity of the injection point. For instance, at a distance of 10 mm away from the injection point in the vertical direction, the excess pore pressure was about 0.85 kPa at a pressure in the orifice of 10 kPa, corresponding to a rate of flow of 135 l/h. This was then increased to 1.5 kPa by increasing the pressure in the orifice to 20 kPa, the point at which flow rate increased to 235 l/h. Following a further increase in the pressure in the orifice to about 27 kPa, the rate of flow increased to 338 l/h while the excess pore pressure reached to a value of 2.2 kPa.

The hydraulic gradient $(\Delta h/\Delta l)$ in the vicinity of the orifice is greater than unity, while further away from the injection point, in about 50 mm from it in the vertical direction, the excess pore pressure decreases linearly with height until it becomes atmospheric at the bed surface. This is only limited to low pressures in the orifice, and thus small flow ranges i.e. 10 kPa corresponding to flow rate of 135 l/h. However, at higher pressures in the orifice i.e. 60 kPa, corresponding to a flow rate of 1042 l/h, the linearity in the excess pore pressure with height was not seen until 150 mm away from the injection point Figure 3.12.

For the same set of data Figure 3.12, following a further increase in the pressure in the orifice to 60 kPa the flow rate increased to 1042.6 l/h. At this point, the excess pore water pressure at the injection point peaked at a value of 7.3 kPa, the point at which the average hydraulic gradient was 2.37. At this point, the hydraulic gradient in the vicinity of the injection point (within the 50 mm of it) was much higher with a value of 8.9; while in the upper 150 mm of the sample was about 1.02.

Beyond this point, a further increase in the pressure in the orifice to 83kPa led to an increase in the rate of flow to a value of 1177 l/h. However, this was associated with an abrupt drop in the pore pressure at the injection point. At this point the pore pressure dropped to a value of 4 kPa. A further drop in the pore pressure to a value of 3.7 kPa occurred when the pressure upstream of the orifice increased to 130 kPa, corresponding to a flow rate of 1233 l/h. At this point the pore pressure readings within the range of 50 mm from the injection point, in the vertical direction, were almost the same, with an average value of 3.7 kPa Figure 3.12.

When the pressure in the orifice increased to 256 kPa, unexpectedly, the rate of flow remained unchanged at a value of 1233 l/h, while the excess pore pressure readings within the 100 mm from the injecting point were steady with an average value of about 2.9 kPa.

Observation of the internally fluidised zone

Once the excess pore water pressure at the injection point peaked at 7.3 kPa, corresponding to flow rate of 1042 l/h, the particles above the injection point were lifted in an upward direction. This was followed by an abrupt drop in the excess pore water pressure at the injection point to a value of about 4 kPa, corresponding to a flow rate of 1177 *l/h*. Figure 3.13 shows a photograph of the bed level before and after the uplift mechanism (i.e. onset of fluidisation). Figure 3.14 and 3.15 shows a contour of the particles movement using the Particle Image Velocimetery (PIV) technique.

Immediately after the uplift of the particles above the orifice had occurred, the particles at the bottom of the bed (i.e. in the vicinity of the orifice) started to fluidise, forming an internally fluidised zone (see Figure 3.16). Inside this zone the particles move with the jet of water (i.e. the particles were picked up by the jet of water and carried out to the top of the jet in the centre and then slowly moved down on the sides), whilst those outside the zone remained fixed in the bed.

After the formation of the internally fluidised zone, it was observed that at each increase in the pressure in the orifice, and thus the rate of flow, the faster the movement of the particles inside the fluidised zone was associated with a slight

enlargement in its size. The growth of the fluidised zone extended from the bottom (i.e. at the orifice) to the top, and the excess pore water pressure in the vicinity of the orifice decreased fairly sharply. In this particular test, the highest fluidised zone obtained was 110 mm above the orifice, at a pressure in the orifice of 256 kPa, corresponding to flow rate of about 1233 *l/h*. It was thought surprising that such a high pressure head could be sustained in the orifice without the internally fluidised zone breaking through to the bed surface.

Pressure-flow rate relationship

Figure 3.17 shows the pressure-flow rate relationship for an orifice opening of 0.336 mm. The height of the bed was 300 mm of silica sand with a mean particle diameter (d_{50}) of 0.9 mm. The figure shows interesting behaviour, with three different phases, marked as A-B, B-C, and C-D on the curve depicted in Figure 3.17. The first phase (A-B) started from the point of injecting flow, i.e. small flow rate and head in the pipe, and continued up to flow rate of 666 *l/h* and head in the pipe of 53 kPa. In this phase the flow rate is linearly proportional to the head in the pipe, adhering to Darcy's Law.

In the second phase (B-C) a deviation from Darcy flow took place, which was characterised by a steep vertical line of the pressure head flow rate relationship (See Figure 3.15, phase B-C). As can be seen in Figure 3.17, in this phase less pressure head in the pipe was required to deliver more flow. Increasing the pressure from 53 kPa into 63 kPa resulted in a jump in the rate of flow from 666 l/h to 1042 l/h.

The third phase (C-D) shows a deviation from the previous two phases, and is characterised by a flat line of the pressure head flow rate relationship (Figure 3.17, phase C-D). This phase started at flow rate of about 1177 *l/h* corresponding to a pressure in the pipe of 83 kPa. At this point an internal fluidised zone in the vicinity of the orifice was formed in which the particles started moving around. It is interesting to note that after this point that, as the pressure in the orifice increased, no further increase in the rate of flow was observed. But as the pressure increased a slight increase in the height of the fluidised zone was observed associated with higher velocity of the particles moving inside the fluidised zone. This indicates that

the pressure head in the orifice (potential energy) was converted into velocity head in the orifice and inside the fluidised zone.

Experiment B

Figure 3.18 shows the profile of excess pore water pressure, in experiment B, when water was injected into a 300 mm bed height of silica sand (d_{50} =0.9 mm) through an orifice opening of 0.234 mm. Behaviour was similar to experiment A, increasing pressure in the orifice led to progressive build up of pore water pressure in the bed of grains, with a maximum values in the vicinity of the orifice. Away from this point, about 150 mm in the vertical direction, the pore pressure decreased linearly with height until it became atmospheric at the bed surface.

The excess pore water pressure at 10mm from the injection point increased dramatically with increasing pressure in the orifice. For example, at a pressure in the orifice of 23 kPa, corresponding to a flow rate of 258 l/h, the excess pore pressure was about 2 kPa. This was then increased to about 3 kPa as pressure in the orifice reached to 44kPa, the point at which the rate of flow was 412 *l/h*. A further increase in the pressure to value of 82 kPa, and flow rate of 811 *l/h*, the excess pore pressure reached to about 7 kPa.

A maximum value of the excess pore pressure was reached at 9.8 kPa; the point at which the system reached its capacity at a pressure in the orifice of 220 kPa, corresponding to a flow rate of 1017 *l/h*. In this particular test no drop in the excess pore pressure was observed as in experiment A, indicating that the uplift mechanism of the particles above the injection point did not occur. However, the hydraulic gradient (in the upper 150 mm of the sample) at this point was about 0.996, suggesting that test sample was very close to the onset of the uplift mechanism.

Experiment C

Experiment C was conducted on a 300 mm bed of LBS-A (d_{50} =1.6 mm) and orifice opening of 0.234 mm. Figure 3.19 shows the profile of excess pore pressure distribution along the bed height. In a similar behaviour to experiments A and B,

increasing pressure in the orifice results in progressive build up of pore pressure, with a maximum value at the injection point.

This particular test, however, was conducted on coarse material i.e. LBS-A, and the rate of increase in the excess pore water pressure was fairly low. For instance, at a pressure in the orifice of 23 kPa, corresponding to a flow rate of 286 *l/h*, the excess pore pressure at 10 mm above the orifice was about 0.8 kPa. This was then increased to just 1.6 kPa as pressure in the orifice reached to 44 kPa, the point at which the rate of flow was 485 l/h. A further increase in the pressure to value of 94 kPa, and flow rate of 768 l/h, the excess pore pressure reached to about 2.4 kPa.

A maximum value of the excess pore pressure was reached at 2.9 kPa; the point at which the system reached its capacity at a pressure in the orifice of 220 kPa, corresponding to a flow rate of 954 *l/h*. Similar to experiment B, no drop in the excess pore pressure was observed in this experiment, suggesting that the uplift mechanism of the particles above the injection point did not occur. The hydraulic gradient (in the upper 150 mm of the sample) at this point was far below the hydraulic gradient of unity, with a value of 0.301.

3.10 Re-design of test procedures based on the outcomes of the preliminary tests

Based on the outcomes the preliminary tests it was concluded that:

- Further tests required flow control, instead of pressure control.
- A flow sensor and/or a rota-meter was required to measure flow rate at the inlet point.
- Pore pressure transducers were required for continuous measurement of excess pore pressure during the experiment
- Further tests were required to investigate the effect of particle characteristics (such as form and size of the grain) on the uplift mechanism of the particles in the bed (i.e. onset of fluidisation).

- Further tests were required to investigate the effect of orifice size on the uplift mechanism of the particles in the bed.

3.11 Experimental setup for final tests

The same apparatus used to carry out the preliminary tests was used during final tests with additional instrumentation for measuring flow rate, pore pressure in the bed of grains, and pressure in the orifice. Figure 3.20 shows a photograph of the final experimental setup with the additional instrumentations.

3.11.1 Instrumentation

Pore pressure measurement

Measurement of pore pressure along the bed sample was made using pressure transducers. Six pressure transducers (RS type 286-658) with pressure range of 0-34.47 kPa were used. The sensors have a full scale output of 50 mV with a sensitivity of 10 mV/psi, and an accuracy of ±0.24 kPa. The null offset is between -1.5 and +1.5.

For calibration of the pore pressure transducers, each sensor was loaded with a column of water, while observing the output voltage. Typical calibration results for these transducers are presented in Appendix C, Figure C-2 to C-7.

The pore pressure transducers were connected into the stand pipes, used in the preliminary experimental setup, to measure the excess pore pressure.

Pressure upstream of the orifice

Pressure upstream of the orifice was measured using a pressure indicator; (Model-DPI 261, Druck products) with a pressure range up to 3447 kPa (500 psi), having an accuracy of 0.04%. The typical calibration results for this indicator are presented in, Appendix C, Figure C-8.

Flow sensor

A magnetic flow meter, model Signet 2551, with an LCD display unit was used to measure the inlet flow in the system. The meter has a function for averaging rate of flow (i.e. setting a time over which the meter averages the flow signals). During the

experimental run, this function was adjusted to 25 seconds to help smooth the display on the LCD. According to the specifications the meter achieves ±2% accuracy of readings, and operating range up to 10 m/s (18241 *l/h*).

In order to get the optimal performance of the flow sensor a full pipe is required. Therefore when installing the sensor a location was selected with sufficient distance of straight pipe immediately upstream and downstream of the system of the sensor; (50 × id[1]) upstream of the sensor and (5 × id) down stream of the sensor to ensure the pipe was always filled, and would not be exposed to air bubbles at any time.

The flow meter was calibrated using the volume method of calibration. A known volume of water was pumped through the flow meter, and then compared to the measured. The typical calibration results of the flow sensor are presented in Appendix C, Figure C-9.

3.11.2 Data acquisition system

An automatic data acquisition system was used to read the output of the pore pressure transducers and write the data to storage. The acquisition system consisted of sensors, an amplifier which also supplied power to the sensors, a data logger (CR1000-model), and a personal computer with CR basic editor.

In total six channels were used to monitor the signals coming from the pore pressure transducers. The monitored signals were logged via CR1000 and converted into engineering units using the calibration constants, as discussed in the above section.

3.12 Test programme and procedures for final tests

The purpose of carrying out final tests was to further explore the mechanism of internal fluidisation due to localised flow, and to assess the effects of particle characteristics (i.e. form and grain size), and orifice size on the onset of this mechanism.

---

[1] id is the internal diameter of the pipe.

A series of tests therefore were designed to accomplish this (see Tables 3.5 and 3.6). In order to study the effect of particle characteristics on the onset of fluidisation, three different bed materials were chosen for the tests; namely Leighton Buzzard sand-Fraction A (LBS-A), Leighton Buzzard sand-Fraction B (LBS-B), and glass ballotini (GB). The particle size distribution of these materials, shown in Figure 3.10, fell between 0.6 and 2 mm for the LBS-A, and 0.6 to 1.18 for the LBS-B and GB. Scanning Electron Micrograph images of the tested materials are shown in Figure 3.9, showing that while the glass ballotini had a high sphericity. The Leighton Buzzard sand was sub-rounded and slightly elongated and flattened. The glass particles were produced from soda-lime glass and procured from Sigmund Linder GmbH, Germany. Leighton Buzzard Sand is natural, uncrushed silica sand free from silt, clay or organic matter and supplied by David Ball Group plc of Cambridge.

For studying the effect of orifice size on the mechanism of fluidisation, four different orifice sizes, ranging between 0.234 mm and 0.92 mm, were selected for the test, (Table 3.6). In all these tests the orifice form was unchanged with square edge of 10 mm thickness.

Test procedures

The test procedures used for preliminary tests (section 3.7) were used for final tests, except that the final tests were conducted at controlled flow rates instead of controlled pressure in the orifice.

During the test, water was injected vertically through the orifice to fluidise a bed of grains. Initially small flow rates were applied (e.g. 50 *l/h*), and this was then increased in increments until fluidisation was observed or the capacity of the system was reached. At each increment in flow rate, the excess pore water pressure in the bed of grains and pressure in the orifice were recorded. The pressure in the orifice was recorded directly from the digital pressure indicator, while the pore pressure readings were collected from the data logger by the end of the test. The data were then plotted using Excel spreadsheets.

The behaviour of the fluidised bed was also monitored, at each increment in flow rate, using a video camera, and the images produced were then analysed using the Particle Image Velocimetery (PIV) techniques, as described in section 3.4. However, for the experiments conducted on glass ballotini, it was found that lack of visual texture prevented the use of PIV.

3.13 Results of final tests

The experimental data obtained and the physical observations are presented in this section and analysed in detail. All experiments run were performed at room temperature of 20 ± 2◦C.

Experiment D

In Experiment D water was injected into a 220 mm bed height of glass ballotini through an orifice opening of 0.62 mm. During the experiment water flow was increased incrementally from 50 l/h to 1500 l/h. Profiles of excess pore pressure as a function of flow rate are presented in Figure 3.21. It can be seen from the figure that, as the rate of flow increased in the early stages of the experiment, the pore pressure along the bed height increased correspondingly, with maximum value in the vicinity of the orifice. For example, at flow rate of 300 l/h, the excess pore pressure was about 1 kPa and, and this was then increased to 2.15 kPa by increasing the rate of flow to 600 *l/h*. A maximum excess pore water pressure of 5.3kPa was reached at flow rate of 1145 l/h. At this point the average hydraulic gradient was about 2.3.

As the peak was reached, uplift of the particles above the orifice was observed. This was followed by an abrupt drop in the excess pore pressure values in the vicinity of the orifice. Beyond this point, at each increase in the rate of flow the excess pore pressure dropped correspondingly. At the same time the height of the internally fluidised zone extended until eventually breakthrough was observed at the bed surface (Figure 3.22). For instance, when the rate of flow increased to 1150l/h the excess pore pressure dropped to 4.4kPa. At this point an internally fluidised zone was formed, in the vicinity of the orifice, with a measured height of 18mm from the orifice. With a further increase in the rate of flow up to 1200 l/h, the pore pressure dropped further to 2.5 kPa, while the height of the internally fluidised zone increased

up to 40mm. When the rate of flow was increased to 1250 l/h, the pore pressure dropped to 2.15 kPa, the point at which the fluidised zone extended up to about 55mm above the orifice. At this point the pore pressure readings within the range of 50mm from the orifice, in the vertical direction were almost the same with an average value of 2.15 kPa.

Following a further increase in the rate of flow up to 1300 l/h, the pore pressure dropped again to about 1.8 kPa. At this point, the height of the fluidised zone reached about 80mm above the orifice. When the rate of flow increased further to 1350 l/h, the behaviour of the internally fluidised zone became unsteady. At this point it started growing continually until it brokethrough to the surface of the bed. This process occurred fairly quickly; in about 10 seconds, (for video see the attached CD).

After fluidisation broke through to the surface, the particles started boiling at the surface like an erupting volcano.

Experiment E

In this experiment water was injected into a 150 mm bed height of LBS-B (d_{50} = 0.9 mm) through an orifice opening of 0.33 mm. During the experiment, flow rate was increased incrementally from 50 *l/h* to 1200 *l/h*. Profiles of excess pore pressure along the bed height as a function of flow rate are shown in Figure 3.23. Behaviour was similar to that in experiment D. As the rate of flow increased, in the early stage of the experiment, the excess pore pressure increased correspondingly, with a maximum value at the injection point. For example, at 10 mm above the injection point, the excess pore pressure value was about 0.28 kPa, at a flow rate of 50 *l/h*. This was then increased to 0.54 kPa when the rate of flow increased to 100 *l/h*.

A maximum excess pore pressure of 2.63 kPa was reached at flow rate of 450 *l/h*, and this occurred at an average hydraulic gradient of 1.68. At this particular point, the hydraulic gradient in the vicinity of the orifice (within 50mm of the orifice) was about 3.6 times higher than that away from the orifice (i.e. in the upper 2/3 of the sample).

As the excess pore pressure peaked, uplift of the particles above the orifice occurred, Figure 3.24 and 3.25. This was followed by an abrupt drop in the pore pressure at the injection point. At this point an internally fluidised zone was seen and continually extended up until it broke through to the bed surface. Figure 3.26 presents photographs showing the development of the internally fluidised zone. In this particular test, the internally fluidised zone developed and broke through to the bed surface fairly quickly (in about 11 seconds). (For video see the attached CD). During the onset of this mechanism the rate of flow jumped from 450 *l/h* to 650 *l/h*, while the excess pore pressure dropped from 2.63 kPa to 1.06 kPa.

After the fluidised zone broke through to the bed surface, the particles started boiling at the surface, and a dune or ridge was formed around the boiling zone. This was due to the deposition of particles washed from the fluidised region (Figure 3.27). Increasing the rate of flow resulted in a more violent boiling condition at the bed surface extended to higher position as the rate of flow increased (see Figure 3.27). At the same time the boundaries of the deposited zone widened as well as deepened, until they formed a concave upward fluidised zone at the higher flow rates i.e. 1000l/h to 1200 l/h, Figure 3.27 e and f.

Experiments F, G, and H

Experiments F, G, and H were carried out on three different bed materials; namely: LBS-B (sub-rounded, d_{50}=0.9 mm), LBS-A (sub-rounded, d_{50}=1.6 mm), and GB (spherical, d_{50}=0.9 mm). In all three experiments bed height and orifice opening were constant at 300 mm and 0.62 mm, respectively. During the experiments, the flow rate was increased incrementally from 50 l/h to 1500 l/h. Figures 3.28, 3.29, and 3.30 show profiles of excess pore water pressure along bed height of the of three materials, i.e. LBS-B, LBS-A, and GB, respectively.

A general observation of the figures shows that increasing flow rate results in progressive build up of the excess pore pressure, with maximum values in the vicinity of the orifice. Away from the this point, about 50 mm in the vertical direction, the excess pore pressure decreases linearly with height until it becomes atmospheric at the bed surface. This is shown at low flow rates e.g. 100 *l/h.*

However, at high flow rates e.g. 1000 *l/h*, the linearity in the excess pore pressure with height was not seen until 150 mm away from the injection point Figure 3.29.

The build up of the excess pore pressure in the LBS-B (i.e. is sub-rounded, d_{50}=0.9 mm) was much higher than that in the LBS-A (is sub-rounded, d_{50}=1.6 mm) and GB (spherical, d_{50}=0.9mm) Figures 3.28, 3.29, and 3.30, respectively. For example, at an applied flow rate of 100 l/h, the excess pore pressure at 10 mm above the orifice was 0.78 kPa, 0.21 kPa, and 0.43 kPa for the LBS-B, LBS-A, and GB, respectively.

For experiment F, conducted on LBS-B, a maximum excess pore water pressure of 7.52 kPa was reached at flow rate of 1050 l/h, Figure 3.28. This occurred at a hydraulic gradient in the vicinity of the injection point (within 50 mm of it) of about 10.37. The average hydraulic gradient along the bed sample at this point was about 2.54. In this particular test, as the pore pressure peaked, the uplift mechanism of the particles above the orifice occurred; this was followed by an abrupt drop in the pore pressure to a value of about 2 kPa. During this stage, an internally fluidised zone developed and broke through to the bed surface fairly quickly, in a similar way to experiment E.

In experiment G, conducted on LBS-A, fluidisation did not occur during the whole experiment. The system reached its capacity at flow rate of 1500 *l/h*, the point at which the excess pore water pressure reached a value of 3.45 kPa, Figure 3.29. The hydraulic gradient in the vicinity of the orifice at this point was about 4.41; while in the upper 150 mm of the sample it was 0.394. The average gradient up the sample bed was about 1.13.

For experiment H, carried out on GB, fluidisation also did not occur even at the high flow rate of 1500 l/h. The maximum excess pore water pressure at this point was about 8.8 kPa, corresponding to an average hydraulic gradient of about 2.93, Figure 3.30. In the vicinity of the injection point (within the 50 mm of it) the gradient was very high of about 13.5; much higher than that in the upper 150 mm of the sample i.e. 0.94.

3.14 Summary

- An experimental apparatus has been designed and built to investigate the mechanism of internal fluidisation of granular materials due to localized (or concentrated) flow.

- Techniques for monitoring the behaviour of a fluidised bed have been developed based on the Particle Image Velocimetery (PIV) technique.

- Experiments were designed to investigate the effect of particle characteristics (i.e. form and grain size) on mechanisms of fluidisation.

- Experiments were designed to investigate the effect of orifice size on mechanisms of fluidisation.

Table 3.1: Maximum and minimum densities, void ratios, void ratio ranges of the materials.

Material	Gs	ρ_{max} [1](Mg/m³)	ρ_{min} [2](Mg/m³)	e_{max}	e_{min}	$e_{max} - e_{min}$
LBS-A	2.665	1.749	1.477	0.804	0.523	0.281
Silica Sand	2.658	1.765	1.470	0.808	0.506	0.302
LBS-B*	2.65	1.793	1.450	0.788	0.463	0.324
GB*	2.5	1.635	1.478	0.675	0.529	0.146

(*) Data of Bui (2009)

1 The maximum density was determined using dry pluviation technique.

2 The minimum density was determined by inverted cylinder method (BS 1377-4:1990)

Table 3.2: Shape parameters of tested materials

Material	Gs	L_{ave} (≡ *Max.Dim.*) (mm)	I_{ave} (≡ *Int.Dim.*) (mm)	S_{ave} (≡ *Min.Dim*) (mm)	Corey's Shape factor, CSF	SEES	ψ_o
GB	2.5	1.008	0.967	0.925	0.936	0.917	0.958
LBS-B	2.65	1.202	0.864	0.616	0.604	0.512	0.717
Silica Sand	2.658	-	-	-	-	-	-
LBS-A	2.665	2.228	1.439	1.006	0.562	0.451	0.663

ψ_o Operational sphericity
CSF Corey's shape factor
SEES Scalene equivalent ellipsoid sphericity
I Intermediate dimension of the particle
L Largest dimension of the particle
S Smallest dimension of the particle

Table 3.3: Initial conditions of the specimens in the test

Material	ID	ρ (Mg/m^3)	e	D_r (%)
LB sand A	LBS-A	1.702	0.565	85
Silica Sand	SS	1.725	0.540	88
LB sand B	LBS-B	1.727	0.534	79
Glass Ballotini	GB	1.593	0.569	75

Table 3.4: Test programme for preliminary tests: bed height 300mm.

Experiment	Test Material	Grain size D50 (mm)	Orifice opening (mm)
A	Silica sand	0.9	0.336
B	Silica sand	0.9	0.234
C	LBS-A	1.6	0.234

Table 3.5: Tests to study the effect of soil characteristics, orifice opening: 0.62 mm.

Test no.	Test Material	Grain size d_{50} (mm)	Grain shape
1	LBS-A	1.6	Sub-rounded
2	LBS-B	0.9	Sub-rounded
3	GB	0.9	Spherical

Table 3.6: Tests to study the effect of orifice opening, material tested: LBS-B (d_{50}=0.9mm).

Test no.	Orifice opening (mm)
1	0.234
2	0.336
3	0.62
4	0.92

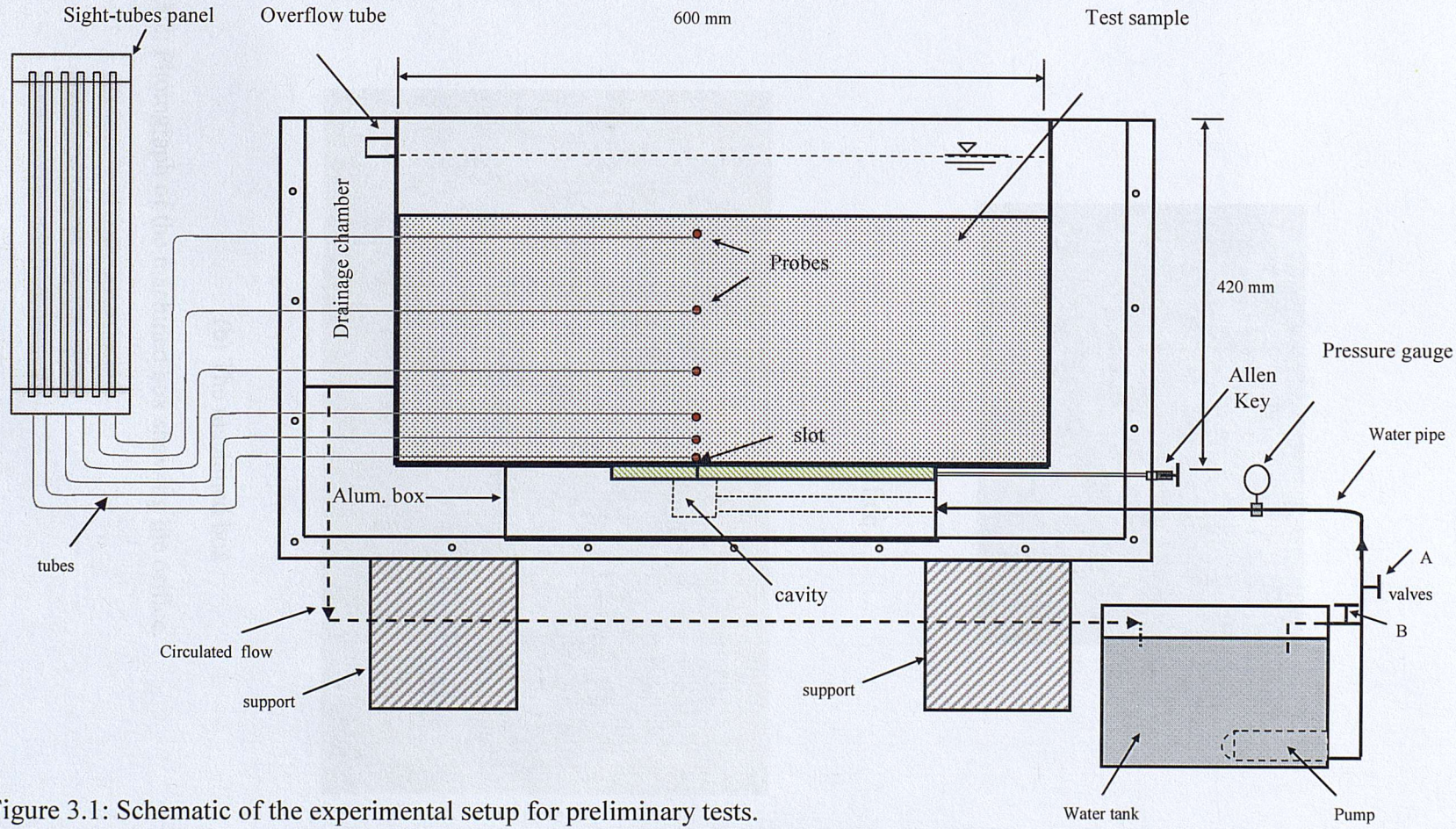

Figure 3.1: Schematic of the experimental setup for preliminary tests.

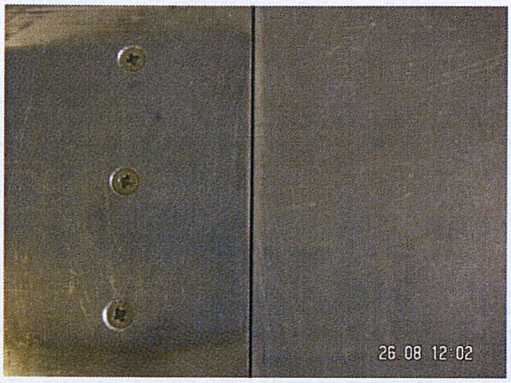

(a) The orifice

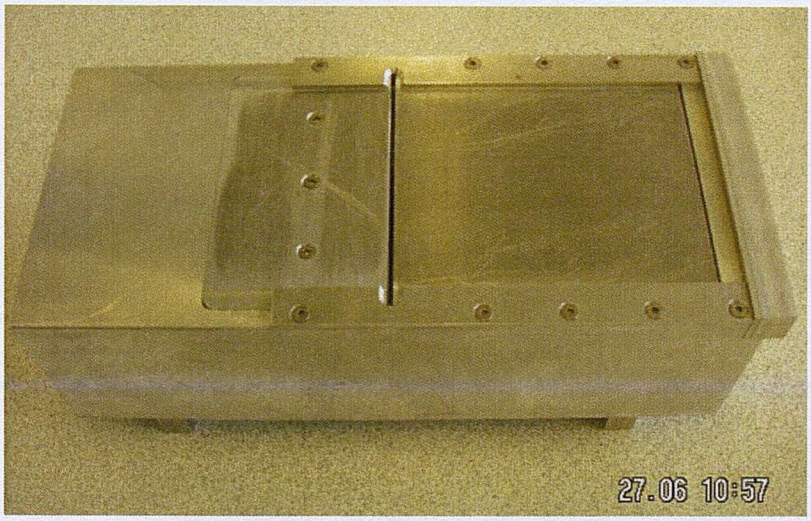

(b) The machined box

Figure 3.2: Photograph of the machined box showing the orifice.

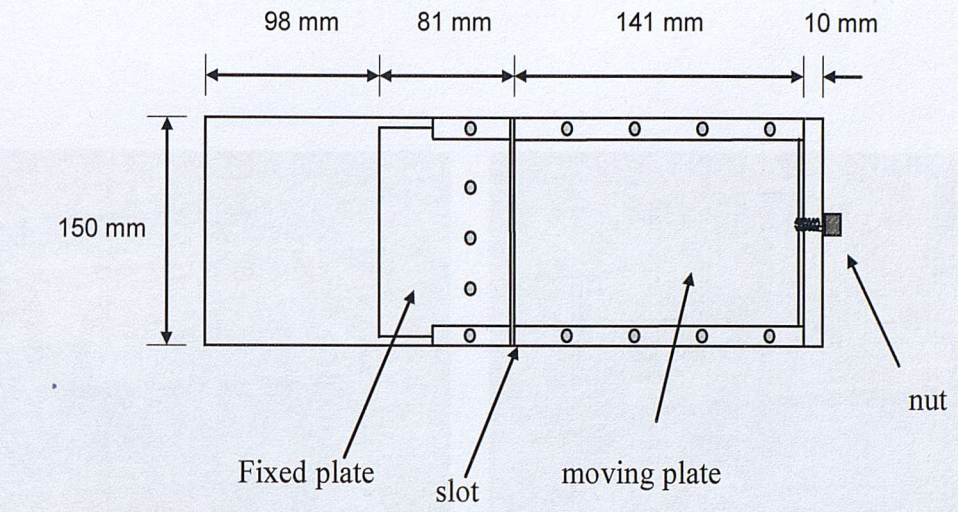

(a)

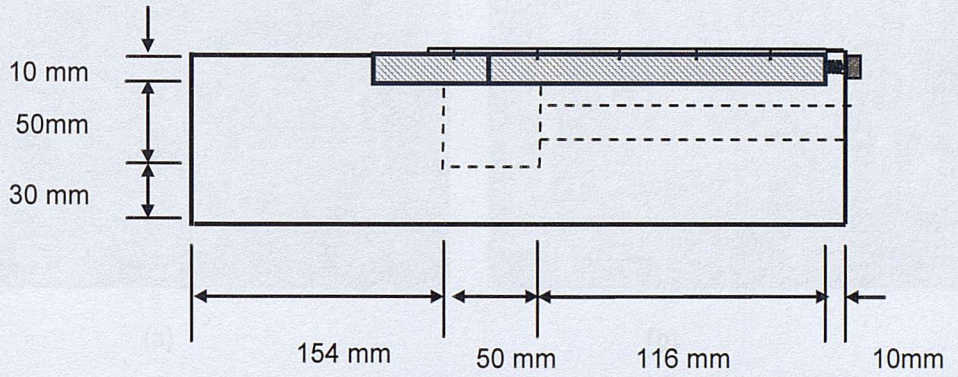

(b)

Figure 3.3: Schematic diagram of the machined box (a) top view (b) front view.

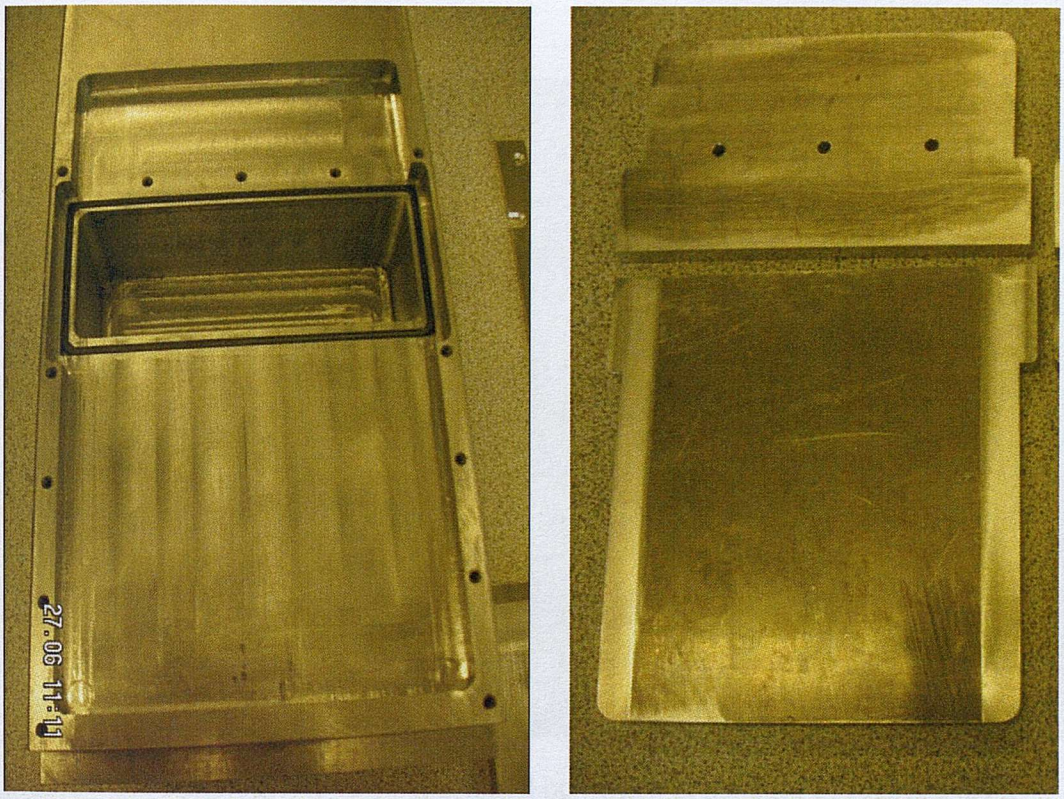

(a) (b)

Figure 3.4: Photographs of the: (a) machined box with an O-ring placed in a groove on the upper flange, and (b) two plates put on top of the machined box to form the crack.

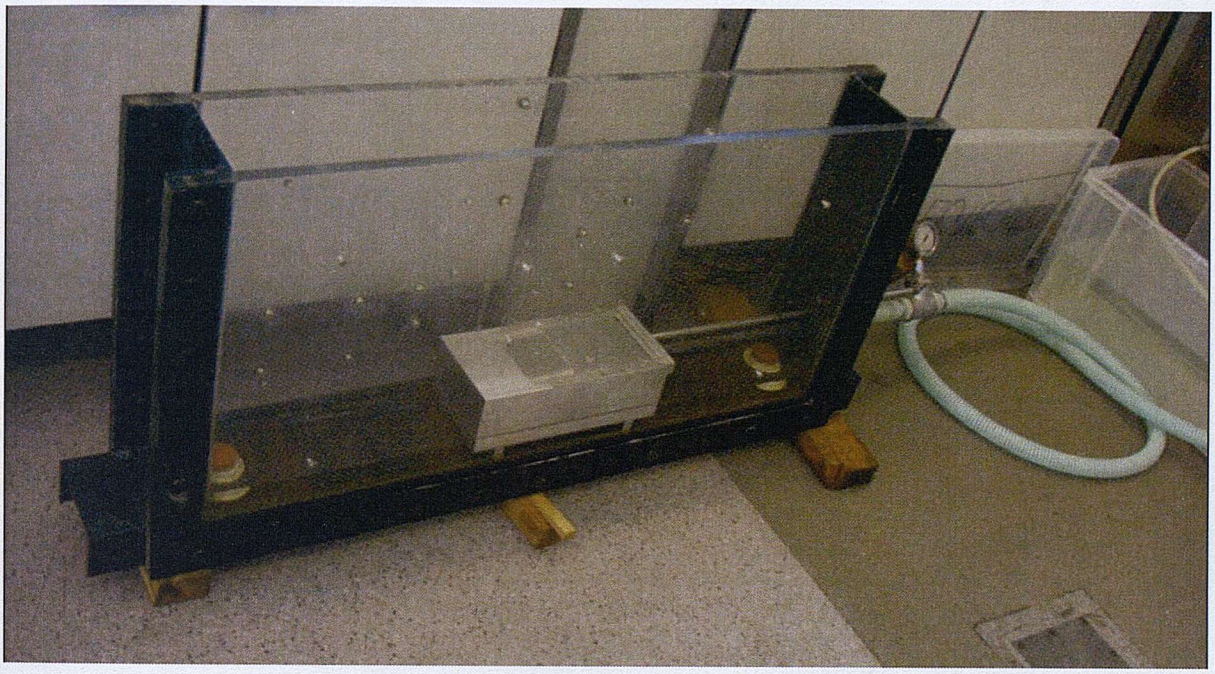

Figure 3.5: A photograph of the machined box fitted at the base of seepage tank.

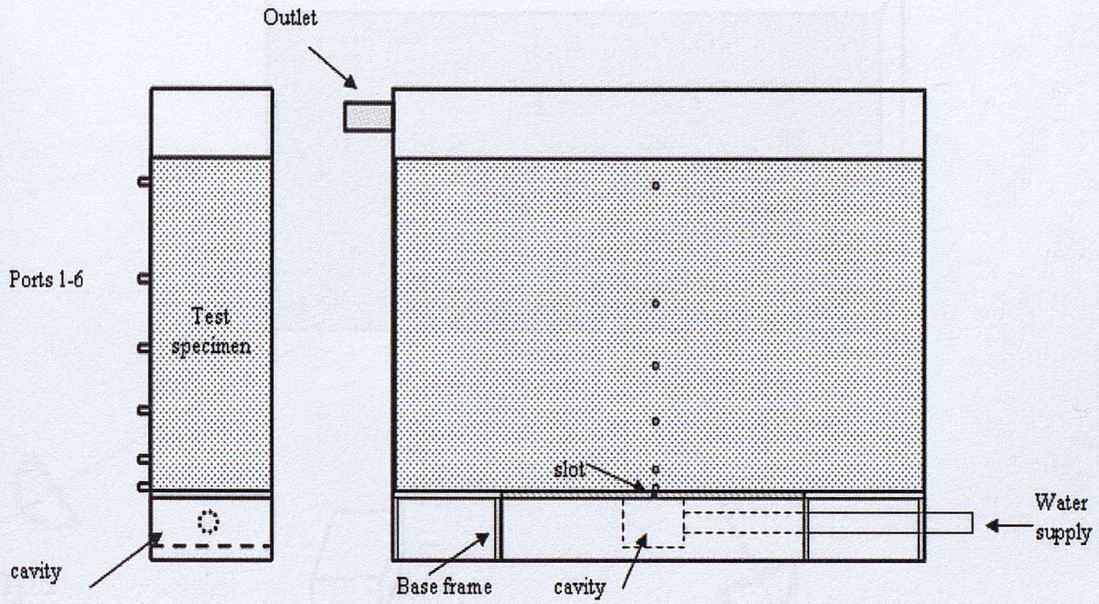

(i) Side view (ii) front view

Figure 3.6: Manometer port locations, and specimen in the apparatus- 6 ports located at 10 mm,53 mm, 102 mm, 150 mm, 220 mm, and 300 mm above the slot.

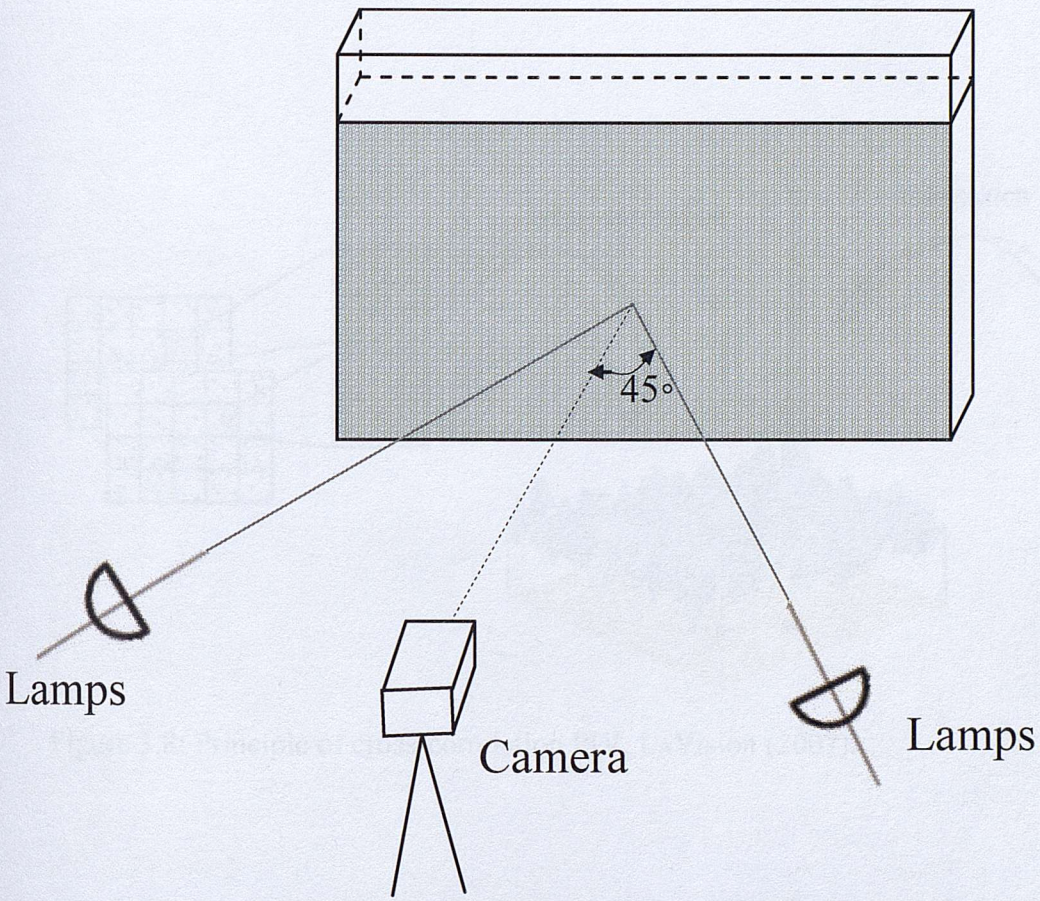

Figure 3.7: Sketch of the experimental setup for PIV.

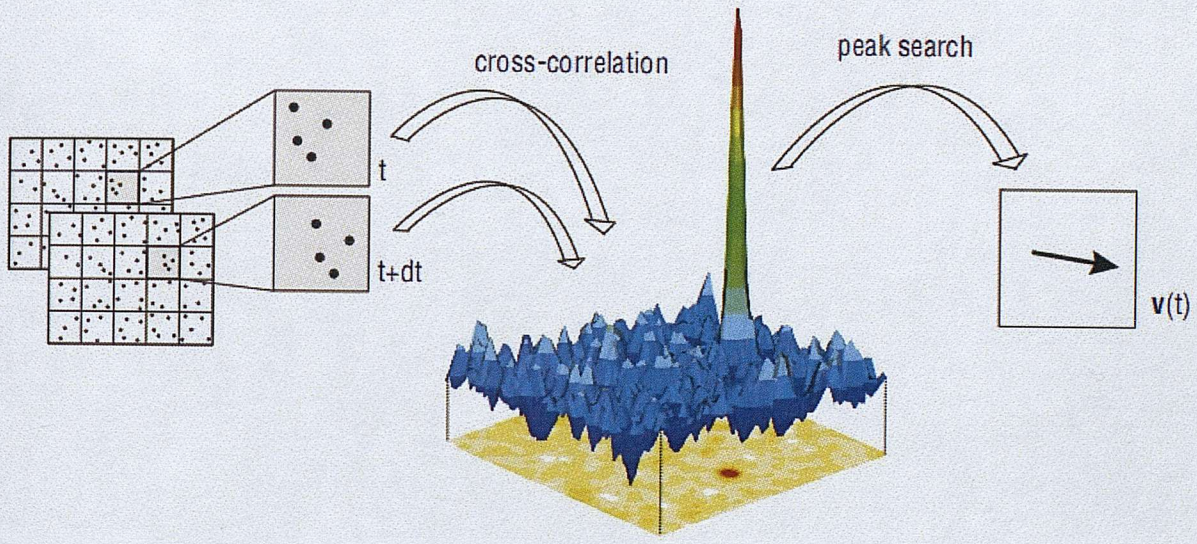

Figure 3.8: Principle of cross-correlation PIV, LaVision (2007).

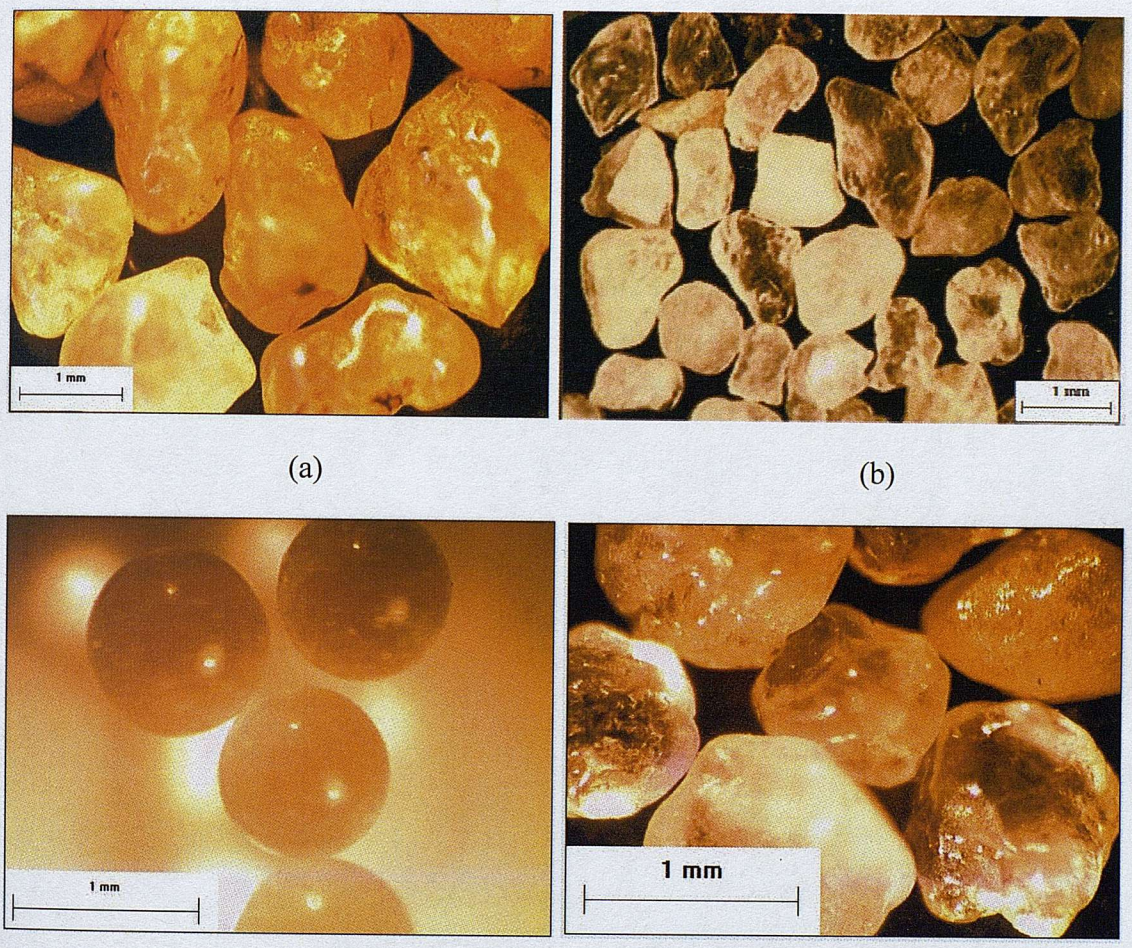

(a) (b)

(c) (d)

Figure 3.9: Scanning Electron micrographs; (a) Light Buzzard Sand –Fraction A, (b) Silica sand. (c) Glass ballotini; and (d) Leighton Buzzard sand- Fraction B.

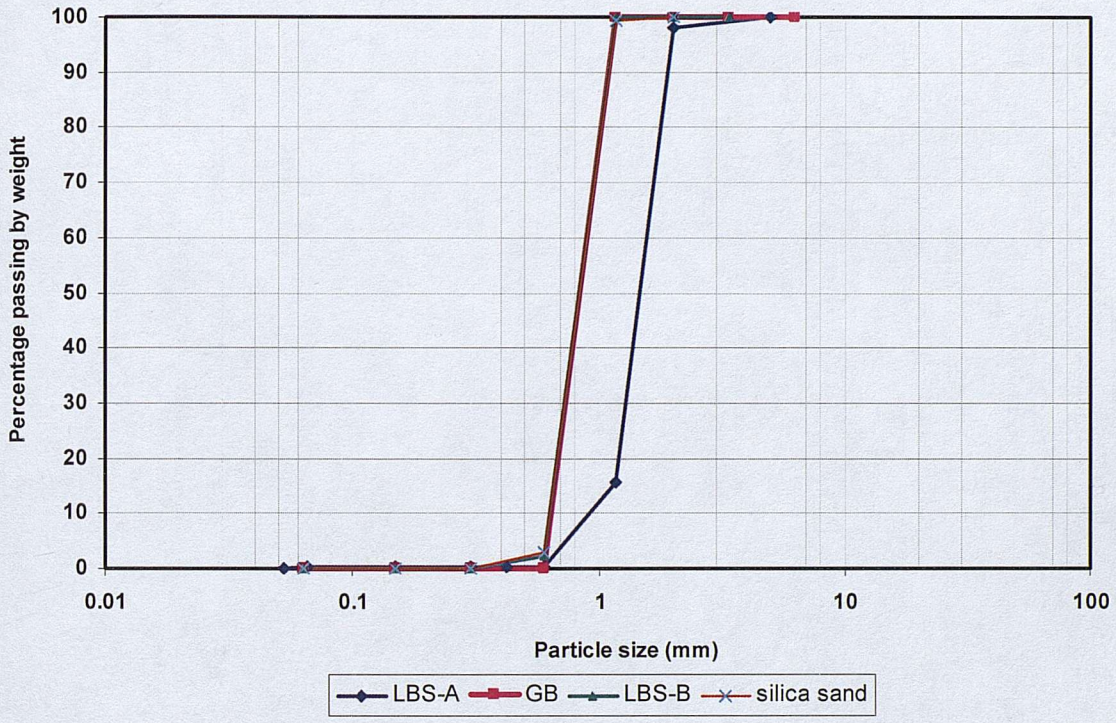

Figure 3.10: Particle size distributions of Leighton Buzzard sand Fraction A and B, and Glass Ballotini.

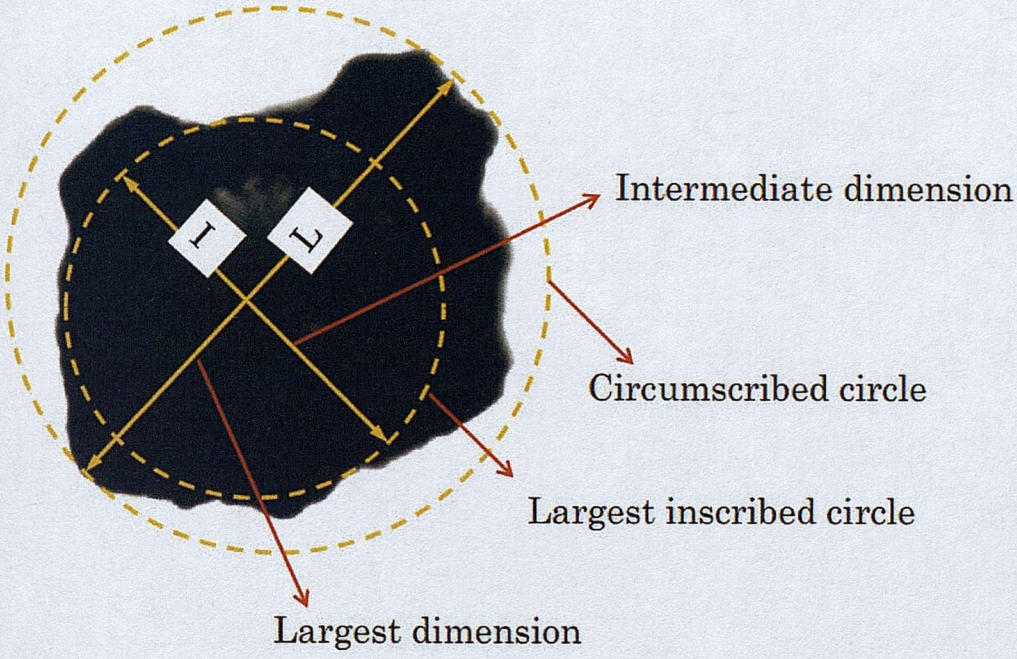

Figure 3.11: Largest (I) and intermediate (I) dimensions from 2D particle image in volume method. (After Reddy, 2008).

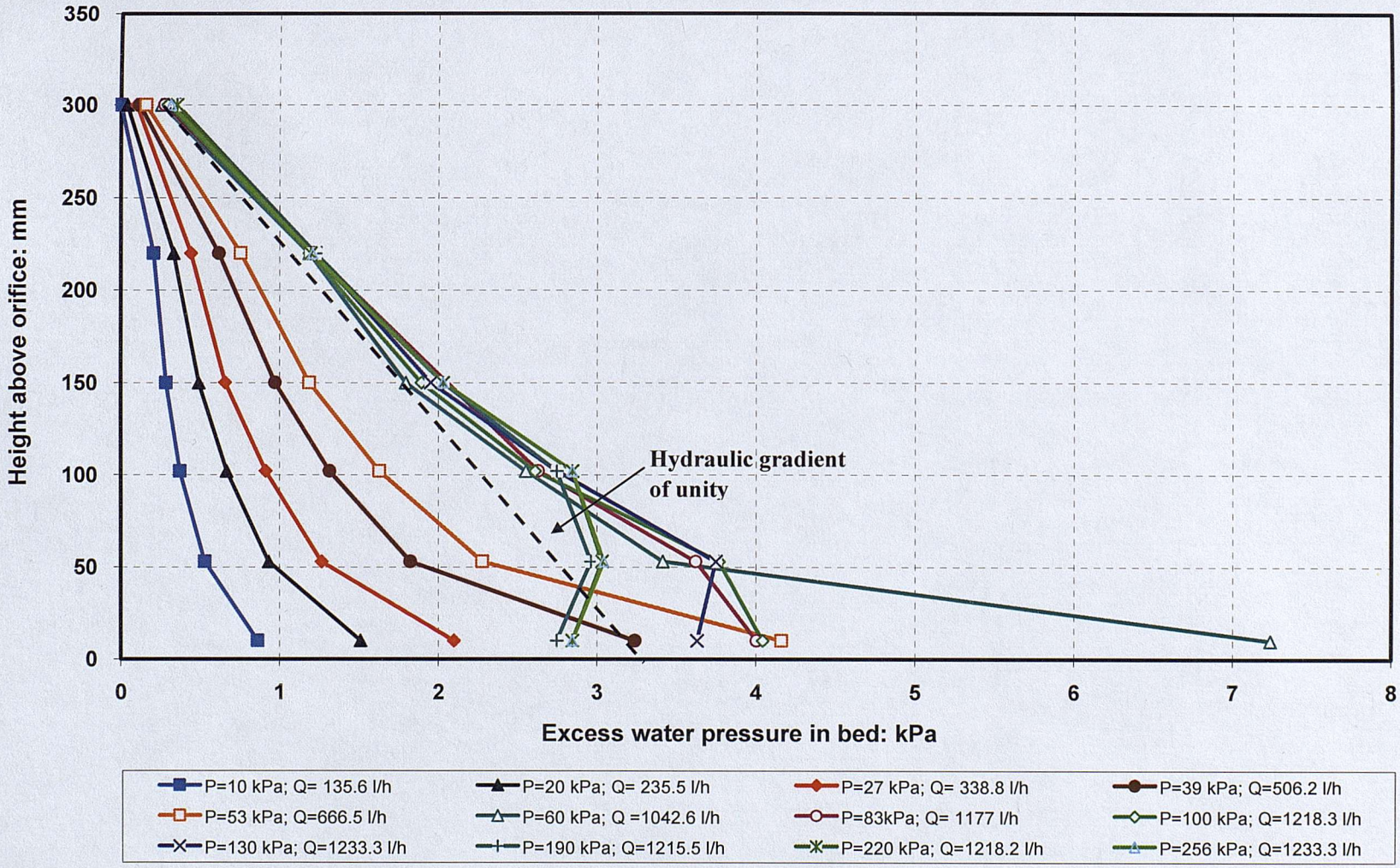

Figure 3.12: Excess pore water pressures at different points along 300mm bed height of silica sand, orifice opening: 0.336mm.

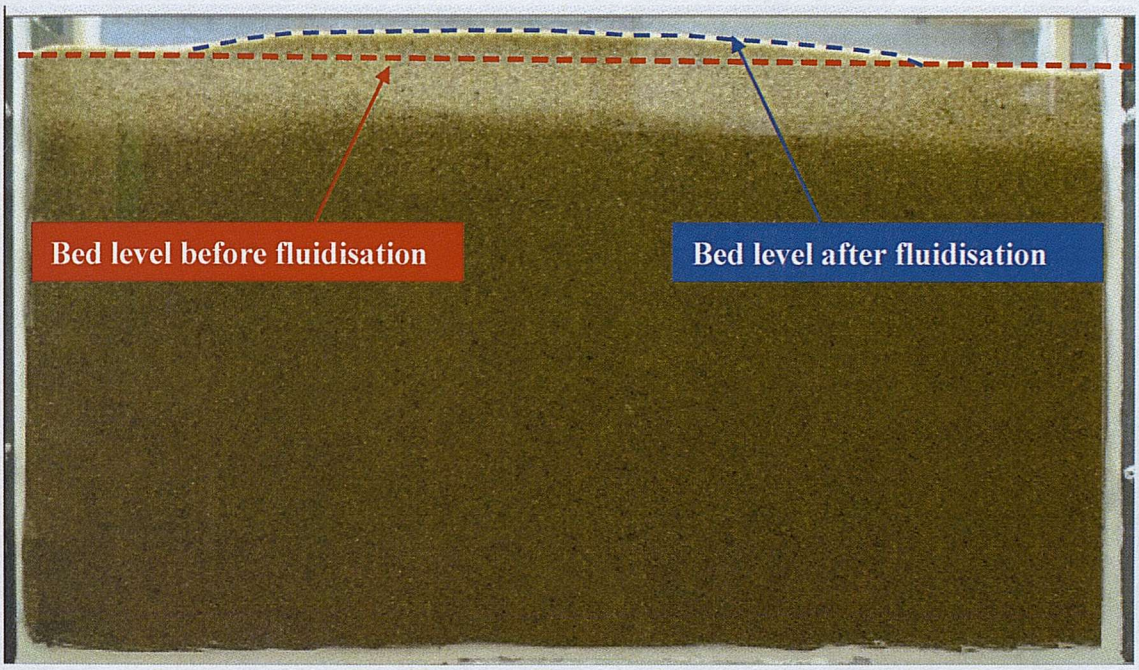

Figure 3.13: Photograph of the level of the bed before and after the onset of fluidisation. The particles in the active bed above the orifice lifted upward to a certain level.

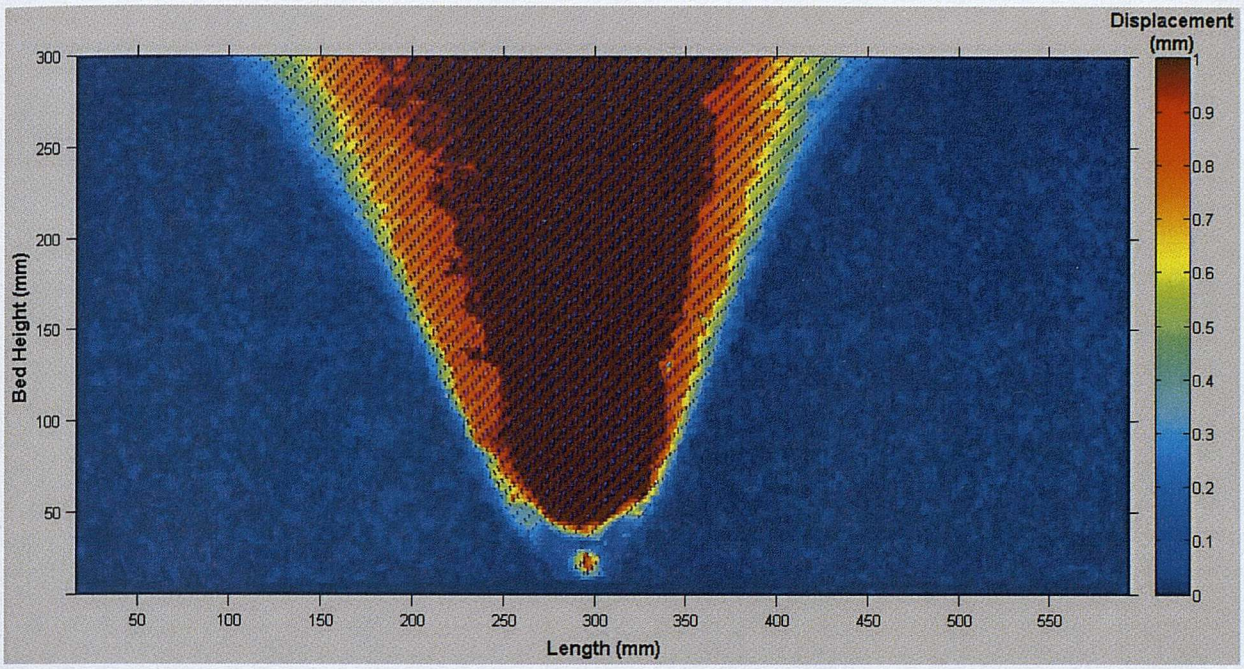

Figure 3.14: The uplift mechanism of the grains above the injection point at the onset of fluidisation. Bed height 300mm of silica sand, and orifice opening: 0.33mm. Pressure in the orifice: 83 kPa, and flow rate: 1177 l/h.

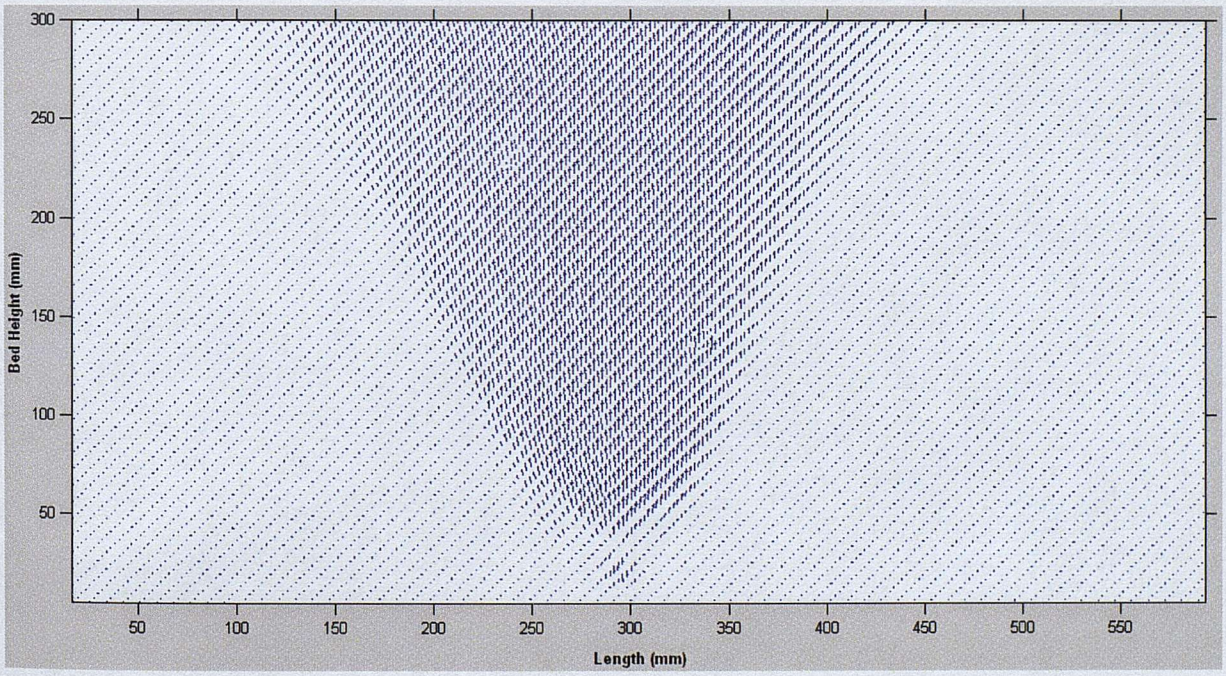

Figure 3.15: Vectors showing the uplift mechanism of the grains above the injection point at the onset of fluidisation. Bed height 300mm of silica sand, and orifice opening: 0.33mm. Pressure in the orifice: 83 kPa, and flow rate: 1177 l/h.

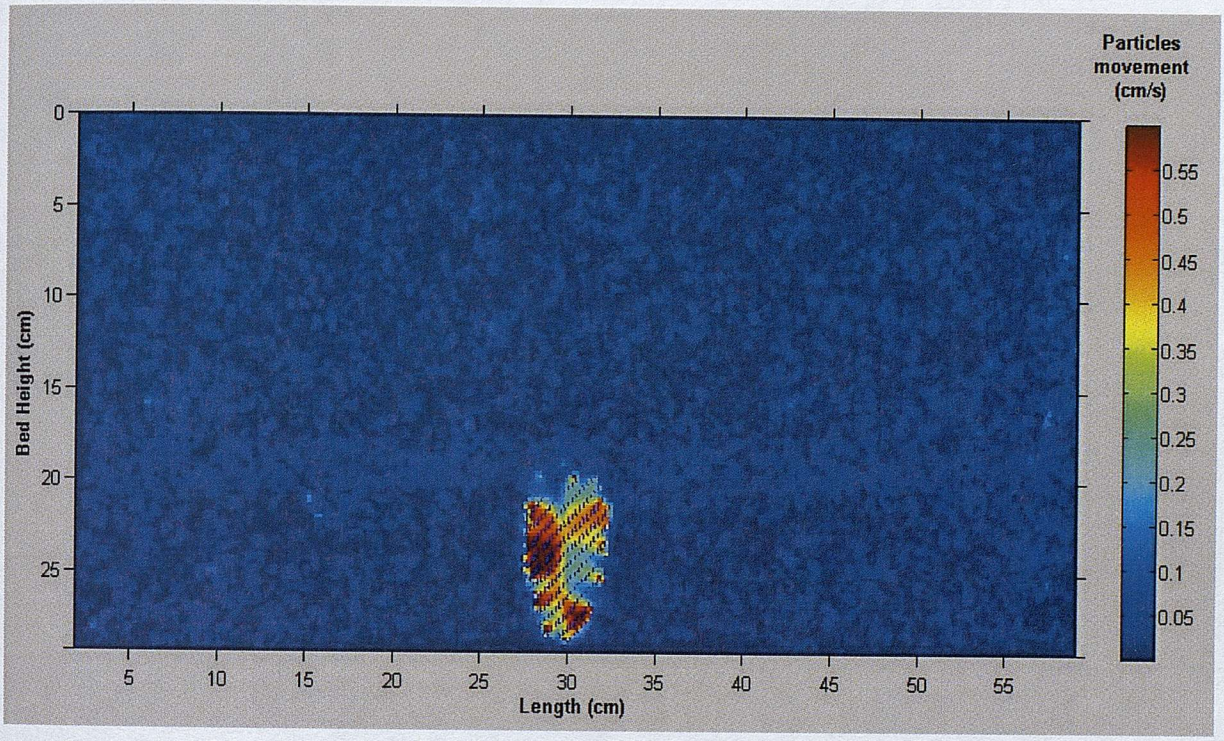

Figure 3.16: Internal fluidised zone in a 300 mm bed height of silica sand. Pressure in the orifice: 256 kPa and flow rate: 1233 l/h.

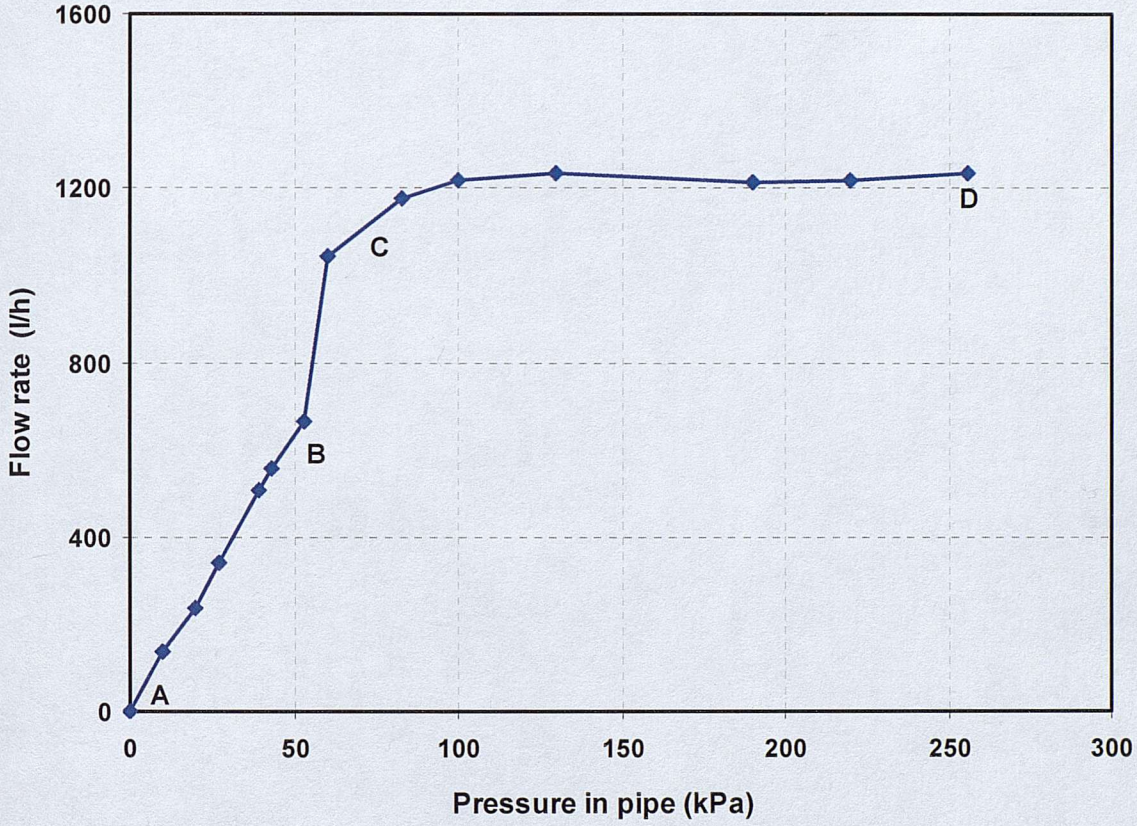

Figure 3.17: Pressure –flow rate relationship, when water was injected into a 300mm bed of silica sand (d_{50} =0.9mm) through an orifice opening of 0.336mm.

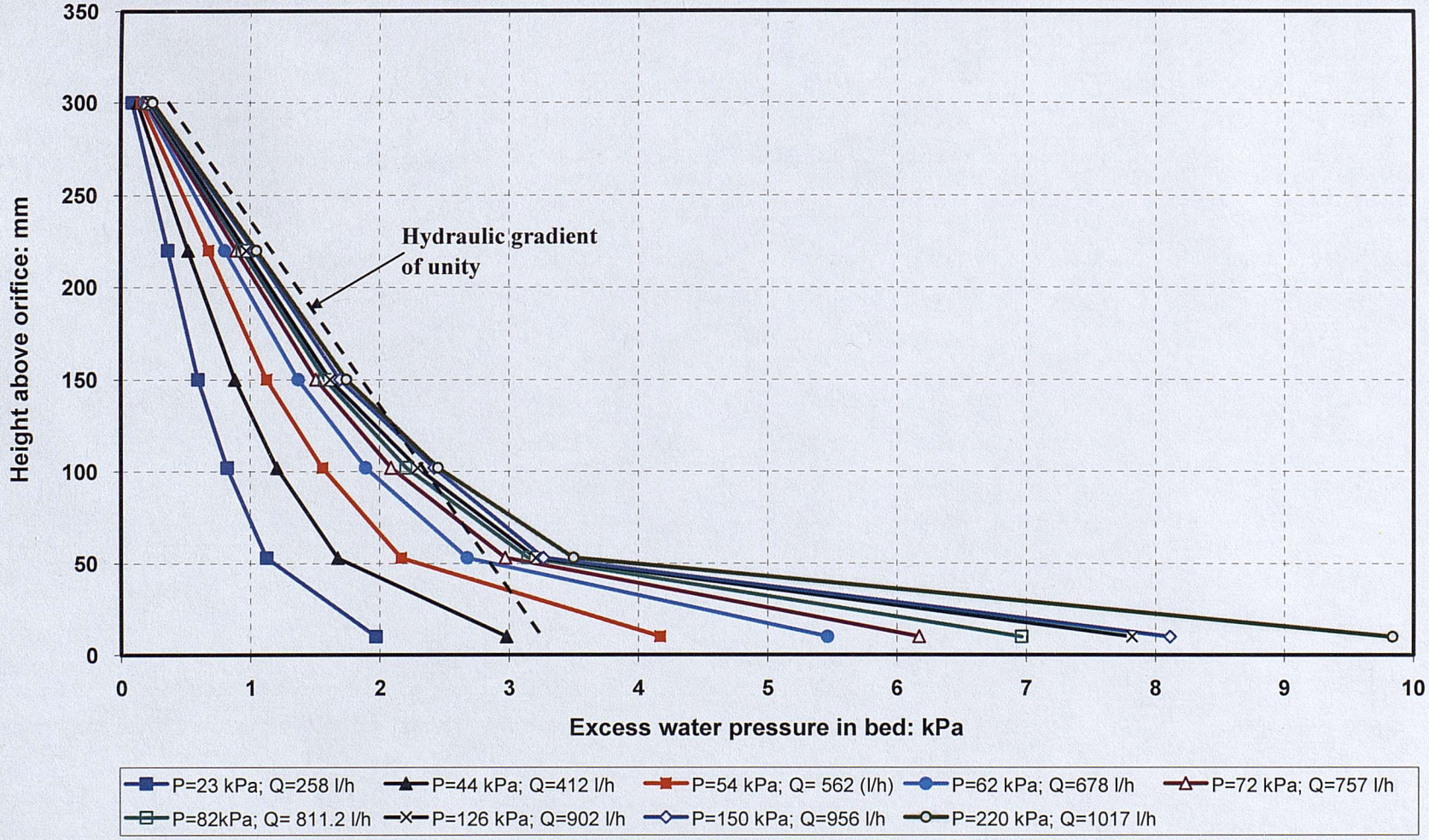

Figure 3.18: Excess pore water pressures at different points along 300mm bed height of silica sand, orifice opening: 0.234mm.

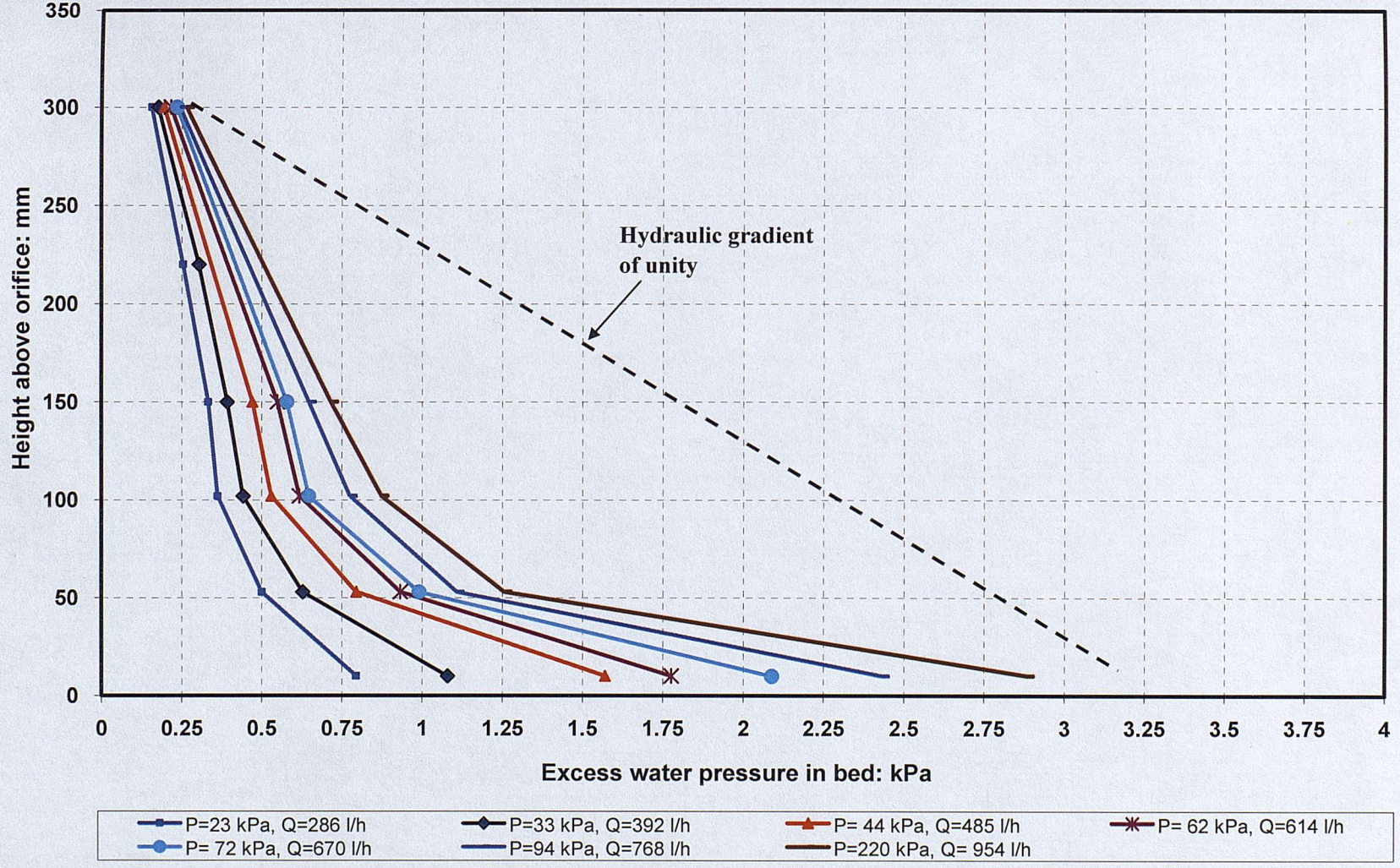

Figure 3.19: Excess pore water pressures at different points along 300mm bed height of LBS-A, orifice opening: 0.234 mm.

Figure 3.20 Photograph of the experimental setup for final tests.

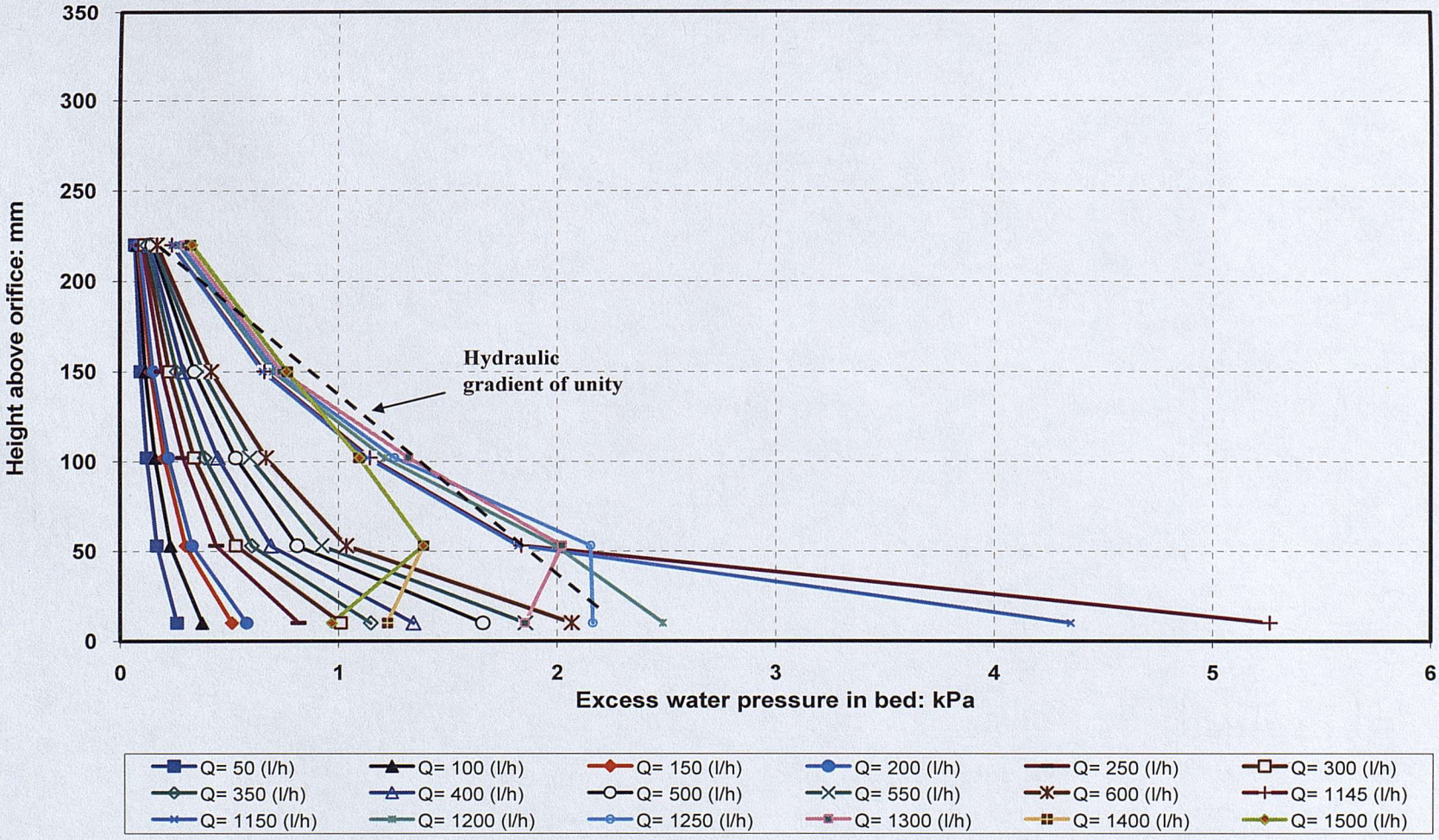

Figure 3.21: Excess pore water pressures at different points along 220 mm bed height of GB, orifice opening: 0.62mm.

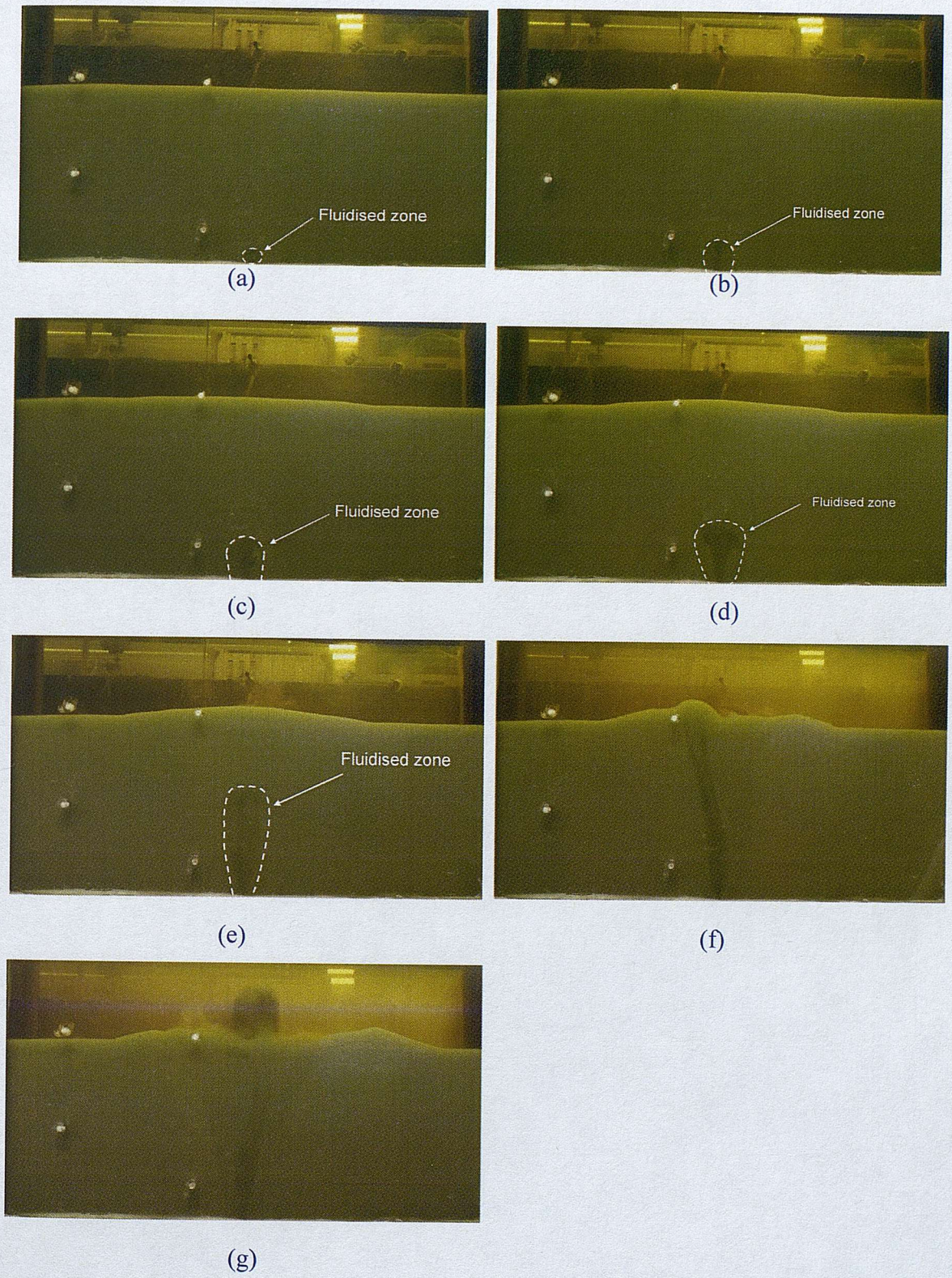

Figure 3.22: Development of internal fluidisation in a 220 mm bed height of GB at different flow rates: (a) 1150 l/h; (b) 1200 l/h; (c) 1250 l/h; (d) 1300 l/h; (e) 1350 l/h; (f) 1400 l/h; (g) 1500 l/h. Orifice opening: 0.62 mm.

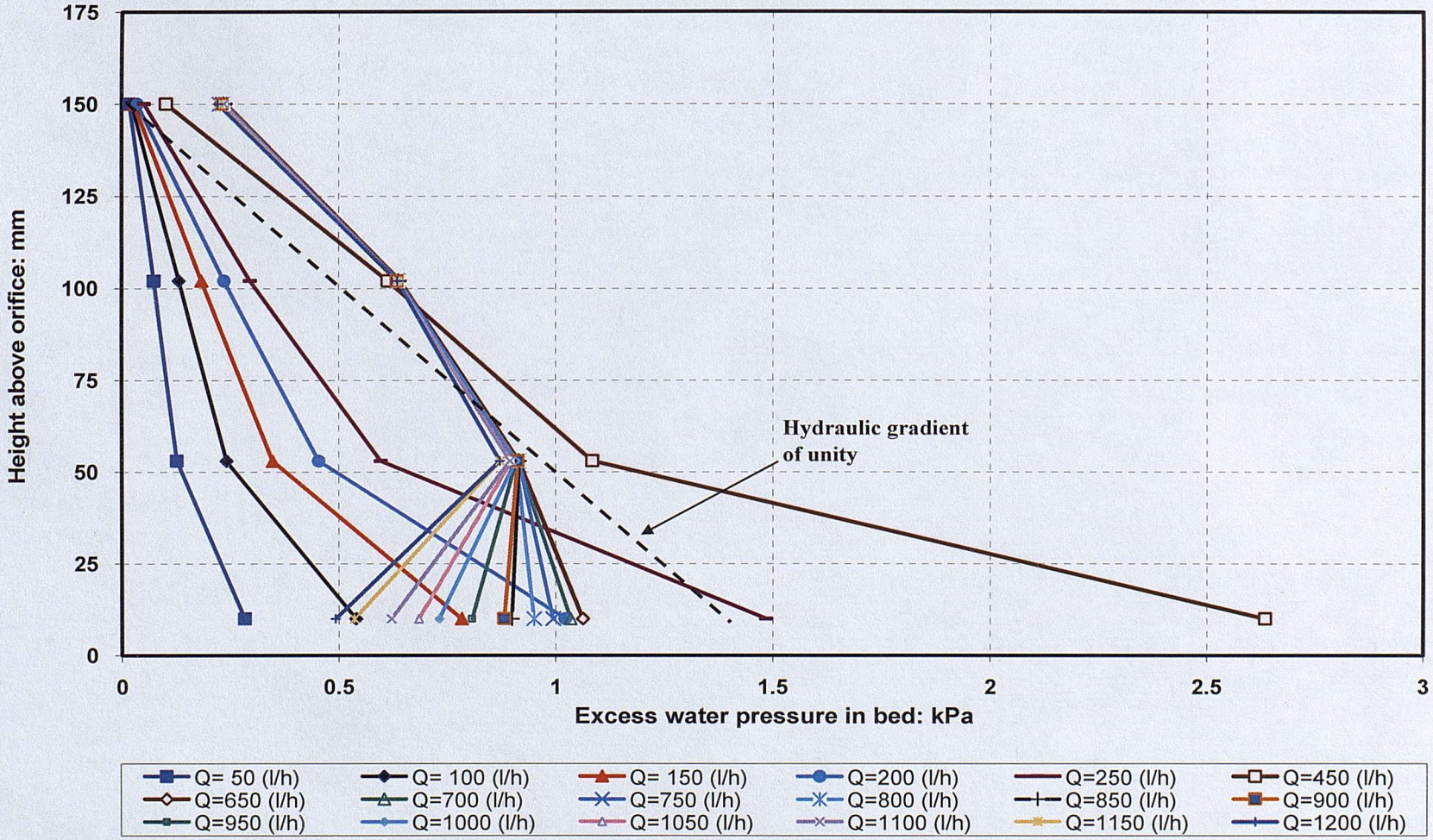

Figure 3.23: Excess pore water pressures at different points along 150mm bed height of LBS-B, orifice opening: 0.33 mm.

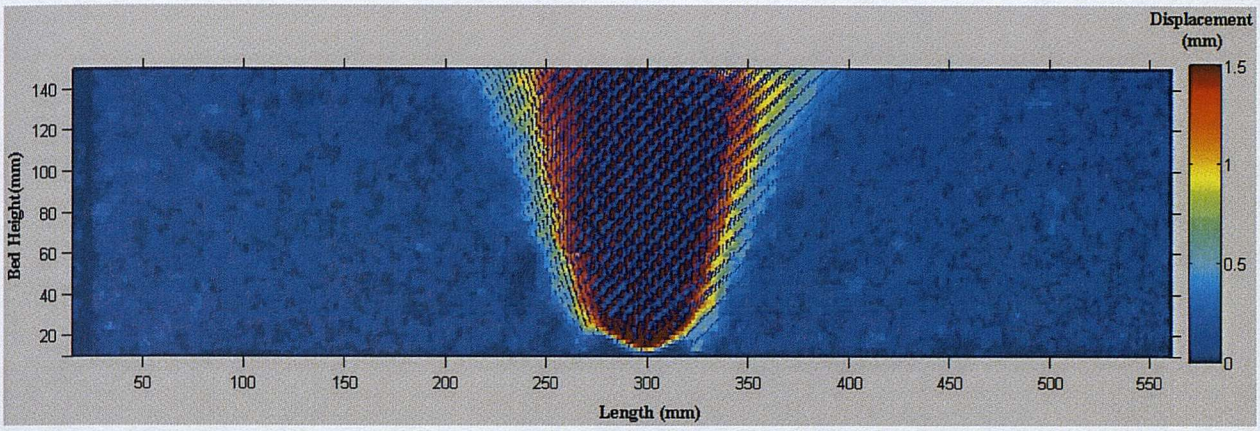

Figure 3.24: The uplift mechanism of the grains above the injection point at the onset of fluidisation. Bed height 150mm of LBS-B, and orifice opening: 0.33 mm.

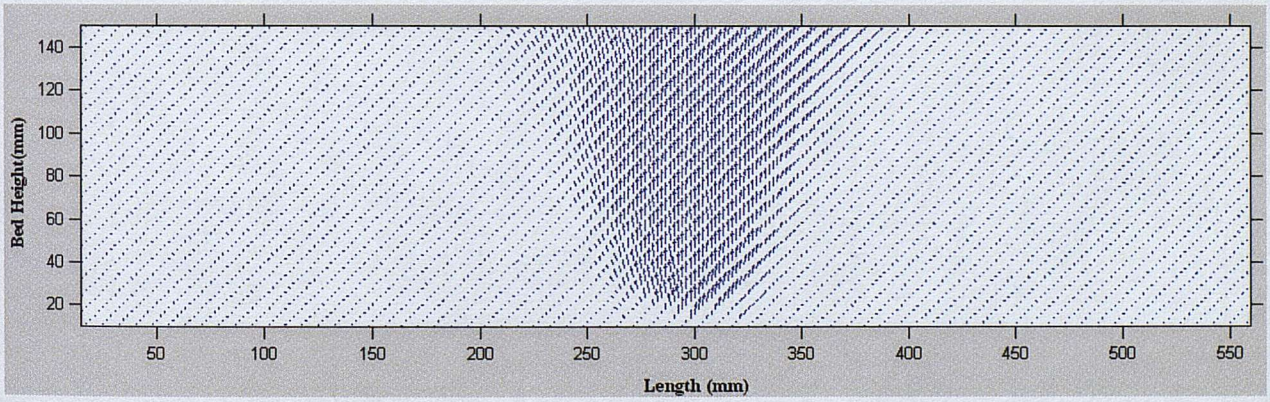

Figure 3.25: Vectors of the uplift mechanism of the grains above the injection point at the onset of fluidisation. Bed height 150mm of LBS-B, and orifice opening: 0.33 mm

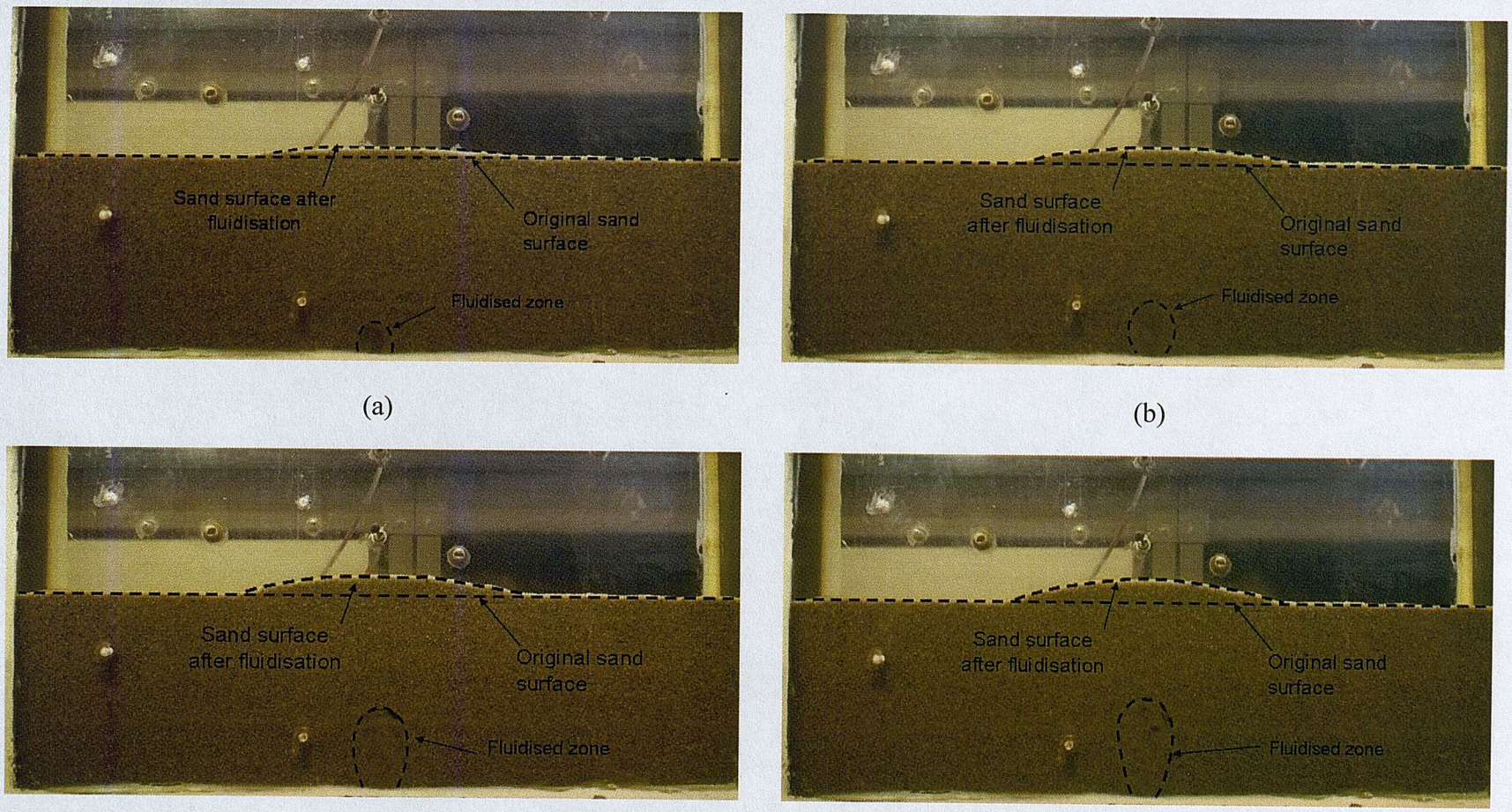

Figure 3.26a: Development of internal fluidisation in a 150 mm bed height of LBS-B. Orifice opening: 0.33mm.

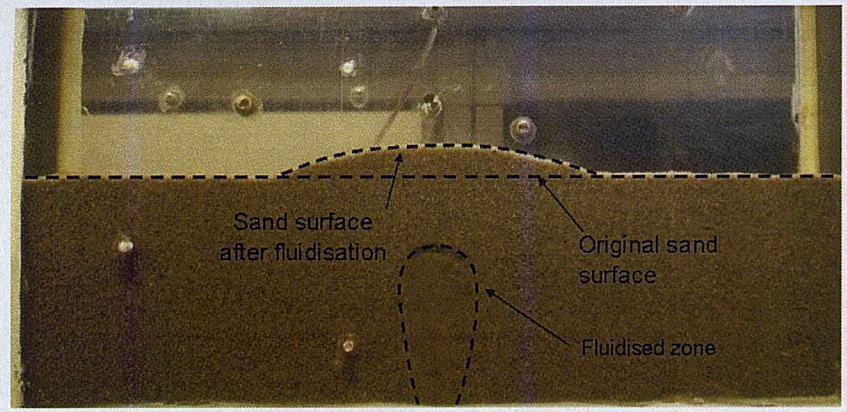

(e)

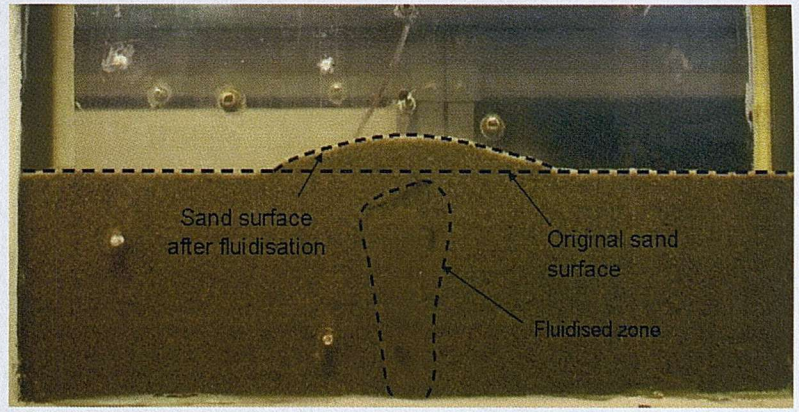

(f)

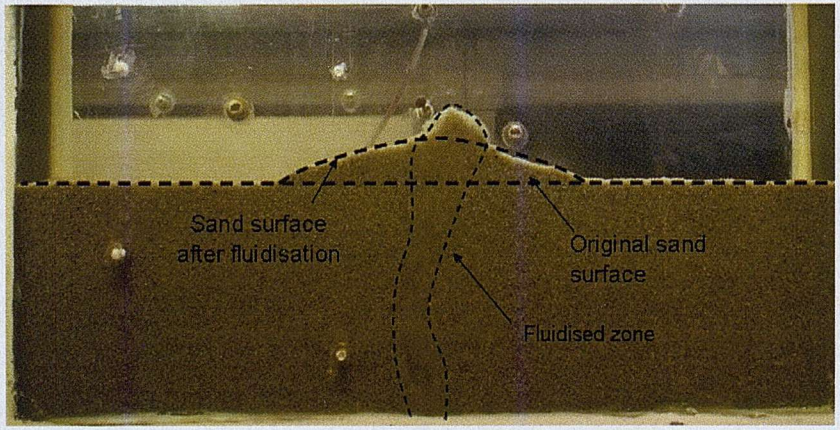

(g)

Figure 3.26b: Development of internal fluidisation in a 150 mm bed height of LBS-B. Orifice opening: 0.33mm.

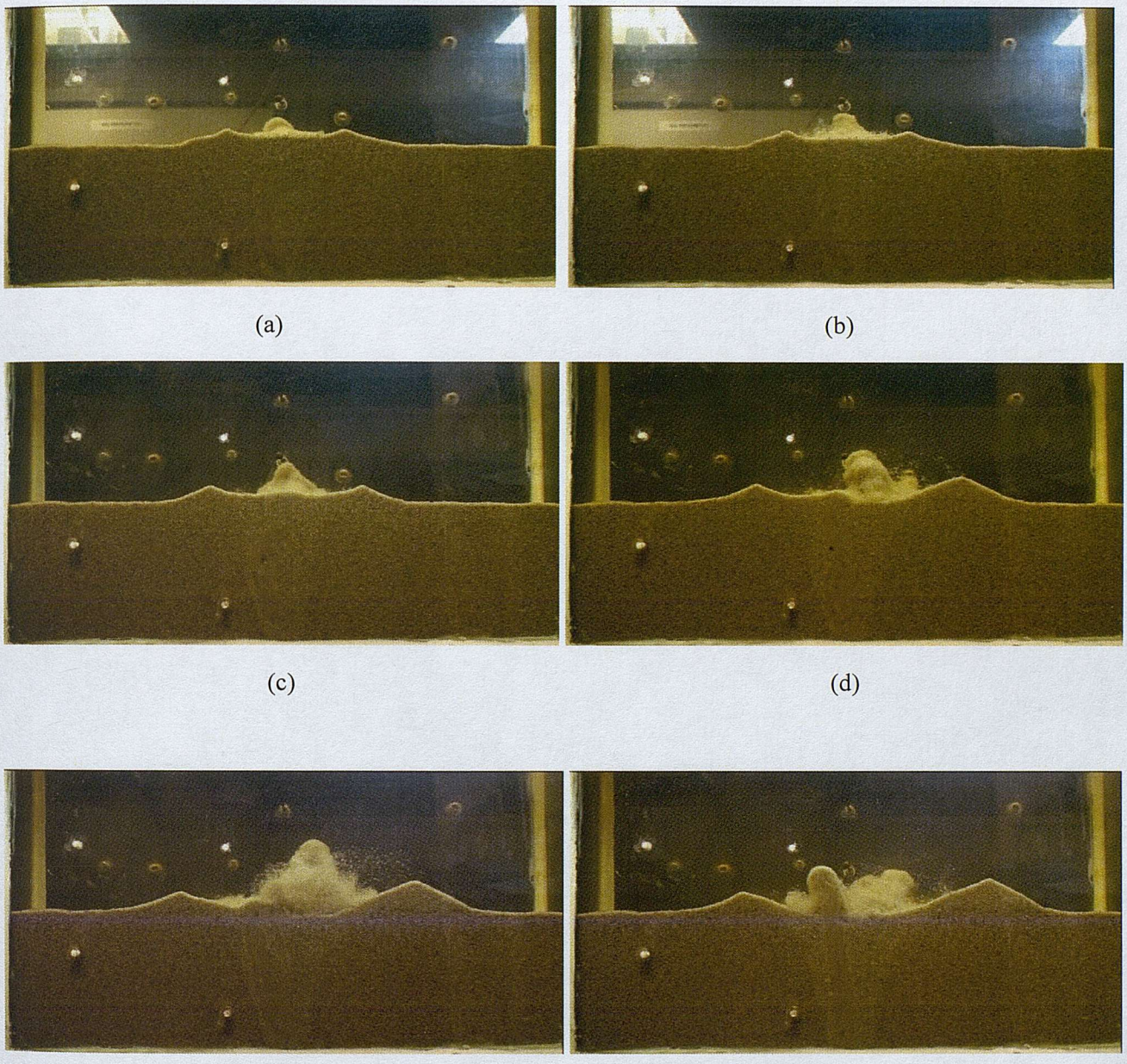

(a) (b)

(c) (d)

(e) (f)

Figure 3.27: Boiling of sand particles at the surface of the bed at different flow rates: (a) 700 l/h; (b) 800 l/h; (c) 900 l/h: (d) 1000 l/h; (e) 1100 l/h; and (f) 1200 l/h. Bed height 150mm of LBS-B, and orifice opening: 0.33mm.

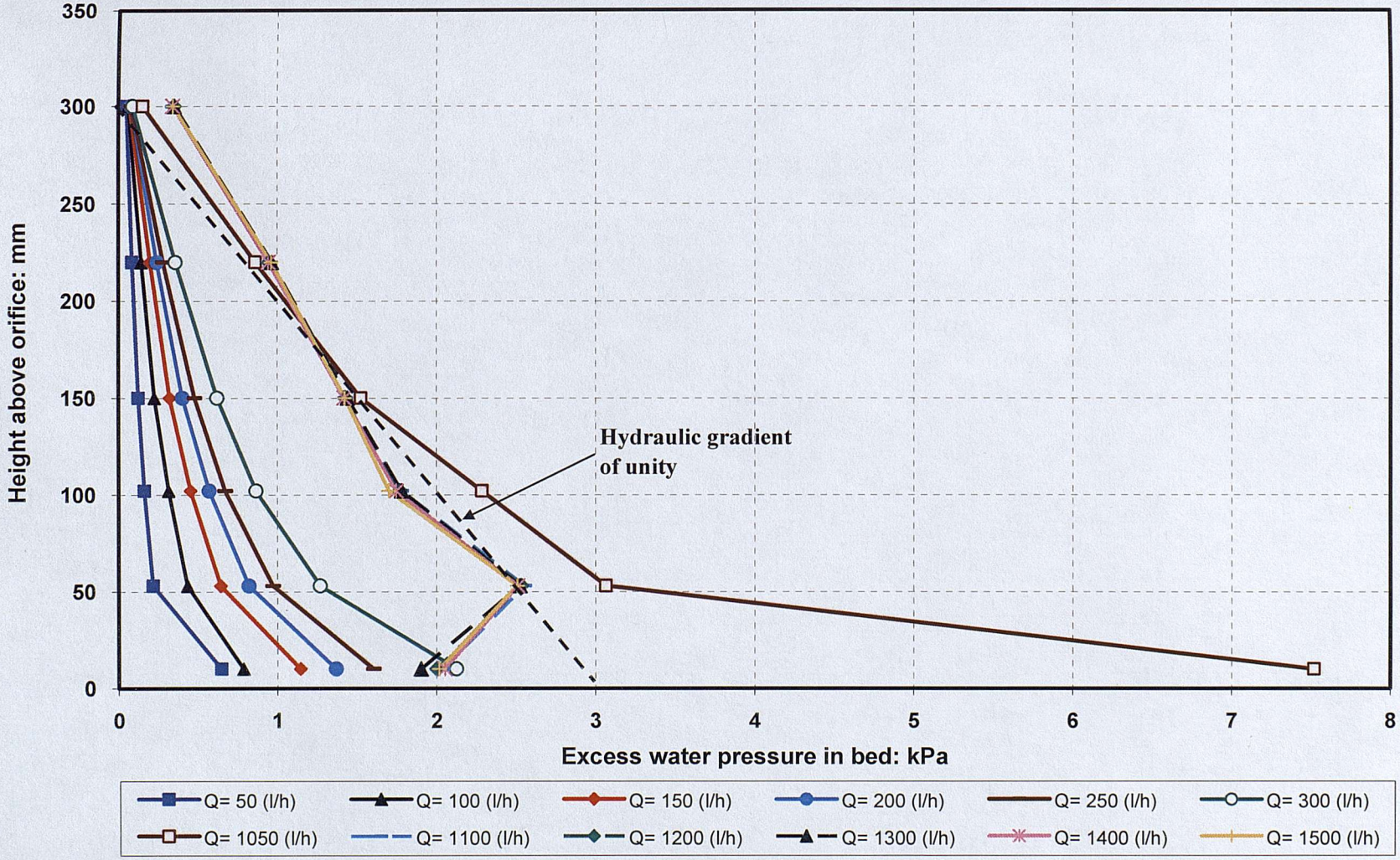

Figure 3.28: Excess pore water pressures at different points along 300mm bed height of LBS-B, orifice opening: 0.62mm.

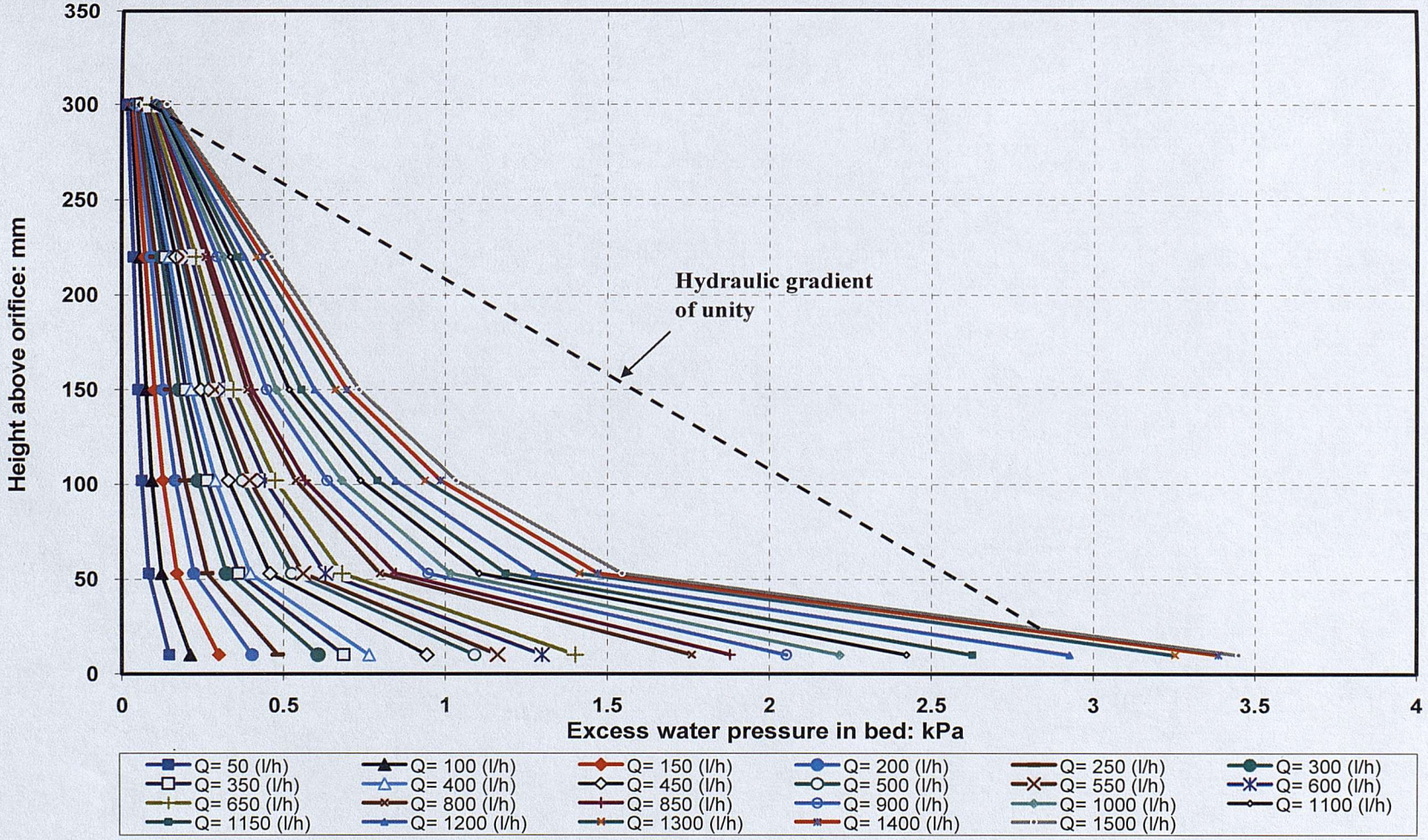

Figure 3.29: Excess pore water pressures at different points along 300mm bed height of LBS-A, orifice opening: 0.62mm.

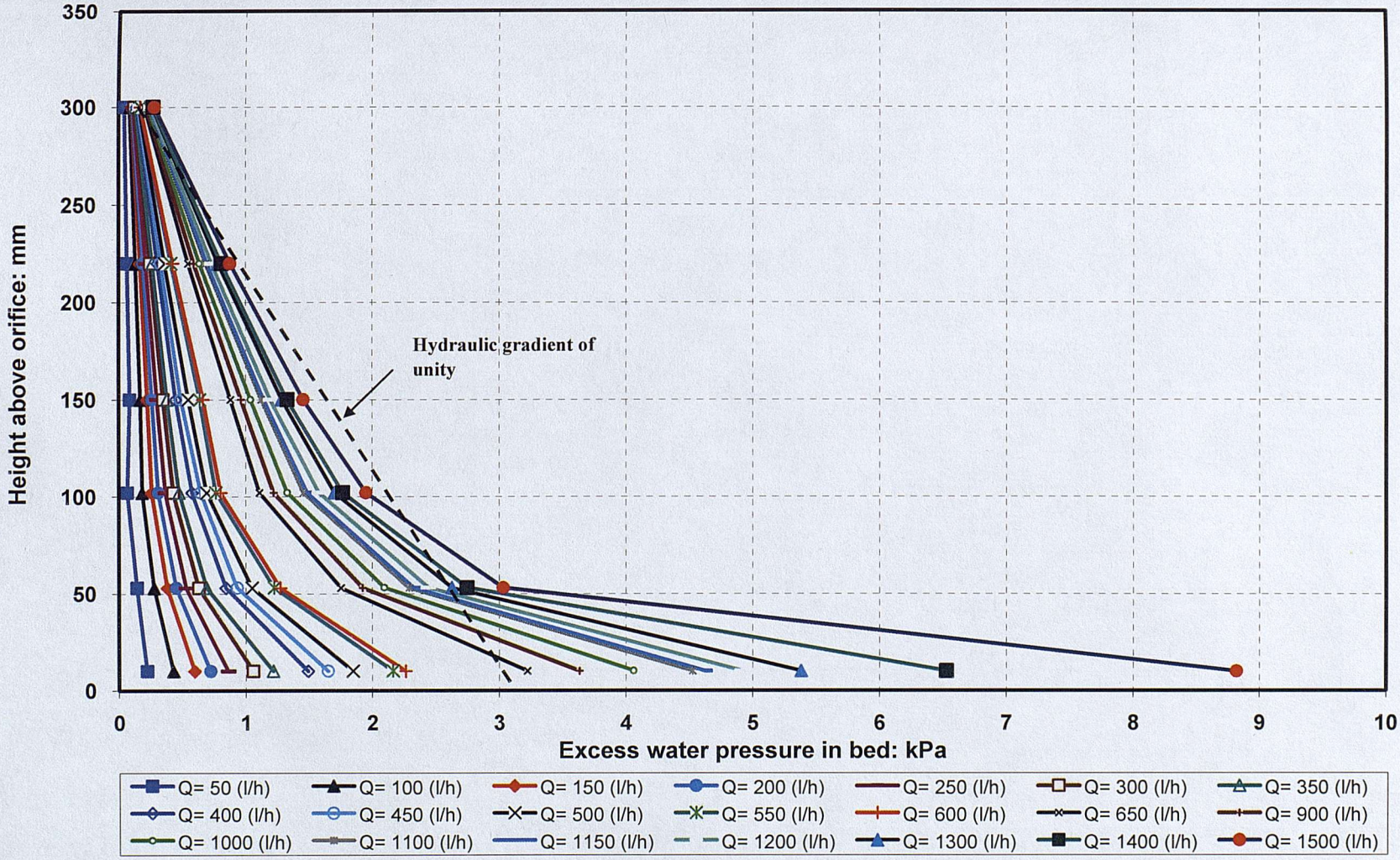

Figure 3.30: Excess pore water pressures at different points along 300mm bed height of glass ballotini, orifice opening: 0.62mm.

CHAPTER 4 DISCUSSION

This chapter presents and discusses the results and observations from this study. These include the observed mechanisms, hydraulic pressure distribution in the bed of materials, and the pressure v. flow-rate relationship. It also presents and discusses the effect of particle characteristics i.e. size and form of the grain, bed height, and size of the orifice opening on the onset of fluidisation. It then presents and discusses a theoretical model for predicting the excess pore water pressure at the onset of fluidisation and compares the predictions with measurements from experiments. Finally, conclusions from the discussion are presented at the end of the chapter.

4.1 Observed mechanisms

An internally fluidised zone was observed in the vicinity of the injection point, due to the build up of water pressure and increase in the hydraulic gradient at the point source of leakage. Analysis of the produced data and images indicate that the onset of this phenomenon is associated with an uplift mechanism of the granular materials above the injection point.

All conducted experiments where internal fluidisation had been observed, suggest that the observed mechanisms occurred in the following sequence:

(i) Fluid flow through the orifice into the bed of granular materials led to the build up of water pressure and an increase in hydraulic gradients in the vicinity of the orifice until they reached a certain point;

(ii) At this point, an uplift mechanism of the particles above the orifice occurred, during which the particles were lifted in an upward direction to a certain level and then remained fixed. Peak water pressure and peak hydraulic gradients were associated with this point.

(iii) Immediately after the uplift mechanism of the particles had occurred, an abrupt drop in the excess pore pressure in the vicinity of the orifice was observed. This was then followed by:

(iv) Formation of an internally fluidised zone in the vicinity of the orifice (in which the particles appeared to move freely, whilst those outside the region remained fixed);

(v) Propagation of the internally fluidised zone as flow rate was increased, until eventually it might break through to the bed surface.

The fluidised zone grew from the bottom (i.e. at the injection point) to the top. At the same time the excess pore pressure in the vicinity of the injection point decreased fairly sharply. The test results showed that a high pressure could be sustained upstream of the orifice without the internally fluidised zone breaking through to the bed surface.

4.1.1 The internally fluidised zone

Observation of the experimental results indicated that as the rate of flow through the orifice was increased by increasing pressure upstream of the orifice, the bed initially remained fixed. At a particular flow rate, i.e. 1177 *l/h* corresponding to pressure of 83 kPa Figure 4.1(a), the particles above the orifice were lifted in an upward direction to a certain level because of equilibrium with the upward drag force caused by the fluid (i.e. water), see Figure 4.1. This is the point of the onset of fluidisation. Immediately after uplift, the particles at the bottom of the bed (i.e. in the vicinity of the orifice) started to circulate rapidly, forming an internally fluidised zone (see Figure 4.2). Inside this zone the particles moved with the jet of water (i.e. the particles were picked up by the jet of water and carried out to the top of the jet in the centre and then slowly moved down on the side), whilst those outside the zone remained fixed in the bed. (See video in Appendix D for supplementary data attached in the CD). This mechanism is similar to the cavity formed in a bed of granular materials, also termed a raceway cavity, in chemical and process engineering, which is produced by injecting air or gas through a

pipe into beds of granular materials (MacDonald and Bridgwater, 1997; Singh et al., 2007). The onset of this mechanism can be attributed to the progressive build up of water pressure and increase in hydraulic gradient at the orifice-particle interface.

The experimental results showed that a high pressure can be sustained upstream of an orifice bedded within a shallow bed of granular material without the fluidised zone breaking through into the bed surface. Figure 4.3 shows the development of the internally fluidised zone as a function of pressure upstream of the orifice. Inspection of the figure shows that in the early stages of its development, as pressure upstream of the orifice increased to a certain limit (i.e. up to 130 kPa) no noticeable enlargement was observed in the size of the fluidised zone. For example, after increasing the pressure from 83 kPa to 100 kPa, the height of the fluidised zone remained unchanged at about 45 mm above the orifice. The rate of flow at these pressure values (i.e. 83 kPa and 100 kPa) increased slightly from 1177 *l/h* to 1218 *l/h*, respectively. When increasing the pressure to 130 kPa, the height of fluidised zone increased to only 60 mm above the orifice, and the rate of flow to 1233 *l/h*.

When the pressure upstream of the orifice was increased to 190 kPa, corresponding to a flow rate of 1215 *l/h*, the height of the fluidised zone increased to about 100 mm above the orifice. Unexpectedly, this point was associated with a slight drop in the rate of flow (by about 1%), measured at the downstream point of the system. This may be because the particles in the fluidised zone moved as an integral part of the fluid. By further increasing the pressure to 256 kPa, the height of the fluidised zone enlarged to just 110 mm above the orifice (see Figure 4.3). Interestingly, such high pressure was sustained upstream of the orifice, and only about one-third of the 300 mm bed height of the granular material was fluidised. This suggests that the pressure head upstream of the orifice was dissipated in the orifice and also inside the fluidised zone.

The mechanism of internal fluidisation observed in this study is different from the widely known piping phenomenon – the classic backward erosion. As seen in this study,

internal fluidisation occurs due to flow along a pre-existing opening which may occur in the middle of the structure due to leakage through cracks or holes in the structure, where the particles move in a localised zone with pore fluid; whereas the piping phenomenon initiates at the exit point of seepage and progresses backward along the structure base, resulting in the formation of a continuous passage or pipe. Rather than being initiated by the Darcy's flow at an exit point, internal fluidisation is initiated by seepage forces in the middle of the body due to localised leakage in which non-laminar flow is expected to occur.

4.1.2 The uplift mechanism

As mentioned above, the experimental results of this study indicate that the onset of fluidisation is associated with an uplift mechanism of the particles above the orifice. During this mechanism the particles were lifted in an upward direction to a certain level and then remained fixed; this was followed by the formation of an internally fluidised zone.

The deformation of the bed material by uplift over the point of fluidisation is shown for an orifice opening of 0.33 mm Figure 4.4. Inspection of the figure indicates that the mechanism resembled an inverted tapered block, surrounded by distributed shear zones extending outwards from the injecting point and widening towards the surface, with a maximum displacement at the uplift mechanism that was in the order of 1.5 mm. It is interesting to note that this observed mechanism is similar to the uplift mechanism of pipes buried in sand which may occur as a result of thermal buckling (Cheuk et al., 2008). For example, oil and gas pipelines normally operate at a high temperature (i.e. 160 C°) and pressure (i.e. 70 MPa) in order to ease the flow. Under such operational conditions axial thermal expansion can be generated which is restrained by friction at the particles-pipe interface and at the end connections. This in turn can generate axial compressive forces (i.e. ~1.5 MN) leading to a vulnerability to buckling in either the vertical or lateral direction (Hooper et al., 2004). The uplift mechanism of the particles

observed in this study is attributable to the build of water pressure and increase in hydraulic gradients in a bed of granular materials as a result of localised leakage.

Vertical displacement profiles during development of an internally fluidised zone in a 150 mm bed height of LBS-B are shown in Figure 4.5. The displacement at different sections (i.e. 20 mm, 50 mm, 75 mm, 100 mm, and 130 mm) of the bed height was obtained at heights of internally fluidised zone of 16 mm, 25 mm, 55mm, and 76 mm (Figure 4.5a-d). The profiles show that very small displacements occurred at the start of the fluidised zone, and these displacements increased with increasing its height. For example, at height of fluidised zone of 16 mm from the source of flow, the displacement along its centreline was in the order of 3.7 mm (Figure 4.5a). This was then increased to about 6.9 mm at a height in the fluidised zone of 25 mm (Figure 4.5b). Higher in the fluidised zone, i.e. 55 mm, the vertical displacement increased to about 18.8 mm. The above data would suggest that if an internally fluidised zone developed in the middle body of a structure it may be difficult to detect or observe without measurements.

The inclination angle of the wedge of the uplifted zone for orifice openings ranging between 0.92 mm and 0.33 mm is shown in Figures 4.6a and 4.6b. The figures show that the angle is neither influenced by the size of orifice opening nor by the height of the bed for the tested conditions. The measured inclination angle, defined by drawing a straight line passing along the shear distributed zone starting at the injection point at the bottom of the bed to the bed surface, ranged between 63.2° and 64.8°; with an average angle of 63.8 °.

4.2 Excess Pore Water Pressure Distribution in the bed of material.

Distribution of excess pore water pressure along the bed height of granular materials shows very interesting behaviour with a critical hydraulic gradient at the onset of fluidisation different from that suggested by seepage failure theory.

Figure 4.7 shows profiles of excess pore water pressure above the injection point in the bed of granular material for an orifice opening of 0.92 mm. A general observation of the pore water pressure distribution on vertical plane showed that increasing the rate of flow resulted in a progressive build up of the excess pore water pressure in the bed of material, with a maximum value in the immediate vicinity of the orifice. The hydraulic gradient ($\Delta h/\Delta l$) in the vicinity of the orifice is greater than unity, while further away from it, within about 50 mm in the vertical direction, the excess pore water pressure decreases linearly with height until it becomes atmospheric at the bed surface. This is limited to a low flow rate, e.g. 100 *l/h*; at a higher flow rate, e.g. 1000 *l/h*, the linearity in the excess pore water pressure with height was not seen until 150 mm away from the injecting point. This observed behaviour can be attributed to the geometry of the flow, as it is expected that a leak from a point source (or localised leakage) will spread radially. The discharge velocity is very large near the orifice but decreases sharply as the jet penetrates further into the granular material. This suggests that the jet flow propagates under turbulent conditions in the inner region of the orifice-soil interaction and under laminar conditions in the outer ones. Assuming a rate of flow of 1042 *l/h*, and cross sectional area of flow at the orifice 10 mm x 147 mm give a Reynolds number (Re) of 196, indicating that the flow in this region is turbulent. Further away from the orifice at cross sectional area of 250 mm x 147 mm, the estimated Re is 7.79 indicating that the flow is laminar in this region.

The progressive build up of pore water pressure in the bed of materials continued to increase as flow rate was increased, until it reached a maximum value at the onset of fluidisation (Figure 4.7). For instance, when the rate flow was increased to 1490 *l/h* the excess pore water pressure at the orifice-grain interface peaked at a value of 6.6 kPa. At this point, the maximum gradient of excess pore pressure against depth was 2.2.

It is interesting to note that the critical hydraulic gradient observed in this mechanism exceeded that suggested by theories of seepage flow (i.e. the critical gradient at which failure will occur is about one, based on Terzaghi's failure theory, 1922). One

explanation for this is that the distribution of internal stress in the bed of granular materials influenced the critical gradient at which fluidisation took place. As discussed above, due to the nature of localised leakage in a bed of granular material the flow velocity tends to be relatively high in the vicinity of the source of leakage; and this is often the place where increasing hydraulic gradients express themselves. This is demonstrated in Figure 4.8 which shows the profile of excess pore water pressure along the 300 mm bed of glass ballotini due to flow through an orifice opening of 0.92 mm. As shown in the figure, at a given flow rate of 1490 *l/h* the hydraulic gradient in the vicinity of the orifice (i.e. within 50 mm from it) was very high at about 8.9, much higher than that in the upper 250 mm of the sample: i.e. 1.02.

The onset of fluidisation due to localised leakage in a bed of granular material is associated with an abrupt drop in excess pore water pressures at the orifice-soil interface. Figure 4.9 shows the local excess pore pressures above the jet in the bed of granular material as a function of flow rate. Observation of the figure indicate that as the rate of flow through the orifice is increased the excess pore pressure in the bed increases correspondingly, most significantly at the orifice-soil interface, and a smaller amount further away from the orifice (i.e. equivalent to a ratio of about 4 to 1). Once fluidisation took place a drop in the excess pore pressure at the orifice-soil interface was observed. The pore pressure dropped from a peak of 6.6 kPa to 4.0 kPa corresponding to flow rates of 1490 *l/h* and 1630 *l/h*, respectively. This observed behaviour can be attributed to the "unblocking" and uplift mechanisms of the particles above the orifice, where it created a space for the particles to form an internally fluidised zone (in which the particles started to circulate allowing conversion of the potential energy into kinetic energy, i.e. velocity head).

4.3 Pressure-flow rate relationship

In order to study the pressure-flow rate relationship and the effect of fluidisation of granular materials on it, it was essential to look at the free flow condition (submerged orifice), and then compare it with the flow into a bed of granular materials. A comparison of the data shows very interesting behaviour with different phases depending on the rate of flow and whether it is free flow, or flow into a bed of granular materials (see Figures 4.10 to 4.12). These phases are discussed below.

Free flow condition (submerged office)

The pressure-flow rate relationship under the free flow condition for different orifice openings; 0.33 mm, 0.62 mm and 0.92 mm was obtained experimentally as well as theoretically (using the standard orifice flow equation) and is plotted in Figure 4.10. Comparison between calculated and measured flow rate for each particular orifice opening is presented in Appendix D.

Inspection of the pressure flow rate relationship shows very interesting behaviour (Figure 4.10). The data show that initially the rate of flow varies with pressure according to the orifice flow theory (i.e. flow rate varies with square root of the applied head). At a particular rate of flow, i.e. 1000 *l/h* for the 0.33 mm orifice opening and 1300 *l/h* for the 0.62 mm orifice opening, a deviation from the orifice flow equation was observed, but not in the case of the 0.92 mm orifice opening (Figure 4.10). At these points, higher pressures were required to deliver more flow. For example, in the case of the 0.33 mm orifice opening, increasing the rate of flow from 1000 *l/h to* 1100 *l/h* resulted in an increase in pressure from 44 kPa to 66 kPa. This deviation from the orifice flow equation may possibly be attributed to the phenomenon of cavitation (flow separation) in the orifice. This phenomenon occurs at very high velocity in the orifice, where the pressure of the liquid drops below its vapour pressure. During this mechanism a vapour region is thought to form inside the orifice resulting in a reduction in the effective area of the flow, until a point is reached where there is no further increase in the rate flow as

pressure increased (Figure 4.11). This observation is consistent with the findings of Koivula (2002) who also observed a similar phenomenon in a small orifice

The theory of fluid mechanics also supports the view that the cavitation phenomenon may occur in these conducted experiments. Using the non-dimensional parameter cavitation number k_c for estimating the resistance of flow to cavitation:

$$K_c = \frac{2(p_d - p_v)}{\rho.v^2}$$

The higher k_c the less likely cavitation is to occur. A critical cavitation number of between 1.5 and 0.2 is reported, below which the cavitation is likely to appear (Lam, 1987). Assuming a pressure downstream of the orifice of 3 kPa (3000Pa), corresponding to a velocity through the orifice of 7.6 m/s, the density and vapour pressure of water at 20C° are 998.2 kg/m³ and 2400 Pa, respectively. This gives a cavitation number (k_c) in these experiments of 0.02, indicating that the cavitation phenomenon may occur at this point.

Flow into bed of granular materials

The pressure-flow rate relationship for the condition of flow into beds of granular materials shows very interesting behaviour. Five different phases have been observed experimentally depending on the rate of flow. These are marked as A, B, C, D and E on the curve depicted in Figure 4.12. The figure shows the pressure flow rate relationship when water was injected into a 220 mm bed height of LBS-B through an orifice opening of 0.33 mm.

Inspection of the flgure shows that the first phase (**A**) occurred at a low flow rate, i.e. from the point of injecting flow until a flow rate of 110 *l/h* was achieved, Figure 4.12. In this phase a linear relationship between pressure and the rate flow was observed, adhering to Darcy's flow. This indicates that in this phase the flow rate was controlled by bed head loss. In the second phase (**B**), a deviation from Darcy flow was observed,

which took place at a slightly higher flow rate (i.e. 150 *l/h* to 250 *l/h*). In this phase higher pressure was required to deliver more flow. For instance, increasing the rate of flow from 150 to 250 *l/h* resulted in an increase in pressure from 7.6 kPa to 20.6 kPa. This is possibly due to the combined effect of orifice and bed material on the pressure-flow rate relationship.

At a certain flow rate, i.e. 300 *l/h*, phase **C** occurred (Figure 4.12). At this point a sudden drop in the pressure upstream of the orifice was observed which was associated with a jump in the rate of flow. In this phase less pressure was required to deliver more flow. For example, an increase in pressure from just 22.6 kPa to 25.7 kPa resulted in a jump in the rate of flow from 300 *l/h to* 750 *l/h*. This can be attributed to the onset of fluidisation, i.e. the uplift mechanism of the particles above orifice.

The fourth phase (**D**) was initiated after the onset of fluidisation; i.e. at flow rate of 750 *l/h* and continued until a flow rate of 1000 *l/h* was achieved (see Figure 4.12). In this phase the pressure upstream of the orifice was proportional to the flow squared, following the orifice flow theory. It is interesting to note that this phase is similar to the first phase of the free flow condition, suggesting that after the point of fluidisation particles have no effect on the rate of flow.

In the fifth phase **(E)**, a deviation from the orifice flow equation was observed at high flow rates (i.e.>1000 *l/h*). In this phase a higher pressure was required to deliver more flow than was predicted by the orifice flow equation. It is interesting to note that this phase is also similar to the behaviour observed at high flow rate (i.e. 1000 l/h) in the free flow condition (see Figure 4.12). Increasing flow rate from 1040 l/h to 1100 l/h resulted in an increase in pressure from 53.6 kPa to 64.4 kPa. This observed behaviour can also be attributed to cavitation development in the orifice due to the high velocity in the orifice as discussed above.

Similar pressure-flow rate relationships were also observed for different orifice openings; 0.62 mm and 0.92 mm (Figures 4.13 and 4.14), respectively.

Inspection of the pressure-flow rate relationship indicates that at the onset of fluidisation, the pressure upstream of the orifice dropped significantly (48%) for the larger orifice size and by a relatively small amount (14%) for the smaller orifice size. This is because for small openings most of the head loss was orifice loss rather than bed loss. The drop in the pressure was associated with a sudden increase in the rate of flow, and thus can be attributed to the uplift mechanism of the granular materials above the orifice as a result of the upward drag force of the fluid.

Figure 4.15 shows the calculated coefficient of discharge C_d for the tested orifice opening of 0.336 mm under the above two conditions: free flow conditions and flow into a bed of granular material, i.e. silica sand. It can be seen that in both cases the value of C_d changes depending on the applied head. Its values range between 0.18 and 0.6 in the case of discharge into soil and between 0.33 and 0.6 for the free flow condition. The results also show that before the point of fluidisation, in the case of flow into silica sand, the value C_d was reduced by approximately 48% of that under conditions of free flow. The reduction in the value of C_d probably resulted from the presence of particles around the orifice, which modified the jet behaviour and also reduced the effective area of the orifice. However, after fluidisation, a jump in the value of C_d was observed. At this point the value of C_d increased to a maximum value of 0.6 corresponding to a head upstream of the orifice of 6.12 m. Beyond this point it started decreasing as the head upstream of the orifice increased. The reduction in the value of C_d in this stage can possibly be attributed to the formation of a vapour region in the orifice, which is thought to form at high velocity, resulting in a reduction in its effective area.

The above data would seem to contradict Walski et al.'s (2006) view that the flow from a leak can generally be modelled with the orifice flow equation. The results of this study

show that there are limits to the validity of this equation. It shows that even when the bedding materials become fluidised, the orifice flow equation still may not be valid due to the occurrence of cavitation (i.e. flow separation) in the orifice as discussed above.

4.4 Effect of particle characteristics and bed height

The results of this study show that characteristics of granular materials such as size and form (i.e. sphericity) of the grains, and the height of the bed have a significant effect on the excess pore water pressure required for the onset of fluidisation.

4.4.1 Effect of particle size

Figures 4.16 and 4.17 show the excess pore water pressure distribution along a 300 mm bed of granular material of two different grain sizes; silica sand (d_{50}=0.9 mm) and LBS-A (d_{50}=1.6 mm), at an orifice opening of 0.234 mm. The figures show that at any given flow rate the finer the particles, (i.e. silica sand), the higher the build up of pore water pressure compared to the coarser particles, (i.e. LBS-A), as this is a function of soil permeability. For example at a flow rate of 812 l/h, the excess pore water pressure at the bottom of the bed was about 7 kPa for the silica sand, compared to only 2.6 kPa for the LBS-A at the same flow rate.

The increase in the build up of pore water pressure within the bed of finer particles led to an increased potential for fluidisation. This is shown in Figure 4.18 when a 0.62 mm orifice opening was used to deliver water into a 300 mm bed of LBS-B (d_{50}=0.9 mm). As a result of the increase in flow rate the build up of pore water pressure in the bed of material increased correspondingly. At a certain rate of flow, i.e. 1050 l/h, the pore water pressure reached its maximum value of 7.6 kPa, the point at which fluidisation of the material took place. For the coarser soil particles, LBS-A (d_{50}=1.6 mm), a higher flow rate was required for the onset of fluidisation; however, due to the limitations of the apparatus, a sufficient flow rate could not be provided to fluidise this type of material.

The system reached its capacity at a flow rate of 1500 l/h, which was not sufficient to fluidise this material (Figure 4.19).

In relation to the amount of energy needed to force water through the pores in the soil bed, the higher the permeability, the lower energy needed. The rate of energy loss for the tested materials was measured by the steepness of the hydraulic gradient. As expected the results showed that a steep hydraulic gradient was obtained for the finer particles; silica sand and LBS-B, both of which have d_{50} of 0.9 mm, and a flat gradient for the coarser particles, LBS-A which have a d_{50} of 1.6, as shown in Figure 4.20.

4.4.2 Effects of particle form

Particle form, i.e. a measure of the overall shape of a particle - sometimes measured in terms of "sphericity" - has a major effect on the excess pore water generation in the bed of granular material. The build up of pore water pressure increased with decreasing form, and this led to increase potential for fluidisation. Figures 4.21 and 4.22 show profiles of excess pore water pressure generation as a function of flow rate for two sands with different forms; Leighton Buzzard sand - fraction B (LBS-B) with a sphericity of 0.552, and glass ballotini (GB) having a high sphericity of about 1. Inspection of the figures indicates that at any given flow rate higher build up of excess pore water pressure occurred for LBS-B compared to that of the glass ballotini. For example, at a rate of flow of 300 l/h the pore pressure for the LBS-B was about 2.12 kPa, compared to only 1 kPa for the GB at the same flow rate (Figures 4.21 and 4.22, respectively). This indicates that particles with high sphericity required much higher flow rate for the onset of fluidisation. In these particular tests, fluidisation of the LBS-B occurred at a flow rate of about 1050 l/h, corresponding to excess pore pressure of 7.52 kPa, whereas for the GB the onset of fluidisation occurred at a flow rate of about 1500 *l/h*, corresponding to pore pressure of 8.8 kPa, as shown in Figures 4.21 and 4.22, respectively.

4.4.3 Effect of bed height

Figures 4.23 to 4.25 show profiles of excess pore water pressure as a function of flow rate for three different bed heights; namely 150 mm, 220 mm, and 300 mm, respectively. The bed material in all three cases was LBS-B with an effective particle diameter of 0.9 mm. Inspection of the data in the figures indicates that the higher the bed materials the larger is the excess pore water pressure required for the onset of fluidisation. For instance, when the height of the bed was 150 mm the pore water pressure required for the onset of fluidisation was 2.63 kPa. By increasing the height of the bed further to 220 mm and then to 300 mm the pore pressures to initiate fluidisation increased further to 4.78 kPa and 7.38 kPa (Figures 4.24 and 4.25) respectively. Similarly for the rate of flow, increasing the bed height resulted in an increase in the rate of flow required to fluidise the bed of materials. For example, at bed heights of 150 mm, 220 mm, and 300 mm the rates of flow required to fluidise these beds were 450 *l/h*, 730 *l/h* and 1042 *l/h* (Figures 4.23 to 4.25) respectively. As expected this is because of the increase in the bulk weight of the bed.

4.5 Effect of the size of the orifice opening

To study the effect of the orifice opening size on the onset of internal fluidisation tests were carried out on four different sizes; namely 0.234 mm, 0.336 mm, 0.62 mm, and 0.92 mm, all of which had squared edges with a wall thickness of 10 mm. The tests were conducted on silica sand and LBS-B, both of which have an effective particle diameter of 0.9 mm. The tests results are shown in Figures 4.26 to 4.29 for orifice openings of 0.234 mm, 0.33 mm, 0.62 mm and 0.92 mm, respectively. A summary of these results is also presented in Table 4.1.

Inspection of Figures 4.26 to 4.29 shows that the size of the orifice does not have an effect on the distribution of excess pore water pressure in the bed of granular materials. However, these profiles were controlled by the discharge flow rate. For example, at flow

rate of 600 l/h, the value of excess pore water pressure at 10 mm above the orifice was of the order of 4.5 kPa regardless of orifice size (Figures 4.26 to 4.29). However, pressure (i.e. upstream of orifice) was very dependent on the size of the orifice. The smaller the orifice size the larger was the pressure upstream of the orifice required for the onset of fluidisation (see Table 4.1). This observation is consistent with Weisman and Lennon's (1994) experiment on the design of fluidiser systems for the coastal environment. Inspection of the table shows that for an orifice opening of 0.92 mm a pressure upstream of the orifice of 15.2 kPa was sufficient to fluidise a 300 mm bed of LBS-B, whereas when the orifice opening was reduced to 0.62 mm a higher pressure, i.e. 23.1 kPa, was required to fluidise a similar bed having the same height. For the smaller orifice opening, i.e. 0.234 mm, much higher pressure upstream of the orifice was applied, i.e. 269 kPa, but it still did not fluidise the bed of sand. This is because the smaller orifice opening did not provide sufficient flow rate to fluidise the bed material.

The ratios of head loss through the orifice to that in the bed of granular material were calculated for orifice openings of 0.234 mm and 0.336 mm and are presented in Tables 4.2 and 4.3 respectively. The tests were conducted on similar bed material, i.e. a 300 mm height of silica sand. Inspection of the tables indicates that most of the head loss was dissipated through the orifice while a relatively small amount was dissipated through the bed of granular materials. For example, for the smallest orifice opening, (i.e. 0.234 mm), an average of 94% of the head upstream of the orifice was dissipated in the orifice, while the remaining 6% was dissipated through the sand bed (Table 4.2). For the larger orifice opening, (i.e. 0.336 mm), the proportion of head loss through the orifice remained the highest Table 4.3. However, at a certain point just before the onset of fluidisation, it reached a minimum of 83%, and the remaining 17% was dissipated through the sand. After the point of fluidisation, the ratio of head loss through the orifice increased until it reached 99% of the high applied head (Table 4.3).

The above data would seem to be consistent with Walski et al.'s (2006) view that the head loss due to Darcy's flow through soil will be generally much smaller than that due

to orifice flow. For example assuming a constant head loss due to Darcy's flow of 0.884 m gives orifice/soil ratio (h_o / h_s) in these experiments that varies from about 5.5 (for the 0.336 mm orifice) to over 20 (for the 0.234 mm orifice). However, the results of this study showed that significant head can be sustained upstream of the orifice, and that the fluidised zone still did not break through to the bed surface, even through this was only 300 mm deep (as discussed in section 4.1.1). This indicates that the pressure upstream of the orifice was actually dissipated in different phases; (i) through the orifice (i.e. conversion into velocity head i.e. kinetic energy), (ii) pressure loss due to cavitation development in the orifice (formation of vapour pressure at high velocity), and (iii) dissipation of velocity head (kinetic energy) downstream of the orifice in the internally fluidised zone.

4.6 Modelling pore pressure at the onset of the internally fluidised zone

Based on the results and observations of the experimental tests of this study a mathematical model is presented for predicting the excess pore water pressure at the onset of fluidisation. The model is based on the concept of force equilibrium exerted on the particles in the bed.

Inspection of the behaviour of the fluidised bed and the obtained results indicates that as the rate of flow through the orifice increased the excess pore water pressure in the bed of material also increased, with a maximum value at the orifice-soil interface. At a particular flow rate, the pore pressure reached its maximum value, the point at which an active zone of the bed (i.e. above the orifice) was lifted in an upward direction to a certain level (See Figure 4-30). This was followed by the formation of an internally fluidised zone in the vicinity of the orifice. The uplift mechanism of the active region of the bed (i.e. the onset of fluidisation) was due to equilibrium of forces; the downward active weight of the bed balancing the upward drag force generated by the fluid (i.e. water).

Observation of the geometry of the active region of the bed at the onset of fluidisation indicated that it resembled a tapered shape, with a cross sectional area that increased continuously from the bottom to the top (See Figure 4-30). The area of the flow region therefore increased with height causing the velocity to decrease. Under such flow geometry non-laminar flow is expected to occur and hence Darcy's flow is not valid (as discussed previously in section 4.2).

The particle drag force, which is proportional to the velocity squared, varies with the height of the bed. It has maximum values near the orifice and continuously decreases up the height of the bed (i.e. in the upward direction-Figure 4-30). In this case the Ergun's model (section 2.3.1), which is developed on the hypothesis of a uniform flow to predict pressure loss in a columnar packed bed, also cannot be applied in its current state because of the variation in the velocity along the height of the bed. Shi et al. (1984) and Peng and Fan (1997) proposed models which incorporated the Ergun's equation to predict the point of the onset of fluidisation in a tapered bed. The approach that they have used is based on the dynamic balance of forces exerted on the particle bed. Adopting the same approach used by Shi et al. (1984) and Peng and Fan (1997), the maximum pore water pressure at the onset of the internally fluidised zone can be predicted. The model has been applied in this study under three assumptions:

(i) At the onset of fluidisation it is assumed that the fluid flows in the vertical direction, and any lateral flow is sufficiently small to be neglected,

(ii) The flow is assumed to be vertical and uniformly distributed at any cross sectional area of the active bed, and

(iii) The friction between the particles and the walls is neglected.

The upward drag force applied by fluid:

Observation of the geometry of the active zone of bed at the onset of internal fluidisation shows that it resembled an inverted tapered block (Figure 4.30). The upward drag force exerted on the particles in the bed therefore is not directly proportional to pressure loss

Shi et al. (1984). This drag force in a differential bed height of (dh) equals the pressure loss through it (i.e. differential pressure) times the cross sectional area of the active bed ($\bar{L}W$), (see Figure 3.30).

$$dF = (\bar{L}W).(dp) \tag{4-2}$$

$$F = \int_{h_o}^{h_o+H} dF \tag{4-3}$$

Where; F is the upward drag force by fluid, $\bar{L}$ length of active bed at height h, W is the width of the bed, and H is the height of the bed.

Pressure loss through a packed bed of a differential height can be determined using the Ergun's equation in its simplest form (Ergun, 1952);

$$\frac{\Delta P}{L} = AU + BU^2 \tag{4-4}$$

Where; U is the velocity, L is the length of a column bed, A and B Parameters of the Ergun's equation:

$$A = \frac{150 \cdot \mu}{\phi_s^2 \cdot d_p^2} \cdot \frac{(1-\varepsilon)^2}{\varepsilon^3}$$

$$B = \frac{1.75 \cdot \rho_w}{\phi_s \cdot d_p} \cdot \frac{(1-\varepsilon)}{\varepsilon^3}$$

For differential bed height the pressure loss take the form:

$$dp = (AU + BU^2)dh \tag{4-5}$$

Thus, the total drag force exerted on the particles in the active bed with height of H is (see Appendix B):

$$F = \int_{h_o}^{h_o+H} (\bar{L}W).(AU + BU^2)dh \tag{4-6}$$

$$F = (A.W.L_o.U_o.H) + (B.W.L_o^2.U_o^2.\frac{H}{L_1 - L_o}.\ln(L_1/L_o)) \tag{4-7}$$

where L_o is the size of the orifice, U_o is the velocity down stream of the orifice (i.e. at the bottom of the bed), L_1 is length of the active bed at height (H) and W is the width of the bed.

Downward force- bulk weight of the particles in the bed at the onset of fluidisation

The active weight of the particles in bed at the onset of internal fluidisation is (see appendix B):

$$W_a = \int_{h_0}^{h_o+H} g\ (1-\varepsilon)\ (\rho_s - \rho_w)\ \bar{L}\ W\ dh \qquad 4\text{-}8$$

Where; W_a is the active weight of the bed, g is the gravitational force.

$$W_a = \frac{1}{2}\ g\ (1-\varepsilon_o)\ (\rho_s - \rho_w)\ W\ H\ (L_1 + L_o) \qquad 4\text{-}9$$

Based on the proposed model, the particles at the bottom of the bed start to fluidise when the upward force by the fluid flow is in balance with the bulk weight of the bed F-W_a=0. Therefore, the critical velocity at which the particles start to fluidise can be calculated by equating the equations 4-7 and 4.9. This gives the critical velocity at the onset of fluidisation.

$$[(A.W.L_o.H)U_c + (B.W.L_o^2.\frac{H}{L_1 - L_o}.\ln(L_1/L_o))\ U_c^2] -$$

$$[\frac{1}{2}\ g\ (1-\varepsilon_o)\ (\rho_s - \rho_w)\ W\ H\ (L_1 + L_o)] = 0 \qquad 4\text{-}10$$

This equation can be written in a simple form;

$$aU_c^2 + bU_c - c = 0 \qquad 4\text{-}11$$

This is a quadratic, polynomial equation of the second degree:

$$U_c = \frac{-b + \sqrt{b^2 + 4ac}}{2a} \qquad 4\text{-}12$$

Where

U_c is the critical velocity at which fluidisation starts,

$a = B.W.L_o^2.\frac{H}{L_1 - L_o}.\ln(L_1/L_o)$

$$b = A.W.L_o.H$$

$$c = \frac{1}{2}\ g\ (1-\varepsilon_o)\ (\rho_s - \rho_w)\ W\ H\ (L_1 + L_o)$$

Knowing the velocity at the bottom of the bed at which fluidisation starts, pressure loss can be calculated from the following derived equation.

Prediction of the pressure loss through the bed at the onset of fluidisation:

Pressure loss through the bed with a differential height of *dh* equals to (Ergun, 1952):

$$dp = (AU + BU^2)dh \qquad 4.13$$

The total pressure loss through the active bed (which varies with height) can be obtained by integrating equation (4.13) (see appendix B).

$$\Delta P = \int_{h_o}^{ho+H} (dp)\ dh$$

$$\Delta P = \int_{h_o}^{ho+H} (AU + BU^2)\ dh \qquad 4.14$$

Integrating equation (4.14) gives (see appendix B):

$$\Delta P = A\ U_o\ \frac{H\ L_o}{L_1 - L_0}\ \ln(L_1/L_0) + B\ U_o^2\ \frac{H\ L_o}{L_1} \qquad 4.15$$

Thus to calculate the maximum pressure loss at the onset of fluidisation, U_o is replaced by U_c:

$$\Delta P_{max} = A\ U_c\ \frac{H\ L_o}{L_1 - L_0}\ \ln(L_1/L_0) + B\ U_c^2\ \frac{H\ L_o}{L_1} \qquad 4\text{-}16$$

This model is based on concept of force equilibrium in a two-dimensional fluidised bed, and takes into account the effect of variation in the velocity along the height of the bed. It incorporates the Ergun's equation (eq. 2.5), which describes the dependence of pressure loss on fluid velocity and packing properties. It takes into account the effect of

pressure loss due to viscous energy loss resulting from laminar flow at low velocity, and losses due to kinetic energy or inertial losses within granular media at higher flow velocity.

To examine the proposed model, the maximum pore water pressures at the onset of fluidisation for different bed materials were calculated and compared with those measured experimentally (see Figure 4.31). These include tests on three different materials; glass ballotini, silica sand, and Leighton Buzzard sand-Fraction-B. Parameters used for the model are presented in Table 4.4. Comparison of the data shows a good match was obtained between the predicted and measured values, with a maximum error of less than 10 % (see Figure 4.31). The experimental data indicate that the proposed model is valid and of practical use.

4.7 Summary

The present study suggests that the mechanism of internal fluidisation in a bed of granular material due to localised leakage occurs in the following sequence:

(i) Fluid flow through the orifice into the bed of granular materials leads to the build up of water pressure and an increase in hydraulic gradients in the vicinity of the orifice until they reached their peaks;

(ii) As the water pressures and hydraulic gradients peak, an uplift mechanism of the particles above the orifice occurs, during which the particles are lifted in an upward direction to a certain level and then remained fixed;

(iii) Immediately after the uplift mechanism of the particles has occurred, an abrupt drop in the excess pore pressure in the vicinity of the orifice is observed. This was then followed by:

(iv) An internally fluidised zone that formed in the vicinity of the orifice (in which the particles appeared to move freely, whilst those outside the region remain fixed);

(v) Propagation of the internally fluidised zone as flow rate was increased, until eventually it might break through to the bed surface.

It was found that a high pressure could be sustained upstream of the orifice without the internally fluidised zone breaking through to the bed surface.

- Deformation of the bed material during the uplift mechanism resembled an inverted tapered block, surrounded by distributed shear zones extending outwards from the point of injection and widening towards the surface. The weight of the bed material within the tapered block is equal to the uplift force due to seepage at the onset of fluidisation. The inclination angle of the wedge of the uplifted zone was neither influenced by the size of orifice opening nor by the height. It ranged between 63.2° and 64.8° with an average angle of 63.8°.

- Very small displacements (i.e. 3.7 mm) occurred during the uplift mechanism, which were associated with shallow heights (i.e. 16 mm) of the internally fluidised zone. This suggests that if an internally fluidised zone develops in the middle body of a structure it may be difficult to detect or to observe without measurements.

- Distribution of excess pore water pressure along the bed height of granular materials is affected by the geometry of the flow, and this produces a critical hydraulic gradient for the onset of fluidisation different from that suggested by piping failures theory. The average critical hydraulic gradients at the onset of fluidisation were found to be in the range of 1.5 and 3 for the tested conditions. The explanation for this is that the distribution of internal stress in the bed of granular materials influences the critical gradient at which fluidisation takes place. Due to the nature of a concentrated leakage in a bed of granular materials, the flow velocity is high in the vicinity of the source

leakage, and this is often the place where increasing hydraulic gradients express themselves.

- The relationship between pressure (i.e. upstream of the orifice) and flow rate is complex. Five different phases have been observed experimentally depending mainly on the rate of flow:

  (i) A linear relationship between pressure and flow rate was observed at low flow rate (i.e. up to 100 to 200 l/h), adhering to Darcy's flow.

  (ii) A deviation from Darcy's flow was observed at a slightly higher flow rate in which higher pressure was required to deliver more flow due to the combined effect of the orifice and bed material on the pressure-flow rate relationship.

  (iii) At a certain point of flow a sudden drop in pressure in the orifice was associated with a jump in the rate of flow due to the fluidisation effect.

  (iv) After the onset of fluidisation, the pressure was proportional to the flow squared, following the orifice flow theory.

  (v) Deviation from the orifice flow equation was observed at high flow rates, due to cavitation development in the orifice.

- Particle characteristics including size and form (i.e. sphericity) of the grain have a significant impact on the build up of excess pore pressure required for the onset of fluidisation. Tests results show that at any given flow rate the finer the particles the higher the build up of pore water pressure compared to coarser particles, as this is a function of soil permeability. This higher increase in the build up of pore water pressure for the finer particles led to an increased potential for fluidisation. Similarly, particle form (i.e. sphericity) has a major effect on excess pore water generation. The build up of pore water pressure increased with decreasing form, and this lead to increased potential of fluidisation.

- The size of the orifice opening does not have an effect on the distribution of excess pore water pressure in the bed of granular materials. But these profiles are controlled by the discharge flow rate. However, pressure (i.e. upstream of the orifice) is very dependent on the size of the orifice. The smaller the orifice size the larger is the pressure upstream of the orifice required for the onset of fluidisation. Tests results also indicate that most of the head losses are dissipated through the orifice while a relatively small amount are dissipated through the bed of granular materials.

- The results of this study show that significant head can be sustained upstream of the orifice, and that the fluidised zone still will not break through to the bed surface, even though this is only 300 mm deep. This indicates that the head upstream of the orifice was actually dissipated through the orifice (as conversion into velocity head i.e. kinetic energy), and head loss due to cavitation development in the orifice (formation of vapour pressure at high velocity), and dissipation of velocity head (kinetic energy) downstream of the orifice in the internally fluidised zone.

- A mathematical model, based on the concept of force equilibrium exerted on the particle in the bed, has been proposed for predicting the excess pore water pressure at the point of the onset of fluidisation. Comparison of the data shows a good fit was obtained between the predicted and measured values, with a maximum error of less than 10%. The data indicate that the proposed model is valid and of practical use.

Table 4.1: Experimental results for different orifice sizes; height of the bed: 300mm and the effective particle diameter 0.9 mm.

Test no.	Tested material	Orifice opening (mm)	Flow rate at fluidisation (l/h)	Pressure upstream orifice at fluidisation (kPa)
1	Silica sand	0.234	B*	B*
2	Silica sand	0.336	1042	60
3	LBS-B	0.62	1050	23.1
4	LBS-B	0.92	1030	15.2

B* A maximum pressure of 269 kPa was applied in the system corresponding to flow rate of 1008 l/h and still the bed of sand did not fluidise.

Table 4.2: Head distributions in the system, 300mm bed of silica sand, and orifice opening of 0.234mm.

Head upstream orifice (m)	head in soil (m)	head in orifice (m)	head loss in orifice %
2.320	0.201	2.119	91
3.340	0.239	3.101	93
4.440	0.304	4.136	93
5.440	0.425	5.015	92
6.248	0.557	5.691	91
7.230	0.629	6.601	91
8.212	0.710	7.502	91
9.194	0.755	8.439	92
10.422	0.783	9.639	92
11.405	0.809	10.596	93
12.633	0.797	11.836	94
15.088	0.827	14.261	95
16.071	0.870	15.201	95
17.053	0.897	16.156	95
18.281	0.941	17.340	95
19.018	0.965	18.053	95
20.000	0.983	19.017	95
20.982	0.995	19.987	95
21.965	1.003	20.962	95
22.947	0.935	22.012	96
23.929	0.945	22.984	96
24.912	0.951	23.961	96
26.876	0.973	25.903	96

Table 4.3: Head distributions in the system, 300mm bed of silica sand, and orifice opening of 0.336mm.

Head upstream orifice (m)	head in soil (m)	head in orifice (m)	head loss in orifice %
1.940	0.159	1.781	92
2.320	0.174	2.146	93
2.900	0.215	2.685	93
3.940	0.306	3.634	92
4.900	0.844	4.056	83
5.756	0.884	4.872	85
6.739	0.759	5.980	89
7.721	0.694	7.027	91
9.194	0.664	8.530	93
10.177	0.644	9.533	94
12.141	0.319	11.822	97
15.580	0.312	15.268	98
18.035	0.295	17.740	98
20.000	0.299	19.701	99
24.912	0.299	24.613	99

Table 4.4: The parameters used in the proposed model for predicting the pore water pressure at the onset of fluidisation.

Parameter	Numerical values adopted
Height of the bed, H (m)	0.3 [a]
Active length of the bed (at the top surface), L1 (m)	0.312 [b]
Orifice opening, Lo (m)	3.30E-04 [c]
Width of the bed, W (m)	0.147
Density of water, ρ_w (kg/m³)	1000
Density of bed material, ρ_s (kg/m³)	1578 [d]
Porosity, n	0.354
Particle shape parameter, sphericity, φ	1 [e]
Diameter of the particle, d_p (m)	0.001
Viscosity of water, ν (kg/m.s)	1.01E-03
Acceleration due to gravity, g (m/s²)	9.81

a- Different bed heights were also modelled including : 0.22 m and 0.15 m

b- Effective length of the bed at the onset of fluidisation is estimated as L1= 2*H*TAN (θ), (see Figure 4.30b).

c- Orifice openings of 0.62 mm and 0.92 mm were also modelled.

d- Density of glass ballotini 1578 kg/m³ and the LBS-B 1725 kg/m³

e- Glass ballotini modelled with sphericity of 1, while the LBS-B by a sphericity of 0.6.

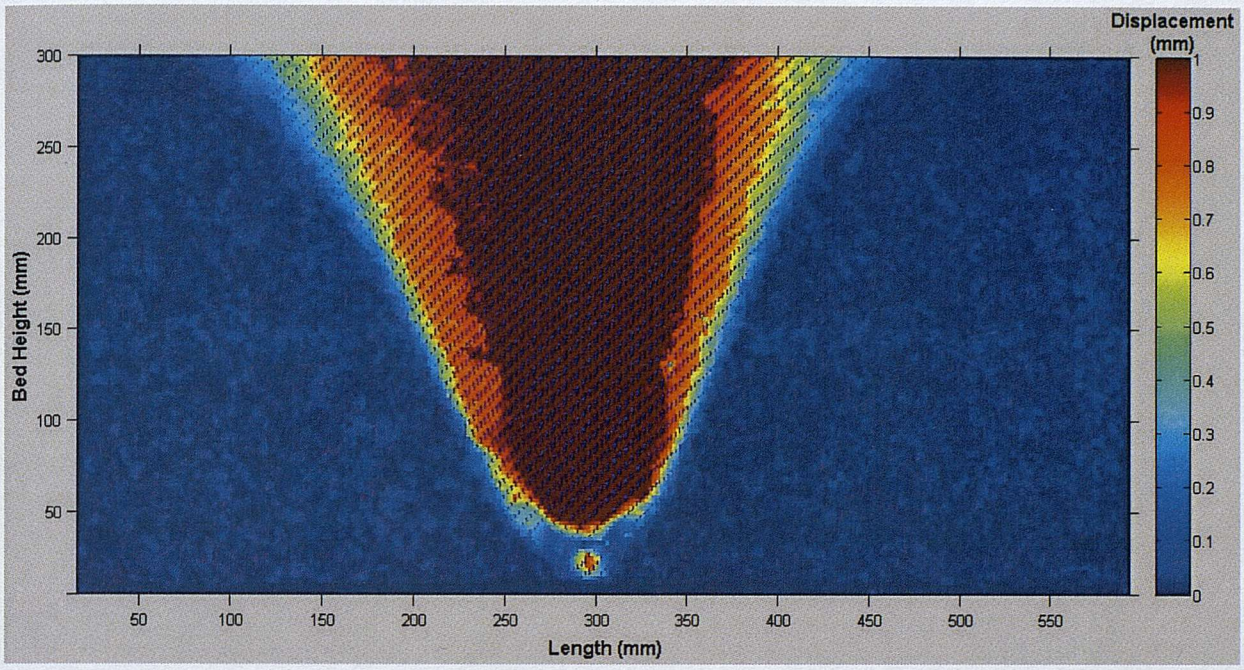

Figure 4.1a: Onset of internal fluidisation at flow rate of 1177 l/h and pressure in pipe of 83 kPa.

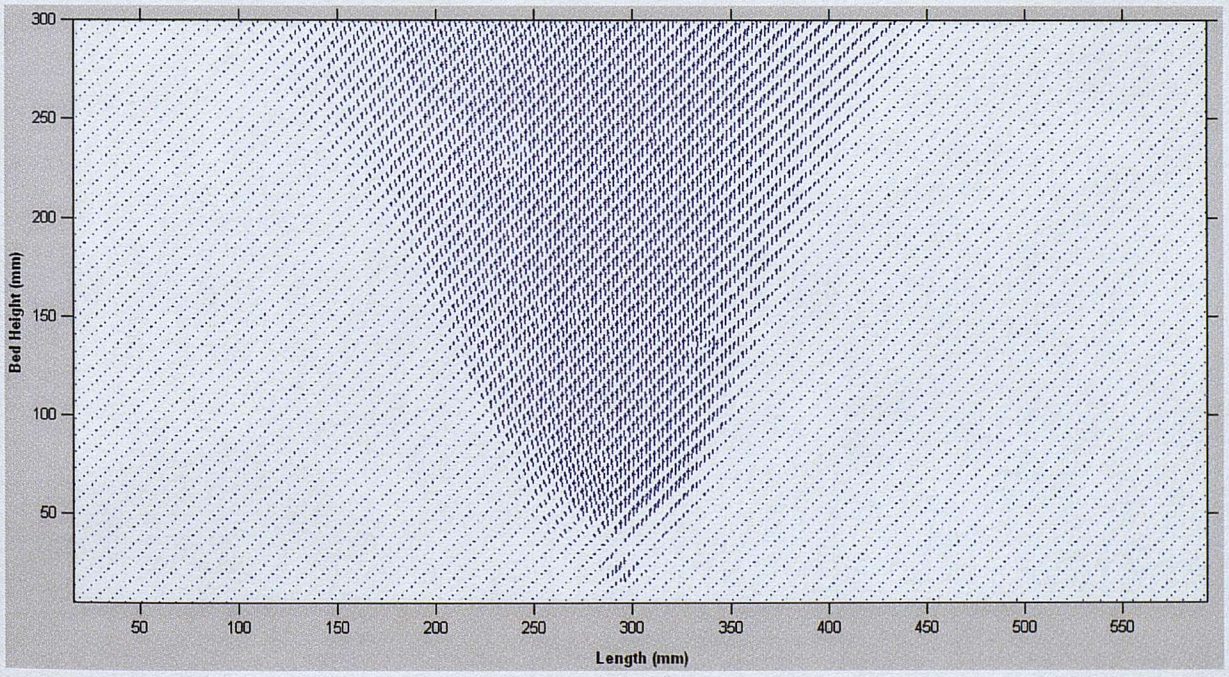

Figure 4.1b: Displacement vectors at the onset of internal fluidisation.

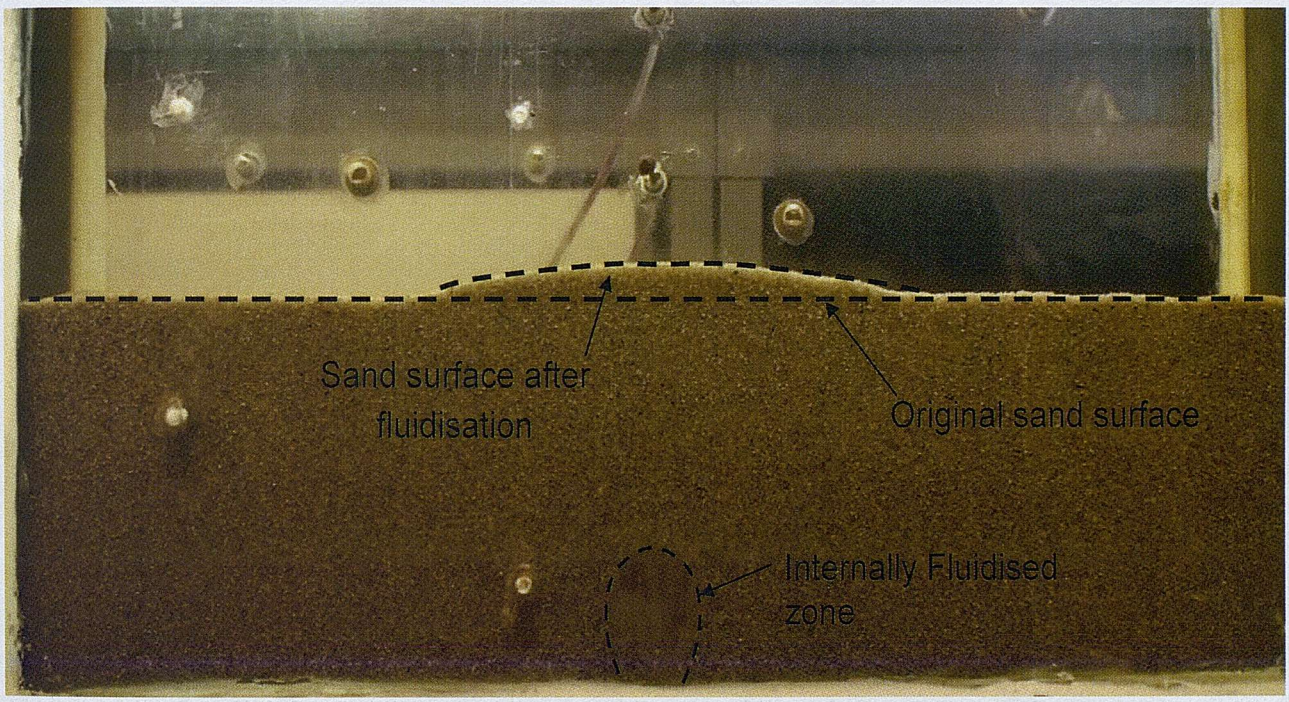

Figure 4.2: Internally fluidized zone in a bed of granular materials due a localised leakage, orifice opening 0.33 mm.

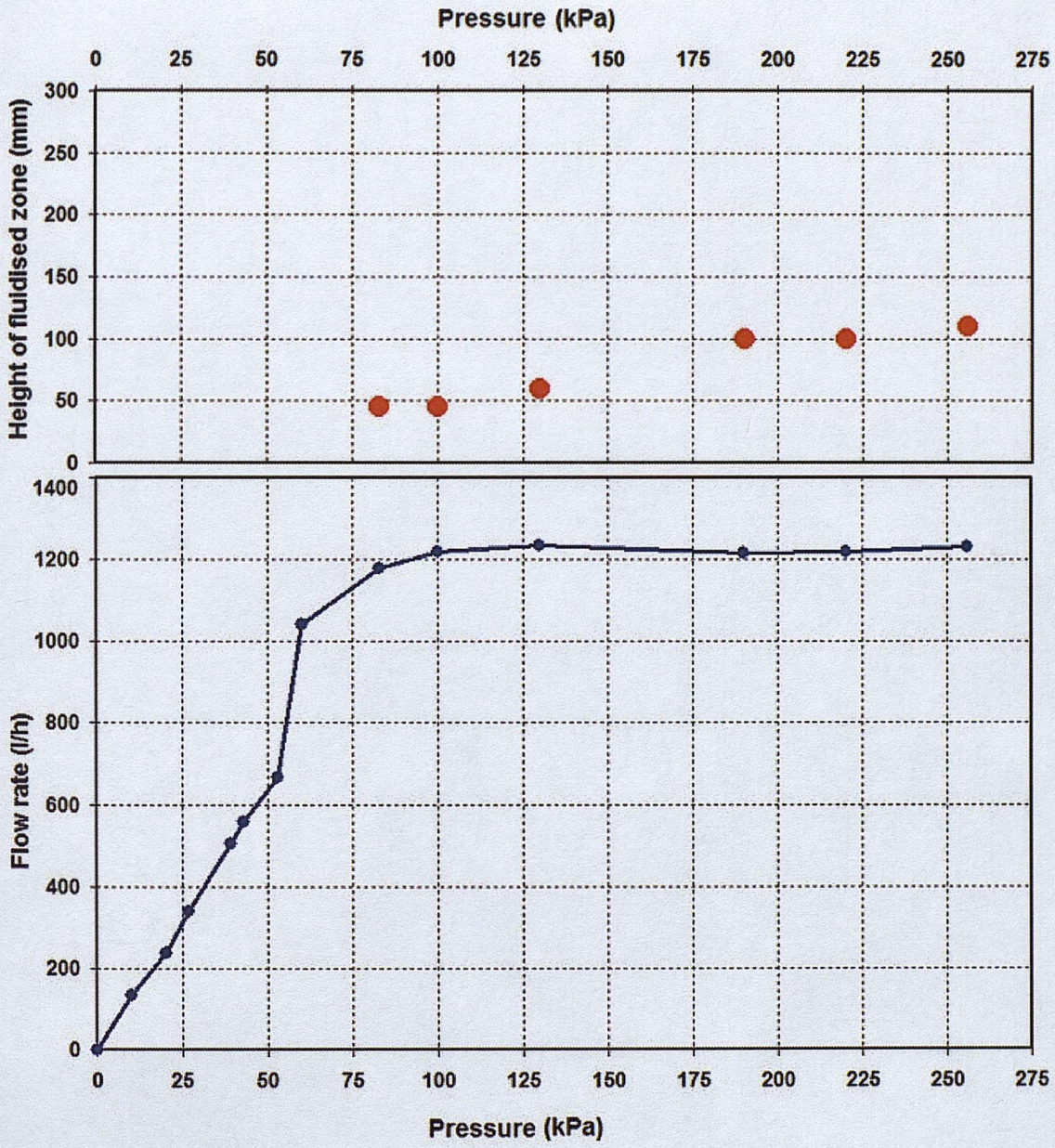

Figure 4.3: Development of the internally fluidised zone, bed height 300 mm of silica sand; and orifice opening 0.336mm.

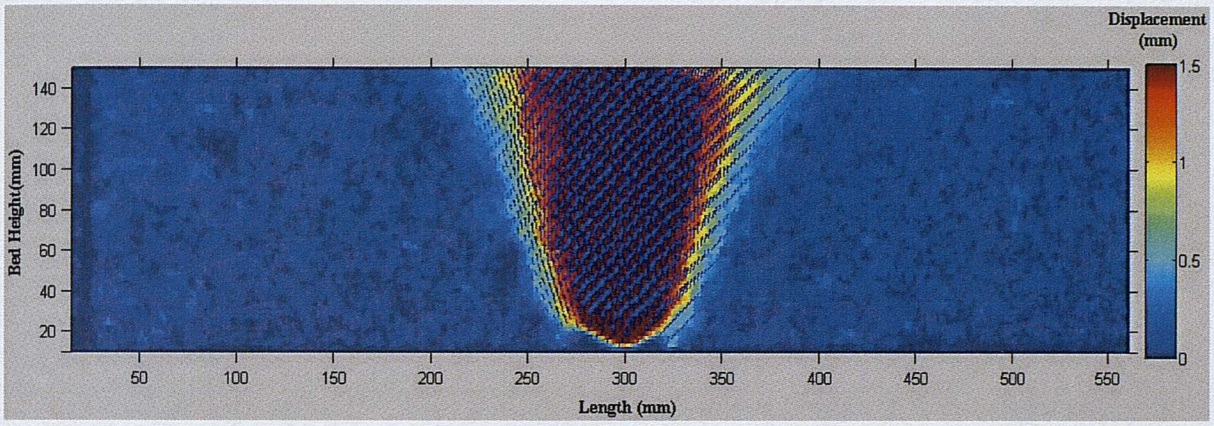

Figure 4.4a: The uplift of the grains above the injection point at the onset of fluidisation. Bed height 150mm of LBS-B, and orifice opening: 0.33mm.

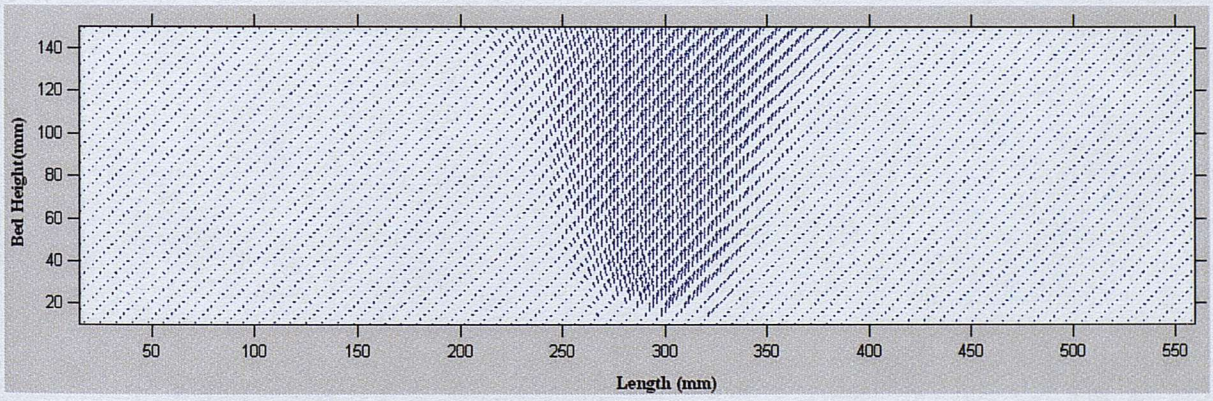

Figure 4.4b: Vectors of the uplift of the grains above the injection point at the onset of fluidisation. Bed height 150mm of LBS-B, and orifice opening: 0.33mm.

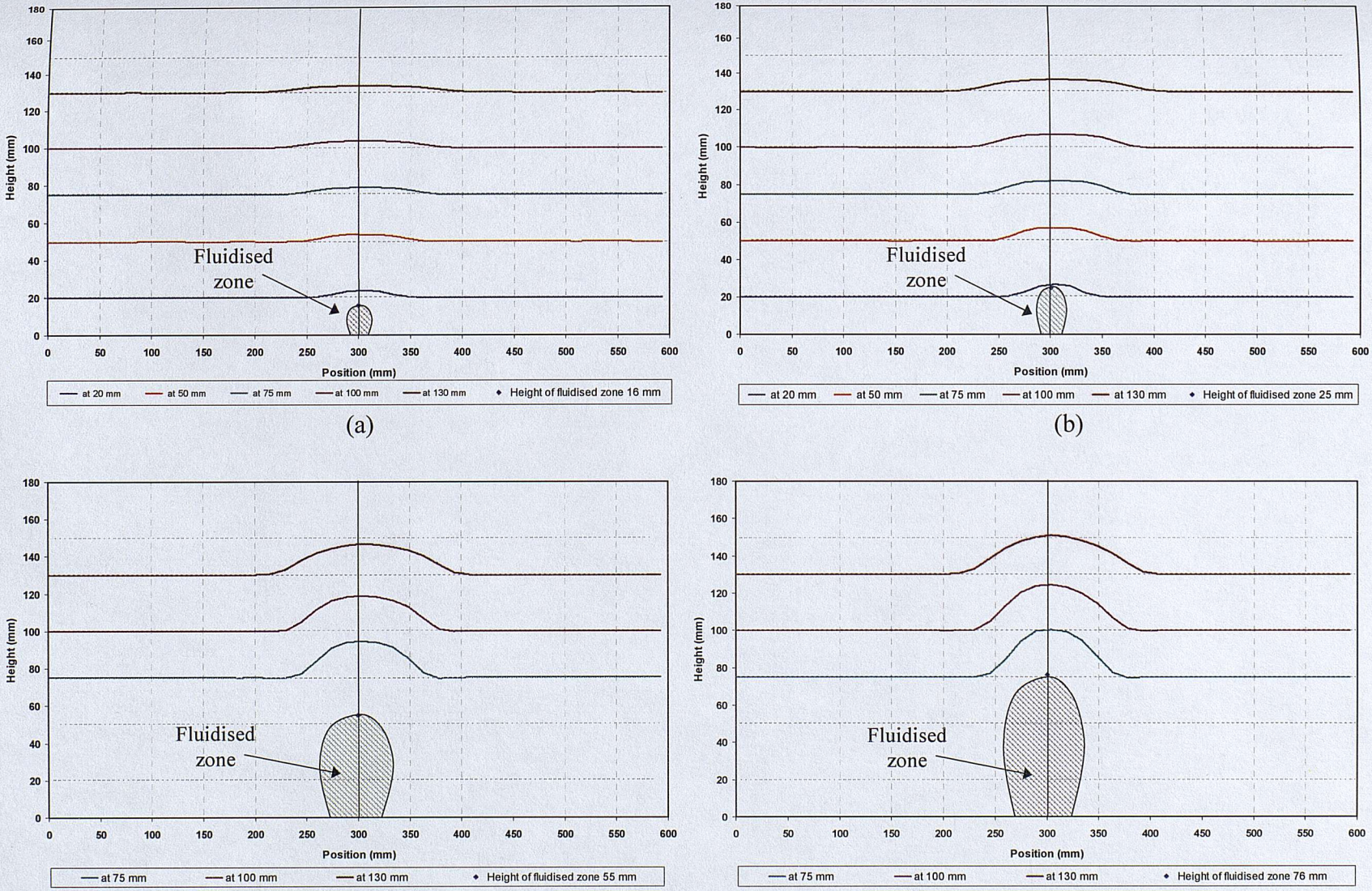

Figure 4.5: Vertical movement profile during fluidization development in 150 mm bed height, orifice opening: 0.33 mm.

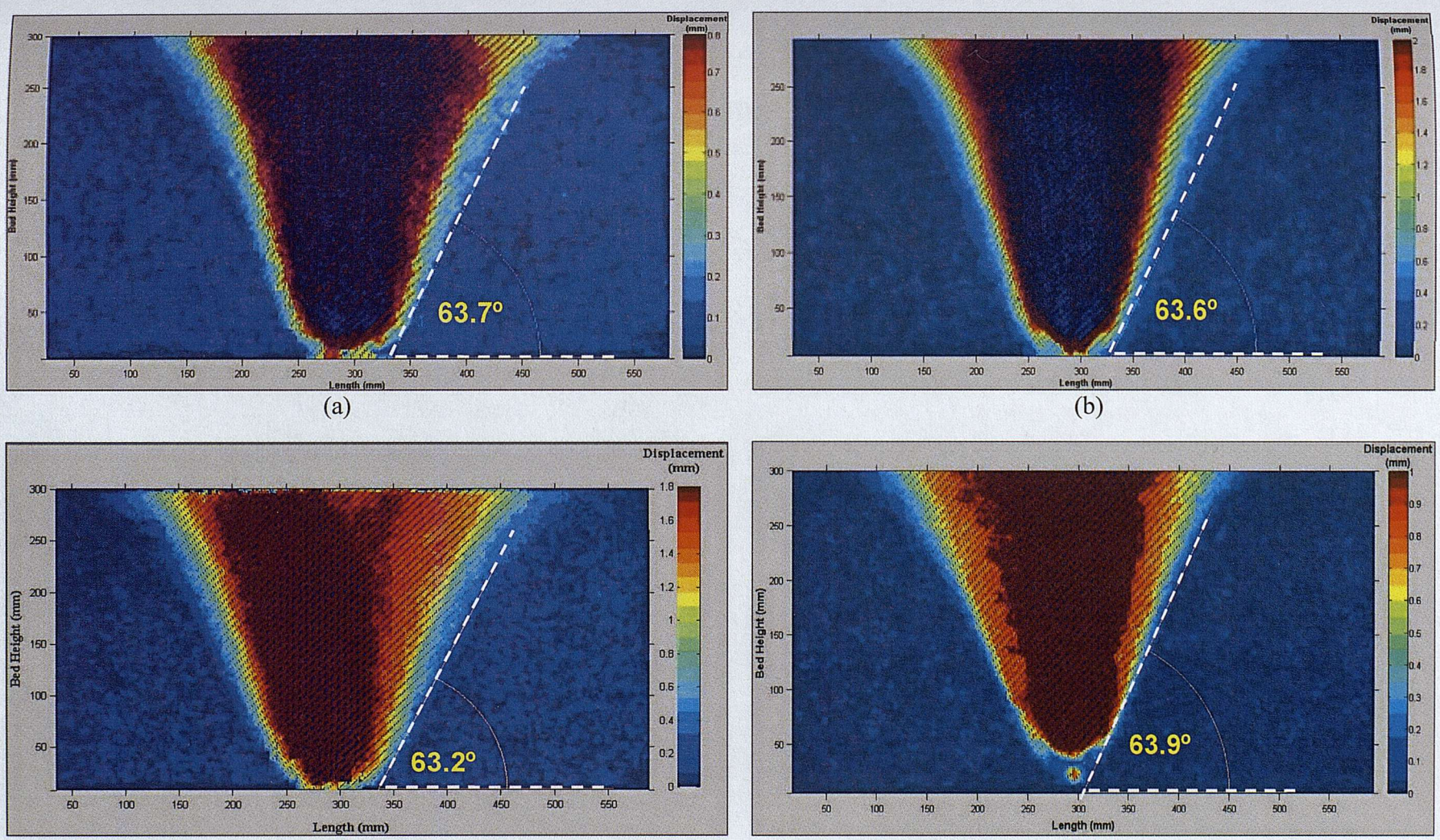

Figure 4.6a: The uplift mechanism at the onset of fluidisation in a 300mm bed height, for orifice openings: (a) 0.92 mm, (b) 0.62 mm, (c) 0.43mm and (d) 0.33mm.

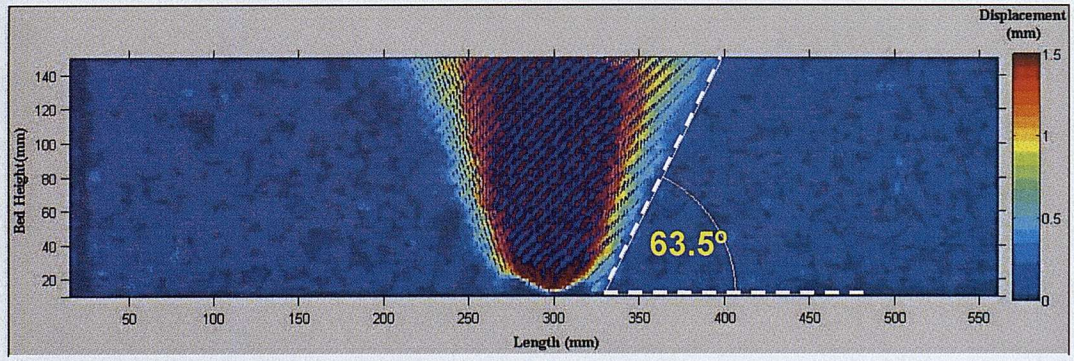

(e)

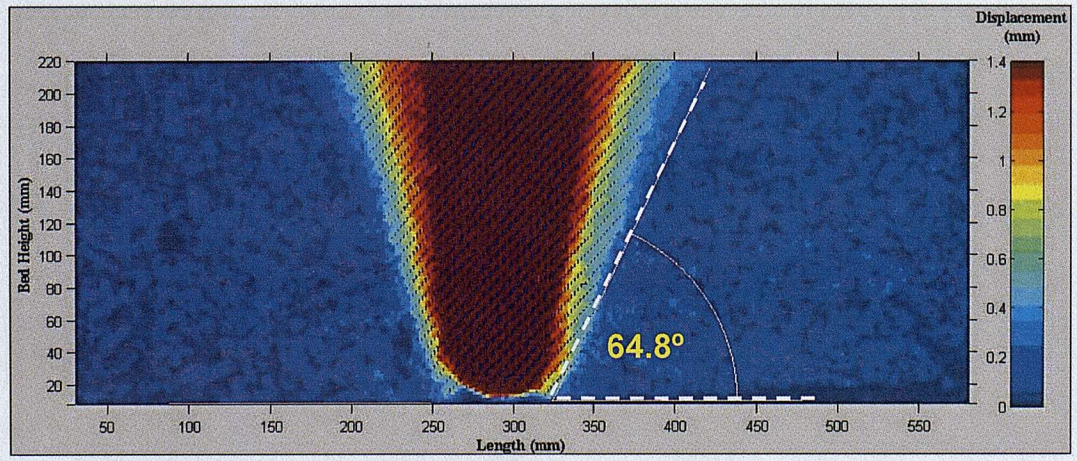

(f)

Figure 4.6b: The uplift mechanism at the onset of fluidisation, bed height: (e) 150 mm and (f) 220 mm. Orifice opening: 0.33 mm.

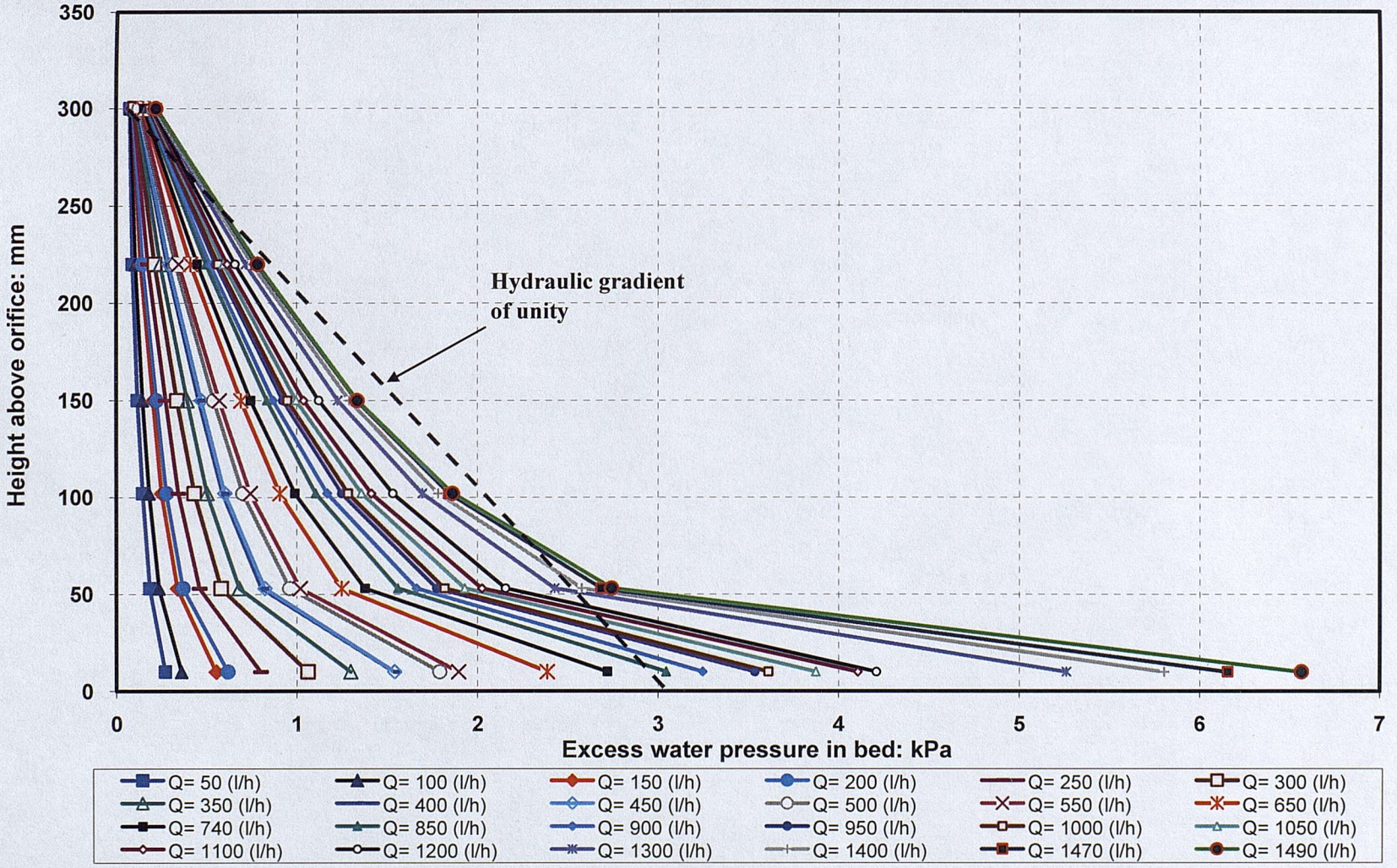

Figure 4.7: Excess pore water pressures at different points along 300 mm bed height of glass ballotini before fluidisation, orifice opening 0.92 mm.

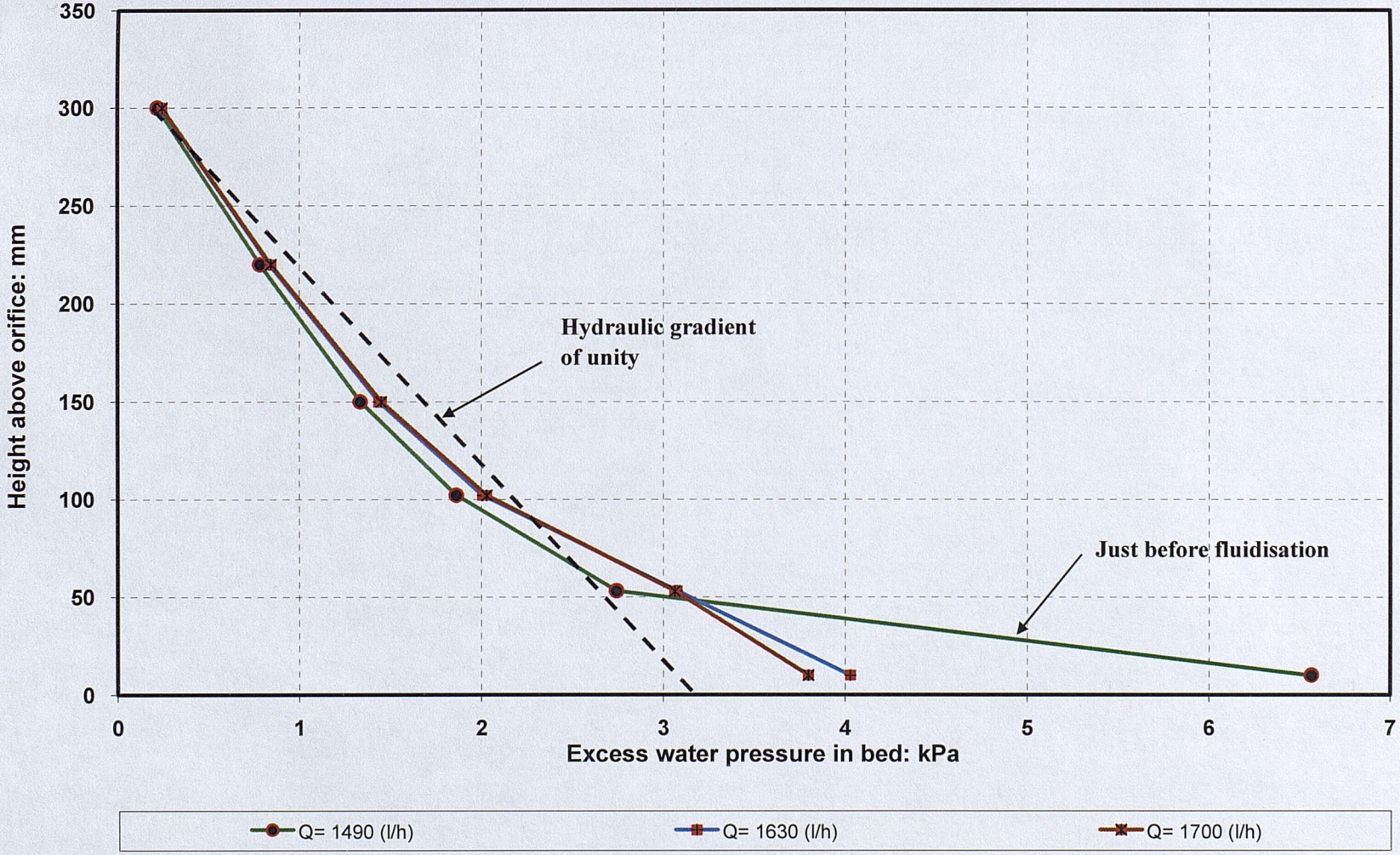

Figure 4.8: Excess pore water pressures at different points along 300 mm bed height of glass ballotini after fluidisation, orifice opening 0.92 mm.

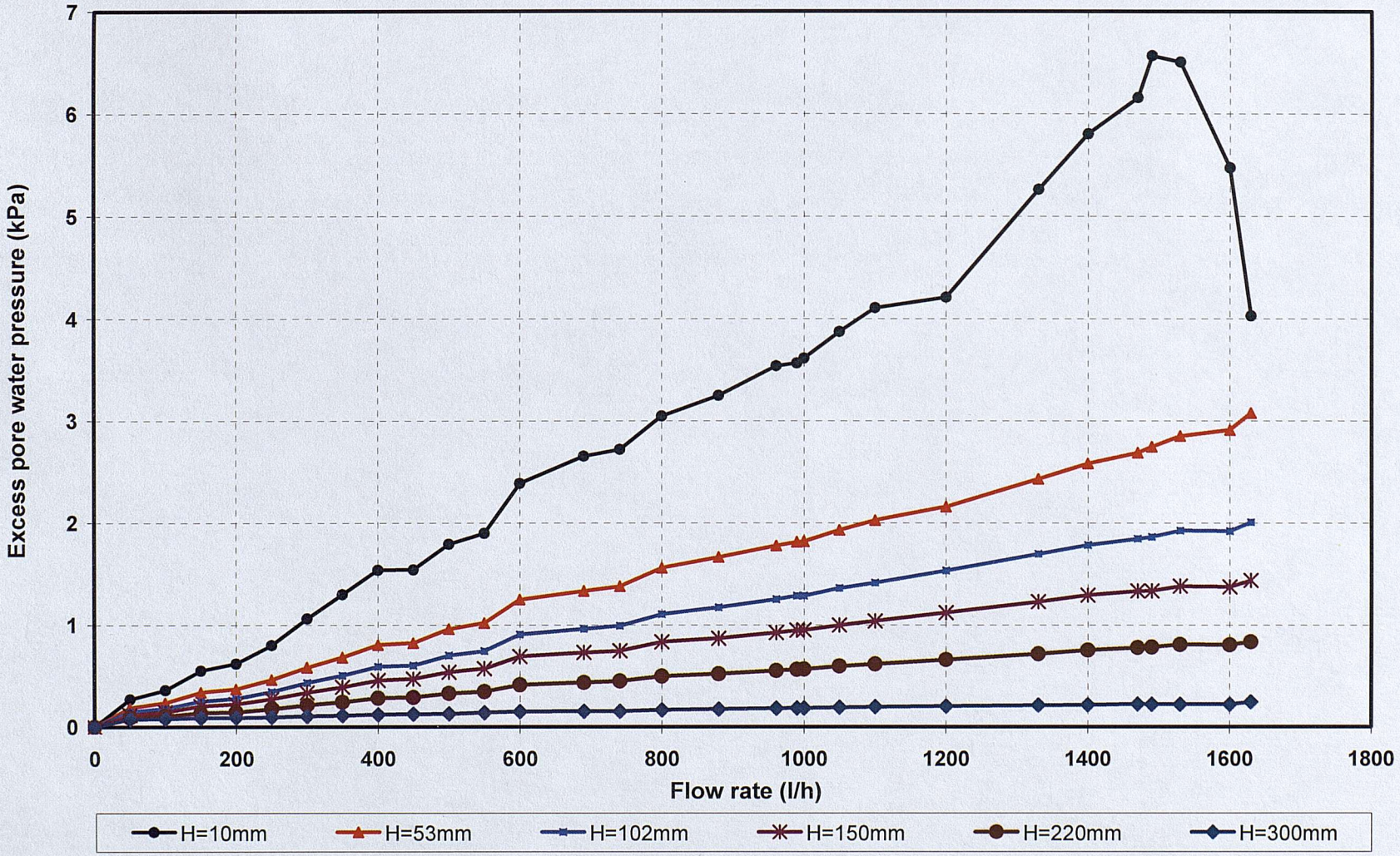

Figure 4.9: Excess pore water pressures distribution at different points along 300 mm bed height of glass ballotini, orifice opening 0.92 mm.

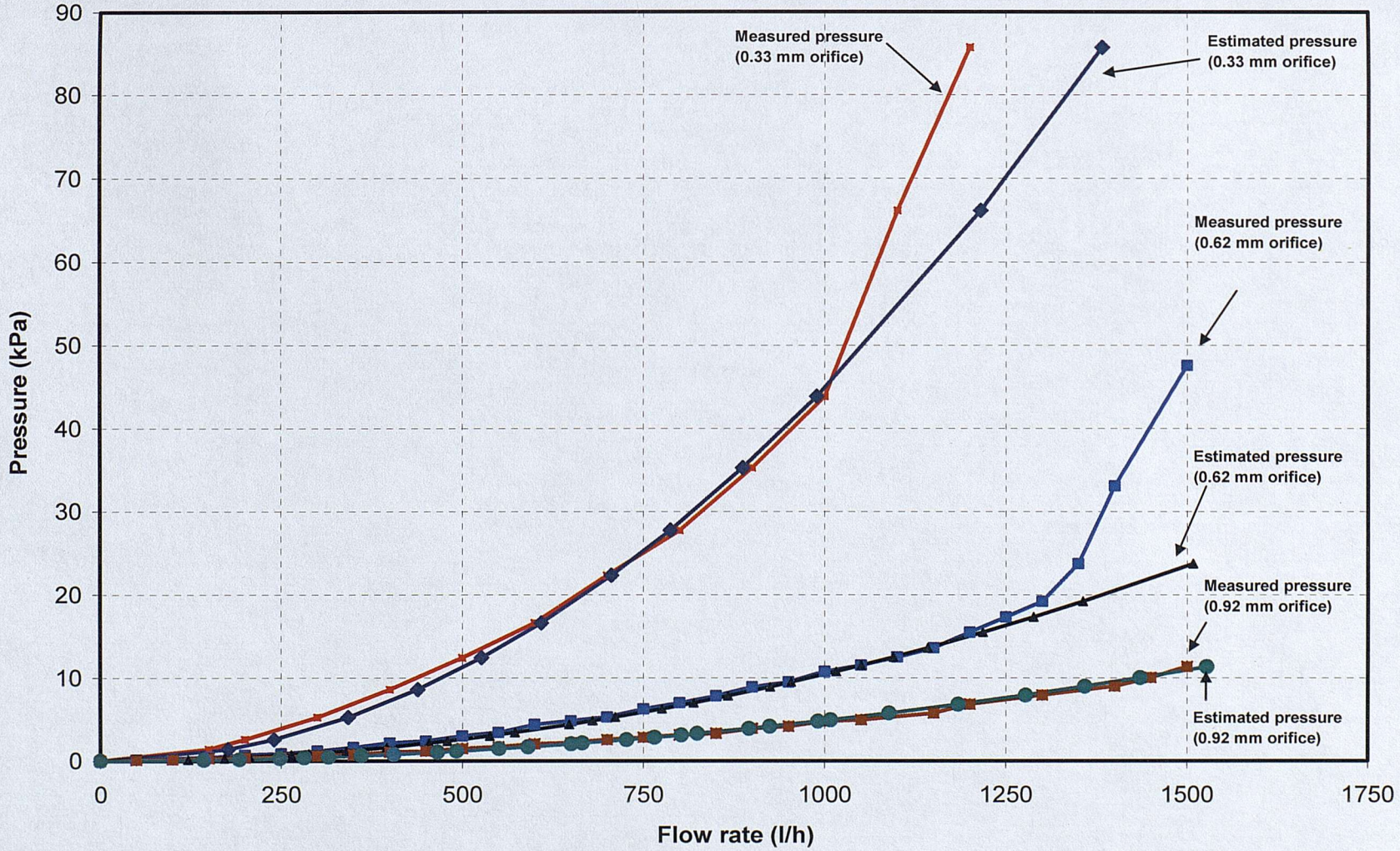

Figure 4.10: Pressure-flow rate relationship under free flow condition for orifice opening of 0.33 mm, 0.62 mm, and 0.92 mm.

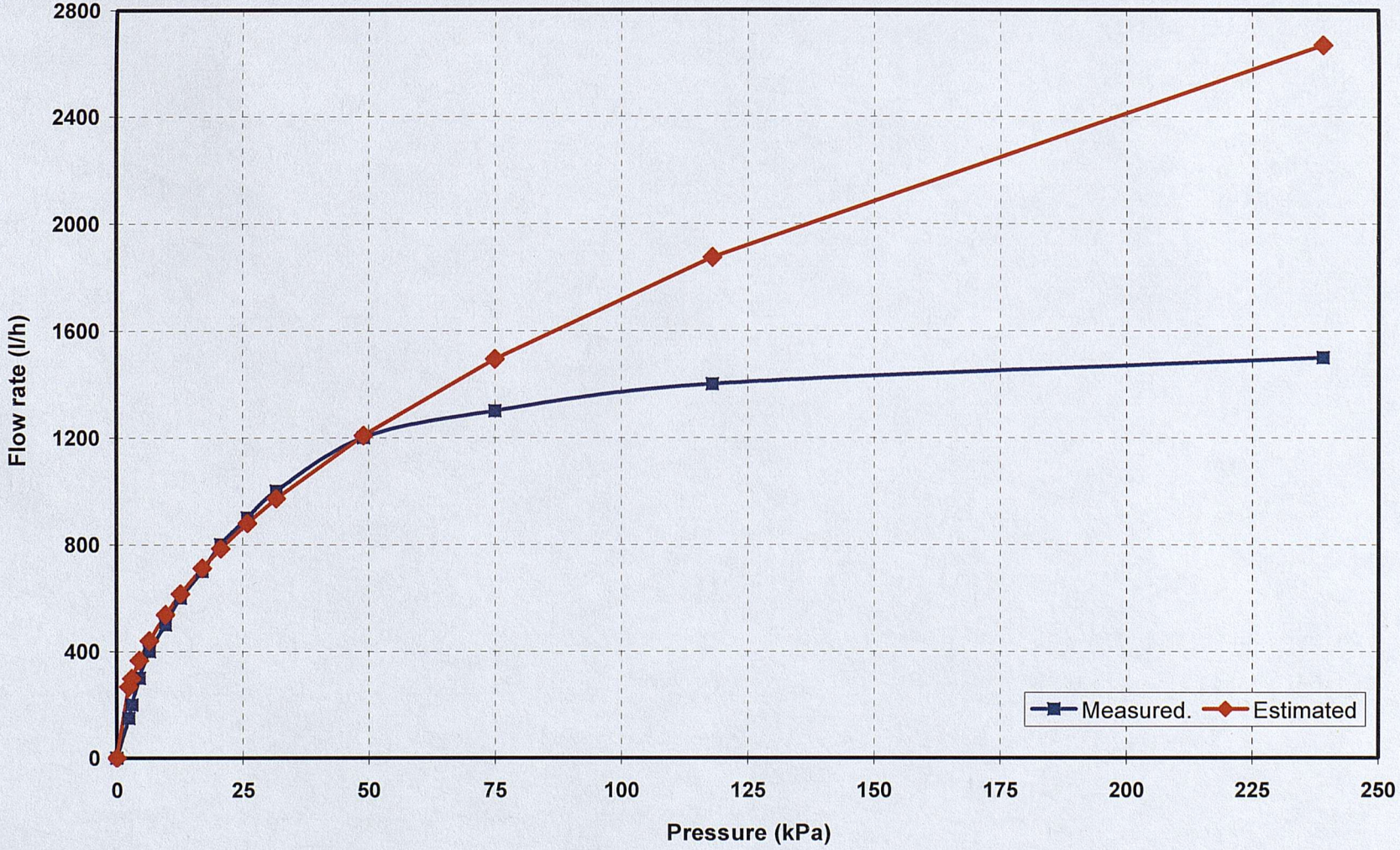

Figure 4.11: Measured and predicted pressure-flow rate relationship for an orifice opening of 0.43 mm.

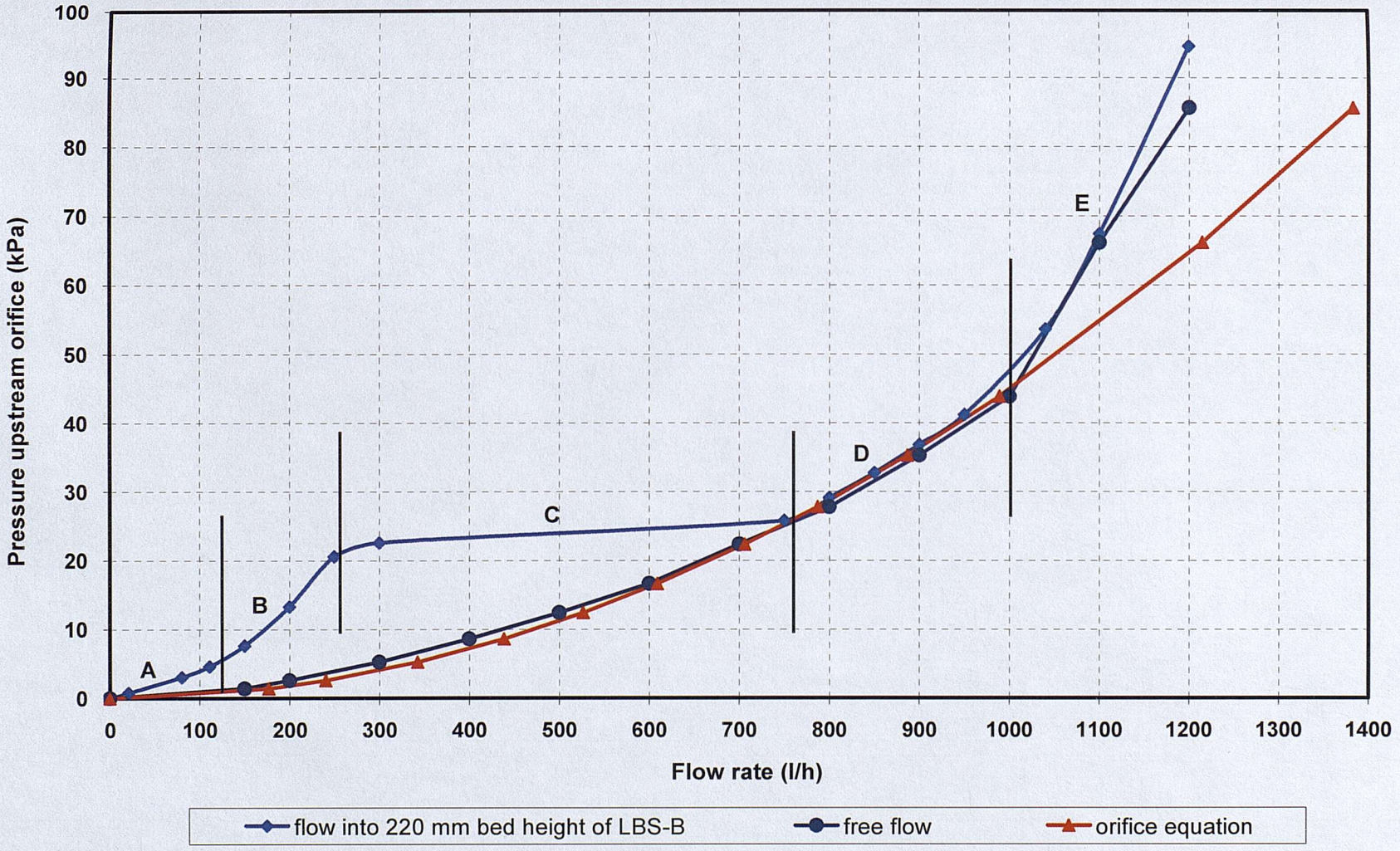

Figure 4.12: Pressure-flow rate relationship for an orifice opening of 0.33 mm.

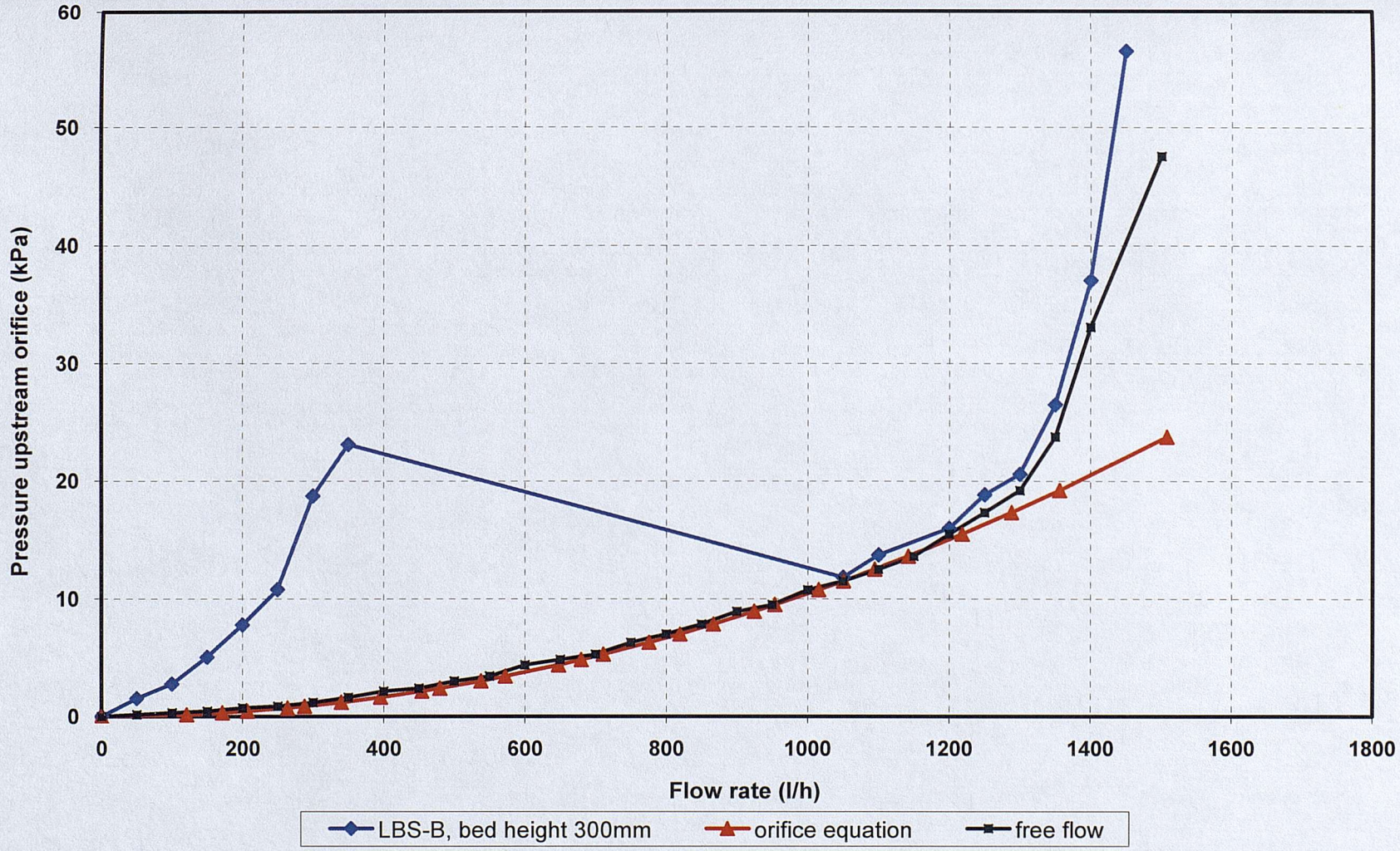

Figure 4.13: Pressure-flow rate relationship for an orifice opening of 0.62 mm.

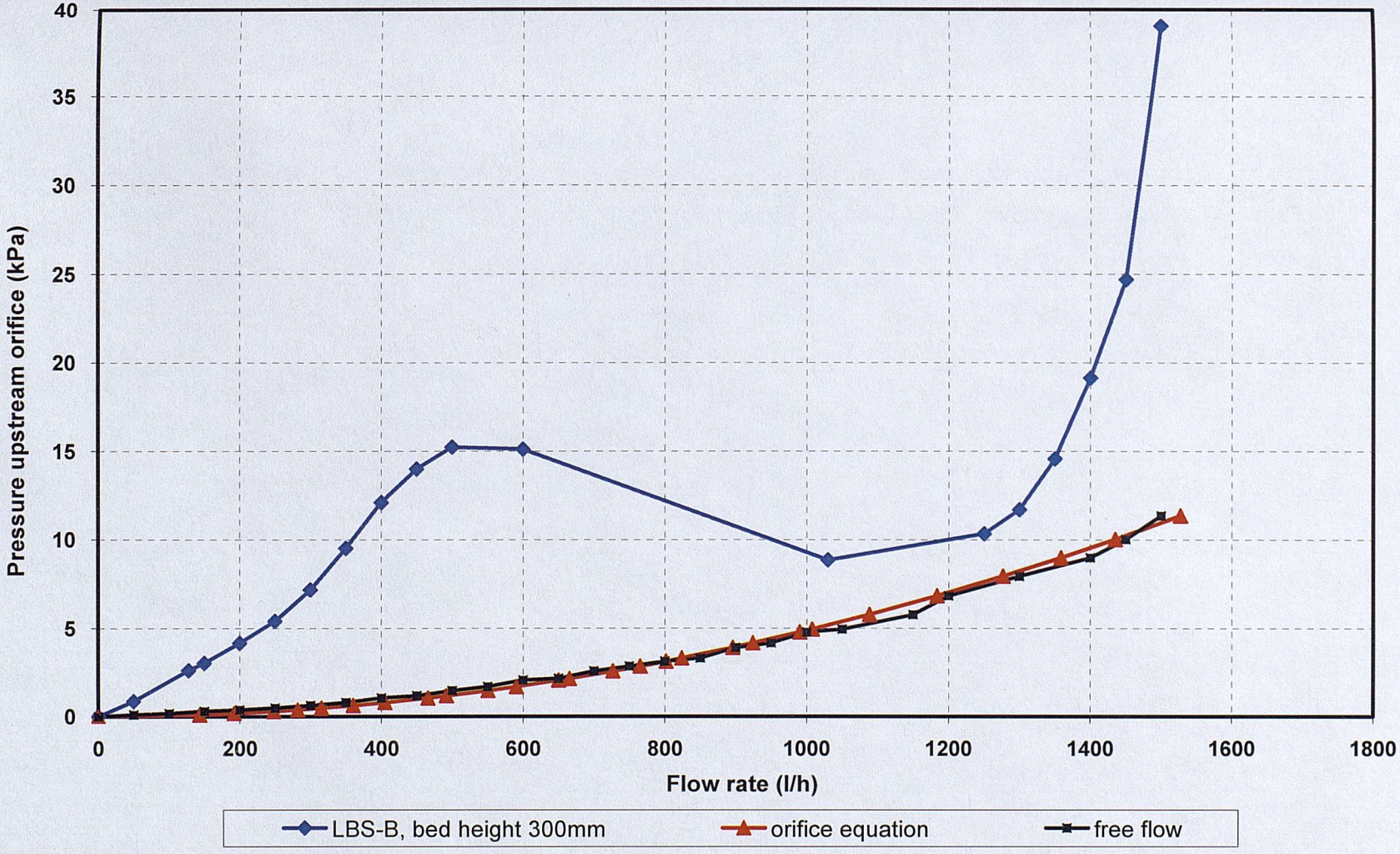

Figure 4.14: Pressure-flow rate relationship for an orifice opening of 0.92 mm.

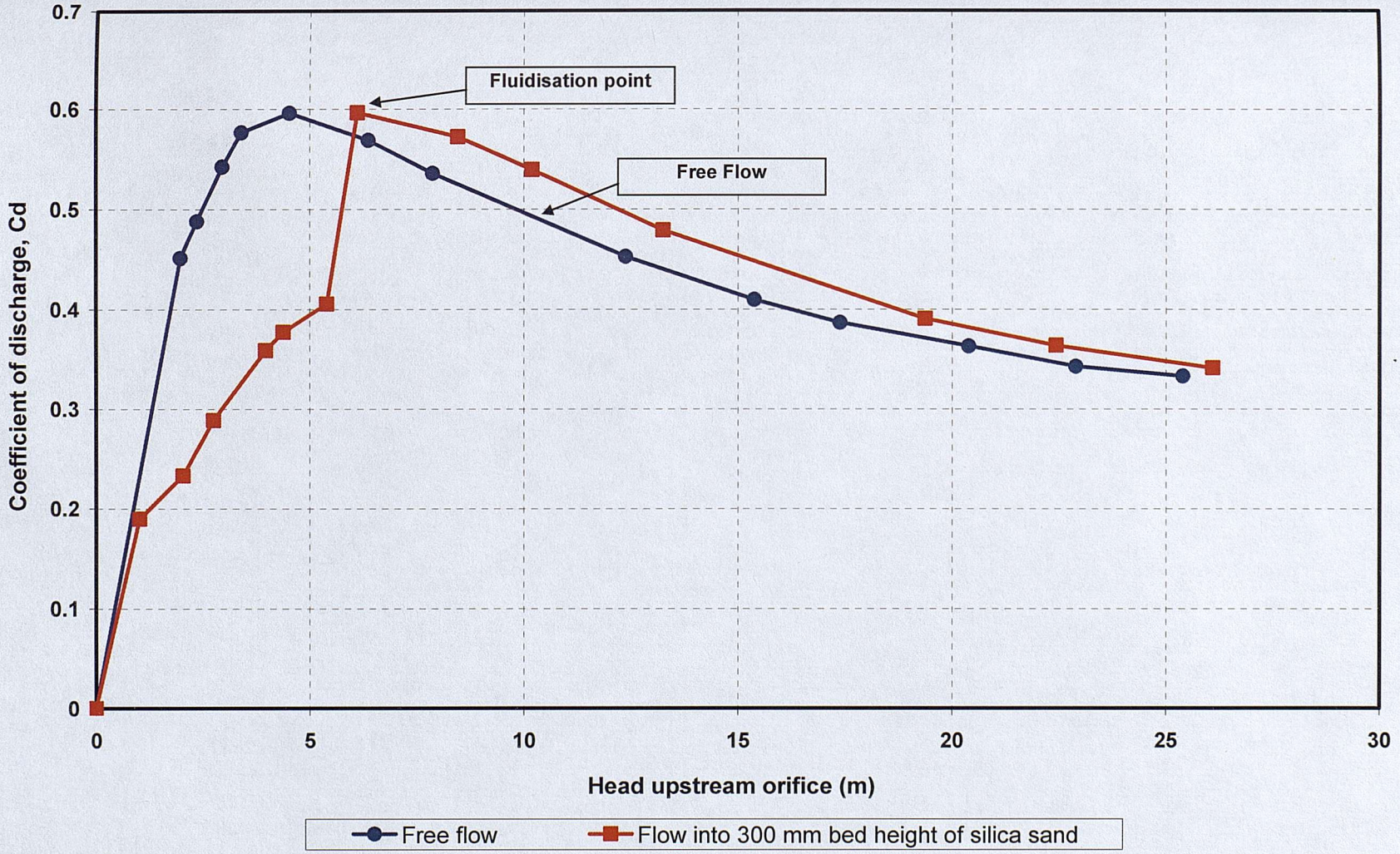

Figure 4.15: Coefficient of discharge as a function of head upstream of the orifice, orifice opening 0.336 mm.

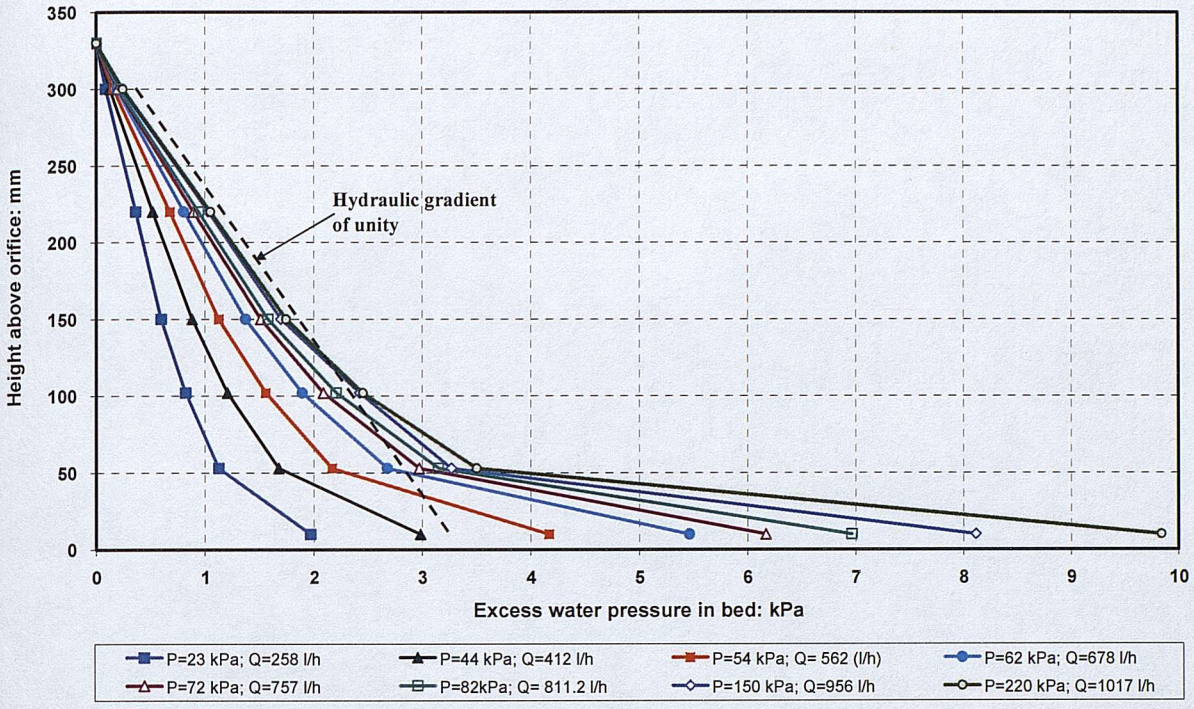

Figure 4.16: Excess pore water pressure at different points along 300mm bed height of silica sand, d_{50} 0.9mm, and orifice opening 0.234 mm.

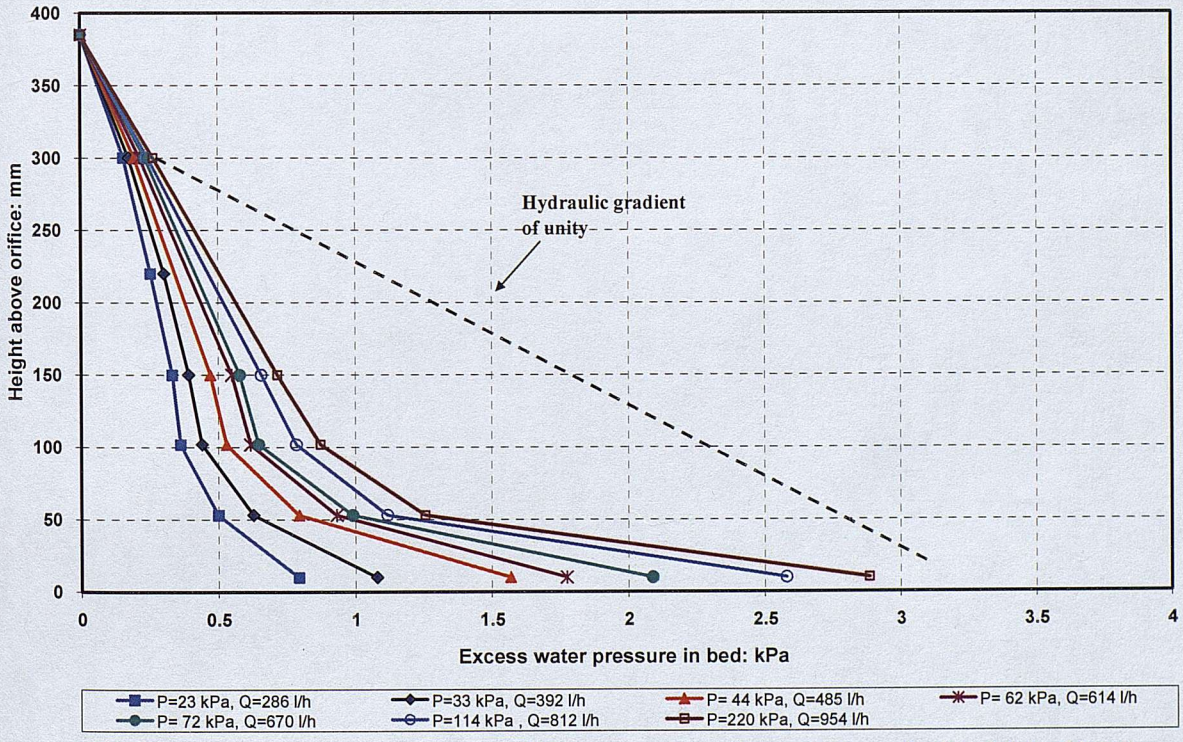

Figure 4.17: Excess pore water pressure at different points along 300mm bed height of LBS-A, d_{50} 1.6mm, and orifice opening 0.234mm.

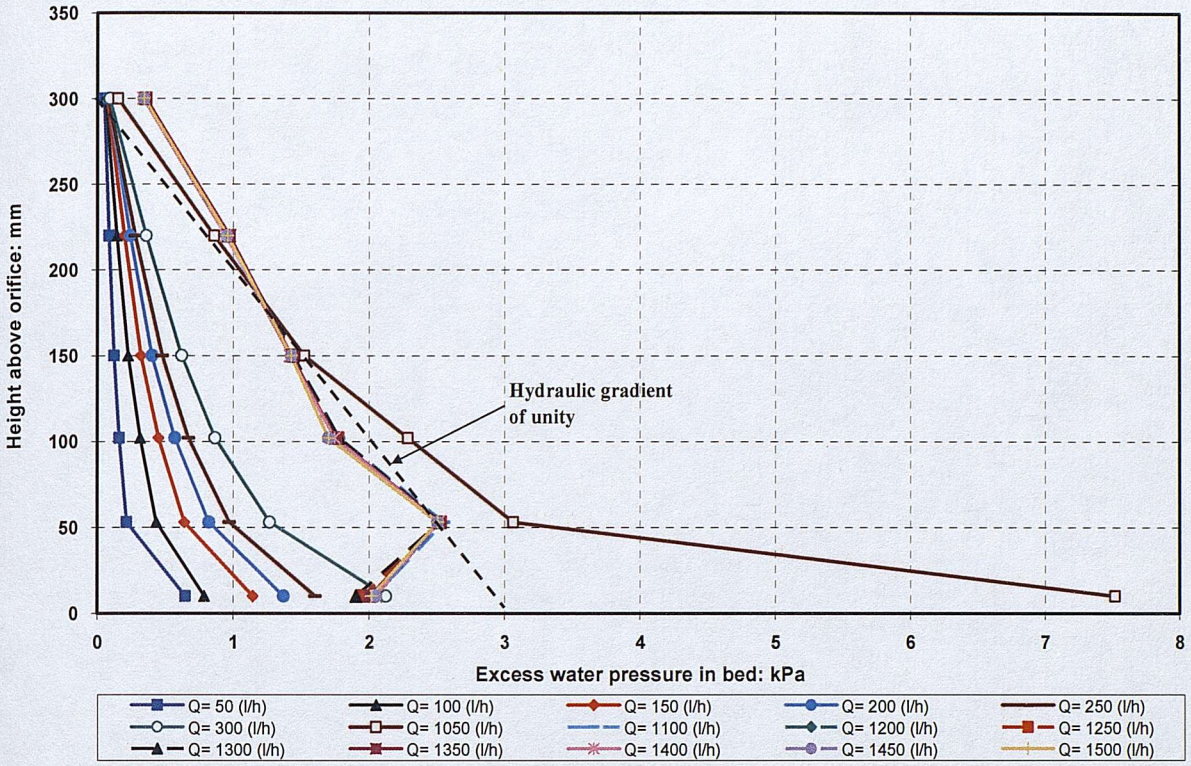

Figure 4.18: Excess pore water pressure at different points along 300mm bed height of LBS-B, d_{50} 0.9mm, and orifice opening 0.62mm.

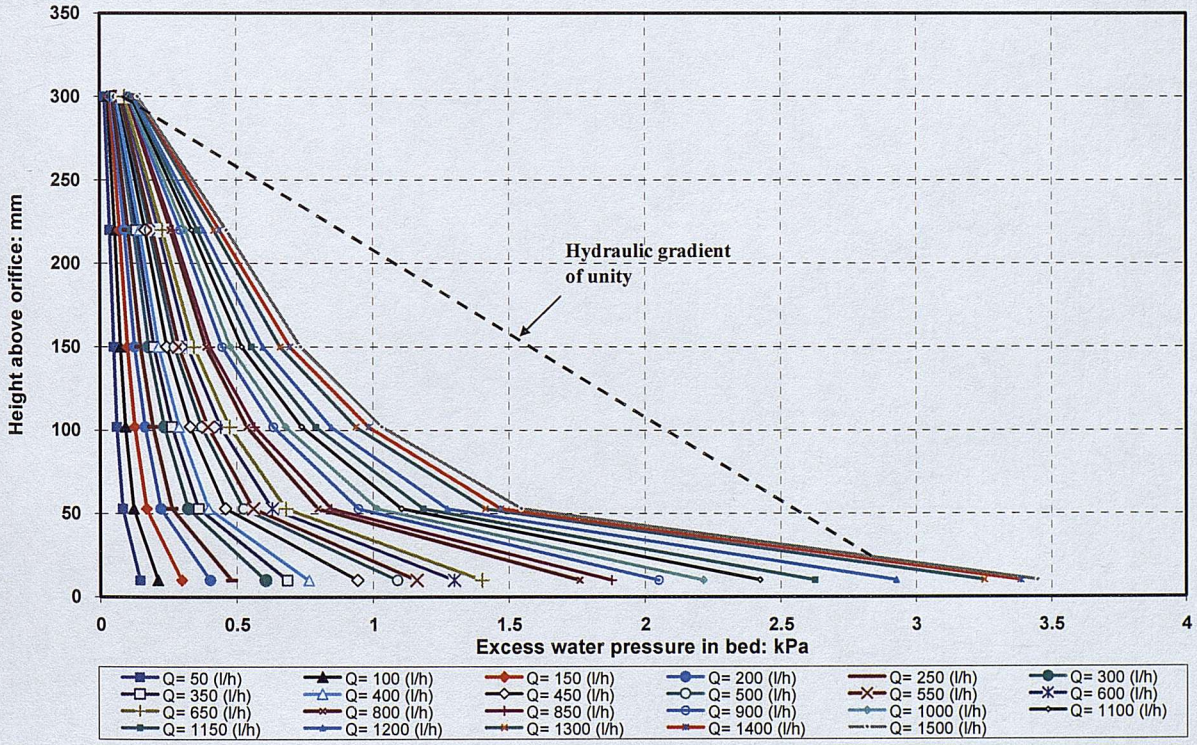

Figure 4.19: Excess pore water pressure at different points along 300mm bed height of LBS-A, d_{50} 1.6mm, and orifice opening 0.62mm.

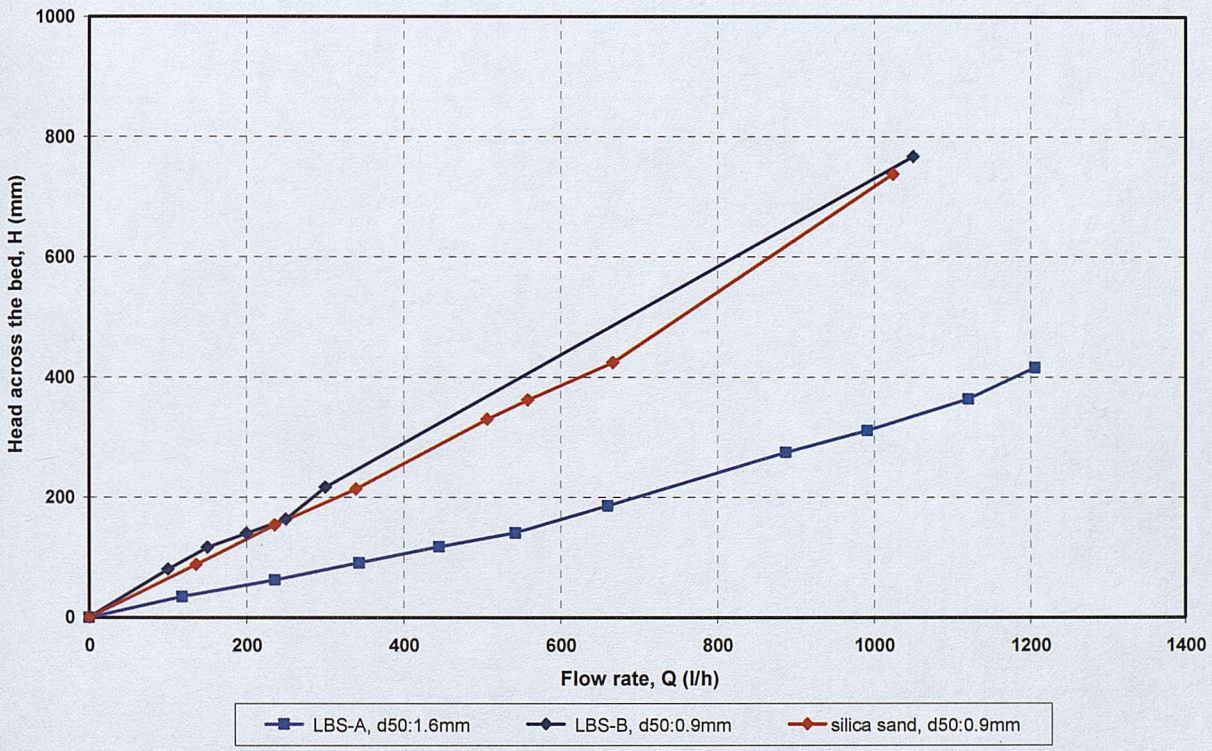

Figure 4.20: Head loss as a function of flow rate for different bed materials: LBS-A, LBS-B, and Silica sand; Bed height 300mm.

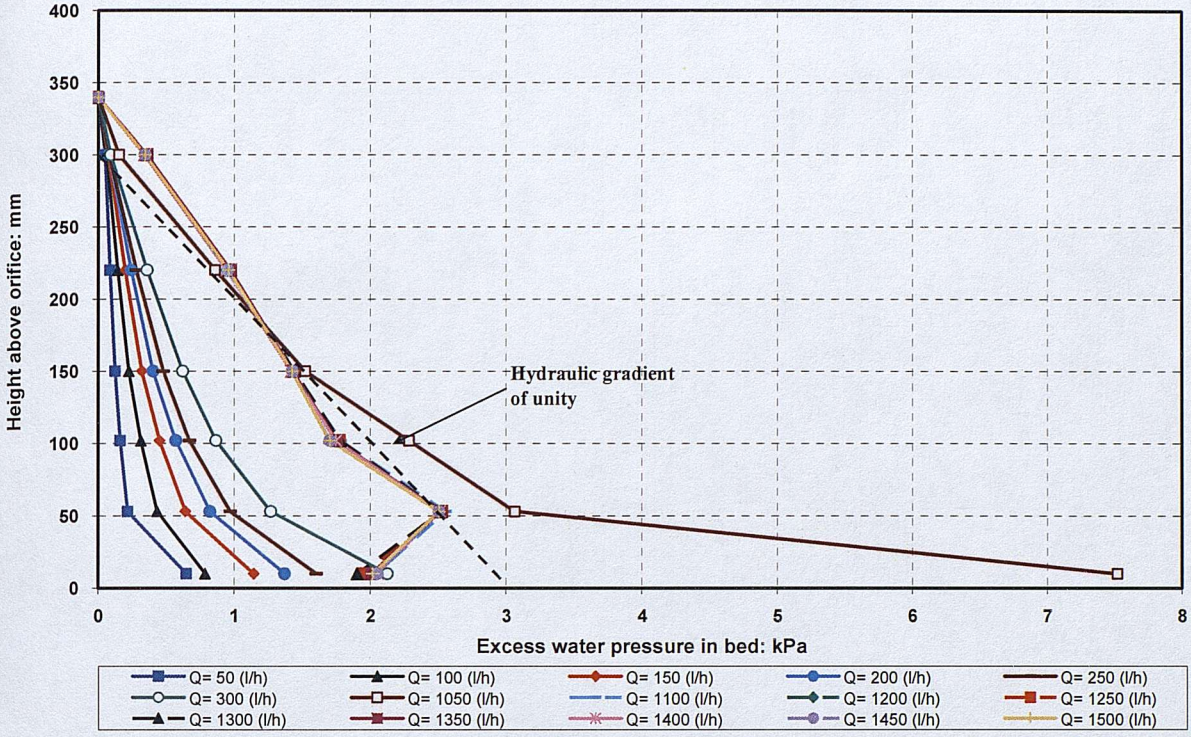

Figure 4.21: Excess pore water pressure at different points along 300mm bed height of LBS-B, d_{50} 0.9mm, and orifice opening 0.62mm.

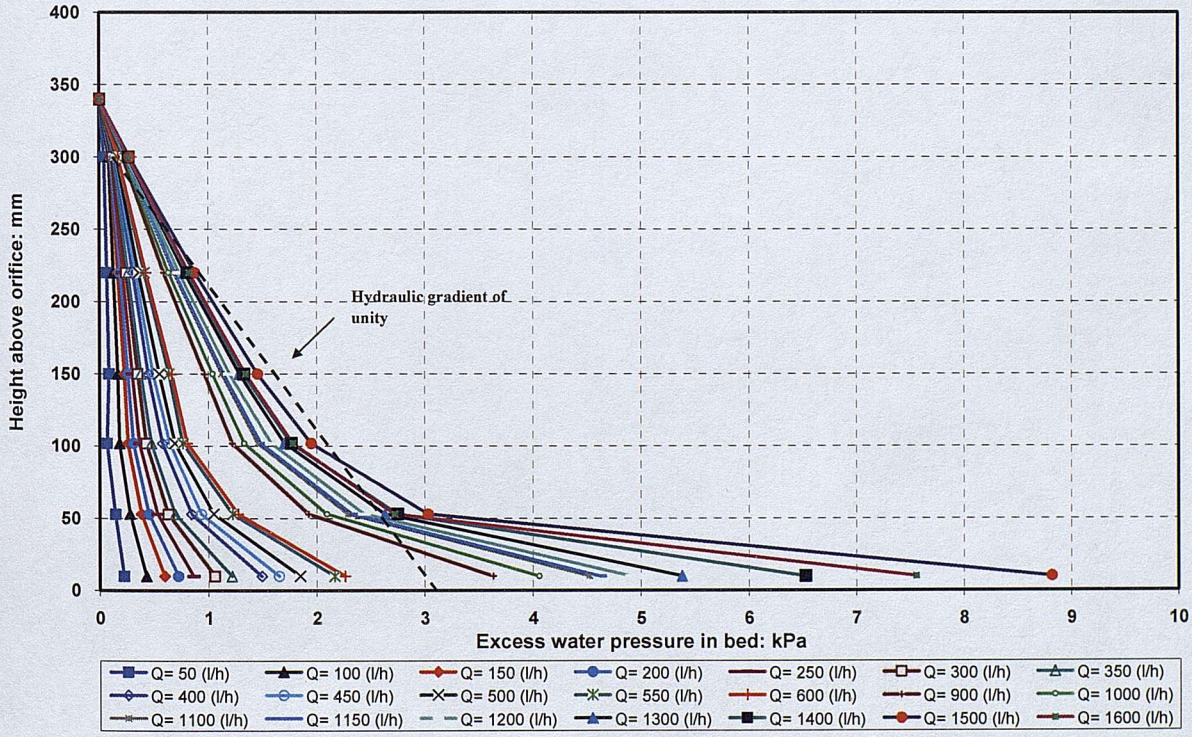

Figure 4.22: Excess pore water pressure at different points along 300mm bed height of glass ballotini, d_{50} 0.9mm, and orifice opening 0.62mm.

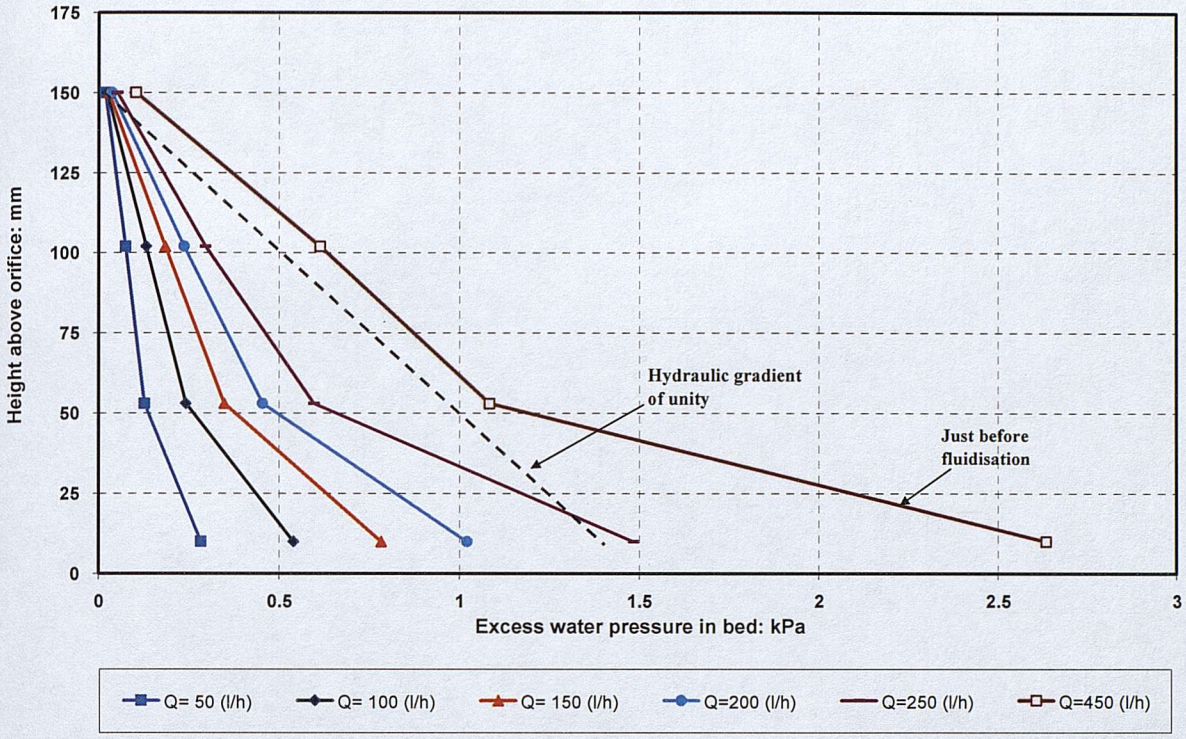

Figure 4.23 Excess pore water pressures along a 150mm bed height of LBS-B, d_{50} 0.9mm, and orifice opening of 0.33mm.

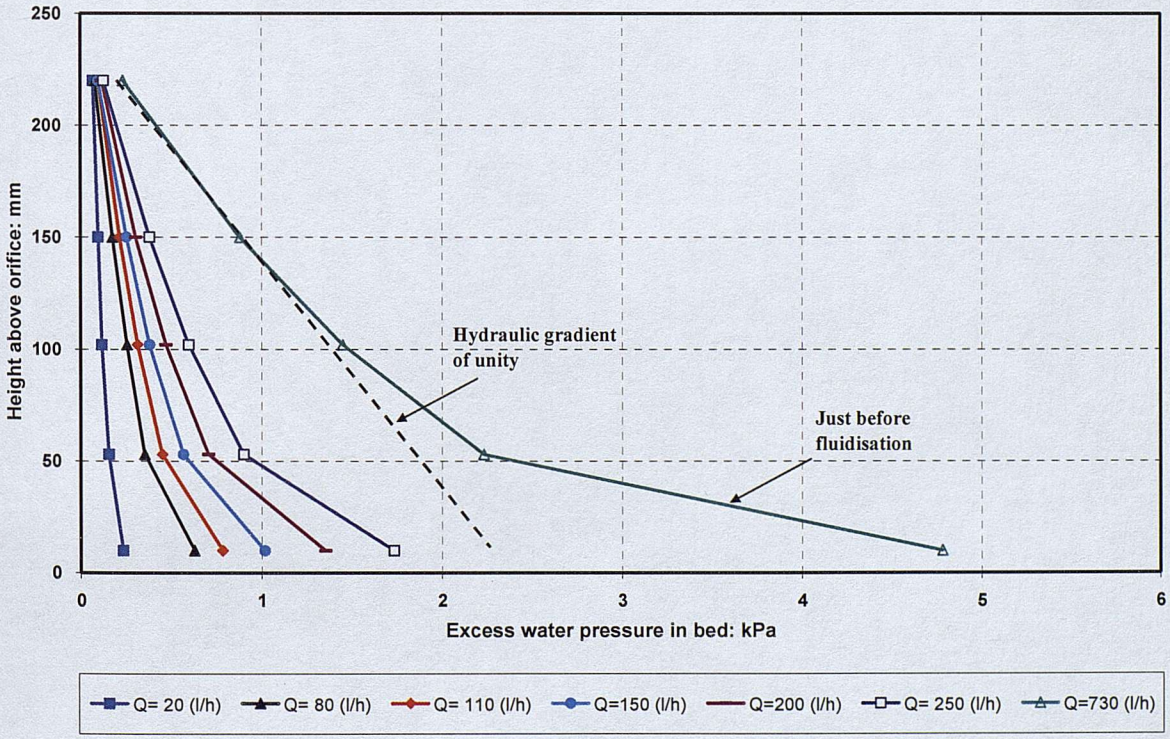

Figure 4.24: Excess pore water pressures along a 220mm bed height of LBS-B, d_{50} 0.9mm, and orifice opening of 0.33mm.

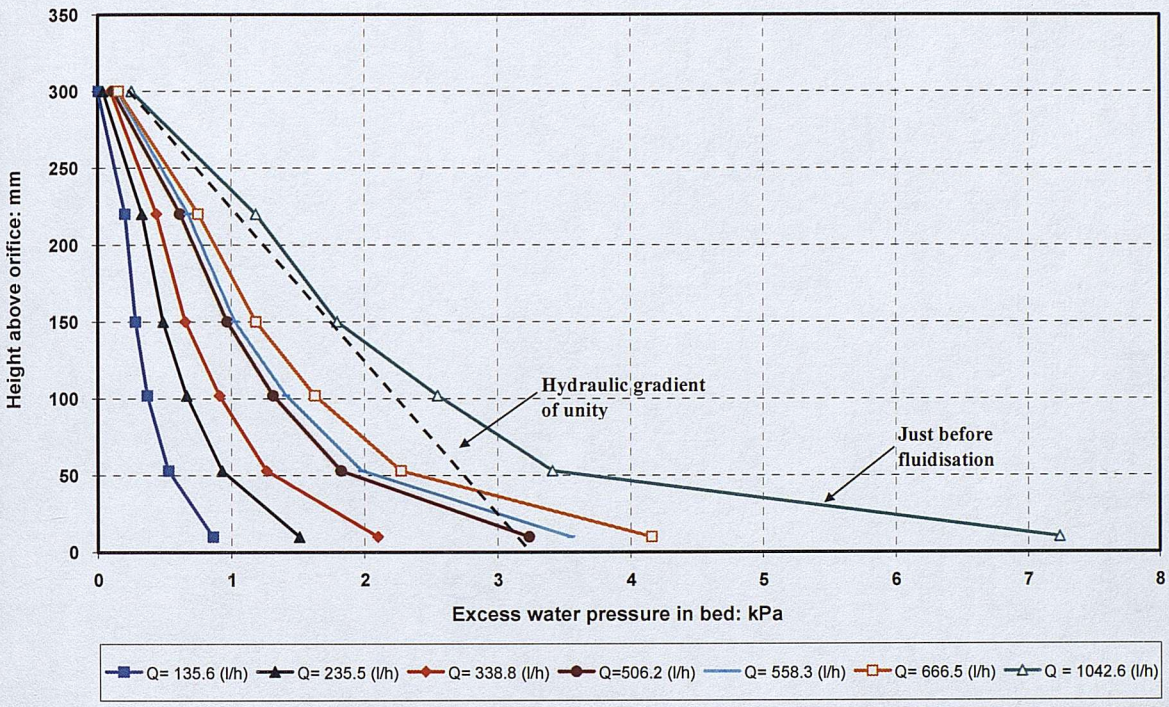

Figure 4.25 Excess pore water pressures along a 300mm bed height of LBS-B, d_{50} 0.9mm, and orifice opening of 0.33mm.

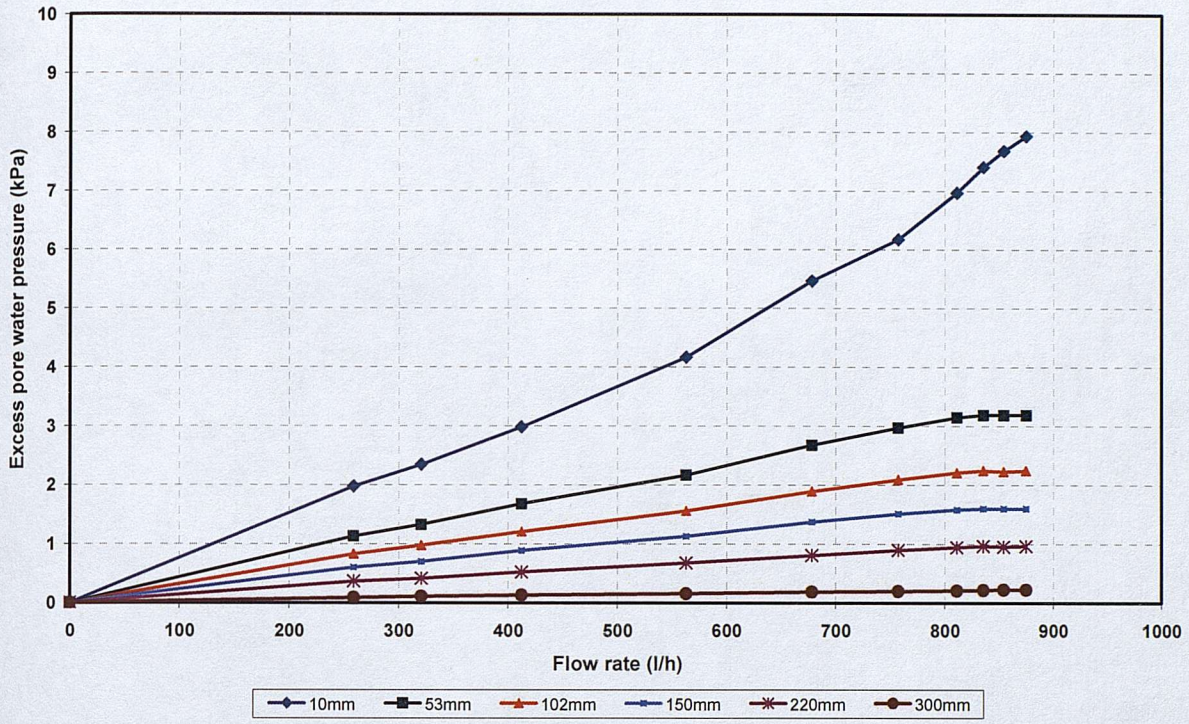

Figure 4.26: Excess pore water pressure at different points along 300mm bed height of silica sand, d_{50} 0.9mm, and orifice opening 0.234mm.

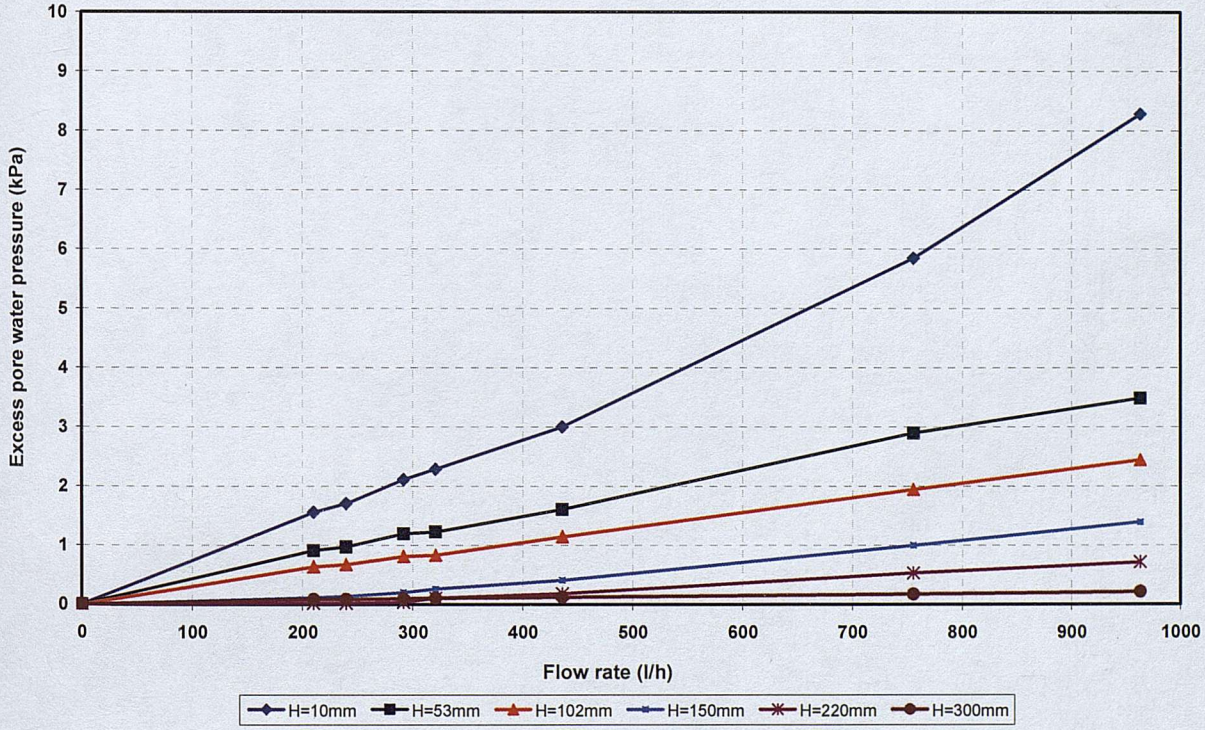

Figure 4.27: Excess pore water pressure at different points along 300mm bed height of silica sand, d_{50} 0.9mm, and orifice opening 0.33mm.

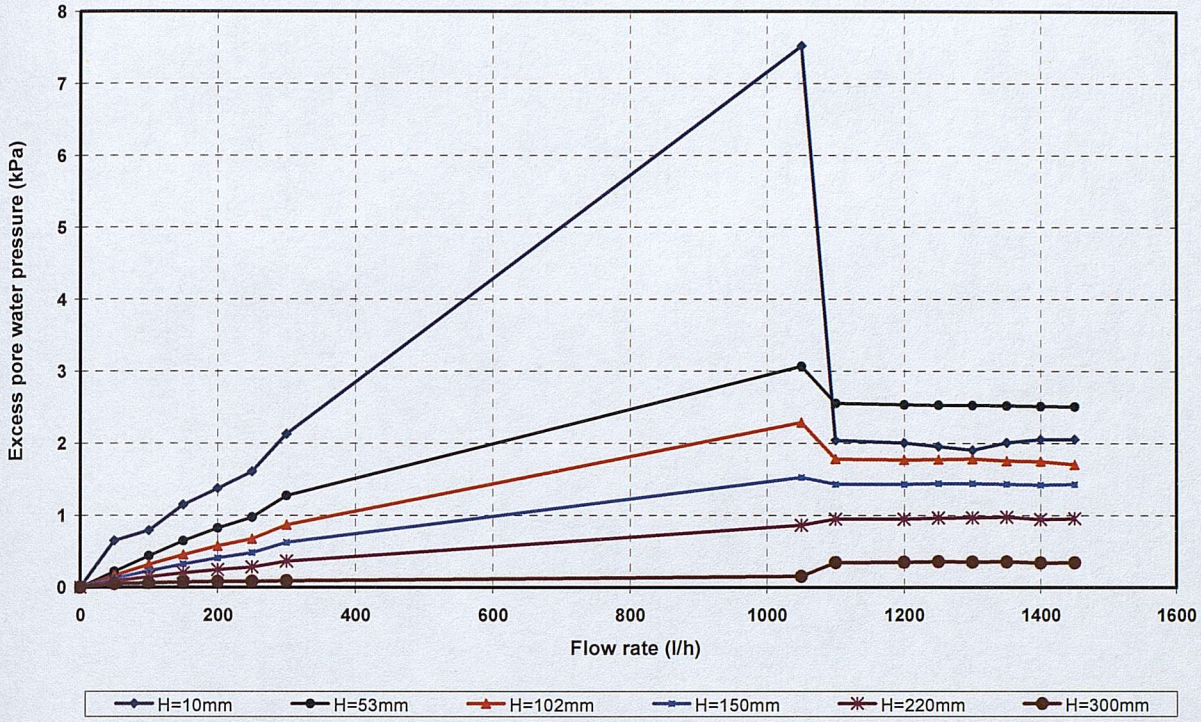

Figure 4.28: Excess pore water pressure at different points along 300mm bed height of LBS-B, d_{50} 0.9mm, and orifice opening 0.62mm.

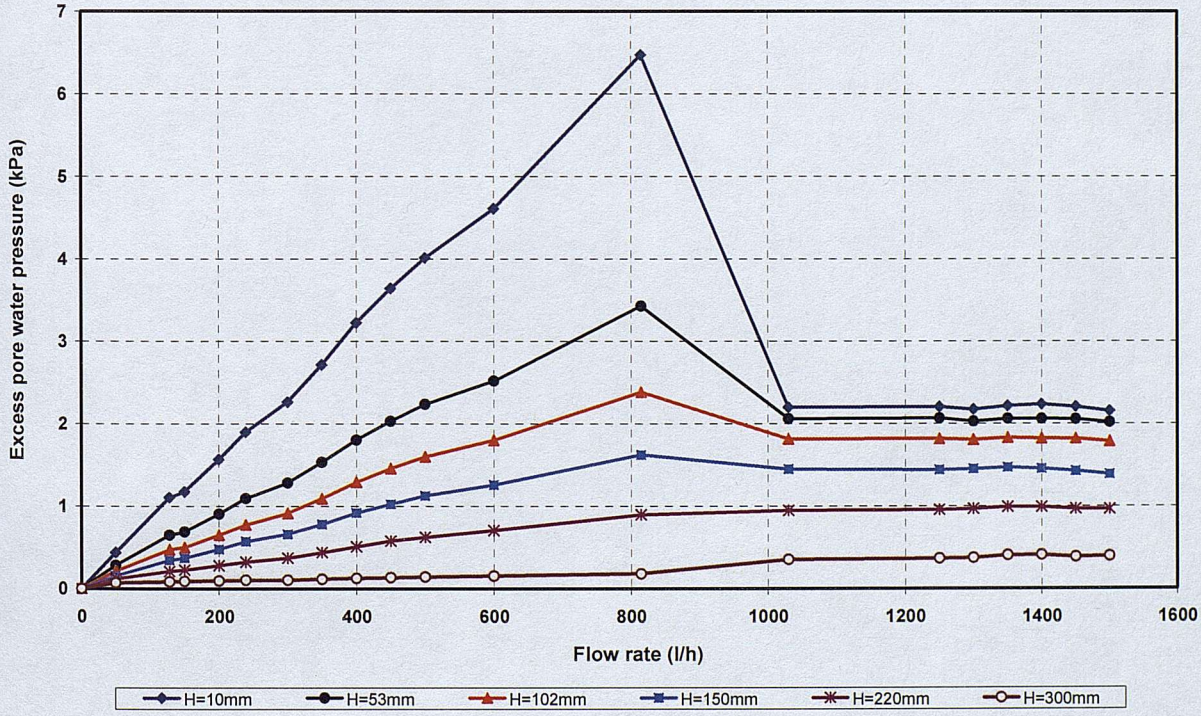

Figure 4.29: Excess pore water pressure at different points along 300mm bed height of LBS-B, d_{50} 0.9mm, and orifice opening 0.92mm.

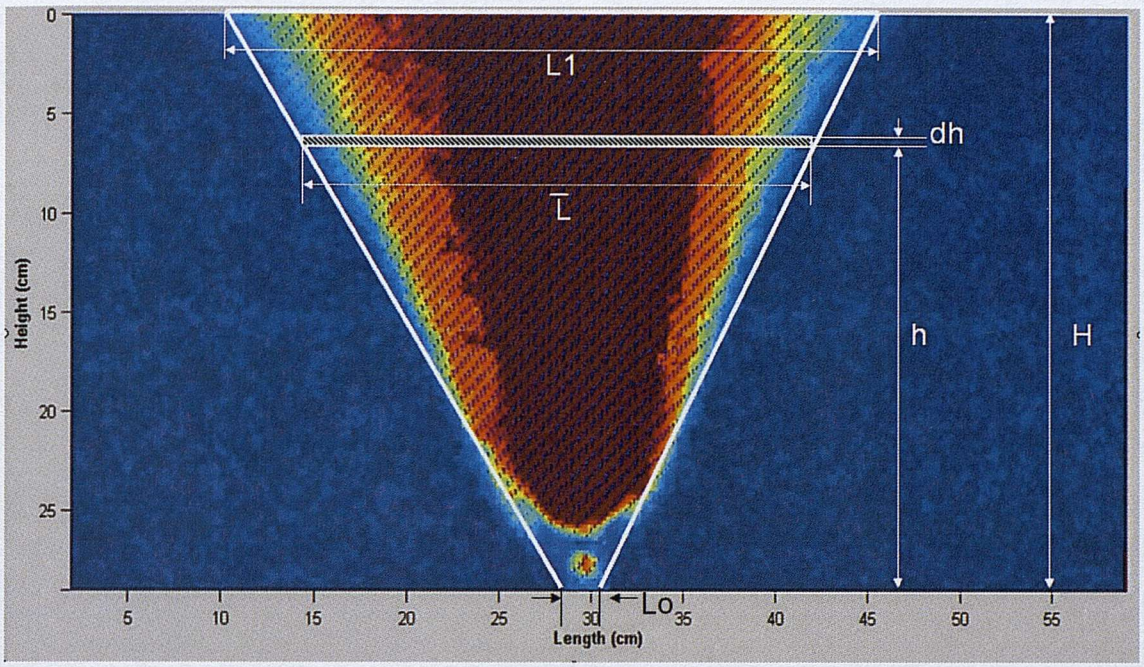

Figure 4-30a: The active weight of the bed at onset of fluidisation (using PIV).

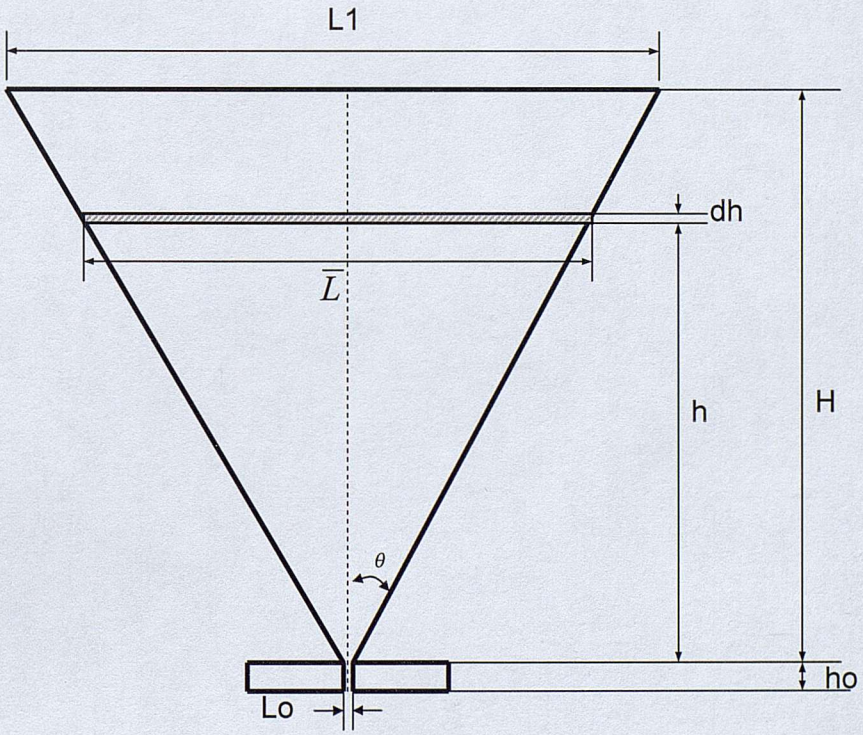

Figure 4.30b: The active weight of the bed at onset of fluidisation.

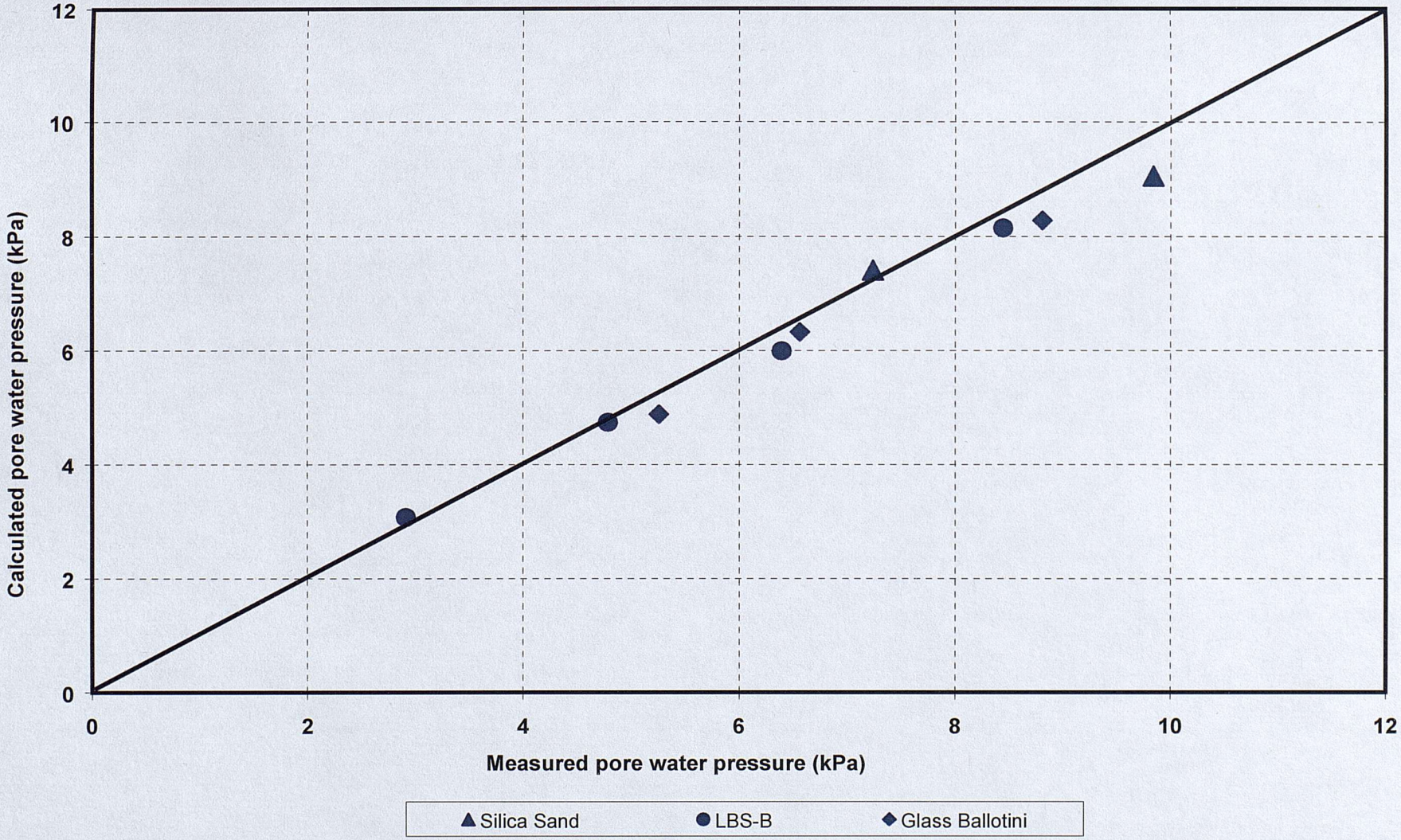

Figure 4.31: Comparison of calculated pore water pressures with experimental at onset of fluidisation.

CHAPTER 5 CONCLUSIONS AND RECOMMENDATIONS FOR FUTURE WORK

Interpretation of the literature

The literature review (Chapter 2) has shown that:

- Uncontrolled seepage flow through defects or imperfect joints in engineering structures such as dams, levees, dry-docks, seepage barriers, sheet piles interlocking or from fractured underground pipes is of great concern. A large number of failures occur due to concentrated leakage from such structures. Failure by seepage flow is considered to cause among the most serious accidents in civil engineering.

- Traditionally, failure by seepage flow is perceived as resulting from piping phenomena, in which erosion of the structure initiates at the exit point of seepage, and progressive backward erosion along its base results in the formation of a continuous passage or pipe. Piping is initiated by Darcy flow at the exit point where the flow is laminar. However, failures by seepage flow are very complex and may involve other mechanisms. Unfortunately when structures fail by seepage flow the evidence is often washed away with the structures.

- This thesis deals with internal fluidisation of granular material due to localised leakage. It is postulated that due to the build-up of pore water pressure and increased hydraulic gradient at the point sources of leakage an internally fluidised zone may occur in the body of the structure without being observed at the surface. Such a phenomenon may be transparency-limited until it has progressed enough to be visible or detected by measurements.

- In soil seepage analysis, Darcy's law is generally applied, which suggests that the rate of flow, and hence seepage velocity, is linearly proportional to the hydraulic

head and inversely proportional to the length of flow path. However, there are limits to the validity of Darcy's law in that it can only be applied to laminar flow. From a theoretical view, flow through defects in a structure does not adhere to Darcy's law. It has been suggested by some researchers that size of the opening may play a critical role.

- The literature review reveals that the mechanical role of the hydraulic gradient on failure is not well known. Seepage theory suggests that the critical hydraulic gradient at which fluidisation would occur is about one (based on Terzaghi's failure theory). However, it is recognised that the actual critical hydraulic gradient can be different from that proposed in the theory. It has been suggested by some researchers that distribution of internal stress may influence failure potential.

- A review of the literature on orifice flow indicates that the orifice flow equation is based on the Bernoulli principle which is only applicable along streamlines of fluid flow. This however may not be relevant for the case of flow through defects in pipes or structures due to the interaction of particles with the orifice, and development of flow separation or cavitation at the orifice.

- Very limited research has been carried out on the interaction of soil particles with orifice flow, for example from a leaking pipe. What has been done suggests that soil has no effect on leakage rate because of fluidisation. It has been indicated that the possibility of soil fluidisation from a point source of leakage is very high. However, related literature (in other fields) suggests that the start of fluidisation from a buried pipe requires an energy input greater than that necessary for the fluidisation itself. This has been referred to as the energy required to overcoming grain interlock and energy dissipation at the orifice.

- Theoretical models for estimating the hydraulic pressure in a packed bed of particulate material are already available in other scientific fields (e.g. the Ergun model), and which take into account the effect of laminar and turbulent flow in the bed. These, however, were developed on the hypothesis of uniform flow in a columnar fluidised bed, and therefore may not be valid when the flow results from concentrated leakage, as in the case of a leak through sheet wall pile interlocking, or from a buried pipe, as a result of hydraulic fracturing in embankment dams, or through the seepage barrier in dams. See Section 2.3.

- Experimental evidence available (in other scientific fields) indicates that an internal fluidised zone can form in a bed of granular material when fluid is injected into it. In most of these studies a jet of gas was used as the injection fluid (See Section 2.6).

- Surprisingly very little is known about the phenomenon of internal fluidisation in the field of civil engineering, although it is seen to be very important in designing, assessing, and monitoring of retaining structures where seepage flow is inevitable. Therefore research is required to develop design methodologies based on a better understanding of the mechanisms involved with a localised flow.

Development of experimental apparatus and techniques

- An experimental apparatus and techniques have been developed to investigate the mechanism of internal fluidisation of granular material due to localised flow. A two-dimensional experimental model has been built for the study, in which a machined box with variable orifice openings was designed to simulate an idealised crack for a concentrated leak. The box was fitted inside a modified seepage tank to fluidise a bed of granular material (See section 3.2). The size of the tank (1060 mm 550 mm 153 mm) was reduced to form a sample with dimensions of 600 mm length, 300 mm height and 146.6 mm width. The tests were conducted with very small orifices i.e. a fraction of a millimetre (ranging between 0.235 mm and 0.92

mm). The tests were conducted on a number of granular materials, LBS-A, LBS-B, Silica Sand, and Glass Ballotini, which had different articles sizes and forms.

- Techniques for monitoring the behaviour of the fluidised bed were developed based on Particle Image Velocimetery (PIV).

Observation of the internally fluidised zone

- Results and observations of the conducted experiments showed that as the rate of flow through the orifice increased, by increasing pressure behind the orifice, the excess pore water pressure inside the bed of material increased correspondingly. At a certain point, the excess pore water pressure reached its maximum value; at which the particles above the injecting point were lifted upward to a certain level because of equilibrium with the upward drag force by the fluid. This was the point of onset of fluidisation. At this point, the particles in the vicinity of the injecting point started to fluidise (i.e. forming an internally fluidised zone, where the particles moved with the jet of water) while further away from the orifice the bed remained fixed. In this state the bed of grains is said to be an internally fluidised bed.

- It was found that a high pressure head could be sustained upstream of the orifice even above a shallow bed of granular material, without the fluidised zone breaking through to the bed surface.

Observations of the uplift mechanism

- Deformation of the bed material during the uplift mechanism was studied using image analysis. In all tested cases where fluidisation occurred, the mechanism resembled an inverted tapered block, surrounded by distributed shear zones extending outwards and widening towards the surface (see Figure3.12). The weight of the bed within the trapezoidal block was equal to the uplift force due to seepage at the onset of fluidisation.

- The inclination angle of the wedge of the uplifted zone was observed to be in the range of 63.2° and 64.8° with an average value of 63.8°. The angle was not affected either by orifice size or by the height of the bed for the tested conditions.

Observations on the hydraulic gradient

- The build-up of hydraulic pressure and increase in hydraulic gradient in the vicinity of the injecting point (within 50 mm of this point) were much higher than the build-up recorded further away from the this point, with a ratio of about 10:1 for the tested conditions.

- The average hydraulic gradient at the onset of fluidisation was found to be greater than unity, with a value ranged between 1.5 and 3 for the tested conditions.

Observations on the pressure-flow rate relationship

- The relationship between pressure in the orifice and flow rate is complex. Five different phases have been observed experimentally depending on various factors the most important of which is the rate of flow:
  (i) A linear relationship between pressure and flow rate was observed at low flow rate (i.e. up to 100 to 200 l/h), adhering to Darcy's flow.
  (ii) A deviation from Darcy's flow was observed at slightly higher flow rates in which higher pressure was required to deliver more flow due to the combined effect of the orifice and bed material on the pressure-flow rate relationship.
  (iii) At a certain point of flow a sudden drop in pressure in the orifice was associated with a jump in the rate of flow due to the fluidisation effect.
  (iv) After the onset of fluidisation, the pressure was proportional to the flow squared following the orifice flow theory.
  (v) Deviation from the orifice flow equation was observed at high flow rates, due to cavitation development in the orifice.

- At the start of fluidisation, the pressure in the orifice dropped significantly for larger orifice sizes and a relatively small amount for the smaller orifice size. This is because for small openings most of the head loss was orifice loss rather than the bed head loss. The drop in the pressure was associated with a sudden increase in the rate of flow due to particles above the orifice being lifted upward to a certain level because of the upward drag force of the fluid.

- Development of cavitation in an orifice has a drastic effect on the pressure-flow rate relationship. This mechanism occurs at very high velocity in the orifice, where the pressure of the liquid drops below its vapour pressure. During this mechanism a vapour region is thought to form inside the orifice, resulting in a reduction in the effective area of the flow, until a point is reached where there is no further increase in the flow rate as pressure increases. Development of such a mechanism in the orifice also leads to its degradation by a process termed cavitation erosion.

Observations on the impact of particle characteristics on the start of fluidisation

The build-up of excess pore water pressure in the bed of granular material was dependent upon the size and form (i.e. sphericity) of the grain. At any given flow rate, the finer the particles, the higher the build-up of pore water pressure compared to the coarser particles, as this is a function of soil permeability. This higher increase in the build-up of pore water pressure for the finer particles led to an increased potential of fluidisation. For coarser soil particles, a higher flow rate is required for the onset of fluidisation compared to the finer particles.

- Particle form has an effect on excess pore water pressure generation. For a given flow rate the build-up of excess pore water pressure increased with decreasing form. This leads to increased potential for fluidisation.

Observation on the impact of orifice opening

- Profiles of excess pore pressure were unaffected by the size of the orifice opening, but were controlled by the discharge flow rate. However, the pressure head in the orifice is very dependent on its size. The smaller the orifice, the larger the pressure head in the orifice required for the onset of fluidisation.

- Most pressure loss was dissipated through the orifice, while a relatively small amount was dissipated through the soil. The pressure in the orifice (i.e. potential energy) was converted into velocity head (i.e. kinetic energy) in the orifice and inside the fluidised zone.

Prediction of the excess pore water pressure at the onset of fluidisation

- A theoretical model, based on the concept of force equilibrium exerted on the particles in the bed, has been presented for predicting the excess pore water pressure at the point of fluidisation (see section 4.6).

Practical implications of this research

Fluidisation of granular material is relevant to various industrial, coastal and geotechnical applications:

- In industries, fluidised beds are commonly used in chemical engineering processing as devices for mixing, and heat and mass transfer; and as chemical reactors. For example in the case of tapered fluidised beds, extensive particle mixing can be achieved leading to various applications such as the biological treatment of wastewater, incineration of waste materials and coating nuclear fuel particles. Understanding the fundamental mechanism and the controlling parameters of such a phenomenon are of importance to these applications.

- Applications of fluidisation in coastal engineering are relevant to the design of fluidiser systems for maintenance of navigable waterways at tidal inlets and

harbour mouths. Prediction of the hydraulic pressures in the bed of material as well as the pressure in the orifice at the start of fluidisation is important in designing such systems.

- The research is also of importance in the case of leakage through sheet pile walls with interlocking joints. Leakage through these interlocking joints leads to the build-up of excess pore water pressure in soil which may lead to the increased potential of fluidisation and loss of stability on the excavated side of the sheet pile wall.

- This study is also of practical importance to the case of leakage from buried pipes. Leakage through defects (i.e. cracks, holes, or joints) in pipes can lead to the build-up of hydraulic pressure in the surrounding soil which increases the potential of the formation of internally fluidised zone, and this can lead to pipe grinding.

- Fluidisation is also invoked as an important process in volcanic systems. It is seen to play an important role in environmental flow, such as pyroclastic flow (Wilson, 1980), and exerts major control over the structure and sorting of deposits in Kimberlite pipes (Walter et al., 2006).

Recommendations for future work

- The developed apparatus in this research has been designed to study the problem in two-dimensions, allowing the fluidised zone to be observed and monitored using image analysis techniques such as the Particle Image Velocimetery (PIV). Further work should be carried out to study the problem in three dimensions, and see what effect this has.

- This study has been limited to a certain type of material, i.e. uniform granular material. However, it has been anticipated that different mechanisms would occur

if other materials were investigated, such as widely graded material and clay which need further investigation.

- In this study, water was used as the injection fluid and was based on unidirectional seepage flow tests in upward direction. Future work could be carried out using different fluids (e.g. gas, glycerol) as well as different flow directions (e.g. horizontal, downwards).

- Further study might incorporate numerical modelling such as Computational Fluid Mechanics (CFD), and develop a model to simulate the phenomenon of the internally fluidised zone.

REFERENCES

Adrian, R. J. (1991) 'Particle image techniques for experimental fluid mechanics', Annual Review of Fluid Mechanics, vol. 23, pp.261-304.

Al-Karni, A. (2000). 'Stability of saturated cohesionless soil layer due to water flowing from a broken underground pipeline.' Journal of King Saud University, Engineering Science, vol.12, no.1: pp 27-44.

Albertson, M. L., Dai, Y. B., Jensen, R. A., and Rouse, H. (1950) 'Diffusion of submerged jets', *Transactions of* the American Society of Civil Engineers, 115, 639-664.

Ambraseys, N. N. (1963). "Cut-Off Efficiency of Grout Curtains and Slurry Trenches." Grouts and Drilling Muds in Engineering Practice, Butterworths, London, 1963, pp 43-46.

Apte, V. B., Wall, T. F., and Truelove, J. S., (1990) 'Stress Distribution in a Packed Bed above Raceway Cavities Formed by an Air Jet'. *AIChE Journal,* vol.36, (no.3): pp. 461-468.

Bear, J. (1972) *Dynamics of fluids in Porous Media,* New York, Dover Publications.
Bird, R. B., Stewart, W. E., Lightfoot, E.N., (2002). Transport Phenomena. John Wiley and Sons, New York.

Bjerrum L., Nash. J. K., Kennard R. M., and Gibson R.E. (1972). 'Hydraulic fracturing in field permeability testing.' Geotechnique, Vol. 22, no. 2, pp.319-332.

Brater, E., King, H., Lindell J., and Wei C. (1996). Handbook of Hydraulics, 7th Edition, McGraw-Hill Book Company, New York.

Bui, M. (2009). Influence of Some Particle Characteristics on the Small Strain Response of Granular Materials. Ph.D. thesis, School of Civil Engineering and the Environment, University of Southampton.

Burnell, D., and Race, J. (2000). 'Water Distribution Systems Analysis: Patterns in Supply Pipe Leakage', Proc. 2000 ASCE EWRI Conf., Minneapolis.

Busciglio, A., Vella, G., Micale, G., Rizzuti, L (2007) 'A Digital Image Analysis Technique For 2-D Gas Solid Fluidized Beds' *The 6th International Conference on Multiphase Flow, ICMF.* Leipzig, Germany, July 9 – 13, 2007.

Caicedo, G. R., Marque´s , J. J., Rui´z, M. G., and Soler, J. G. (2003). 'A study on the behaviour of bubbles of a 2D gas-solid fluidized bed using digital image analysis.', Chemical Engineering and Processing, vol. 42, 2003, pp. 9 -14.

Casagrande, A. (1961). "Control of Seepage through Foundations and Abutments of Dams." Geotechnique, Vol.11 (Septemebr,1961), pp:161-181.

Cedergren, H. R. (1989). Seepage, Drainage, and Flow Nets. John Wiley & Sons, Inc., Canada.

Chen, Y., Zhu, X., Wu, Y., Zhu, Z. (2007). "The investigation of pressure drop in moving-beds." Chem. Eng. China, vol.1(no.2): pp:184-189.

Cheuk, C. Y., White, D. J., and Bolton, M. D., (2008). "Uplift Mechanisms of Pipes Buried in Sand." Journal Of Geotechnical and Geoenvironmental Engineering © ASCE Vol. 134 (No. 2): pp:154–163.

Ciottoni, A. (1983). 'Computerized Data Management in Determining Causes of Water Main Breaks: The Philadelphia Case Study', Proceedings of the 1983 international symposium on urban hydrology, hydraulics and sediment control, University of Kentucky, Lexington, Kentucky.

Clayton, C.R.I., Xu, M., Whiter, J., Ham, A., and Rust, M. (2010). 'The influence of seasonal swelling and shrinkage of clay soils on the stresses in cast-iron water distribution pipes', Proceedings of ICE, Water Management, Vol.163 (No.2), pp:157-162.

Clayton, C. R. I., Abbireddy, C. O. R. and Schiebel, R., (2009). "A method of estimation the form of coarse particulates." Geotechnique. Vol.59 (No.6): pp:493-501.

Corey, A. T. (1949). Influence of the shape on the fall velocity of sand grains. Master's thesis, Colorado A & M College, Fort Collins, Colorado, USA.

Darcy, H. (1856). "Les Fontaines publiques de la ville de Dijon (The Public Fountains of the City of Dijon)." English translation by Patricia Bobeck, Kendall Hunt Publishing Co., 2004.

Davidson, L. (1990). "Performance of the concrete diaphragm wall at Navajo Dam." *Proc., Dam Foundation Engineering, 10th Annual USCOLD Lecture*, U.S. Committee on Large Dams, New Orleans, 1–21.

Douglas, J. F., Gasiorek, J.M., Swaffield, J.A. (1979). Fluid Mechanics. Pitman Publishing Limited, England, p.648.

Ergun, S. (1952). 'Fluid flow through packed columns', Chemical Engineering Progress, vol. 48 (No.2), 1952, pp.89-94.

Fell, R., MacGregor, P., Stapledon, D. and Bell, G. (2005). Geotechnical engineering of dams. Balkema, Leiden, ISBN 041536440x.

Field, M., Scott Smith, B.H., (1999). Contrasting geology and near-surface emplacement of kimberlite pipes in southern Africa and Canada. Proceedings of the VIIth International Kimberlite Conference, vol.1, pp. 217-237.

Forchheimer, P. (1901), "Wasserbewegung Durch Boden." Z Ver Deutsch Ing, Vol. 45, pp 1782-1788.

Foster, M., and Fell, R., Ed. (1999). A framework for estimating the probability of failure of embankment dams by internal erosion and piping using event tree methods. UNICIV Report No. R-377, School of Civil and Environmental Engineering, University of New South Wales, Sydney, Australia. ISBN 85841 344 2.

Foster, M., Fell, R. & Spannagle, M. (2000). "A method for assessing the relative likelihood of failure of embankment dams by piping." Canadian Geotechnical Journal, vol. 37 (no.5), pp:1025-1061.

Foster, M., Fell, R. & Spannagle, M. (2002). "Dicussion: A method for assessing the relative likelihood of failure of embankment dams by piping." Canadian Geotechnical Journal, 30 (2002), pp: 497-500.

Foster, M., Fell, R., and Spannagle, M., (2002). "Discussion: A method for assessing the relative likelihood of failure of embankment dams by piping: Reply1." Canadian Geotechnical Journal, vol. **39** (2002), pp: 497-500.

Foster, M.A. (1999). "The probability of failure of embankment dams by internal erosion and piping". PhD thesis, School of Civil and Environmental Engineering, University of New South Wales, Sydney, Australia.

Garber, H. J. (1972). "Memorandum review of hydraulic fill, Crane Valley Storage Dam and Reservoir, No. 95-3." *California Division of Water Resources Internal Memorandum.*

Gernon, T. M., Gilbertson, M.A., Sparks, R.S.J., Field, M. (2009). "The role of gas-fluidisation in the formation of massive volcaniclastic kimberlite." Lithos 112S (2009), pp: 439-451.

Gernon, T. M., Gilbertson, M.A., Sparks, R.S.J., Field, M., (2008). "Gas-fluidisation in an experimental tapered bed: insights into processes in diverging volcanic conduits." Journal of Volcanology and Geothermal Research, vol.174(No.1–3), pp:49–56.

Global Water Leakage Summit (2008) 'Adapting the Most Effective Strategies for Water Efficiency and Leakage Management'. *The 3rd Annual leakage Summit for international water utilities.* London, UK, 17-18 June 2008.http://www.global-leakage-summit.com/index.asp. Last Accessed 6/04/2008.

Guertin, J. D., and McTigue, W. H., "Groundwater Control Systems for Urban Tunneling," Groundwater Control in Tunneling, Vol 1, Report No. FHWA-RD-81-073, Apr 1982, U. S. Department of Transportation, Federal Highway Administration, Washington, D. C. Available from: Technical Information Center, U. S. Army Engineer Waterways Experiment Station, P. O. Box 631, Vicksburg, MS 39180-0631.

Habibian, A. (1994). 'Effect of Temperature Changes on Water Main Breaks.' Journal of Transportation Engineering, vol.120, no. 2, pp. 312-321.

Halvorsen, B. (2005) 'An experimental and computational study of flow behaviour in bubbling fluidised beds', PhD Thesis, Department of Technology, Norwegian University of Science and Technology, P153.

Harr, M. E. (1962) *Groundwater and Seepage,* New York, M.cGraw Hill.

Hartman, M., and Coughlin, R. W. (1993) 'On the incipient of fluidised state of solid particles'. Collection of Czechoslovak Chemical Communications, vol.58, pp.1213-1241.

Hawthorne, J. B. (1975). "Model of a kimberlite pipe. ." Physics and Chemistry of the Earth, vol.9 (1975), pp: 1-10.

Hlushkou, D., and Tallarek, U. (2006). "Transition from creeping via viscous-inertial to turbulent flow in fixed beds." Journal of Chromatography A, vol.1126 (No.1-2), pp: 70-85.

Holtz, R. D. and Kovacs, W. D. (1981) *An Introduction to Geotechnical Engineering*, Prentice-Hall, Inc., Englewood Cliffs, N. J., 733 p.

Hooper, J., Maschnes, E., and Farrant, T., (2004). "Penguin pipeline system—Design challenges for the world's longest snaked lay HP/HT PIP tie-back." Offshore Pipeline Technology Conf., Amsterdam, The Netherlands.

Idelchik, I. E. (1994), *Handbook of Hydraulic Resistance*, 3rd edition, Begell House, New York.

Independent Panel to Review Cause of Teton Dam Failure (1976). Report to the U.S. Department of the Interior and State of Idaho on Failure of Teton Dam. Idaho Falls, Idaho. December 1976.

Jaworski, G., Duncan, J., and Seed, H., (1981). "Laboratory study of Hydraulic Fracturing." ASCE, Journal of Geotechnical Engineering, vol.107 (GT6), pp: 713-733.

Keane, R. D., Adrian, R. J. (1992) 'Theory of cross-correlation analysis of PIV images', Applied Scientific Research, vol.49, no.3, pp.191-215

Kjaernsli, B., Torblaa, I. (1968). "Leakage through horizontal cracks in the core of Hyttejuvet dam." Norwegian Geotechnical Institute Publication, No.80, pp: 39-47.

Koivula, T. S. (2002). Cavitation in Hydraulic Valves-Aspects on the Effect of Oil Type, Erosion, and Detection Methods. PhD Thesis. Institute of Hydraulic and Automation, Tampere University of Technology.

Koivula, T. S., and Ellman, A. U., (1998). "Cavitation behaviour of hydraulic orifices and valves." Society of Automotive Engineers Transaction, vol.107(1998): pp:387–394.

Krumbein, W. C. (1942). "Measurement and geological significance of shape and roundness of sedimentary particles." Journal of Sedimentary Petrology, vol.11 (1942): pp: 64–72.

Krumbein, W. C., and Sloss, L.L., (1963). Stratigraphy and sedimentation. Second edition. W.H. Freeman and Company, San Francisco. P.660.

Kulhaway, H., and Gurtowski, T. M. (1976). "Load transfer and hydraulic fracturing in zoned dams." Journal of the Geotechnical Engineering Division, vol. 102 (No.9), pp. 963-974.

Kunii, D., and Levenspiel, O. (1991). Fluidization Engineering A Butterworth-Heinemann, Stoneham.

Kunkel, G., Laven, K., and Mergelas, B. (2008). "Does Your City Have High Risk Pipes?" American Water Works Association Journal, vol.100 (no.4): pp.70.

Lamb, W. S. (1987). Cavitation and aeration in hydraulic systems. Bedfordshire, UK. BHRGroup, pp:114.

Laverman, J. A., Roghair, I., Van Sint Annaland, M. and Kuipers, J.A.M. (2007) 'Experimental study on solids mixing and bubble behaviour in a pseudo-2D, freely bubbling, gas-solid fluidized bed using PIV and DIA'. The *6th International Conference on Multiphase Flow (ICMF).* . Leipzig, Germany, July 9 – 13, 2007.

LaVison, (2007). FlowMaster, Advanced PIV/PTV systems for quantitative flow field analysis, LaVison LTD, United Kingdom.

Ledwith, C., Weisman, R. N., and Lennon, G. P. (1990) 'Selection of Hole size for Fluidisation Pipes'. *Proc. Nat. Hydr. Conf., ASCE,* New York, N.Y., pp: 933-938.

Lennon, G. P., Chang, T. and Welsman, R.N. (1990). "Predicting incipient fluidization of fine sands in unbounded domains." Journal Hydraulic Engineering, vol.116(No.12): pp:1454-1467.

Leva, M. (1959) Fluidization, McGraw-Hill Book Co., New York, 327pp.

Lofquist, B. (1986). "Discussion paper concerning Sherard, J. "Hydraulic fracturing in embankment dams"." Journal of Geotechnical Engineering © ASCE Vol.112 (No.10), pp: 905-927.

Lueptow, R. M., Akonur, A., AND Shinbrot, T. (2000) 'PIV for granular flows'. *Experiments in Fluid,* Vol.28, no.2, pp.183-186.

MacDonald, J., and Bridgwater J. (1997). 'Void formation in stationary and moving beds', Chemical Engineering Science, vol. 52, no. 5, pp. 677-691.

Makar, J. (1999). 'Failure Analysis for Grey Cast Iron Water Pipes', AWWA Distribution System Symposium, Reno, Nevada.1-8.

Makar, J., Desnoyers, R., and McDonald, S. (2001).'Failure modes and mechanisms in grey cast iron pipe', Underground Infrastructure Research: Municipal,

Industrial and Environmental Applications, Proceedings, Kitchener, Ontario.1-10.

Massey, B. S., Ward-Smith, J.1998)). Mechanics of fluid. Taylor and Francis, ISBN 0748740430 , p.744.

Massimilla, L., Volpicelli, G. and Zenz, F., (1963), Flow of fluid particle suspensions from liquid-fluidised beds. Industrial and Engineering Chemistry Fundamentals. vol. 2 (3), 194-199.

Mu1ller, C. R., Davidson, J. F., Dennis, J. S., and Hayhurst, A. N. 2007. 'A study of the motion and eruption of a bubble at the surface of a two-dimensional fluidized bed using Particle Image Velocimetry (PIV)'. Ind. Eng. Chem. Res., vol. 46, no. 5, pp. 1642- 1652.

Murdoch, L. C. (1993). "“Hydraulic fracturing of soil during laboratory experiments: methods and observations." Geotechnique, vol.43(No.2): pp:255-265.

Muskat, M. e. (1937). The Flow of Homogenous Fluid through Porous Media, Mcgraw Hill Book Company, Incorporated. Reprinted by J.W. Edwards, Inc., Ann Arbor, Michigan, 1946.

Myllykylä, J. (1999). Semi-empirical model for the suction capability of an external gear pump. Ph.D thesis., Tampere University of Technology.

Nichols, R. J., Sparks, R. S., and Wilson, C. J. (1994). "Experimental studies of the fluidisation of layered sediments and the formation of fluid escape structures." Sedimentology, vol. 41: pp.233-253.

Niven, R. K. (2002) 'Physical insight into the Ergun and Wen & Yu equations for fluid flow in packed and fluidised beds'. *Chemical Engineering Science,* vol.57, no.3, pp. 527-534.

Niven, R. K. (2003) 'Discussion paper concerning D.W. Barr. 'Turbulent Flow Through Porous Media'. *Ground water,* vol. 39, no.5, pp. 646-650.

Niven, R. K., and, Khalili, N. (1998). 'In Situ Fluidization by a Single Internal Vertical Jet', Journal of Hydraulic Research, vol. 36, no. 2, pp. 199-228.

Noack, C., and Ulanicki, B. (2006). Modelling of Soil Deffusility on Leakage Characterstics of Burried Pipes. 8th Annual Water Distribution Systems Analysis Symposium, Cincinnati, Ohio, USA.

Nurick, W. H. (1976). "Orifice cavitation and its effects on spray mixing." Journal of Fluids Engineering, Transactions of the ASME, vol.98 (No.4): pp:681-687

O'Day, D. (1982). 'Organizing and analyzing leak and break data for making main replacement decisions', American Water Works Association, vol. 74, no.11, pp. 589-594.

O'Shea, P. J. (2000), 'Failure Mechanisms for small diameter cast iron water pipes', PhD Thesis, Department of Civil and Environmental Engineering, The University of Southampton.

Peng, Y., and Fan, L. (1997) 'Hydrodynamics Characteristics of Fluidisation in Liquid-Solid Tapered Beds'. *Chemical Engineering Science,* vol. 52, no.14, pp. 2277-2290.

Perkins, W. A. (1932). "Memorandum to Mr. Hawley, Crane Valley Dam #95–3, Inspected March 14, 1932." *California Division of Water Resources Internal Memorandum.*

Pillai, V. S., Muhunthan, B., Sasiharan, N. (2004). The Failure Of Teton Dam – A New Theory Based on "State Based Soil Mechanics." The fifth International Conference on Case Histories in Geotechnical Engineering, New York, NY, April 13-17, 2004

Rajani, B. B., Zhan, C., and Kuraoka, S. (1996).'Pipe-soil interaction analysis of jointed water mains', Canadian Geotechnical Journal, vol.33, no, 3, pp. 393-404.

Ramamurthi, K. and Nandakumar, K. (1999). 'Characteristics of flow through small sharp-edged cylindrical orifices', Flow Measurement and Instrumentation, vol.10 (1999) 133–143.

Reddy, A. C. O. (2008). Particle Form and its Impact on Packing and Shear Behaviour of Particulate Materials. Ph.D. thesis, School of Civil Engineering and the Environment, University of Southampton.

Reitz, R. D. a. B., F.V., (1982). "Mechanism of atomization of a liquid jet." Physics of Fluids. Vol.25 (No.10): pp:1730–1742.

Rice, J., Duncan, J. , and Davidson, R. (2007). 'Identification of Failure Mechanisms Associated with Seepage Barriers in Dams'. *Embankments, Dams, and*

Slopes: Lessons from the New Orleans Levee Failures and Other Current Issues (GSP 161), ASCE Conference Proceedings, pp:1-11.

Rice, J. D. a. D., M. (2010). "Findings of Case Histories on the Long-Term Performance of Seepage Barriers in Dams." Journal of Geotechnical and Geoenvironmental Engineering © ASCE vol.136 (No.1), pp: 2-35.

Richards, S., and Reddy, K. (2007). "Critical appraisal of piping phenomena in earth dams." Bulletin of Engineering Geology and the Environment, vol.66 (No.4), pp: 381-402.

Santana, D., Nauri, S., Acosta, A., Garcia, N., and Macias-Machin, A. (2005) 'Initial particle velocity spatial distribution from 2-D erupting bubbles in fluidized beds'. *Powder Technology,* vol.150, pp.1-8.

Sastry, G. S., Gupta, G.S., and Lahiri, A.K., (2003) 'Void formation and breaking in a packed bed'. *ISIJ International,* vol. 43, no.2, pp.153-160.

Scheidegger, A. E. (1960) *'The physics of flow through porous media'.* 2nd ed. Toronto, University of Toronto Press.

Shavit, U., Lowe, R. J., and Steinbuck, J. V. (2006) 'Intensity Capping: a simple method to improve cross-correlation PIV results'. *Experiments in Fluid,* vol. 42, no.2, pp. 225-240.

Shen, L., Johnsson, F., Leckner, B. (2004) 'Digital image analysis of hydrodynamics two-dimensional bubbling fluidised beds'. *Chemical Engineering Science,* vol. 59, 2607-2617.

Sherard, J. L. (1986). "Hydraulic fracturing in embankment dams." Journal of Geotechnical Engineering, ASCE, vol.112(No.10), pp: 905-927.

Sherard, J. L., Woodward, R. J., Gizienski, S. F. & Clevenger, W. A. (1963). Earth and earth rock dams, engineering problems of design and construction. John Wiley & Sons, New York.

Shi, Y., Yu, Y., and Fan (1984) 'Incipient Fluidisation Condition for a Tapered Fluidised Bed'. *Industrial & engineering Chemistry Fundamentals,* Vol.23, pp.484-489.

Silinis, P., and Franks, S. 2007. 'Understanding failure rates in cast iron pipes using temporal stratification', Urban Water Journal, vol. 4, no. 1, pp. 1 - 7.

Singh, V., Gupta, G.S. , and Sarkar, S. (2007). "Study of gas cavity size hysteresis in a packed bed using DEM " Chemical Engineering Science, vol. 62 (2007): pp. 6102-6111.

Skempton, A. and Brogan, J. (1994). 'Experiments on Piping in Sandy Gravels.' Geotechnique, vol. 44, no. 3, pp: 449-460.

Sneed, E. D. F., R.L., (1958). "Pebbles in the lower Colorado River, Texas, a study in particle morphogenesis." Journal of Geology, vol.66 (1958): pp. 114–150.

Sparks, R. S. J. (1976). "Grain-size variations in ignimbrites and implications for the transport of pyroclastic flows." Sedimentology, vol.23 (No.2): pp:147-188.

Sparks, R. S. J., Baker, L., Brown, R., Field, M., Schumacher, J., Stripp, G., Walters, A., (2006). "Dynamical constraints on kimberlite volcanism." Journal of Volcanology and Geothermal Research, vol.155(2006): pp:18–48.

Squier, L. (1970). " Load transfer in earth and rockfill dams." Journal Geotechnical Engineering Division. 96 (SM1) (1970): pp. 213-233.

Su, T. F., Farell, P.V., and Nagarajan, R.T., (1995). ""Nozzle Effect on High Pressure Diesel Injection"." SAE Paper 950083.

Sveen, J. K. (2004) *An introduction to MATPIV v. 1.6.1'*, eprint series, Dept. Of Math, University of Oslo, Mechanics and Applied Mathematics, No.2 ISSN 0809–4403, August 2004.

Taylor, D. W. (1948). Fundamentals of Soil Mechanics, John Wiley, New York.

Telling, R. M., Menzies, B K, SIMONS, N E (1978). "Effectiveness of Jointed Cut-Off Walls beneath Dams on Pervious Soil Foundations." Ground Engineering, vol.11(No.4), pp:27-37.

Terzaghi, K. (1922). "Der Grundbruch an Stauwerken und seine Verhutung (The failure of dams by piping and its prevention)." Die Wasserkraft, vol 17, pp 445–449. Reprinted in (1960) from theory to practice in soil mechanics. Wiley, New York.

Terzaghi, K. (1925). Earthwork mechanics on the basis of groundphysics (Erdbaumechanik, in German). Franz Deuticke, Leipzig, Germany.

Terzaghi, K. (1939). "Soil mechanics: a new chapter in engineering science." Institution of Civil Engineers, vol. 12(1039), pp: 106:141.

Terzaghi, K. (1943). Theoretical Soil Mechanics. John Wiley and Sons, New York.

Valverde, J. M., Ramos, A., Castellanos, A., Watson P.K. (1998). "The tensile strength of cohesive powders and its relationship to consolidation, free volume and cohesivity." Powder Technology, vol.97(1998): pp:237–245.

Van Zyl, J. E., Clayton C.R.I. 2007. 'The Effect of Pressure on Leakage in Water Distribution Systems', Proceedings of the Institution of Civil Engineers - Water Management, vol.160, no.WM2, pp.109 - 114.

Van Zyl, J. E., Clayton, C.R.I. 2005. 'The Effect of Pressure on Leakage in Water Distribution Systems, CCWI2005 Water Management for the 21st Century, Vol. 2, ISBN 0-9539140-3-8, Savic, D. A., Walters, G. A., Khu, S. T., King, R. (Eds.), Centre for water systems, university of Exter, UK, 131-136.

Wadell, H. (1932). "Volume, shape, and roundness of rock particles." Journal of Geology, vol. 40(1932): pp:443–451.

Wadell, H. (1933). "Sphericity and roundness of rock particles." The Journal of Geology, vol. 41(1933): pp: 310 - 331

Walski, T., Bezts, W., Posluzny, E., Weir, M., and Whitman, B. 2004. 'Understanding the Hydraulics of Water Distribution System Leaks', Proceeding of the 6th ASCE/EWRI Annual Symposium on Water Distribution System Analysis, Salt Lake City.

Walski, T., Bezts, W., Posluzny, E., Weir, M., and Whitman, B. 2006. 'Modelling Leakage Reduction Through Pressure Control', Journal of the American Water Work Association, vol. 98, no. 4, pp. 147-152.

Walters, A. L., Phillips, J.C., Brown, R.J., Field, M., Gernon, T., Stripp, G., Sparks, R.S.J., (2006). "The role of fluidisation in the formation of volcaniclastic kimberlite: grain size observations and experimental investigation." Journal of Volcanology and Geothermal Research, vol. 155 (2006), pp: 119-137.

Watson, I., and A.D. Burnett. 1993. Hydrology: An environmental approach. CRC Press, Boca Raton, FL.

Watson, P. K., Valverde, J.M., and Castellanos, A. (2001). "The tensile strength and free volume of cohesive powders compressed by gas flow." Powder Technology, vol. 115(2001), pp:45–50.

Weisman, R., Lennon, G., and Roberts, E. 1988. 'Experiment on Fluidization in Unbounded Domains', Journal of Hydraulic Engineering, vol.114, no. 5, pp. 502- 515.

Weisman, R. N., and Lennon, G. P., (1994) 'Design of Fluidiser Systems for Coastal Engineering', *Journal of Waterway, Port, Coastal, and Ocean Engineering, ASCE* vol. 120, no.5, PP. 468-487.

Wen, C. Y., and Yu, Y. H. (1966). Mechanics of fluidization. Chemical Engineering Progress Symposium, vol. 62, no.62, pp:100-111

White, D. J. (2002) An investigation into the behaviour of pressed-in piles. PhD thesis *Engineering Department*, University of Cambridge.

White, D. J., Take, W. A., and Bolton, M. D. (2003) 'Soil deformation measurement using Particle Image Velocimetry (PIV) and photogrammetry'. Geotechnique, vol. 53, no.7, PP. 619-631.

Wiklund, P. E. and Svedberg, G. C. (1996). The Cavitation properties of an axial piston pump using a vegetable and a mineral oil. 9th Bath international fluid power workshop, Bath, Uk.

Wilson, C. J. N. (1980). "The role of fluidisation in the emplacement of pyroclastic flows: an experimental approach." Journal of Volcanology and Geothermal Research, vol.8 (1980): PP:231-249.

Wilson, C. J. N. (1984). "The role of fluidisation in the emplacement of pyroclastic flows, 2: experimental results and their interpretation." Journal of Volcanology and Geothermal Research, vol. 20 (no.1-2), pp: 55-84.

Woolsey, T. S., McCallum, M.E. and Schumm, S.A., (1975). "Modeling of diatreme emplacement by fluidization." Physics and Chemistry of the Earth, vol.9 (1975): pp:24–42.

Zhang, B., Liu, X., and Zhu, H. (2003). "Mechanism of local fluidisation in converging packed beds." The Canadian journal of chemical Engineering, vol. 81 (October 2003): pp. 949-956.

Zoccola, M. F., Haskins, T. A., and Jackson, D. M. (2006). "The problem is the solution: A history of seepage, piping, and remediation in a Karst Foundation at Wolf Creek Dam." *Proc., 26th USSD Conf.— The Role of Dams in the 21st Century*, United States Society on Dams, Denver, 141–150.

Zoueshtiagh, F., and Merlen, A., (2007). "Effect of a vertically flowing water jet underneath a granular bed." Physical Review E 75, 056313-1-1056313-12.

Appendix A: MATPIV

In this study the Particle Image velocimetery technique has been performed using a computer code MatPIV written in MATLAB by Sveen (2004). The process for PIV was started by first defining a coordinate system to transformation from local camera coordinates (pixels) into physical world coordinates in the experiment. This was done by inserting a grid with points into the field of view and taken an image of it (Figure A.1). Thereafter masking out the region of the flow was applied to avoid performing calculations where there were no particles. Then the images were interrogated using the window shifting techniques to calculate the velocity field. A series of filters were then applied before finally all the identified outliers were interpolated using a nearest neighbour interpolation.

An example of the PIV run is presented below:

```
>> definewoco('mpwoco.jpg','.');
Please give the approximate width of your points (in pixels -default is 20). Type 0
here to get old behaviour of definewoco: 8
hsize =
  8.50000000000000  8.50000000000000
....calculating....this may take a few seconds.
...Done!
Now mark the dots you whish to use as coordinate points
Please mark your world coordinate points with left mouse button.
Press ENTER when finished!
Now you need to give the physical coordinates to each of the points specified!
----------
Please enter the world coordinates for the white circle marked in the current figure
(in square parenthesis):  [5,30]
Please enter the world coordinates for the white circle marked in the current figure
```

(in square parenthesis): [5,0]

Please enter the world coordinates for the white circle marked in the current figure

(in square parenthesis): [30,30]

Please enter the world coordinates for the white circle marked in the current figure

(in square parenthesis): [30,0]

Please enter the world coordinates for the white circle marked in the current figure

(in square parenthesis): [60,30]

Please enter the world coordinates for the white circle marked in the current figure

(in square parenthesis): [60,0]

Mapping function. (N)onlinear or (L)inear (N/n/L/l): l

Error (norm) = 4.4251

Save coordinate file....specify number >> 1

Coordinate mapping factors saved to file: worldco1

>> mask('mpim1b.jpg','worldco1.mat');

Mark your polygon points with the left mouse button.

Press the middle button when you are finished, press

<BACKSPACE> or <DELETE> to remove the previously selected vertex.

Do you whish to add another field to mask? (1 = yes, 0 = no) >> 0

* Calculating the pixel to world transformation using linear mapping - DONE

>> [x,y,u,v,snr,pkh]=matpiv('mpim1b.jpg','mpim1c.jpg',...

[64 64;64 64;32 32;32 32;16 16;16 16],...

0.32,0.5,'multin','worldco1.mat','polymask.mat');

* Pass No: 1

No. of vectors: 0 , Seconds taken: 0.013052,
No. of vectors: 1 , Seconds taken: 0.023128
No. of vectors: 70 , Seconds taken: 0.627552
No. of vectors: 139 , Seconds taken: 1.196350
No. of vectors: 208 , Seconds taken: 1.761530
No. of vectors: 277 , Seconds taken: 2.343857
No. of vectors: 346 , Seconds taken: 2.913907
No. of vectors: 415 , Seconds taken: 3.499115

No. of vectors: 484 , Seconds taken: 4.066173
No. of vectors: 553 , Seconds taken: 4.628333
No. of vectors: 622 , Seconds taken: 5.191381
No. of vectors: 691 , Seconds taken: 5.778626
No. of vectors: 760 , Seconds taken: 6.342545

No. of vectors: 829 , Seconds taken: 6.905337
No. of vectors: 898 , Seconds taken: 7.467838
No. of vectors: 967 , Seconds taken: 8.052264
No. of vectors: 1036 , Seconds taken: 8.614312
No. of vectors: 1105 , Seconds taken: 9.199314
No. of vectors: 1174 , Seconds taken: 9.765729
No. of vectors: 1243 , Seconds taken: 10.332250
No. of vectors: 1312 , Seconds taken: 10.896551
No. of vectors: 1381 , Seconds taken: 11.459867
No. of vectors: 1450 , Seconds taken: 12.024843
No. of vectors: 1519 , Seconds taken: 12.609333
No. of vectors: 1588 , Seconds taken: 13.177519
No. of vectors: 1657 , Seconds taken: 13.739328
No. of vectors: 1726 , Seconds taken: 14.305846
No. of vectors: 1795 , Seconds taken: 14.890402
No. of vectors: 1864 , Seconds taken: 15.457165
No. of vectors: 1933 , Seconds taken: 16.029969
No. of vectors: 2002 , Seconds taken: 16.596471
No. of vectors: 2071 , Seconds taken: 17.162379
No. of vectors: 2140 , Seconds taken: 17.725746
No. of vectors: 2209 , Seconds taken: 18.353391
No. of vectors: 2278 , Seconds taken: 18.940354
No. of vectors: 2347 , Seconds taken: 19.558744
No. of vectors: 2416 , Seconds taken: 20.123284
No. of vectors: 2485 , Seconds taken: 20.733880
No. of vectors: 2533 , Seconds taken: 21.161450.

Global filter running - with limit: 3 *std [U V] ..... 205 vectors changed

Local median filter running: .....7 vectors

changed.

Interpolating outliers: .....212 Nan's interpolated.

Expanding velocity-field for next pass

Interpolating outliers: .....59 Nan's interpolated.

* Pass No: 2

No. of vectors: 0 , Seconds taken: 0.000911
No. of vectors: 1 , Seconds taken: 0.009168
No. of vectors: 70 , Seconds taken: 0.637338
No. of vectors: 139 , Seconds taken: 1.257832
No. of vectors: 208 , Seconds taken: 1.885019

No. of vectors: 277 , Seconds taken: 2.504961
No. of vectors: 346 , Seconds taken: 3.132369
No. of vectors: 415 , Seconds taken: 3.749778
No. of vectors: 484 , Seconds taken: 4.333762
No. of vectors: 553 , Seconds taken: 4.955975
No. of vectors: 622 , Seconds taken: 5.557032
No. of vectors: 691 , Seconds taken: 6.183259
No. of vectors: 760 , Seconds taken: 6.775976
No. of vectors: 829 , Seconds taken: 7.402403
No. of vectors: 898 , Seconds taken: 8.027545
No. of vectors: 967 , Seconds taken: 8.606401
No. of vectors: 1036 , Seconds taken: 9.230370
No. of vectors: 1105 , Seconds taken: 9.808415
No. of vectors: 1174 , Seconds taken: 10.407372
No. of vectors: 1243 , Seconds taken: 11.033316
No. of vectors: 1312 , Seconds taken: 11.664046
No. of vectors: 1381 , Seconds taken: 12.288183
No. of vectors: 1450 , Seconds taken: 12.879047
No. of vectors: 1519 , Seconds taken: 13.504254
No. of vectors: 1588 , Seconds taken: 14.129027
No. of vectors: 1657 , Seconds taken: 14.708971
No. of vectors: 1726 , Seconds taken: 15.333815
No. of vectors: 1795 , Seconds taken: 15.927783
No. of vectors: 1864 , Seconds taken: 16.554324
No. of vectors: 1933 , Seconds taken: 17.179468
No. of vectors: 2002 , Seconds taken: 17.804623
No. of vectors: 2071 , Seconds taken: 18.397185
No. of vectors: 2140 , Seconds taken: 19.023492
No. of vectors: 2209 , Seconds taken: 19.648727
No. of vectors: 2278 , Seconds taken: 20.228863
No. of vectors: 2347 , Seconds taken: 20.854292
No. of vectors: 2416 , Seconds taken: 21.449371
No. of vectors: 2485 , Seconds taken: 22.076209
No. of vectors: 2533 , Seconds taken: 22.502906.

Global filter running - with limit: 3 *std [U V] ..... 186 vectors changed

Local median filter running: .....8 vectors changed.

Interpolating outliers: .....194 Nan's interpolated.

Expanding velocity-field for next pass

Interpolating outliers: .....272 Nan's interpolated.

* Pass No: 3

No. of vectors: 0 , Seconds taken: 0.002053

No. of vectors: 1 , Seconds taken: 0.010511

No. of vectors: 10009 , Seconds taken: 23.615792.

Global filter running - with limit: 3 *std [U V] ..... 641 vectors changed

Local median filter running:
.....36 vectors changed.

Interpolating outliers: .....677 Nan's interpolated.

Expanding velocity-field for next pass

Interpolating outliers:
.....206 Nan's interpolated.

* Pass No: 4

No. of vectors: 0 , Seconds taken: 0.002028

No. of vectors: 1 , Seconds taken: 0.010163

No. of vectors: 10009 , Seconds taken: 23.731063.

Global filter running - with limit: 3 *std [U V] ..... 633 vectors changed

Local median filter running:
.....37 vectors changed.

Interpolating outliers: .....670 Nan's interpolated.

Expanding velocity-field for next pass

Interpolating outliers:
.....688 Nan's interpolated.

* Pass No: 5

No. of vectors: 0 , Seconds taken: 0.005813

No. of vectors: 39740 , Seconds taken: 35.900719.

Global filter running - with limit: 3 *std [U V] ..... 1857 vectors changed

Local median filter running:
.....194 vectors changed.

Interpolating outliers:
.....2051 Nan's interpolated.

* Final Pass

- Using 16*16 interrogation windows!

No. of vectors: 0, Seconds taken: 0.012229

No. of vectors: 39740, Seconds taken: 43.208070

Calculating the pixel to world transformation using linear mapping – DONE

>> [su,sv]=snrfilt(x,y,u,v,snr,1.3);

SnR filter running with threshold value = 1.3 - finished... 46 outliers identified

>> [pu,pv]=peakfilt(x,y,su,sv,pkh,0.5);

Peak height filter running ..... 4 vectors changed

>> [gu,gv]=globfilt(x,y,pu,pv,3);

Global filter running - with limit: 3 *std [U V] ..... 999 vectors changed

>> [mu,mv]=localfilt(x,y,gu,gv,2,'median',3,'polymask.mat');

Local median filter running:

.....

.....6434 vectors changed.

>> [fu,fv]=naninterp(mu,mv,'linear','polymask.mat',x,y);

Interpolating outliers:

.....

.....7481 Nan's interpolated.

>> quiver(x(1:4:end),y(1:4:end),fu(1:4:end),fv(1:4:end),2); axis tight

>> w=magnitude(x,y,fu,fv);

>> pcolor(x,y,w), shading flat, colorbar

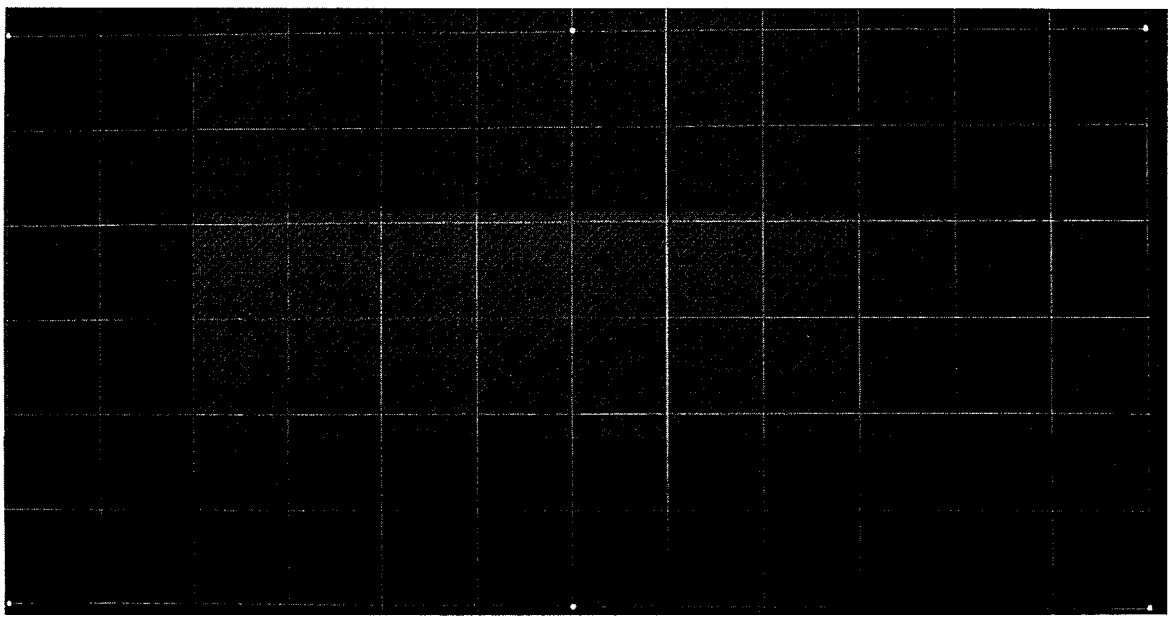

Figure: A-1 Image of the grid for coordinate system.

Appendix B: Mathematical derivations of the equations for predicting the pore water pressure at the onset of fluidisation

The model is based on the concept of force equilibrium exerted on the particles in the bed.

The upward drag force applied by fluid:

$$P = \frac{F}{A} \Rightarrow F = P.A \qquad \text{B-1}$$

The force is not proportional to pressure drop. This force in a differential bed height of (dh) equals the pressure drop through it (i.e. differential pressure) time the cross sectional area of the active bed ($\overline{L}W$) Shi et al. (1984), (see Figure B-2).

$$dF = (\overline{L}W).(dp) \qquad \text{B-2}$$

$$F = \int_{h_o}^{h_o+H} dF \qquad \text{B-3}$$

Head loss through a packed bed of a differential height (Ergun, 1952)

$$\Delta P = AU + BU^2 \qquad \text{B-4}$$

$$dp = (AU + BU^2)dh \qquad \text{B-5}$$

$$F = \int_{h_o}^{h_o+H} (LW).(AU + BU^2)dh \qquad \text{B-6}$$

$\overline{L}$, U varies with height

$$\frac{\overline{L}}{L_o} = \frac{h}{h_o} \Rightarrow \overline{L} = \frac{L_o}{h_o}.h$$

$$U.h = U_o.h_o$$

$$\frac{U}{h_o} = \frac{U_o}{h} \Rightarrow U = \frac{U_o.h_o}{h}$$

$$F = \int_{h_o}^{h_o+H} (L.W.A.U + L.W.B.U^2)dh \qquad \text{B-7}$$

$$F = \int_{h_o}^{h_o+H} \left(\frac{L_o.h}{h_o}.W.A.\frac{U_o.h_o}{h} + \frac{L_o.h}{h_o}.W.B.\frac{U_o^2.h_o^2}{h^2}\right)dh \qquad \text{B-8}$$

$$F = \int_{h_o}^{h_o+H} \left(A.W.L_o.U_o + B.W.L_o.U_o^2.h_o.\frac{1}{h}\right)dh \qquad \text{B-9}$$

$$F = A.W.L_o.U_o \int_{h_o}^{h_o+H} dh + B.W.L_o.U_o^2.h_o. \int_{h_o}^{h_o+H} \frac{1}{h}dh \qquad \text{B-10}$$

$$F = A.W.L_o.U_o.h \Big|_{h_o}^{h_o+H} + B.W.L_o.U_o^2.h_o.\ln(h) \Big|_{h_o}^{h_o+H}$$

$$F = A.W.L_o.U_o[h_o + H - h_o] + B.W.L_o.U_o^2.h_o.\ln\left(\frac{h_o+H}{h_o}\right)$$

$$F = (A.W.L_o.U_o.H) + \left(B.W.L_o.U_o^2.h_o.\ln\left(\frac{h_o+H}{h_o}\right)\right) \qquad \text{B-11}$$

Since; $\frac{h_o+H}{h_o} = \frac{L_1}{L_o} \Rightarrow h_o = \frac{(H.L_o)}{(L_1 - L_o)}$ to remove h_o;

$$F = (A.W.L_o.U_o.H) + \left(B.W.L_o^2.U_o^2.\frac{H}{L_1 - L_o}.\ln\left(L_1/L_o\right)\right) \qquad \text{B-12}$$

where F is the upward drag force by the fluid, A and B are parameters in the Ergun's equation, L_o is the size of the orifice, U_o is the velocity down stream of the orifice (i.e. at the bottom of the bed), L_1 is length of the active bed at height (H) and W is the width of the bed.

Downward force- bulk weight of the particles in the bed at the onset of fluidisation

$F = m.g$

$volume\ of\ particles = (1-\varepsilon)AH$

$Weight\ of\ particles\ (m.g) = (1-\varepsilon).(\rho_s - \rho_w).A.H.g$

W_a = bulk weight of the particles in the bed

$$W_a = \int_{h_0}^{h_o+H} g\ (1-\varepsilon)\ (\rho_s - \rho_w)\ \bar{L}\ W\ dh$$

$$\frac{\bar{L}}{L_o} = \frac{h}{h_o} \Rightarrow \bar{L} = \frac{L_o}{h_o}.h$$

$$W_a = \int_{h_0}^{h_o+H} g\ (1-\varepsilon)\ (\rho_s - \rho_w)\ W\ \frac{L_o}{h_o}.h\ dh \qquad \text{B-13}$$

$$W_a = g\ (1-\varepsilon_o)\ (\rho_s - \rho_w)\ W\ \frac{L_o}{h_o}.\int_{h_o}^{h_o+H} h\ dh$$

$$W_a = g\ (1-\varepsilon_o)\ (\rho_s - \rho_w)\ W\ \frac{L_o}{h_o}.(\frac{h^2}{2})\ |_{h_o}^{h_o+H}$$

$$W_a = g\ (1-\varepsilon_o)\ (\rho_s - \rho_w)\ W\ \frac{L_o}{h_o}.(\frac{H^2+2h_oH}{2})$$

$$W_a = \frac{1}{2}\ g\ (1-\varepsilon_o)\ (\rho_s - \rho_w)\ W\ \frac{L_o}{h_o}.[H^2+2h_oH]$$

To remove h_o;

$$\frac{h_o+H}{h_o} = \frac{L_1}{L_o} \Rightarrow h_o = \frac{(H.L_o)}{(L_1-L_o)} \qquad \text{B-14}$$

$$W_a = \frac{1}{2}\ g\ (1-\varepsilon_o)\ (\rho_s - \rho_w)\ W\ \frac{L_o\ (L_1-L_o)}{(H.L_o)}.[H^2+2\frac{(H.L_o)}{(L_1-L_o)}H] \qquad \text{B-15}$$

$$W_a = \frac{1}{2}\ g\ (1-\varepsilon_o)\ (\rho_s - \rho_w)\ W\ H\ (L_1+L_o). \qquad \text{B-16}$$

Based on the proposed model, the particles at the bottom start to fluidise when the upward force by the fluid flow is in balanced with the effective weight of the bed F-W_a=0. Therefore, the critical velocity at which the particles start to fluidise can be calculated by equating the equations B-12 and B-16. This gives the critical velocity at the onset of fluidisation

$$[(A.W.L_o.H)U_c + (B.W.L_o^2.\frac{H}{L_1 - L_o}.\ln(L_1/L_o))\ U_c^2\ ] -$$

$$[\frac{1}{2}\ g\ (1-\varepsilon_o)\ (\rho_s - \rho_w)\ W\ H\ (L_1 + L_o)] = 0 \qquad \text{B-17}$$

$$a = B.W.L_o^2.\frac{H}{L_1 - L_o}.\ln(L_1/L_o)$$

$$b = A.W.L_o.H$$

$$c = \frac{1}{2}\ g\ (1-\varepsilon_o)\ (\rho_s - \rho_w)\ W\ H\ (L_1 + L_o)$$

This equation can be written in a simple form;

$$aU_c^2 + bU_c - c = 0 \qquad \text{B-18}$$

This is a quadratic equation, a polynomial equation, of the second degree:

$$U_c = \frac{-b + \sqrt{b^2 + 4ac}}{2a} \qquad \text{B-19}$$

U_c is the critical velocity at which fluidisation start,

Knowing the velocity at which fluidisation starts, head loss can be estimated from the following derived equation.

Prediction of the Pressure loss through the bed at the onset of fluidisation:

Head loss through the bed with a differential height of dh equals to (Ergun, 1952):

$$dp = (AU + BU^2)dh \qquad \text{B-20}$$

$$A = \frac{150 \cdot \mu}{\phi_s^2 \cdot d_p^2} \cdot \frac{(1-\varepsilon)^2}{\varepsilon^3}$$

$$B = \frac{1.75 \cdot \rho_w}{\phi_s \cdot d_p} \cdot \frac{(1-\varepsilon)}{\varepsilon^3}$$

The total pressure loss through the active bed height (which varies with height) can be obtained by integrating eq.(B-20)

$$\Delta P = \int_{h_o}^{ho+H} (dp)\ dh$$

$$\Delta P = \int_{h_o}^{ho+H} (AU + BU^2)\ dh$$

$$U.h = U_o.h_o$$

$$\frac{U}{h_o} = \frac{U_o}{h} \Rightarrow U = \frac{U_o.h_o}{h}$$

$$\Delta P = \int_{h_o}^{ho+H} [A \cdot (\frac{U_o.h_o}{h}) + B(\frac{U_o^2.h_o^2}{h^2})]\ dh$$

$$\Delta P = A \cdot U_o \cdot h_o \int_{h_o}^{h_o+H} \frac{1}{h}\ dh\ +\ B \cdot U_o^2.h_o^2 \int_{h_o}^{h_o+H} \frac{1}{h^2} dh$$

$$\Delta P = A \cdot U_o \cdot h_o \cdot \ln(h)\Big|_{h_o}^{h_o+H} + B \cdot U_o^2 \cdot h_o^2 (-\frac{1}{h})\Big|_{h_o}^{ho+H}$$

$$\Delta P = A \cdot U_o \cdot h_o \cdot \ln(\frac{h_o + H}{h_o}) + B \cdot U_o^2 \cdot h_o^2 (\frac{1}{h_o} - \frac{1}{h_o + H})$$

$$\Delta P = A \cdot U_o \cdot h_o \cdot \ln(\frac{h_o + H}{h_o}) + B \cdot U_o^2 \cdot h_o^2 (\frac{(h_o + H)}{h_o(h_o + H)} - \frac{h_o}{h_o(h_o + H)})$$

$$\Delta P = A \cdot U_o \cdot h_o \cdot \ln(\frac{h_o + H}{h_o}) + B \cdot U_o^2 \cdot h_o^2 [\frac{(h_o}{h_o(h_o + H)} + \frac{H}{h_o(h_o + H)} - \frac{h_o}{h_o(h_o + H)}]$$

$$\Delta P = A \cdot U_o \cdot h_o \cdot \ln(\frac{h_o + H}{h_o}) + B \cdot U_o^2 \cdot h_o^2 [\frac{H}{h_o(h_o + H)}]$$

$$\Delta P = A \cdot U_o \cdot h_o \cdot \ln(\frac{h_o + H}{h_o}) + B \cdot U_o^2 \cdot \frac{h_o \cdot H}{(h_o + H)}]$$

To remove h_o:

$$\frac{h_o + H}{h_o} = \frac{L_1}{L_o} \Rightarrow h_o = \frac{(H.L_o)}{(L_1 - L_o)}$$

$$\Delta P = A\ U_o\ \frac{H\ L_o}{L_1 - L_0}\ \ln(L_1 / L_0) + B\ U_o^2\ \frac{H\ L_o}{L_1} \qquad \text{B-21}$$

Thus to calculate the head loss at the onset of fluidisation, U_o is replaced by U_c:

$$\Delta P_{max} = A\ U_c\ \frac{H\ L_o}{L_1 - L_0}\ \ln(L_1 / L_0) + B\ U_c^2\ \frac{H\ L_o}{L_1} \qquad \text{B-22}$$

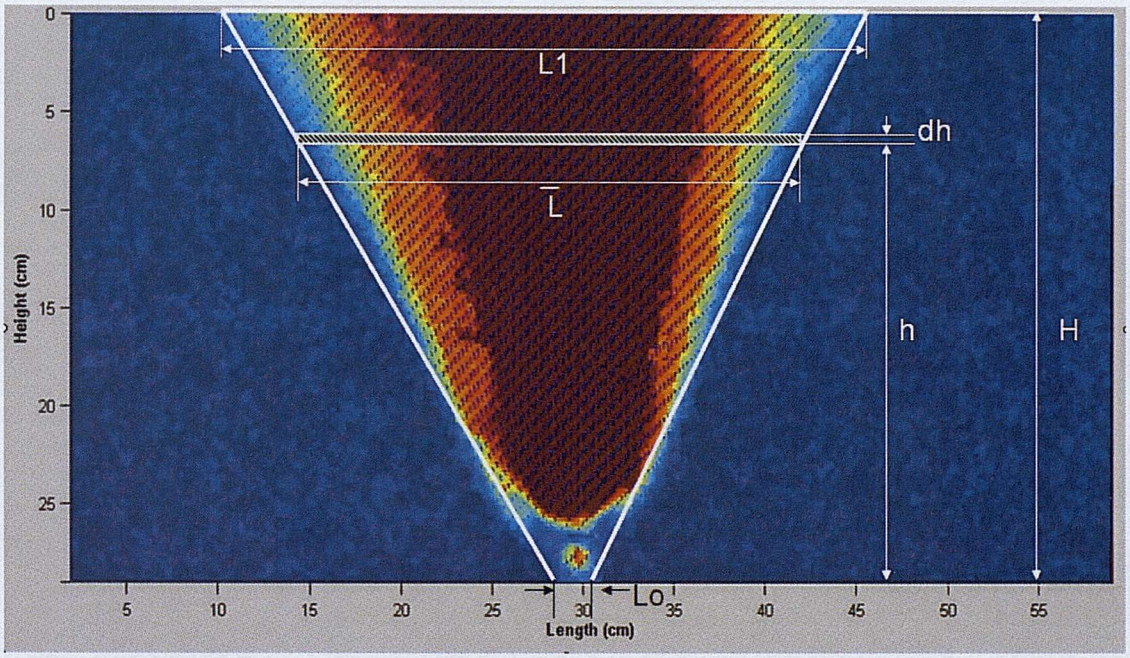

Figure B-1: The active weight of the bed at the onset of fluidisation using PIV.

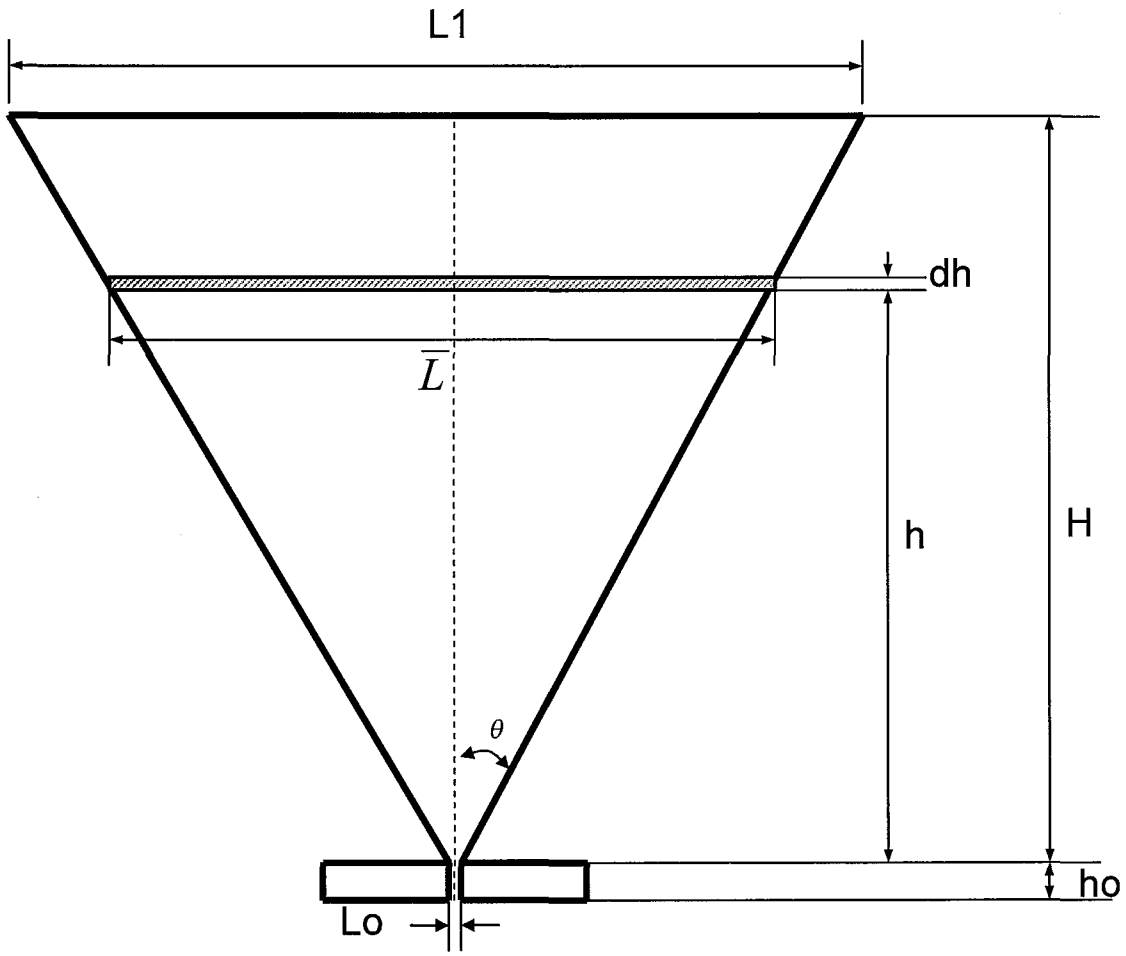

Figure B-2: The active weight of the bed at the onset of fluidisation.

Appendix C:

C-1 Pressure gauge calibration-Bourdon gauge used for preliminary tests

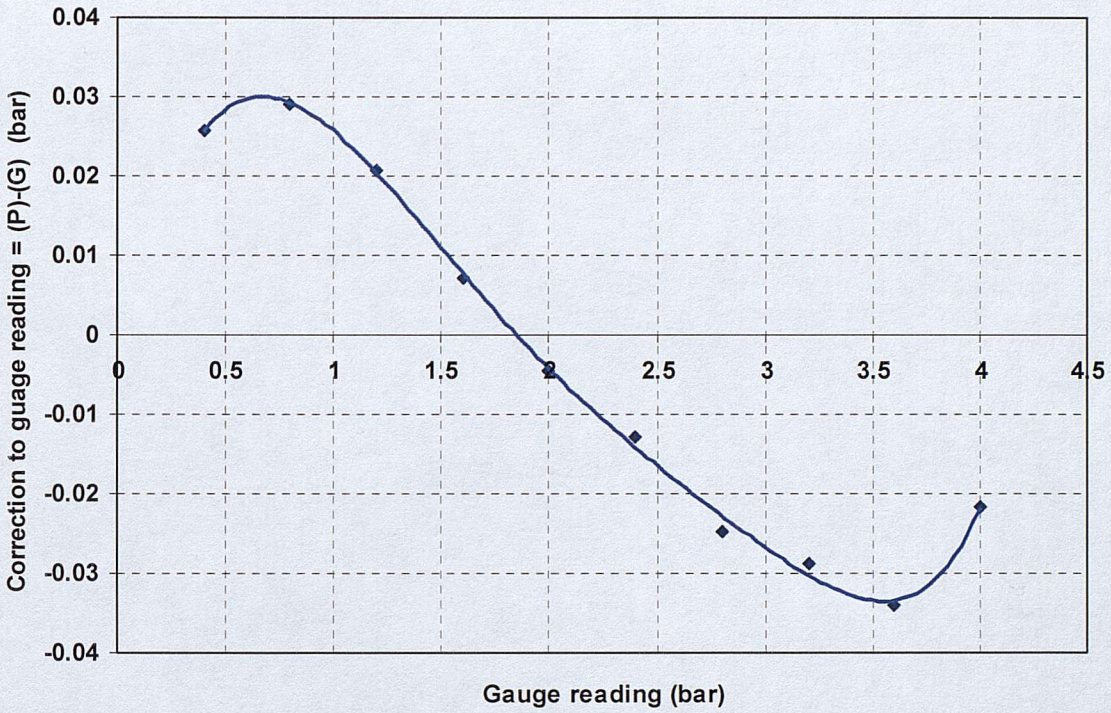

Figure C-1: Typical calibration result of the pressure gauge.

C-3 Pore Pressure transducers calibration

Six pressure transducers (RS type 286-658) with pressure range of 0-34.47 kPa (0-5 psi) were used. To calibrate the pressure transducers, the sensor was loaded with a column of water giving a static head according to the equation:

$$P_{water\ column} = \rho_{water} \cdot g \cdot h_{water\ column}$$

The sensor has a full scale output (FSO) of 50 mV with a sensitivity of 10 mV/psi. The null offset is between -1.5 and +1.5., and accuracy of $\pm$ 0.24 kPa.

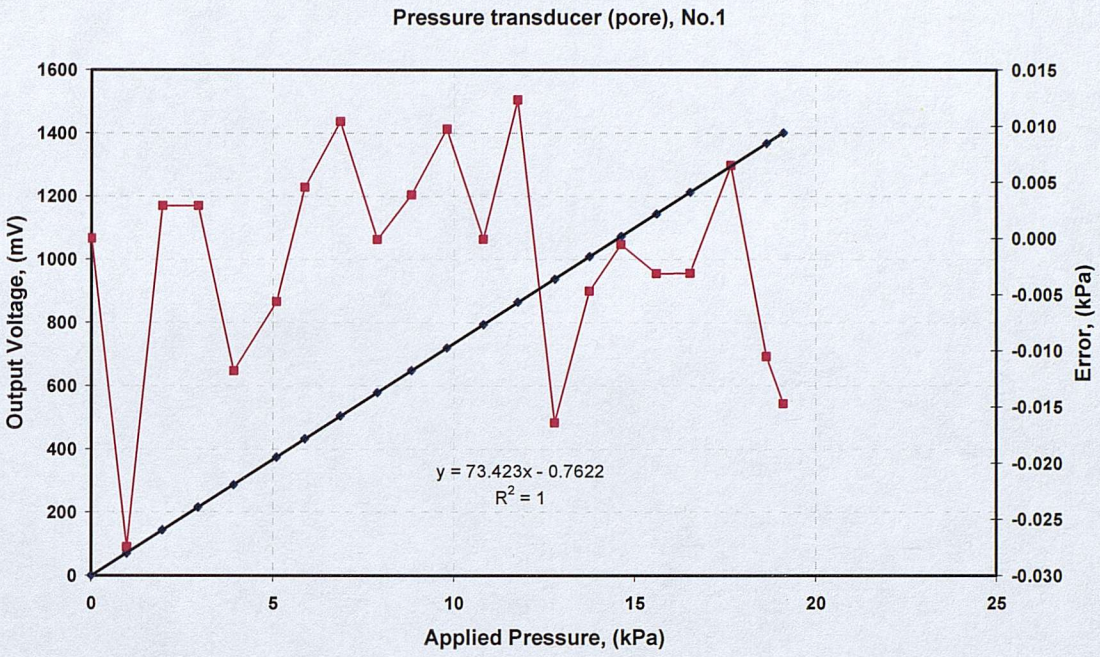

Figure C-2: Calibration result of the pore pressure transducer (no.1).

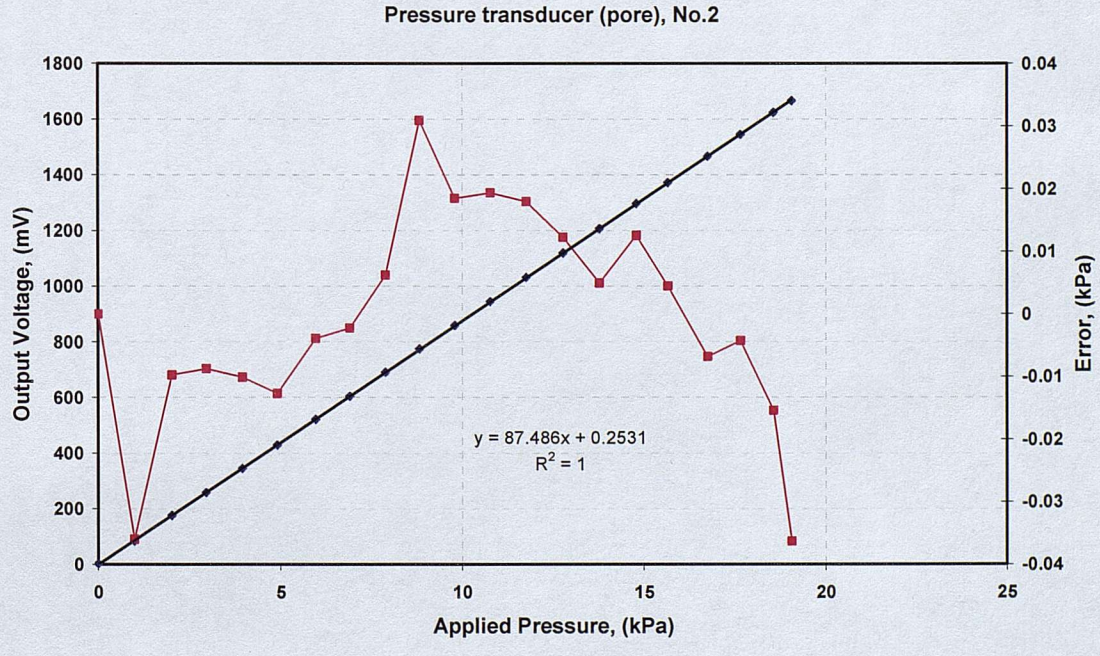

Figure C-3: Calibration result of the pore pressure transducer (no.2).

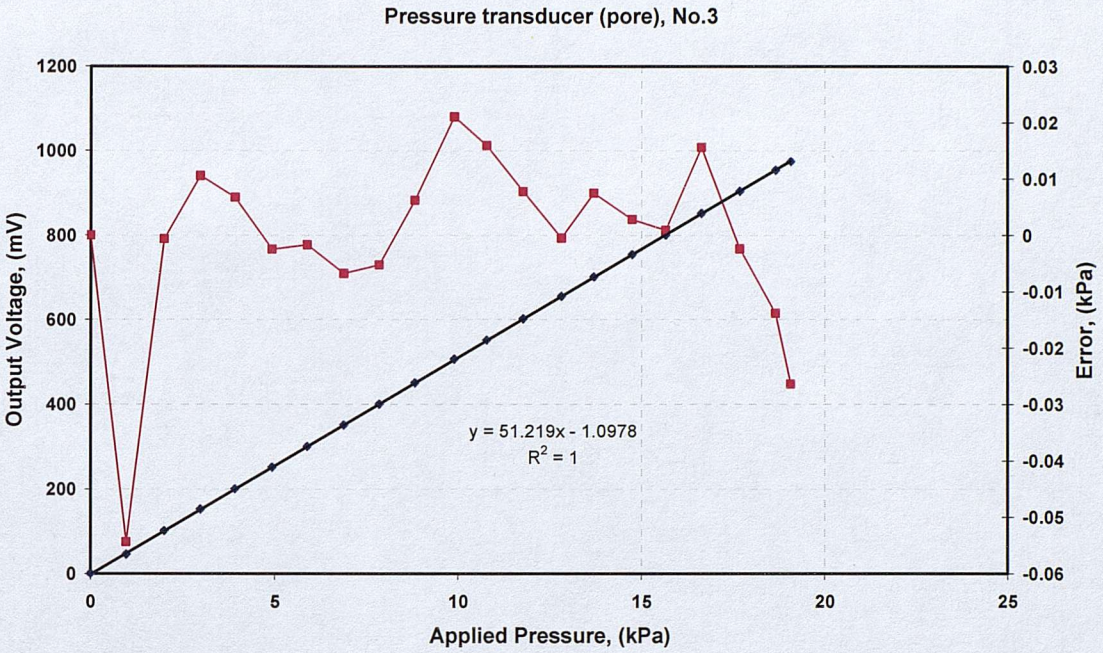

Figure C-4: Calibration result of the pore pressure transducer (no.3).

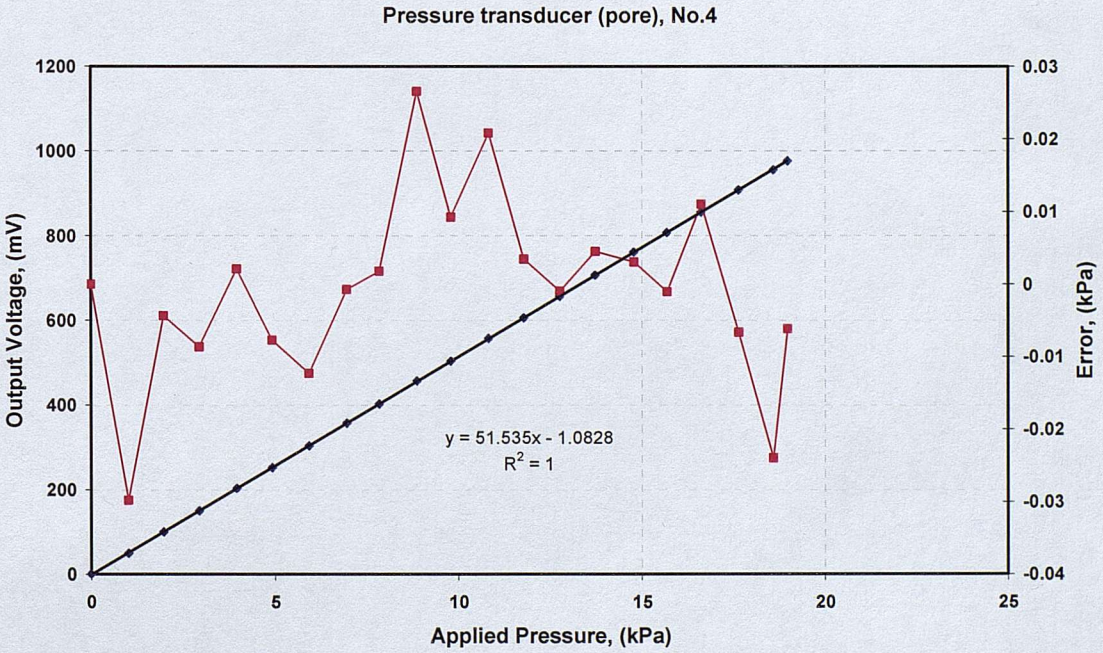

Figure C-5: Calibration result of the pore pressure transducer (no.4).

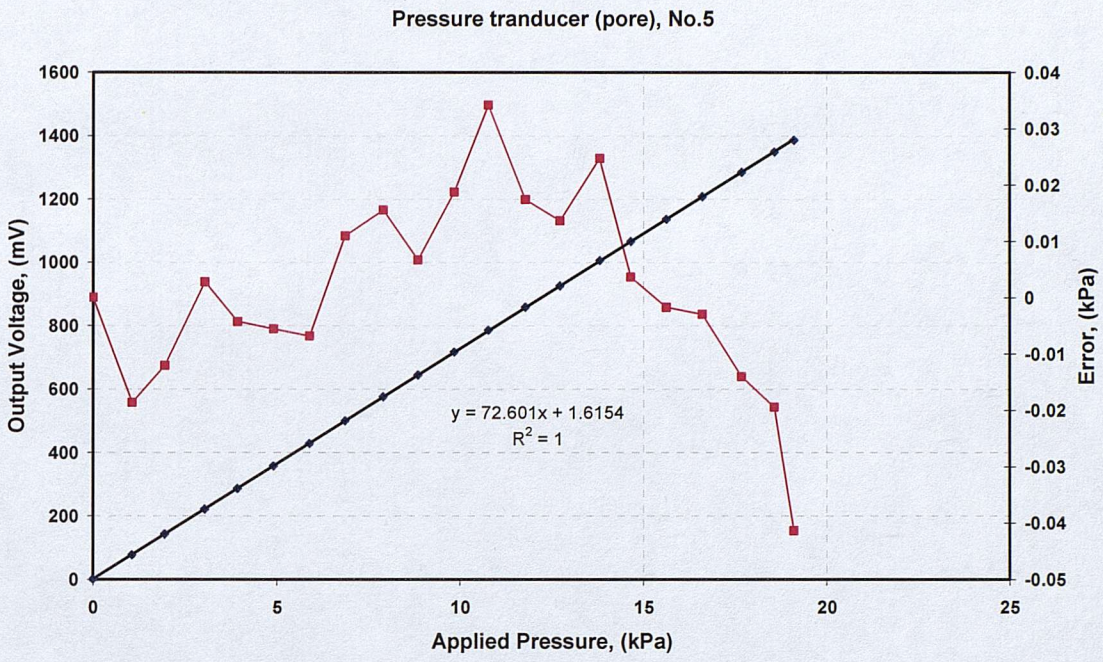

Figure C-6: Calibration result of the pore pressure transducer (no.5).

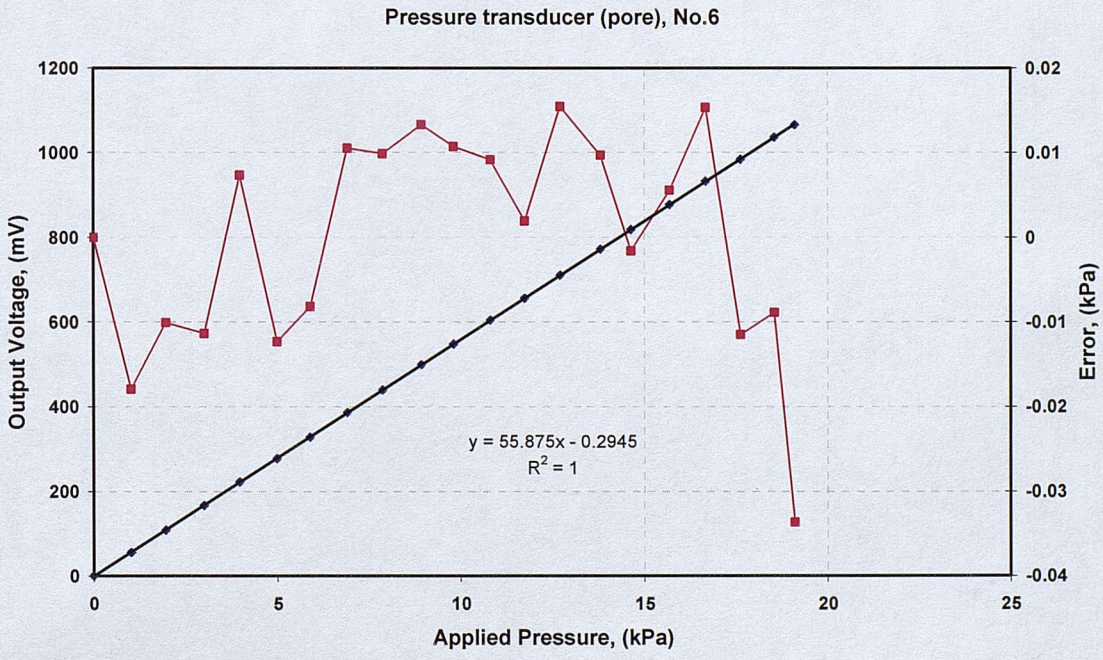

Figure C-7: Calibration result of the pore pressure transducer (no.6).

C-2 Pressure transducer (for measuring pressure upstream of the orifice)

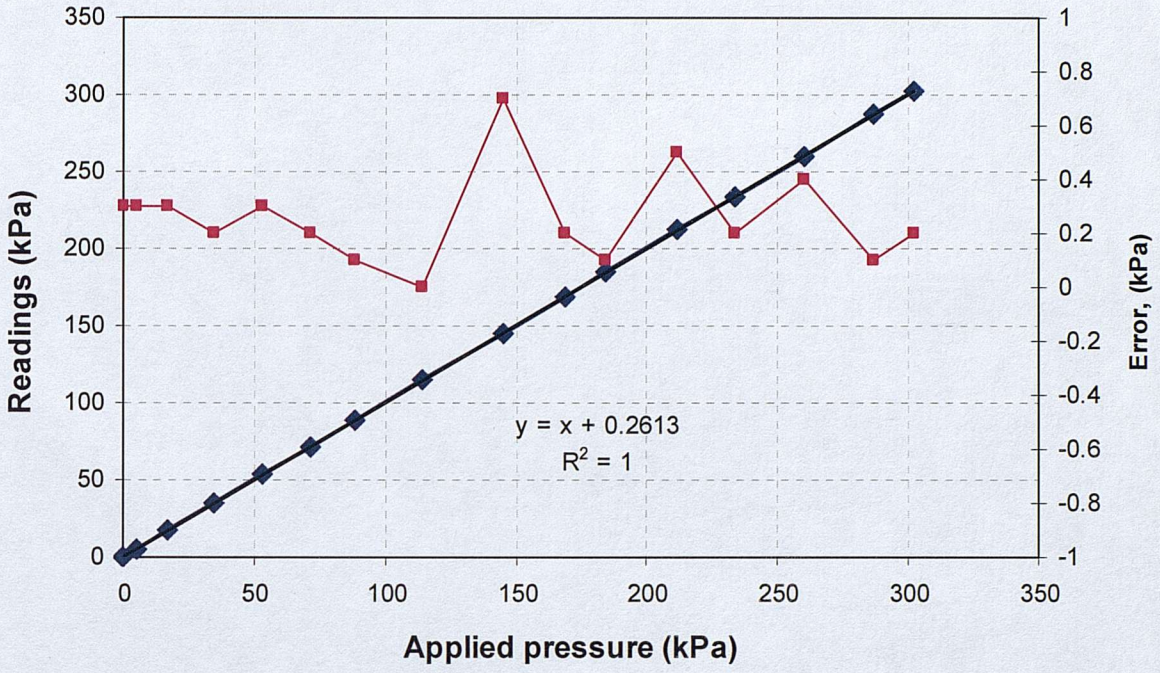

Figure C-8: Calibration result of the pressure transducer.

C-3 Flow sensor calibration

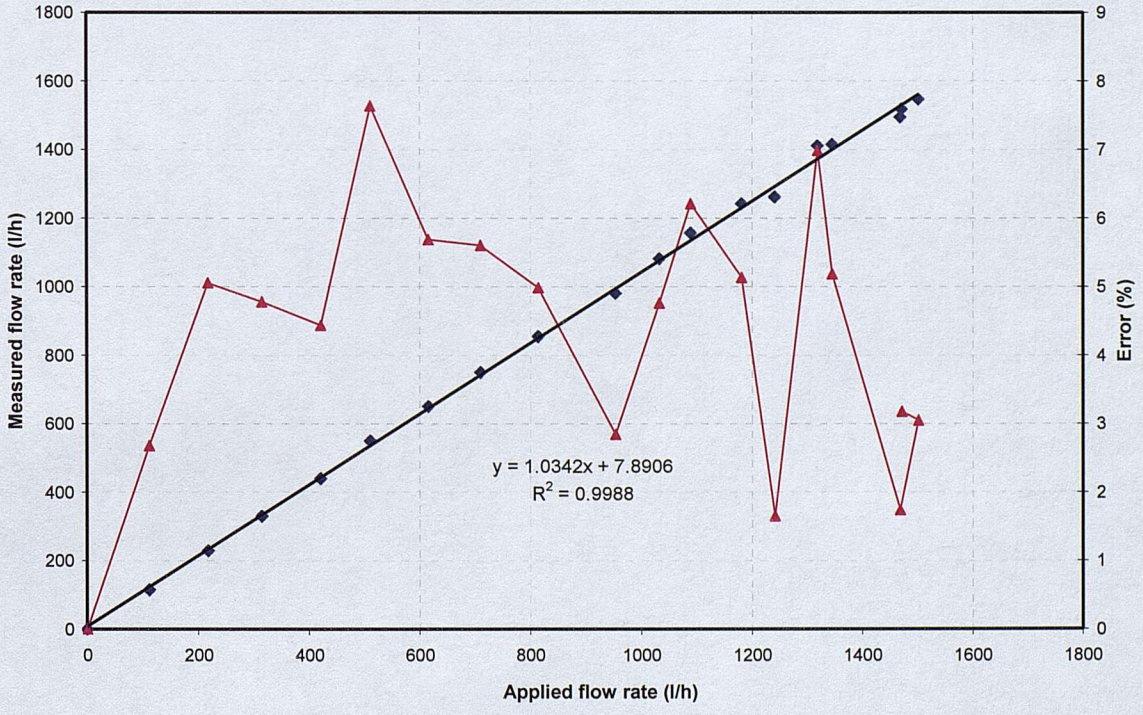

Figure C-9: Calibration result of the flow sensor.

Appendix D: comparison between calculated and measured flow rate for different orifice openings.

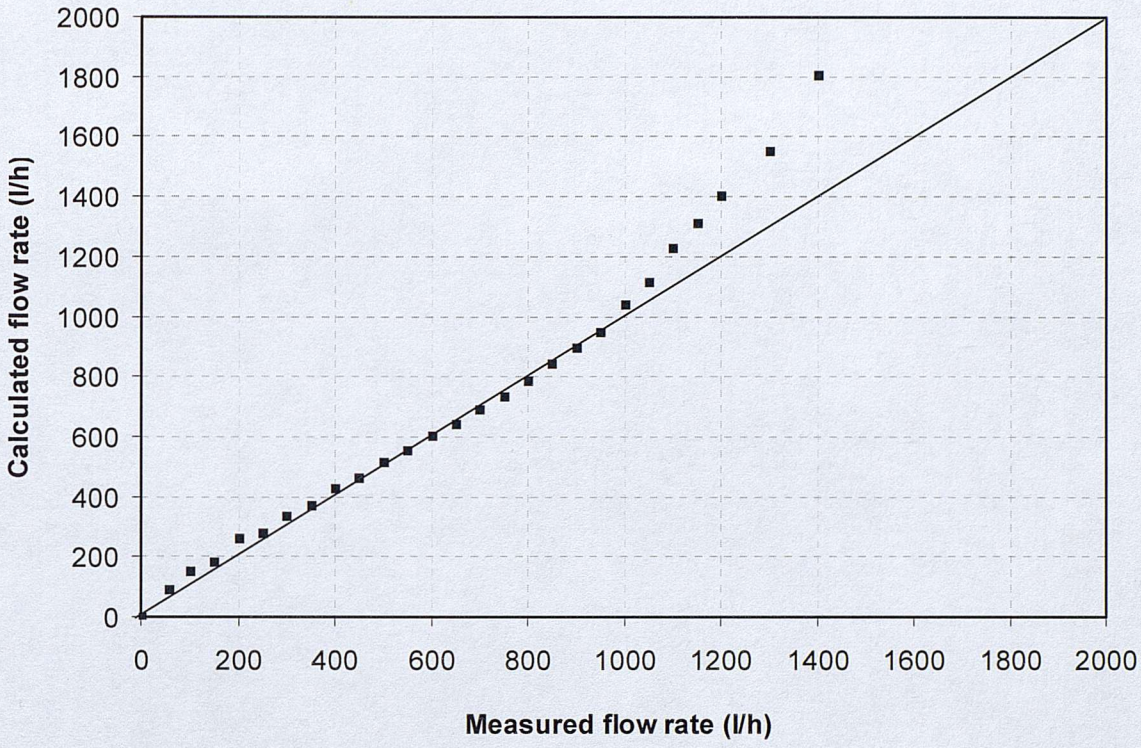

Figure D-1: Calculated and measure flow rate for 0.33 mm orifice opening.

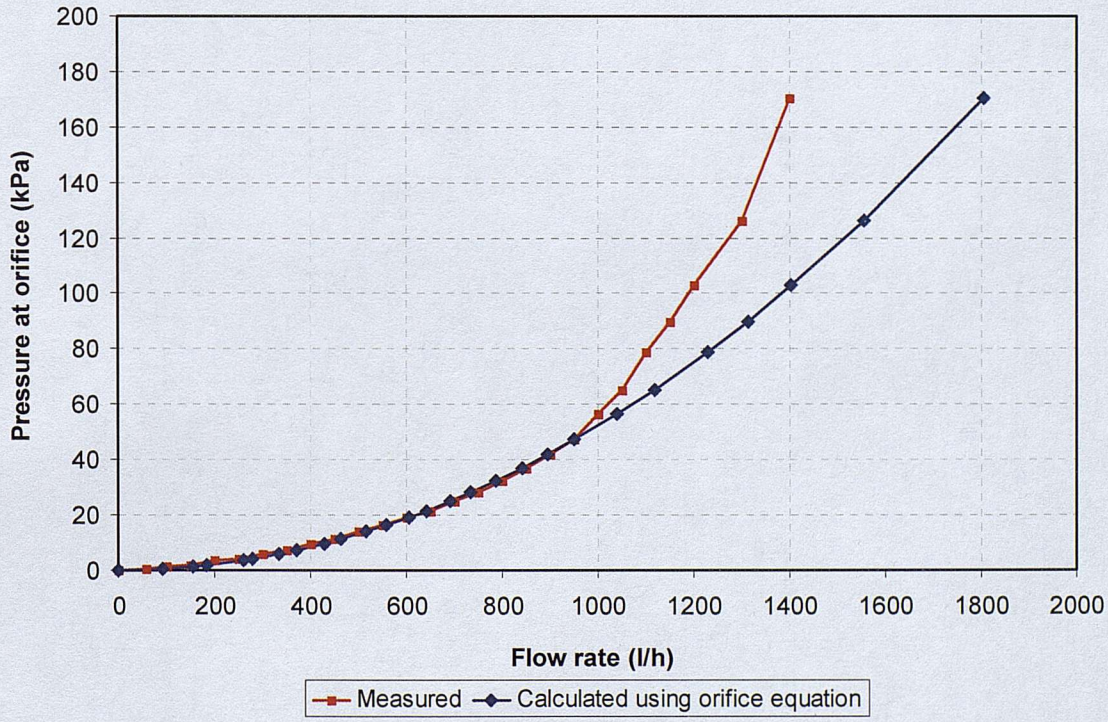

Figure D-2: Pressure flow rate relationship for 0.33 mm orifice opening.

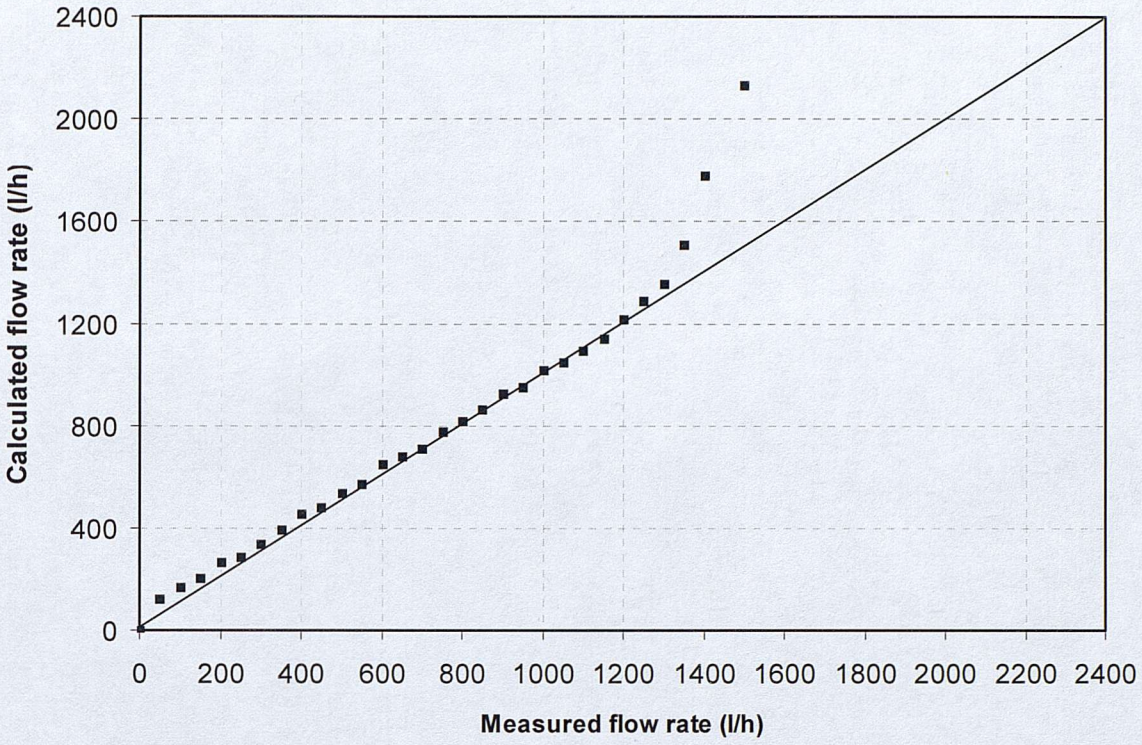

Figure D-3: Calculated and measure flow rate for 0.62 mm orifice opening.

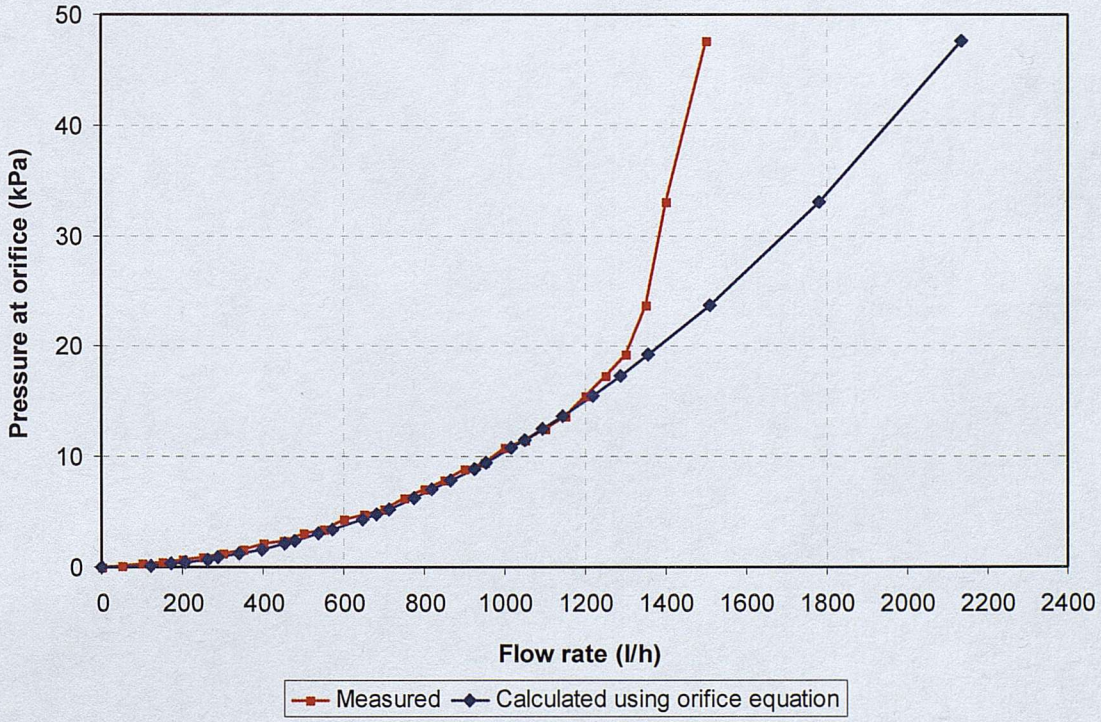

Figure D-4: Pressure flow rate relationship for 0.62 mm orifice opening.

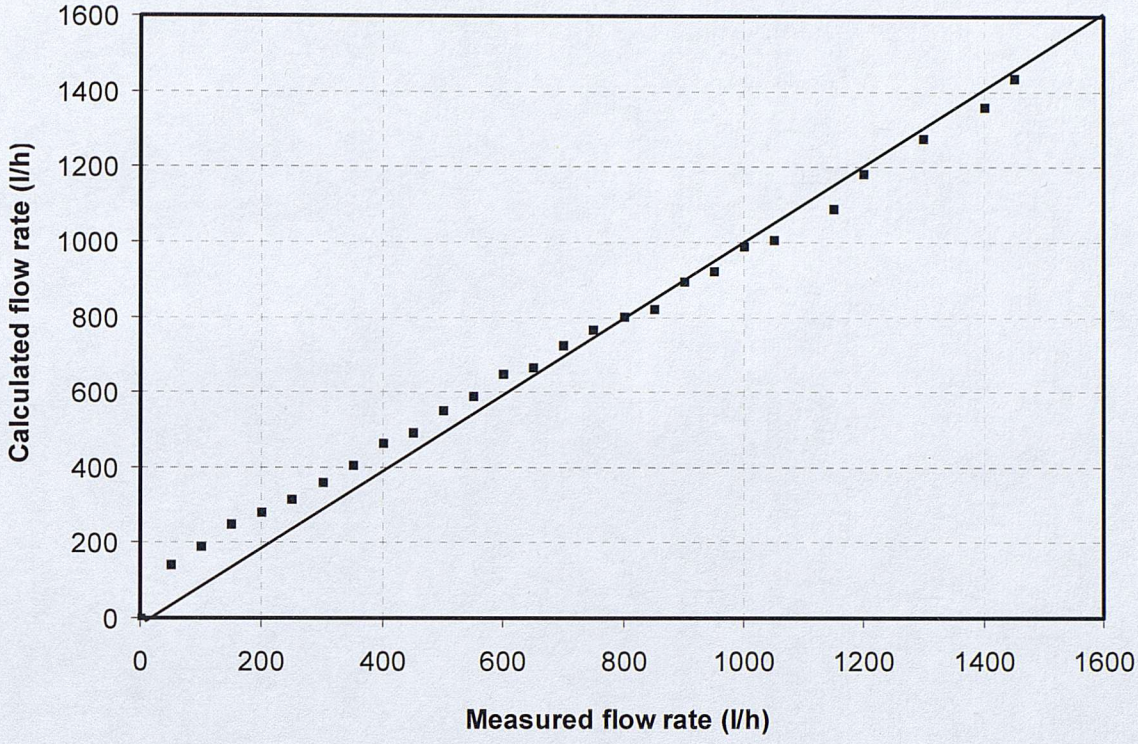

Figure D-5: Calculated and measure flow rate for 0.92 mm orifice opening.

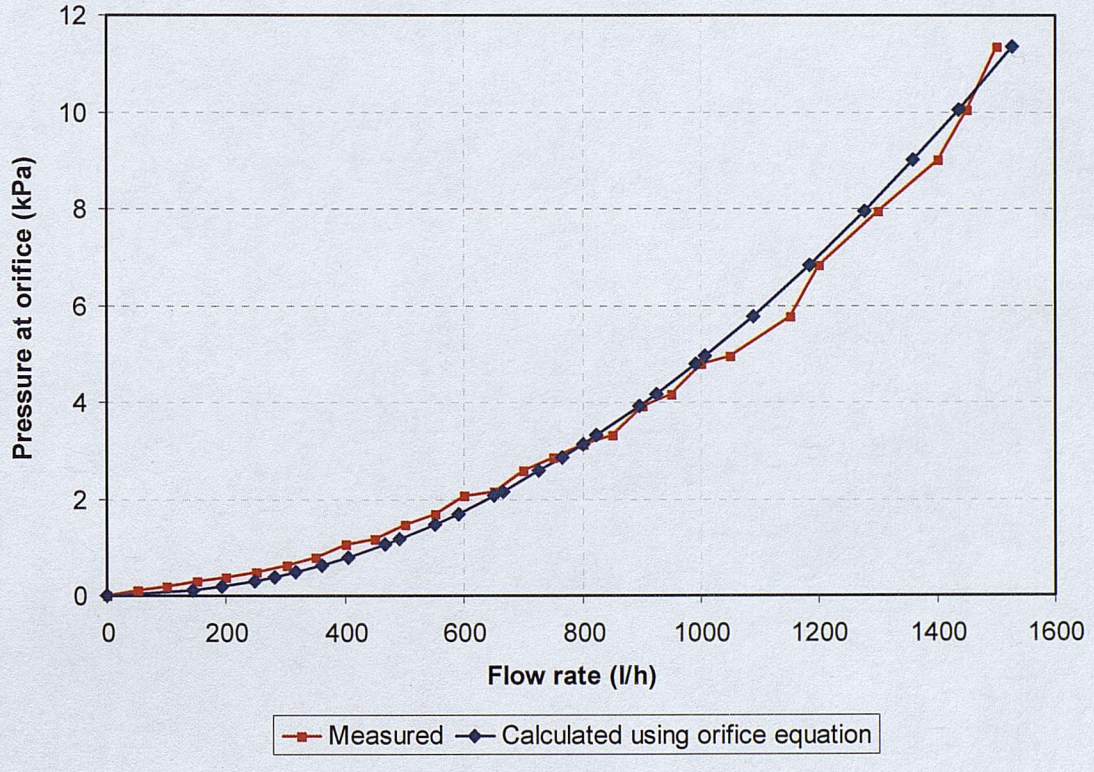

Figure D-6: Pressure flow rate relationship for 0.92 mm orifice opening.